

# SCIENTIFIC & TECHNICAL REPORT **2020**



:csem

## IMPRINT

---

**Full report title** CSEM Scientific and Technical Report 2020

**Editor and publisher** CSEM SA  
[info@csem.ch](mailto:info@csem.ch)  
T +41 32 720 5111

**Publication** Frequency yearly  
Media printed and electronic  
Website [www.csem.ch/str2020](http://www.csem.ch/str2020)

**Cover page design** Contreforme  
[www.contreforme.ch](http://www.contreforme.ch)

**Printing** Imprimerie Baillod SA, Bevaix (Switzerland)

# PREFACE

Dear Reader,

This year has seen the COVID-19 pandemic impact every part of our lives; it has also inspired a sense of togetherness, leading to acts of generosity, collaboration, and human kindness both personally and professionally. Crucially, during this time digital technologies have proven themselves essential in securing businesses' futures and keeping the economy going. Their accelerated adoption, along with that of automation (a key element of digital transformation), has provided many companies with new advantages, including the speeding up of their business operations and improved efficiency and precision.

Moreover, it is also widely recognized that the rapid evolution of biological screening tests, contact-tracing apps, or vaccine development could not have been as fast and efficient without digital health technologies: telemedicine, information and communication technologies (mobile phones, apps, and handheld devices), robotics, virtual reality, AI, or genomics. Even ten years ago, we would have struggled to innovate at the same pace as we have today.

Of course, CSEM has not emerged from the pandemic completely unscathed, and there has been some disruption to our research objectives. While our digital researchers and AI experts have been able to continue working from home, this has not been the case for all of our colleagues, especially those working on projects that need access to equipment and clean rooms.

Despite this, CSEM remains committed to helping businesses unlock their digital potential by developing the personalized tools, hardware, and software they need: whether that be smart sensing devices, wearables, machine/deep learning algorithms, or digital twins that connect products to the IIoT.

We are extremely proud of this report as well as of our colleagues, who have worked hard to overcome difficult circumstances while still achieving these exceptional highlights:

- Blood pressure measurement via a smartphone camera for early detection, prevention, and management of hypertension (p. 91).
- From a MIP to a product—a custom PV watch dial for the Tissot T-Touch Connect Solar (p. 61).
- Electrochemical point-of-care device for rapid diagnostic tests in low-resource settings (p. 51).
- DropWatch, an optical tool for in-flight, high-speed monitoring of liquid droplets (p. 47).
- The best models for model predictive control in buildings (p. 66).

While this is the last time my signature will appear here, I leave confident that CSEM's researchers will continue on their road to excellence and provide our partners with the best technologies.

Mario El-Khoury  
CEO, CSEM SA



# CONTENTS

## PREFACE

## MULTIDISCIPLINARY INTEGRATED PROJECTS—MIPS

- AUDIENCE—An Ultra-low-power and Smart Sound Acquisition System for IoT Applications  
UC-MORE—Ultra-compact Multispectral Snapshot Camera based on Optical Resonant Nanostructures  
ROBIN—Robust Battery Monitoring  
YOU-ON-CHIP—Automated *in vitro* 3D Systems and Diagnostics  
CHAMELEON—Compliant Mechanism with Embedded Sensing  
SIOSCAPE—Flexure-based Escapements for Mechanical Watches

## MICROSYSTEMS

- Bolometer for Plasma Diagnostics in ITER Tokamak  
Processing of SU8 Dry Film Laminates and Multilevel Processing  
Advances in Microfabricated Electron Gun for Atomic Clocks  
Wafer-scale in-plane Micro-optical Interconnects for Integrated Photonics Circuits (PICs)  
An Electro-optics Integrated Photonic Circuits (PICs) Platform based on Lithium Niobate  
High Thermal Conductive Die Attach Material for High-power Semiconductor Devices in Space Applications  
Advanced Packaging for Simultaneous Hermetic Lid Sealing and Chip Backside Heat Removal  
Photonic Multi-domain Integration Trends  
SWaP—Smart Wall Pipes and Ducts  
Development of Metal Matrix Composites by Laser Powder Bed Fusion  
3D-printed Multi-material 3/2-way Valves for Soft Actuators

## SURFACE ENGINEERING

- PLASMEX—Plasmonic Structures for Exosome Analysis  
Modelling Optical Effects in Water Splitting  
Photoelectrodes  
Molecular Imprinted Polymer as a Sensing Layer for Various Analytes Detection  
Micro-nanostructuring of 3D Surfaces: on the Manufacturing of Functional Parts for the Medical and Watchmaking Industry  
Imprint of High Refractive Index Micro- and Nano-optical Structures

1	Smartphone Readable Digital Scrambled Pixelated Microstructures for Part Identification and Brand Protection	36
7	High-efficiency Gratings at 1.55 μm Fabricated by UV Imprint	37
9	Freeform Micro Optics: Design, Manufacturing, Characterization	38
10	Freeform Microlenses for High-quality Lighting	39
11	Smart Laser-based Manufacturing for Precision Industry 4.0	40
12	Silver Electroless Coating of 3D-Printed Parts	41
13	Patterning Metal Grids on Heterojunction Solar Cells using Self-assembled Monolayers	42
14	PDMS Replacement in Organ-on-Chip Systems and <i>in vitro</i> Assays	43
15	Organoid Technology Platform for Tissue Engineering	44
18	MUSTANG—Automated Screening Platform for Skeletal Muscle Contractility Assays	45
19	Calibration-free Air Flow-rate Sensor for Monitoring Dispensing Systems	46
20	DropWatch—High-speed Volumetric Measurement System for Nanoliter Droplets in Flight	47
21	Development of Digital Droplet Nucleic Acid Amplification Platform for Field-deployable Diagnostics	48
22	Optical Sensor for Glucose Monitoring in Cell Cultures	49
23	ACEnano—New Tools for Nanomaterials Risk Assessment	50
24	NIIDS—Digital Urine Analysis with Printed Electrochemical Sensors	51
25	Multiplex Photonic Sensor Platform for Plasmonic-based Detection of Contaminants in Milk	52
26	Porous Material Assisted Lateral Flow Immunoassay (LFIA) for Improved Sensitivity and Detection Limit	53
27	Inkjet Printed Pt-electrode Array for <i>in vivo</i> Neural Recordings	54
28	Artificial Ear Canal with Integrated Pressure Sensors	55
29	<b>PHOTOVOLTAICS &amp; ENERGY MANAGEMENT</b>	57
31	Deep Black Solar Cells for Energy Harvesting	60
32	From an Internal Research Project to a Product: The Wear-a-Watt Project and a Production Platform for IOT Energy Harvesters	61
33	Optical Coating for Fluorescence-based Diagnostics and Advanced Microscopy	62
34	DIPPS—Upscaling of Perovskite/Silicon Tandem Cells	63
35	Development of Sputtered Passivating Contacts for Industrial, High-efficiency Silicon Solar Cells	64
	AMPERE—Silicon Heterojunction for High-performance Photovoltaics	65
	Finding the Best Models for Model Predictive Control in Buildings	66

A Software Solution to Manage Local Energy: from the House to the District	67	Soft Structure Designs for 3D-printed Wheelchair Seat Cushions	100
Integration of Advanced Diagnostic Capabilities in Battery Management Systems	68		
Multi-site PV Forecasting using Spatio-temporal Machine Learning Models	69	<b>ULTRA-LOW-POWER INTEGRATED SYSTEMS</b>	<b>101</b>
DC Distribution in Low-energy Buildings with Innovative, Compact Hybrid Storage System	70	Efficient Un-supervised Neural Network Learning for Image Restoration and Generation	103
A Building Model Library for Simulation and Control of Energy systems	71	Efficient Neural Vision Systems Based on Convolutional Image Acquisition	104
<b>SYSTEMS</b>	<b>73</b>	AI-based Hand Gesture Recognition System for Improved Human Machine Interaction in Cockpits	105
A Stable Mode-locked Laser as Local Oscillator for a Photonics-based Radar	75	A ULP 22 nm System-on-Chip with Dual-engine Hardware Acceleration for Edge ML Inference	106
MEMS Cells for High Stability Miniature Atomic Clocks	76	An Ultra-low-power System-on-Chip with Adaptive Body Bias	107
macQsim—Towards Reliable Miniature Quantum Sensors	77	Towards fully Integrated Cooperative Sensors for Vital Signs Monitoring	108
LiDAR Use in Sunlight: Pathway to New Opportunities	78	$\mu$ 111MP—Porting the $\mu$ 111 RTOS on Dual-core Cortex-A7 Processor	109
PULSAR—Development of a Mirror Tile Prototype for Future Large Telescopes Robotically Assembled in Space	79	Porting Low-power Wireless protocols on the $\mu$ 111 Real-time Operating System	110
SMARTES—Slip Ring Assemblies based on Additive Manufacturing for Space Applications	80	IoT SPAT—Security and Privacy Analysis Toolbox for IoT Applications	111
Compliant Mechanism built by Additive Manufacturing	81	Bluetooth Dual Mode Transceiver in 22 nm CMOS	112
CITCOM—Automated 3D Quality Control of MEMS	82	A 60 GHz FMCW RADAR-on-Chip Front-end Integrated in 22 nm CMOS	113
AI-based Generic Machine Health Monitoring	83	A Novel Joint Phase Processing Algorithm for MIMO Sensor Imaging	114
CSEM Visard Enables AI for Industrial Quality Control	84	Multipurpose Optically Transparent Planar High-gain Passive Antenna	115
Pignosis—Hierarchical Time Series Forecasting using Multiple Machine Learning Methods	85	High-gain Sectorial Antenna for Localization Applications Dedicated to Healthy Ageing	116
Metal Working Fluid Monitoring for Industry 4.0	86	Dynamic Authorization and Consent in an IoT Ecosystem Dedicated to Healthy Ageing	117
Solving the Data Problem: Deep Learning based Image Synthesis for Industrial Applications	87	IR-UWB for Precise Ranging and Localization	118
Detecting the Source of Defects in Condition-based Maintenance	88		
Life-long Learning: Handling the Complete Data Pipeline	89		
Machine Learning Approaches for PPG-based Blood Pressure Monitoring: Validation against Invasive Arterial Line Measurements	90	<b>ANNEXES</b>	<b>119</b>
Blood Pressure via Smartphone Camera: Validation against Auscultatory Measurements	91	Publications	119
Wearable Multiparametric Monitoring System with Embedded Intelligence: towards Seamless Atrial Fibrillation Detection	92	Proceedings	122
Pulse Oximetry and Respiration Rate Assessment at the Wrist: towards the Unobtrusive Detection of Sleep Apnea	93	Conferences and Workshops	125
ELAINE—Electronic Fetal Monitoring System	94	Research Projects	126
Interoperable Pig Health Tracking	95	Innosuisse – Swiss Innovation Agency	128
Remote Automatic Fall Detection and Activity Monitoring using Smart Wearables	96	European Commission Projects	132
SBra—Development of a Sensor-equipped Bra to Evaluate the Feasibility of Detecting Breast Cancer through Temperature and Bioimpedance Measurements	97	European Space Agency, Swiss Space Office, and Swiss Space Center Projects	135
Wireless Powering of Ultra-low-power Sensors	98	Industrial Property	136
Tissue Discrimination via Electrical Impedance Spectroscopy for Neurosurgical Robots	99	Collaboration with Research Institutes and Universities	136
		Teaching	142
		Theses	142
		Commissions and Committees	144
		Prizes and Awards	147

# CSEM SA

CSEM is a private, non-profit research and technology organization (RTO) with over 35 years of technological transfer experience and know-how in digitalization, precision manufacturing, and sustainable energy technologies. A source of Swiss industrial competitiveness, CSEM offers end-to-end services, powerful R&D capabilities, and world-class engineering prowess—all, of course, “Made in Switzerland”.

The center’s research strategy is built around five main programs:

**Microsystems**—Dedicated to the development of complete and reliable microsystems solutions using MEMS and additive manufacturing technologies, with packaging and integration concepts.

#additivemanufacturing #AM #mems #3Dprinting #packaging #photonics

**Systems**—Design, simulation, prototyping, and integration of micro/nano technologies and advanced algorithms to create (sub-) systems for use within applications such as scientific instrumentation, automation and robotic systems, and wearable and medical devices.

#medicaldevices #wearable #automation #robotics  
#quantumtechnology #timefrequency #laser

**Ultra-Low-Power Integrated Systems**—Addresses the key challenges to, and the technologies required in, developing embedded autonomous smart systems or remote sensing nodes, including deep learning and ultra-low-power electronics and wireless communication.

#visionsensors #machinelearning #AI #edgecomputing #zerobattery #IOT #SystemOnChip #wireless #neuralnetworks  
#datascience

**Surface Engineering**—Focused on the functionalization of surface structure and composition (topographical and/or chemical), alongside the optimization of (bio-) chemical, optical, and electrical properties. In addition, the program develops related competitive manufacturing technologies that are suitable for use in industrial applications.

#functionalization #biosensing #biosurface #nanocoating  
#printedelectronics #nanostructuring #lifesciences

**Photovoltaics & Energy Management**—Fostering innovation while accelerating the pace of technology transfer in the fields of photovoltaics, energy storage, and systems, to support the Internet of Things, cleantech, and the energy transition.

#smartgrid #storage #energydata #bipv #solarenergy #HJT  
#perovskite #thinfilm #photovoltaics



# MULTIDISCIPLINARY INTEGRATED PROJECTS—MIPS

Harry Heinzelmann

Multidisciplinary integrated projects (MIPs) form an interdisciplinary program that mostly builds on technologies developed in the five topical research programs, **Microsystems, Surface Engineering, Integrated Systems, Ultra-Low-Power Integrated Systems, and Photovoltaics & Energy Management**. The goal of the MIP program is to better exploit synergies and to create innovative solutions.

Every year CSEM dedicates an important part of its resources to the program, targeting demonstrators with a high level of maturity (i.e., a high technology readiness level (TRL)) for novel applications with high market potential in relatively short development times. Classical MIPs typically last 1–2 years, while Technology MIPs address longer term co-developments with different technologies.

The MIP program is re-evaluated annually and consists of new proposals and ongoing projects. In this way, CSEM's MIPs complement its five topical research programs in an ideal way. The program enables CSEM to offer its industrial clients an even richer portfolio of technologies, beyond the scope of its thematic research programs alone.

An overview of 2020 MIPs is given in the text below; the projects are presented in more detail in the following pages. Due to the particular sanitary situation in 2020 and the consequent delays in development work, most of these projects were still ongoing at the time these reports were written. Final results are expected during 2021.

## Classical MIPs

### Audience—An ultra-low-power, smart sound acquisition system for IoT applications

The ability of IoT devices to acquire sound enables applications in voice control and in monitoring physiological signals. As in most IoT use cases, ultra-low power consumption represents a decisive advantage where long battery life is essential.

In the project Audience, such a sound acquisition system is realized based on a dedicated low-power ASIC and a commercial neural network processor for sound analysis and keyword recognition. The goal is to integrate all components together with a passive microphone in a system-in-package, allowing this “smart microphone” solution to be realized in a volume of only 10x10x4 mm<sup>3</sup>.

### UC-MORE—Ultra-Compact Multispectral Snapshot Camera Based on Optical Resonant Nanostructures

Imaging at multiple wavelength ranges has proven useful in numerous applications in very diverse areas, such as agriculture and geology, environmental imaging and meteorology, and astronomy. Advances in low-cost miniaturized multispectral cameras would help to integrate this technology—for example, into smartphones—and thus allow consumer markets such as well-being and cosmetics, or food analysis, to be addressed.

The use of novel nanostructured optical filters with characteristic angular transmission properties allows a more compact design of hyperspectral cameras. Simulations show that software

algorithms will be able to extract the encoded spatial and spectral information with satisfactory resolution.

## Technology MIPs

### ROBIN—Robust Battery Monitoring

Advances in reliable storage solutions for electrical energy are key for the transformation of the global energy landscape toward renewable sources. Driven by the electric vehicle market, the energy density of Li ion batteries has increased substantially over the years. More recently, other aspects such as battery management solutions (BMSs) have gained in importance.

The project ROBIN aims at optimizing electrochemical impedance spectroscopy (EIS) sensing for an improved BMS. In a first evaluation, a measurement precision better than 1% has been achieved. The use of powerline communication for data transmission and cell synchronization allows the necessary wiring to be minimized. A demonstrator featuring the above innovations is expected in summer 2021.

### YOU-ON-CHIP—Automated in vitro 3D Systems and Diagnostics

Organoid and organ-on-chip (OOC) systems allow the simulation of cell complexes and entire organs, opening up new possibilities for studying human physiology in in-vitro models well beyond the capabilities of lab-on-a-chip fluidic systems. Great hope is placed on this technology eventually replacing animal tests in drug development and toxin testing.

This project further develops the “YOU-ON-CHIP™” platform for the automated maintenance and monitoring of biological entities, hopefully in the future helping to reduce time-consuming and contamination-prone interventions by lab personnel.

### CHAMELEON—Compliant Mechanism with Embedded Sensing

Additive Manufacturing (AM) has introduced unprecedented design flexibility into the production process, in particular where tool-less and small-series production are important. The integration of functional elements, such as sensors and actuators, will further contribute to the potential of AM technologies in flexible and resource-efficient manufacturing.

The project CHAMELEON aims at developing the technologies required for fabricating metal-based 3D parts with embedded functionalities. Novel design concepts and the use of advanced printing technologies have allowed us to demonstrate the integration of well-performing sensing elements and electrical connectivity in a high-precision flextec-based translation stage. This technology is particularly interesting for applications in preventive maintenance.

### SILOSCAPE20—Flexure-based Escapements for Mechanical Watches

The precise structuration of silicon, on scales from micrometers (MEMS) up to centimeters (MacroMEMS), with techniques such as deep reactive ion etching (DRIE) has allowed the development of mechanical parts with novel properties. Flexure-based watch parts in particular benefit from the excellent elastic

behavior of silicon as well as from its amagnetic and corrosion free nature.

The project series SILOSCAPE has the objective to design, produce, and characterize silicon-based oscillators and escapements. In this way, development risks can be lowered prior to proposing the technology to our partners from the Swiss watch industry. Recent developments include innovative escapements with improved power reserve and precision.

# AUDIENCE—An Ultra-low-power and Smart Sound Acquisition System for IoT Applications

S. Devise, G. Yilmaz, M. Crettaz, V. Schaffter, P.-A. Beuchat, K. Badami, B. Putter, R. Catteneoz, P. Pad, P. Nussbaum, S. Emery

The project Audience aims to build an ultra-low-power sound acquisition system in a small system-in-package (SiP). The platform will be utilized for keyword spotting and speaker identification in mobile and IoT applications where power, processing resources and footprint are extremely limited. An integrated circuit (ASIC) comprising a low noise audio amplifier, a 16-bit Sigma Delta ADC is developed together with new algorithms running on a neural network processor. In parallel, a passive microphone is developed and integrated in a complete system meant to acquire sounds and other physiological signals for medical applications.

The main challenges faced while designing mobile autonomous IoT product are (a) keeping power consumption as low as possible to extend battery life and (b) to reach high level of integration for an easier and cost-effective integration in the system. Audience addresses these goals specifically for ultra-low-power sound acquisition systems and demonstrates it with two applications. The first one, a smart microphone, is designed for device activation by the voice by detecting keywords. The second, a wearable patch, will acquire multiple body sounds together with physiological signals (ECG).

The main building blocks that will be developed are a passive microphone and an ultra-low-power front-end ASIC while a commercial neural network (NN) processor will be configured.

The passive microphone is fabricated with a thin film piezoelectric material (PVDF). The mono oriented PVDF film has been curved along its poling direction and clamped from both non-curved ends to a rigid frame. This approach [1] provides a mechanical amplification as a function of the radius of curvature. The piezoelectric sensor can be modelled as a lossy capacitance in series with this voltage source. Practical value of this capacitance is lower than 100 pF, necessitating an analogue front-end capable of working with high source impedance.

The smart microphone relies on an ultra-low-power audio front-end ASIC designed in 22 nm CMOS (Figure 1).

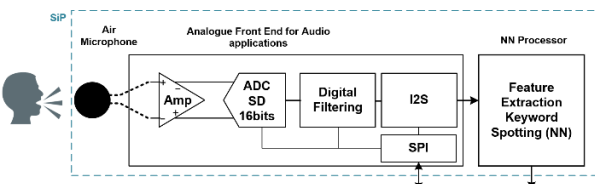


Figure 1: Smart microphone block diagram.

The input analogue stage consists of a buffer with a high input impedance and a low-noise amplifier with programmable gain that can be interfaced with high impedance passive microphones as well as COTS analogue microphones. The amplified signal is then digitized with a third order  $\Sigma\Delta$  modulator (block diagram in Figure 2) employing state of the art techniques such as mixing continuous time and discrete time integrators with switched capacitor degenerated integrator [2, 3], two FIR filters in the loopback [4] and chopping to reach the 16 bit resolution while keeping the power budget within 400  $\mu$ W for an input signal with

24 kHz bandwidth. The  $\Sigma\Delta$  modulator output is then filtered and decimated to remove the out-of-band noise and finally transmitted to the external speech processor through I2S or PDM.

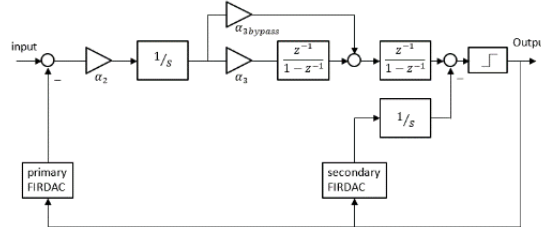


Figure 2: 16-bit third order Sigma Delta Modulator.

The first application that will be developed is a smart microphone that will showcase the performance of a system dedicated to keyword spotting. The algorithms to detect keywords will be implemented on an external NN processor. In addition, a feasibility study to build a microphone in a System in Package (SiP) is also undertaken. The envisioned SiP is shown in Figure 3 where the microphone, the ASIC and the NN processor are embedded in a 10x10x4 mm<sup>3</sup> casing.

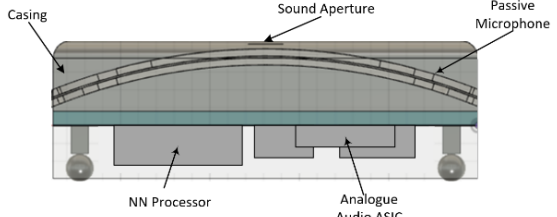


Figure 3: System in Package design.

The second system that will be developed is a wearable patch capable of measuring 1-lead ECG (in accordance with IEC 60601-2-47) with CSEM's proprietary dry electrode technology (EP2101408) and acquiring thoracic sounds as well as ambient sounds. Thoracic sounds are acquired via a contact microphone, while ambient sounds are captured with a capacitive MEMS microphone. Thanks to its semi-flexible structure, the device can conform to the curved surfaces of the body. The patch features a BLE SoC for instant visualization of the acquired vital signs. Although the device is designed for infants, its use cases can easily be extended for adults, particularly for monitoring progressive respiratory diseases, such as COPD, under real-life conditions of patients.

[1] H. Naono, et. al., "Design of an Electro-Acoustic Transducer Using Piezoelectric Polymer Film", presented at the Audio Engineering Society Convention 58, Nov. 1977, Accessed: Jun. 29, 2020.

[2] B.M. Putter, "SD ADC with Finite Impulse Response Feedback DAC", in International Solid-State Circuit Conference proceedings, San Francisco (2004).

[3] K. Badami, et. al., "A switched-capacitor degenerated, scalable gm-C filter for acoustic front-ends," in IEEE International Symposium on Circuits and Systems (ISCAS), Montreal (2016).

[4] S. Pavan, "Finite-Impulse-Response (FIR) Feedback in Continuous-Time Delta-Sigma Converters", in CICC proceedings, San Diego (2018).

# UC-MORE—Ultra-compact Multispectral Snapshot Camera based on Optical Resonant Nanostructures

C. Gimkiewicz, S. A. Bigdeli, C. Schneider, L. A. Dunbar, R. Ferrini, B. Gallinet

A multispectral camera with a form factor of less than 3 mm thickness is reported. It is ideal for integration in a smartphone and it gives a strong improvement in color reproduction. The knowledge of the object spectrum also opens up further applications, such as food analysis.

Multispectral cameras are able to capture an image of a scene with a high number of spectral channels, which makes them highly attractive for accurate color rendering in smartphone cameras. However, current multispectral cameras are limited by their physical size and the cost of components. Here, we present a design of multispectral snapshot camera with a small form factor and a thickness of < 3 mm, which is ideal for integration into a smartphone [1]. Our design uses standard imaging optics and image sensor, with nanostructured filters and a microlens array inserted in the optical path creating a negligible additional thickness in the optical stack.

Figure 1 shows the working principle of the multispectral camera. The light-field emanating from an object point is imaged onto a microlens array. A filter whose transmission spectrum depends on the incidence angle is placed between the imaging optics and the microlens array. After transmission through the filter, the light angular distribution is associated to a spectral distribution. The purpose of the microlens array is to image light transmitted by the filter onto the image sensor. As a result, the light spectral distribution is imaged under each microlens. The signal in the image sensor under all microlenses of the array can be reconstructed to form a multispectral image.

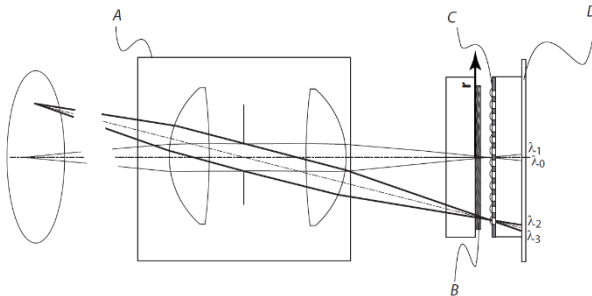


Figure 1: Multispectral imaging optics based on imaging optics (A), nanostructured filters with angle-dependent transmission (B), microlens array (C) and an image sensor (D).

The nanostructured filter is based on a hybrid dielectric-metallic periodic nanostructure, sketched in Figure 2a [2]. Incident light is coupled and propagating in the hybrid waveguide, yielding a peak at resonance wavelength as shown by the simulations of Figure 2b. A cladding of low refractive index ensures minimal optical losses from the metallic layer during propagation in the core. Due to the grating and waveguide dispersion, the resonance wavelength strongly varies with the incidence angle, as shown in Figure 2b. Another essential component of the multispectral camera is the microlens array (Figure 2c).

[1] Patent pending

It originated by photolithography and reflow and replicated by UV imprint lithography on a substrate with absorbing microapertures.

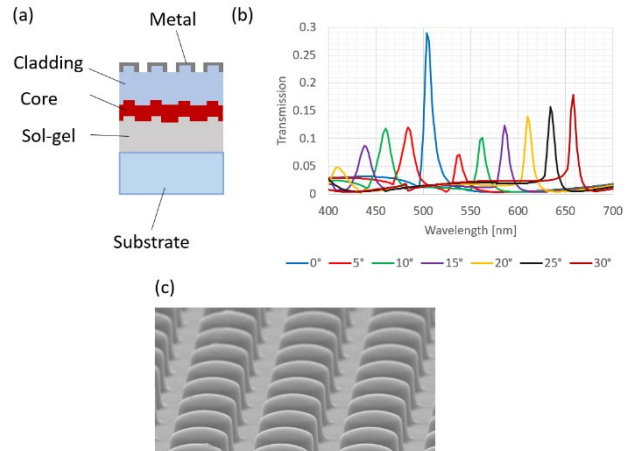


Figure 2: Optical components of the multispectral camera. a) Schematic cross section of the nanostructured filter. b) Transmission spectrum as function of the incidence angle. c) Scanning electron micrograph of fabricated microlenses.

The response of the full optical system is computed by ray tracing coupled with electromagnetic simulation of the grating transmission (Figure 3). In this example, a homogeneous monochromatic image is used as input for simulations. At different wavelengths, the image under each individual microlens is different, due to the nanostructured filter dispersion. The knowledge of individual patterns as a function of the wavelength will be used in the reconstruction of multispectral images.

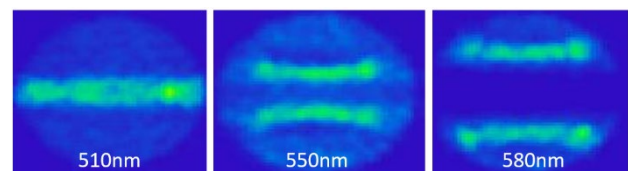


Figure 3: Simulated image under a single microlens at different wavelengths, showing the effect of grating dispersion.

In summary, a compact light-field multispectral camera has been presented, based on nanostructured filters and a microlens array. Preliminary simulation results show its ability to reconstruct a multispectral image. Next steps of the development include the integration and characterization of a full prototype, as well as optimization of the spatial and spectral resolution for accurate color reconstruction.

[2] G. Quaranta, C. Schneider, B. Gallinet, "Hybrid plasmonic-dielectric resonant waveguide grating for wavelength-selective diffraction", SPIE Conf. Proc., 11289, 112890U (2020).

# ROBIN—Robust Battery Monitoring

C. Brivio, E. Namor, D. Piguet, E. Le Roux, O. Vorobiov

CSEM is developing its own platform for a smarter Battery Management Systems (BMS) by moving intelligent processes at the cell level and realizing the so-called Cell Management Systems (CMS). MIP ROBIN proposes to improve the battery cell-based monitoring solution by optimizing the use of electrochemical impedance spectroscopy (EIS) sensing and by demonstrating the relevance of powerline communication (PLC) for data transmission between the cell management units.

ROBIN MIP contributes to lay the basis for the next generation of battery management solutions. In recent years, the industry of batteries was characterized by an average price reduction at pack level of 89% in 10 years (from 1'100 \$/kWh in 2010 down to 137 \$/kWh in 2021<sup>[1]</sup>). While this evolution was driven by improved cell design and materials, the optimization of other components – like for instance the Battery Management System (BMS) – is only now gaining importance.

MIP project ROBIN is the result of the joined forces between div-V and div-M and it is the continuation of Innosuisse feasibility project BATMAN (also mentioned in the present STR). It is characterized by the following overarching objectives:

- Proving PLC is a viable solution to transmit traditional BMS sensed quantities (voltages, currents, temperatures) and newly sensed quantities (impedances).
- Optimising EIS sensing capabilities and designing life-enhancing battery management logic based on that.
- Realising a 24 V battery module based on fully fledged CMSs featuring PLC and EIS. The resulting prototype will be an evolution of the one developed during project BATMAN (Figure 2).

Project is due to finish in 2021. Nonetheless some promising results have been already achieved in 2020.

As regards of the first point, the ROBIN project evaluates the feasibility of using the power lines that interconnect the cells to transmit data for two main reasons: (i) allowing communication and synchronization between the CMSs, which is essential to ensure a coordinated management of the cells; (ii) minimizing the impact of additional wiring. A key aspect is how the communication signal is injected on the power line while keeping the electrical isolation with the CMS electronics. The solution proposed by ROBIN is electro-magnetic coupling with Rogovski coils (Figure 1). The transceiver is a Yamar DCB1M and a robust CSMA/CA protocol with priority arbitration, which has been developed to ensure a timely delivery of the messages with real-time constraints and to provide accurate 1 ms synchronization to support simultaneous actions on the cells.

As regards of the second point, ROBIN introduces the integration and exploitation of impedance measurements in BMSs. In the first part of the project, a measurement campaign to evaluate the performance of the EIS acquisition developed within project BATMAN has been carried out. A measurement precision below 1% has been observed within the frequency range of interest (10 mHz–1 kHz) and the effectiveness of such measures to evaluate cell temperature and state of health is being evaluated.

In the second part of the project, algorithms to modulate the usage of each cell in a module based upon this information will be tested, and resulting advantages quantified.

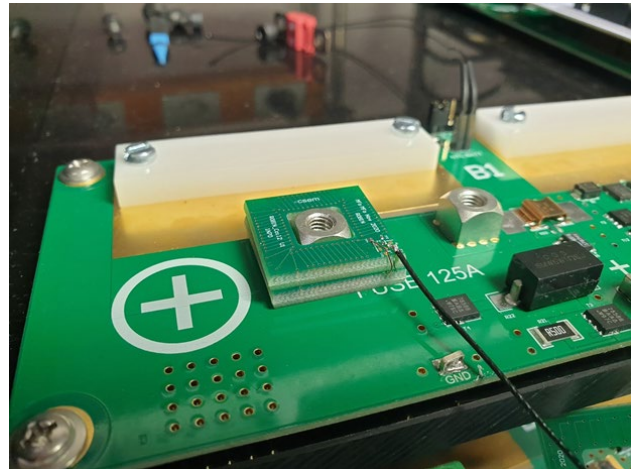


Figure 1: Rogovski coil designed according to CMS specification.

As regards of the third point, most of the prototyping work is forecasted to take place in the first semester of 2021. The promising results obtained on both sides of EIS and PLC will allow to proceed in the development of the new generation of CMS boards. The CMS will be miniaturized both in term of electronics components and overall assembly. The wireless solution (namely PLC) will be integrated, wiring harness eliminated, and low-power processor options investigated. The final prototype will be assembled and tested with real-life cycle scenario (e.g. dynamic discharge profiles for BEV as per IEC 62660-1) to assess its performances in implementing the new BMS balancing logic and exchanging EIS data through PLC.

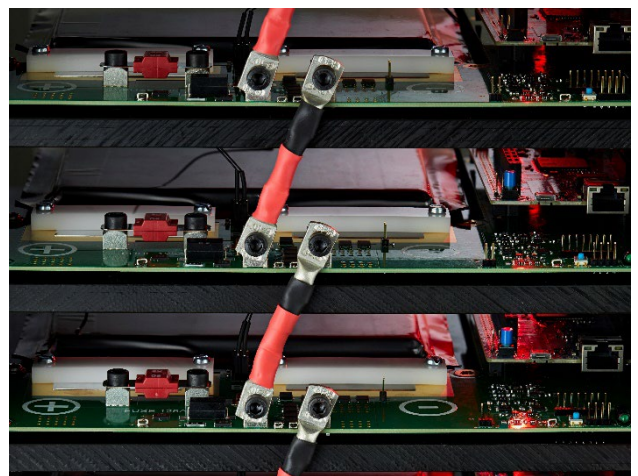


Figure 2: CMS 24 V prototype under development at CSEM.

<sup>[1]</sup> Bloomberg New Energy Finance (BNEF), December 16, 2020.

# YOU-ON-CHIP—Automated in vitro 3D Systems and Diagnostics

S. Heub, S. F. Graf, F. Kurth, N. Glaser, M. Zinggeler, S. Boder-Pasche, N. Baladari, N. Schmid, T. Volden, E. Györvary, S. Paoletti, V. Revol, G. Weder

Personalized medicine is driving the development of organ-on-chip and organoid systems for drug discovery, diagnostics, and therapy planning. Following these trends, CSEM has started the development of the technology platform YOU-ON-CHIP™ aiming at automating organ-on-chip maintenance, differentiation, sampling, and monitoring. New solutions are indeed needed to meet the requirements and regulatory issues of the life science industry in terms of standardization and parallelization. The project YOU-ON-CHIP™ is providing smart lid solutions for the maintenance and biomonitoring of biological tissues grown in the internationally recognized microwell plate standard.

Microwell plates containing between 6 and 1536 individual reaction wells have become a standardized platform in analytical research and clinical diagnostic laboratories including handling by robots. This international standard is increasingly adopted by organoid production and organ-on-chip testing platforms. Within the research activities of organ-on-chip systems, CSEM has established a roadmap towards tools for drug screening and diagnostics (Figure 1).



Figure 1: CSEM roadmap on organ-on-chip technology for drug testing and diagnostics applications.

The production and testing of in vitro organoid and/or organ-on-chip systems rely on highly parallelized and automated approaches for high throughput drug screening. These microwell plate-based processes typically involve a base plate and a lid. The common denominators remain continuous maintenance (tissue perfusion) and monitoring (biosensing).

In this context, the research project YOU-ON-CHIP™ aims at providing intelligent lids that are compatible with most existing base-plate solutions. This unique concept combines automated maintenance, regular readout using electrochemical sensors and sampling for offline analysis on demand.

The YOU-ON-CHIP™ concept is a combination of two lids (Figure 2) that are compatible with the standard 24-microwell plate format. The development is driven to be compliant with standard practices in cell culture. The compact units must typically guarantee sterility and environmental conditions (temperature, humidity, gas) to maintain and monitor the organ-on-chip and organoid systems for several weeks.

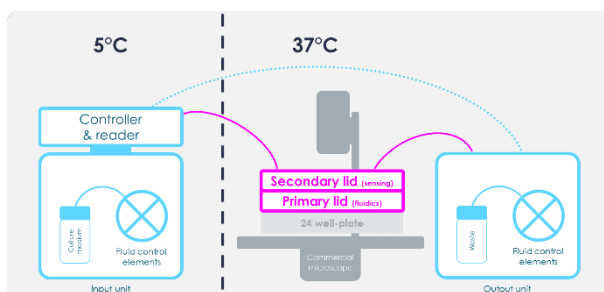


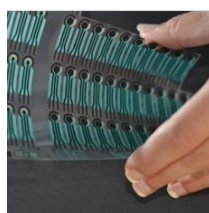
Figure 2: The YOU-ON-CHIP platform consists of two smart lids that enable the automated maintenance and analysis of biological models on a standard microwell plate format for several weeks.

Microfluidic channels integrated in the primary lid (Figure 3) enable automated and programmable medium exchange to ensure a periodic supply of fresh nutrients and oxygen to the biological tissues within the plate over several weeks. The lid is composed of a single liquid inlet and one outlet to control 24 liquid channels in parallel. A prototype system has been successfully tested with 2D cell culture. The next step is the development of a disposable lid to be validated using 3D human cell models over several weeks.



Figure 3: Testing of the primary lid prototype for automated maintenance of 2D cell culture in a 24-microwell plate. The system is validated on an inverted microscope inside an incubator (37°C, 5% carbon dioxide, high humidity) to monitor cell morphology.

The secondary lid will integrate microfluidic features enabling sampling of a small volume (microliter range) for biomonitoring. CSEM is developing glucose sensing technologies based on electrochemical sensors. They are disposable, automatically calibrated and show stable performances from 0 to 5 mM (Figure 4). CSEM is further combining the glucose sensing technology together with the intelligent lid concept to enable parallelized and robust glucose monitoring of organ-on-chip and organoid systems.



Dynamic range	0 - 5 mM
Linear range	0 - 2.5 mM
Limit of detection (LOD)	0.2 - 0.3 mM
Limit of quantification (LOQ)	0.5 mM

Figure 4: The glucose enzymatic sensors have been optimized for improved performances in fully supplemented culture medium.

With YOU-ON-CHIP™, CSEM will deliver a new set of tools for organ-on-chip and organoid platforms. They will be tested by various CSEM Swiss academic and industrial partners. The smart lids will be easily adaptable to different cell culture platforms.

# CHAMELEON—Compliant Mechanism with Embedded Sensing

S. Lani, N. Hendricks, S. Zabihzadeh, G. Perruchoud, L. Kiener, F. Cosandier, N. Marjanovic, J. Disser

Structural health monitoring for preventive maintenance, control feed-back of moveable mechanisms, integrated actuation and adaptive objects necessitate a heterogeneous integration of numerous technologies. To bring Additive Manufacturing (AM) beyond state-of-the-art technologies of topology optimization, it is important to develop concepts and technologies allowing such functionalities while keeping the versatility and flexibility advantages of AM. Hence, CHAMELEON aims at developing technologies to manufacture metal-based 3D parts with embedded functionalities such as compliant mechanisms, electrical/pneumatic feedthroughs, sensors, and actuators by combining advanced design, ink-jet printing (IJP), AerosolJet Printing (AJP), polymer casting, Laser Powder Bed Fusion (L-PBF), and surface post treatment. The main applications will focus on markets already using AM in production (space, aeronautic, and medical) that are requesting additional functionalities.

AM is taking more and more importance for producing high-end components in applications like space, aeronautics, and medical fields. Such industries have critical needs for which AM has appealing features. Among them, they benefit from a manufacturing technology able to produce components with complex geometries that are suitable for moderate production volume as well as weight reduction thanks to topology optimization. However, most of today's applications, for which AM is used, is for manufacturing "passive" elements with no functionality except providing a mechanical structure. To grow the market attractiveness of AM, it is important to develop technologies to bring new functionalities while keeping the advantages of flexibility and versatility of AM. Hence, CSEM is investigating the opportunity to combine 3D printing with 2D printing to obtain 3D compliant mechanisms with embedded sensors in order to elaborate complex AM -based Mechatronics devices.

The technology milestones that have been demonstrated so far:

- Low stress and high precision stainless steel 17-4PH Laser Powder Bed Fusion (L-PBF) manufacturing with high fatigue resistance to manufacture flexure blades down to 0.1 mm and with a 45° angle. During this manufacturing phase, electrical wiring through the structure is also fabricated.
- Advanced surface polishing of the LPBF structures down to 100 nm Ra to be compatible with sensor printing.
- 2D printing (InkJet or AerosolJet Printing) of an insulation and a conductive layer to form the strain sensor. Sensor performances are currently: gauge factor (sensitivity) superior than 2 (equivalent to or better than a commercial thin film metal strain gauge), linearity better than 99.9% and yield of 100%. R variation within a fabrication batch is in the range of +/- 15%, opening the way to produce thermally compensated strain gauges by the mean of a Wheatstone bridge.

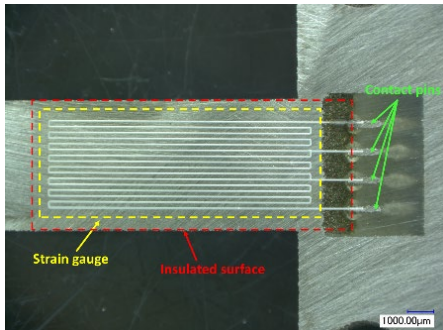


Figure 1: Printed insulation and strain gauge by AerosolJet Printing on a 300  $\mu\text{m}$ -thick flexure element.

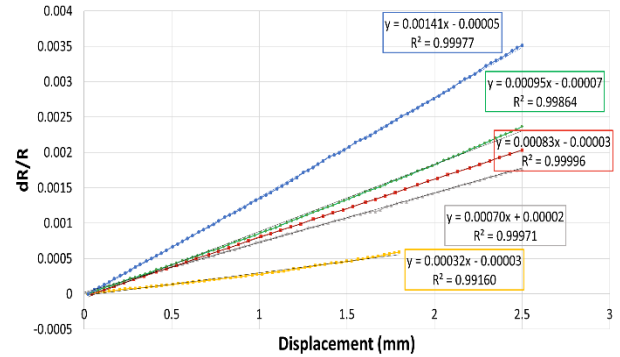


Figure 2: Performance of strain gauges from AerosolJet Printing for difference printing and/or curing conditions.

A first demonstrator has been fabricated and consists of a  $\pm 5$  mm-stroke XY stage with a laser mounted on the output platform. The high precision linear motion is achieved by integrating 300  $\mu\text{m}$ -thick flexure elements, including built-in electrical wires, to supply the laser source and to provide an interface for the printed strain sensors. The total structure will represent a volume of about 80x50x80  $\text{mm}^3$ . The actuation of the demonstrator is ensured by servo motors. The sensor integration is currently in progress.

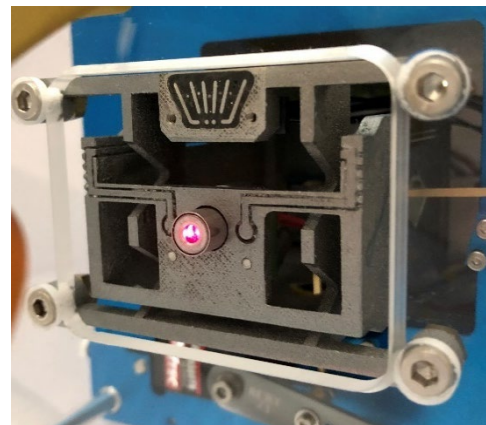


Figure 3: 3D printed XY-stage with embedded sensor and external actuator. A laser pointer is integrated to the moving platform to illustrate the capacity of the demonstrator to power a device through flexure blades.

Additionally, a new material has been developed by L-PBF that present a low CTE (<1 ppm) and consists of a FeNi alloy (INVAR).

This work is supported by the state of Neuchâtel and the state of Basel Land.

# SILOSCAPE—Flexure-based Escapements for Mechanical Watches

F. Barrot, G. Musy, O. Laesser\*, R. Winiger\*, F. Cosandier, L. Giriens, E. Dominé, Y. Petremand, M. Amine, S. Ischer, F. Rigoletti

Combining its expertise in the domains of micro-manufacturing techniques and precision mechanisms, CSEM has been a pioneer in the design and production of centimeter scale silicon parts featuring fine mechanical functions, opening up new opportunities for the design and production of novel and innovative watch mechanisms. In the frame of the SILOSCAPE MIP, CSEM is focusing on the design and production of novel high-performance watch oscillators and escapements.

Silicon is an interesting material for the design of precise mechanical parts such as the ones encountered in watch mechanisms: it is amagnetic, corrosion free, and characterized by an ideal elastic behavior, a high fracture strength and a low density. Using microfabrication techniques inherited from the microelectronic industry (DRIE), it can be batch processed with a micrometric precision for the production of large quantities of centimeter scale mechanical parts that can comprise several levels with fine mechanical functions such as flexure blades. Thanks to all these interesting properties, Silicon offers new opportunities for the design and production of novel and innovative watch mechanisms. In the late 90's CSEM was a precursor in this field [1], paving the way for a new trend that is now followed by several key players in the Swiss watch industry. Since then, CSEM has kept carrying on its pioneering work by pushing back the frontiers of the micromechanical structuration of silicon and by improving its mastery of the production of such delicate parts [2,3].

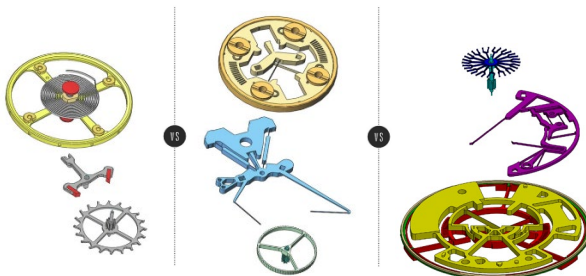


Figure 1: The Swiss anchor escapement (left), The Genequand escapement (middle), the Siloscape escapement (right).

The oscillator and the escapement, are the most delicate and high added-value technical parts of a mechanical watch; for the past ten years, CSEM has proposed several original designs of mechanical watch oscillators [4] and, in a close partnership with Vaucher Manufacture Fleurier, integrated at the watch level, the very original FlexTech and Silicon based Genequand [5] escapement, the first flexure based watch regulator (escapement + oscillator) ever designed and implemented at the watch scale. With the use of silicon as a base material for the design of a watch regulator, the conventional ruby pivots can be replaced by

flexure blade pivots, allowing a very precise and frictionless oscillations of the guided components.



Figure 2: The Siloscape escapement integrated in a watch (left) and its latest updated design (right).

The Siloscape escapement [6], the latest escapement invented at CSEM, is also FlexTech based and paired with a Wittrick oscillator. This innovative escapement is characterized by a power reserve three times better than a conventional system, a good precision performance and is auto-starting by nature, which means that a large accidental shock cannot stop it. Besides, unlike the Swiss anchor and the Genequand escapements, the anchor of the Siloscape escapement is not made of a single part: the impulse planes are implemented on the oscillator itself, while the resting planes are implemented on two detents integrated together in a specific monolithic part which also plays a second function by allowing a fine tuning of the system's isochronism.

Pursuing its pioneering role, CSEM is now working on the design of two novel escapements adapted to flexure-based oscillators and targeting a very precise time keeping (typ. +/- 2s/d) rather than a large increase of the power reserve. The first escapement concept under investigation at CSEM aims at keeping the oscillator amplitude as constant as possible during operation to improve the time keeping precision of the watch. The second escapement concept under investigation at CSEM aims at simplicity and precise time keeping when paired with a flexure based oscillator such as the CR4 [4] oscillator. With these two novel escapements, a regular power reserve is targeted, the goal being to address a market segment complementary to the ones targeted by the Genequand and the Siloscape escapement.

• External key contributors: "Olivier Laesser" and "Winiger Horloger"

[1] A. Perret, "Le silicium comme matériau dans la fabrication de pièces mécaniques", SSC, 2001.

[2] O. Dubochet, et al., "L'hybridation du silicium : vers une simplification de l'intégration de composants silicium dans les mouvements horlogers", SSC, 2015.

[3] M. Despont, et al., "Tic-Tac" made in Silicon", SSC, 2019.

[4] F. Barrot, et al., "SILSOCAPE—Flexure based oscillators for mechanical watches", CSEM Scientific and Technical Report (2018) 19.

[5] F. Barrot, et al., "Un nouveau régulateur mécanique pour une réserve de marche exceptionnelle", SSC, 2014.

[6] F. Barrot, et al., "SILSOCAPE—a novel silicon-based flextech watch escapement", CSEM Scientific and Technical Report (2019) 20.

# MICROSYSTEMS

Michel Despont

The use of microsystem technology continues to grow, fueled by the need for ever-smaller, lower-power, smart devices. Integration of different technologies and miniaturization are at the heart of CSEM, and its Microsystems program aims to bring innovation through the development of new micro-manufacturing technologies, the use of MEMS technology, and the introduction of advanced packaging concepts.

The microsystems market, according to different studies, enjoys a healthy 13–14% CAGR and is approaching a market size of 15 billion dollars. Microsystems are used almost everywhere in devices that sense and monitor our environment and control actions in our daily lives. As an example, today's cars can make use of dozens of integrated sensors and actuators for monitoring and controlling engine functions as well as for safety, navigation, and passenger comfort. Similar trends can be seen in portable devices such as smartphones, with a dozen sensors incorporated into the most recent models. Moreover, global technology trends, including the Internet of Things (IoT), Smart City, Industry 4.0, or personalised medicine, require a massive use of connected sensors and promise large new markets for ultra-miniaturized microsystems for applications in, for example, building automation, healthcare and life sciences, consumer and home automation, transportation, industrial and environment monitoring security, and retail and logistics. All of these applications are looking for autonomous, low-power, small-form-factor, and low-cost sensor and actuator devices.

A large part of the microsystems market is taken by multinational companies such as ST Microelectronics, Bosch, or Texas Instruments, targeting mainly the consumer and automotive markets and exerting strong efforts in process standardization in order to cope with the permanent cost pressure of such applications. Beyond these mass markets, a large fraction of sensors and actuators are fabricated in moderate volumes for specialty, high added value markets. The fabrication of these moderate volumes of microsystem devices requires customization and necessitates the significant know-how of multiple disciplines, such as process technology, packaging, material science, and reliability. Hence, although the fabless model may be gaining some momentum, providers of MEMS-based microsystems are mostly relying on the Integrated Device Manufacturing (IDM) model, and use their own, dedicated manufacturing facilities.

Swiss industry, and in particular its SMEs, has recognized the potential of developing specialty microsystem-based products as a strong differentiator and is present in many niche markets, successfully competing on a global level. For SMEs in particular, it is crucial to fill the pipeline of innovation from fundamental research to the industrialization of new technologies in order to be able to continue to offer innovative products. CSEM has a track record in bringing microsystems technologies to the market, and is uniquely positioned to be an essential partner in bringing ideas to market for many Swiss high-tech SMEs active in the domain of highly miniaturized microsystems. Moreover, CSEM is looking at cross-disciplinary solutions—benefiting from nanotechnology, bioscience, and material science—in order to deliver innovations in MEMS and enable new microsystems.

MEMS play a major role in the Microsystems program, and this role will be supported by increased efforts to develop advanced manufacturing and integration technologies. Recent advances in digital manufacturing, meanwhile, open new opportunities to create and optimize MEMS devices and microsystems. CSEM strongly believes that “traditional” MEMS technologies will be augmented by these new manufacturing technologies to provide new functionalities and deliver the versatility required for fast market introduction. Packaging, meanwhile, no longer serves mainly as a “device protection” and increasingly integrates added features. These include an interface to the outside world (optical paths, electrical leads, actuators ...), environmental compatibility (biocompatibility, withstanding high temperatures, etc.), or built-in sensors or quality monitoring features (antennas, pressure sensitive surfaces, etc.). This makes the border between the package and the device fuzzier. Hence, it is essential to elaborate a common strategy with regard to developing—under one roof—new processes, new devices, and new packaging that will enable the creation of novel microsystems. With its Microsystems program, CSEM aims to create an environment that is adapted to the new challenges of microsystems and that benefits Swiss industry.

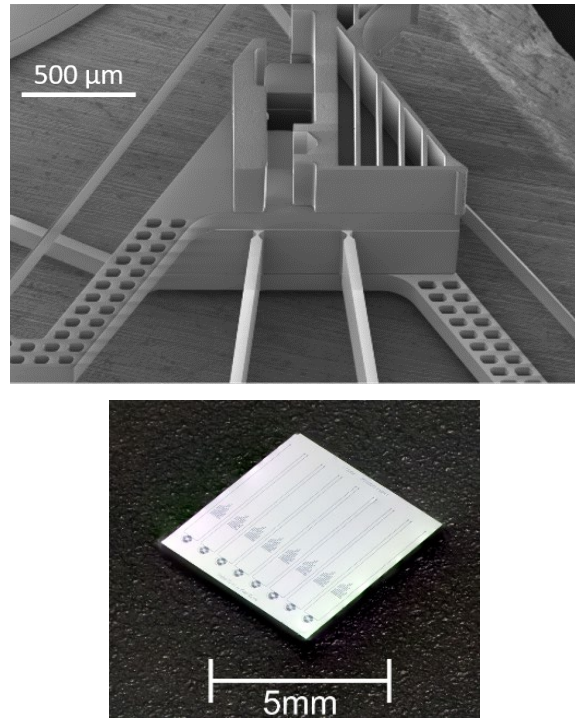


Figure 1: (top) Multi-level silicon component; (bottom) Photonics-MEMS test chip with an array of ring resonators as a building block of a new class of high-sensitivity miniaturized temperature sensors.

Looking back over recent years, the Microsystems program has seen significant progress related to the development of micro-components for mechanical watches and integrated optoelectronic devices. Although those topics are of great importance to Swiss industry, the technology spectrum being developed within the program must address a broader range of applications. The program has, therefore, over the last few years, incorporated several new initiatives in order to diversify into new application fields, including instrumentation, aerospace, and

medical devices, all of which are important markets for Swiss industry.

Hence, at CSEM, the microsystems strategy is oriented along several lines of action, encompassing design, microfabrication, and packaging technologies. They are:

- 1) Innovation for mechanical watches, at the crossover point of high-performance materials, advanced manufacturing, and innovative designs.
- 2) Excel in microsystem technology for harsh environments, for a broad range of applications ranging from medical to aerospace.
- 3) Develop key technologies in the field of infrared sensing and imaging.
- 4) Enhance the technology portfolio in photonics-MEMS and optoelectronic device assembly.
- 5) Life-interacting microsystems for applications in medtech and engineered environments for biological models.

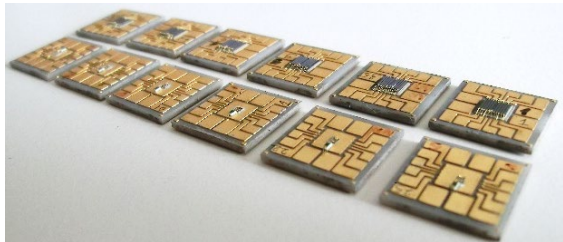


Figure 2: (top) Silicon and GaN samples after bonding with silver sinter on a test substrate for heat dissipation testing; (bottom) cost-effective hybrid opto-mechanical sensor.

### Long-term objectives

The global objective of the Microsystems program is to establish MEMS devices, advanced micro-manufacturing, and packaging technologies for CSEM's partners and to offer to Swiss and international industries a full product-development platform from feasibility demonstration of new device ideas to industrialized, qualified fabrication processes including the production of MEMS in small volumes. Therefore, the activities of this program are aimed at continuing to excel and to build up new competences in microsystems technology—in particular for application fields such as watch technologies, scientific instrumentation, optoelectronics, and medical device technology—with a strong focus on packaging, reliability, and cost reduction for demanding applications.

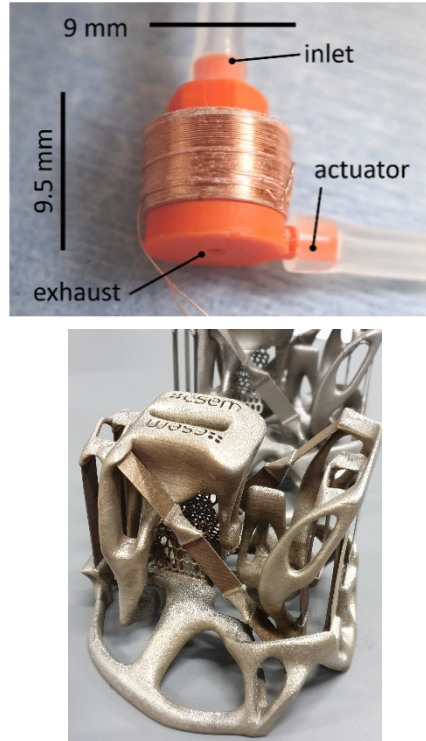


Figure 2: (top) 3D-printed pneumatic electromagnetic microvalve for haptic application; (bottom) 3D-printed translation to rotation mechanisms made in INVAR-36.

The Microsystems program strategy has been organized into three activities—namely, (1) **MEMS Devices**, (2) **Functional Packaging**, and (3) **Advanced Micro-Manufacturing**.

The **MEMS Devices** activity deals with the development and industrialization of specific MEMS in a wide spectrum of applications. The global objective of this activity is to maintain a state-of-the-art platform capable of developing and fabricating reliable MEMS products, from prototypes to small volume production or for technology transfer. This platform, at the service of Swiss SMEs and industries, consists of a fully equipped MEMS fabrication clean room, a reliability laboratory, and an R&D infrastructure focusing on the pursuit of advanced and novel MEMS-based devices. Today, development is underway in the fields of watches and timekeeping, instrumentation and aerospace, and health, biotech, and lifestyle. These are domains in which Swiss industry is highly successful at the global level and that have a large impact on the Swiss economy.

For industrial applications, reliability is of the utmost importance and CSEM's reliability and microstructure characterization capabilities are a powerful tool for supporting process development aiming at eliminating defect- and stress-generated failure modes and performance limitations. The continuous improvement and systematic documentation of development and production process flows within ISO-9001 ensures the successful exploitation of the technology platforms developed. This enables a systematic approach to MEMS development, from feasibility demonstration, via prototyping, to industrialization.

The **Functional Packaging** activity focuses on (i) the development of new integration platforms for CSEM's customers, and (ii) the realization of new products based on these platforms. The chosen approach allows CSEM to serve a large number of customers in different application fields and markets. The

activity's primary objectives are the integration of active MEMS devices, sensors, and actuators into prototype systems and products for different applications and markets. The activity addresses today's global packaging challenges in sensor platforms for medical and environmental monitoring, the integration of measurement solutions for harsh environments, and optoelectronics. The integration of microsystems continues to be a key element of many future high-technology application areas. Hybrid integration technologies—from embedded silicon in polymer to M(O)EMS—find broad uses in markets such as healthcare and energy. Combined with hermetic sealing and embedded self-testing, they open up additional applications for sensors in harsh environments, including in the medical field. In addition, miniaturization in optoelectronics continues to be an innovation driver, from devices to architecture.

The goal of the **Advanced Micro-Manufacturing** activity is to answer the need of Swiss industry to fabricate small-dimension components (typically  $<1\text{ cm}^3$ ) that can take advantage of a 3D aspect and that would not be achievable using existing technology such as clean room microfabrication (MEMS and CMOS). The envisaged solution is to develop a new combination of manufacturing technologies to improve the performance of microsystems. The core technology is based on additive manufacturing (AM), a worldwide “big trend” linked to digitalization, the IoT, and Industry 4.0. This technology brings with it more flexibility and can increase the complexity of systems. It is, however, still lacking with regard to user confidence, and still needs to be developed in order to achieve the small dimensions and structure quality required for its use in microsystems. The combination of its skill sets in material, microfabrication, surface engineering, and characterization is allowing CSEM to tackle the challenge of combining different technologies and of making these new manufacturing techniques available to Swiss industry. Hence, CSEM's attention is focused on two points: (1) the process optimization of 3D printing for the fabrication of small structures made of functional materials, and (2) heterogeneous integration of 3D printing with other microfabrication technologies (in particular with MEMS).

Needless to say, the Microsystems program will continue to work closely with the other CSEM programs (Surface Engineering, Ultra-Low-Power Microelectronics, Systems, and Photovoltaics & Energy Management) to create unique solutions for our industries. One of the major USPs of CSEM, we will continue to cultivate this multidisciplinary approach to answer the needs of our customers.

## Highlights

Lithium niobate on insulator (LNOI) is one of the most promising emerging platforms for photonics integrated circuits (PICs), and comprises a unique set of interesting optical properties: a high electrooptic coefficient, high intrinsic 2nd and 3rd order nonlinearities, and a large transparency window (350–5500 nm). Lithium niobate (LiN) is currently the best choice for high-performance modulators (high speed, high linearity). Currently they are made from bulk LiN crystals but recent advances in the bonding of single crystal thin films of LiN onto silicon substrates open a new avenue via which to explore the advantages of LiN in the context of PICs and to benefit from their cost reduction, scalable manufacturing, and integration. This allows mode volumes to be reduced by more than ~100X, which not only results in even better modulators (more efficient and faster) but

also in significantly smaller bending radii and PIC footprints. This ultimately allows one to design complex PICs with tens of components in a millimeters-sized chip. Over the past year, CSEM has optimized an Ar+ ion milling etching recipe that allows for smooth sidewalls, resulting in state-of-the-art optical losses of  $<0.2\text{ dB/cm}$  and optical ring resonators of  $Q>10^6$ .

CSEM has uniquely versatile packaging and hybridization facilities for the development and small volume production of complex microsystems for niche and demanding applications. Medical is one of these, and a laparoscopy-compatible measurement device has been developed, featuring biocompatible, small-size sensor integration for blood pressure and flow with optical and mechanical functionality. The device replaces an expensive doppler laser perfusion monitor with much simpler technology, delivering 10–20 times cost reduction and a small size of less than 1 cm in length. The development is completed with a lab version monitor to control the probe and visualize measurement data, together with algorithms for data filtering and post processing.

CSEM's main differentiation in additive manufacturing is to focus on high resolution and small feature sizes with high performance materials. Hence, we are extending our material portfolio into materials such as FeNi (low CTE), NiTi (shape memory), and metal matrix composite and PEEK (biocompatibility; high performance). This year we have demonstrated AM processing of INVAR36 with a coefficient of thermal expansion smaller than 1 ppm CTE for a temperature range of 0 to 150°C while keeping its mechanical properties. This allows us to fabricate demanding thermostable components via a simple manufacturing technology from a material otherwise known to be challenging to process with standard machining techniques. The technology has been used to make complex rotation-to-translation mechanisms based on compliant structures for space application (e.g., mirror positioning systems used in beam steering). Low CTE is key in space application as temperature fluctuation is a significant challenge for scientific instruments.

# Bolometer for Plasma Diagnostics in ITER Tokamak

M. A. Dubois, P. Surbled, D. Faralli, O. Dubochet

A large international consortium is developing the world's largest tokamak to prove the feasibility of fusion as a large-scale and carbon-free source of energy. The building of this huge infrastructure by 35 nations is taking place in Saint Paul-les-Durance in the south of France. The first plasma is expected by the end of 2025. In that frame, CSEM is manufacturing bolometer-sensors which are the key components of one of the 50 diagnostic systems necessary to monitor the plasma during operation. The bolometers are manufactured on very thin ceramic substrates. The produced prototypes withstand thermal cycling and meet the electrical specifications set for the application. The delivered sensors still need to be submitted to irradiation testing in order to verify their suitability for the Tokamak environment.

In the quest for sustainable energy production, an international joint experiment has been launched, called ITER. The goal is to build a magnetic fusion reactor which will be capable of delivering net energy for the first time, paving the way to the power plants of tomorrow. The device consists in a toroidal vacuum chamber in which a very high temperature plasma is formed and confined. This plasma will host the fusion reactions between deuterium and tritium nuclei and produce energy in the process. A schematic view of the reactor is shown in Figure 1.

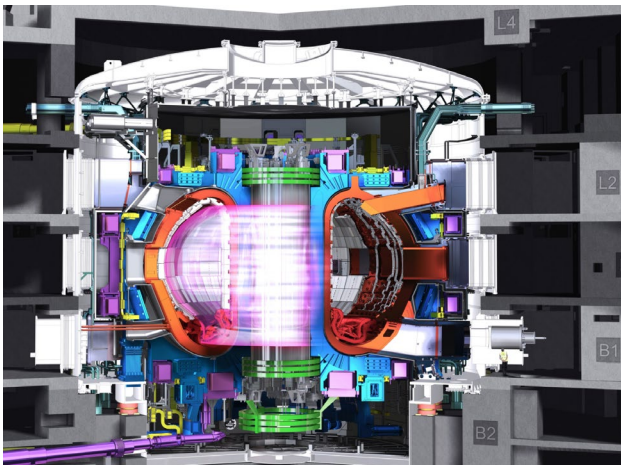


Figure 1: Schematic view of ITER tokamak.

In order to control the extreme conditions necessary for the reactions to take place, a very large battery of monitoring systems has to be developed. One of them is the bolometer diagnostic, which consists of about 100 5-channel bolometer sensors, the purpose of which is to measure the profile of total radiated power emitted by the plasma in the part of the electromagnetic spectrum situated between X-rays and infrared. Each sensor is basically a thin membrane, with on one side a metallic radiation absorber, and on the other side thin film resistors. The latter are connected in a Wheatstone bridge, enabling the detection of any temperature variation through the monitoring of the resistance value.

At CSEM, a complete process flow has been developed for the fabrication of bolometers on 20- $\mu\text{m}$  thick YSZ (yttrium-stabilized zirconia) substrates. This includes the temporary bonding of the substrates on carriers, and all the thin film deposition and patterning steps. An example of produced bolometers is shown in Figure 2. The visible side contains all the platinum resistors and contact lines of the sensors. Figure 3 shows a detail of the second side, where gold absorbers are created by electro-deposition. The thickness of these absorbers is 20  $\mu\text{m}$ , i.e. as large as the substrate itself. The role of the Au absorber is to extend the spectral sensitivity of the sensor, and its thickness is a compromise between sensitivity and heat capacity. Stress management is hence very important for ensuring reasonably flat and crack-free devices.



Figure 2: 5-channel bolometer sensor ( $25 \times 22 \times 0.02 \text{ mm}^3$ ).

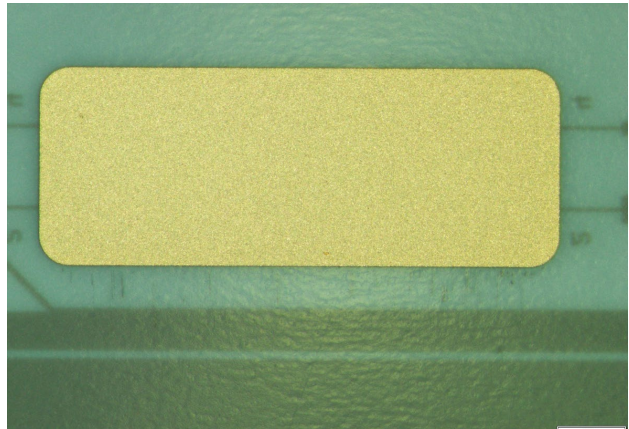


Figure 2: Detail of absorber with electrical contact lines seen through the thin substrate.

The produced devices meet stringent specifications. Specifically, they withstand thermal cycling and exhibit excellent electrical stability. Some sensors have even been trimmed by laser to improve further the equilibrium of the Wheatstone bridge. Resistance variations across a full 5-channel sensor below 0.3% have been reached. The delivered sensors await irradiation testing, which will confirm their suitability for the tokamak environment.

This development is commissioned by the European Joint Undertaking for ITER and the Development of Fusion Energy (or F4E, Fusion for Energy).

# Processing of SU8 Dry Film Laminates and Multilevel Processing

P. Surbled, F. Cardot, O. Dubochet

SU8 is an epoxy-based photoresist which is widely used in microfabrication for its ability to generate high aspect ratio patterns with vertical sidewalls. Most common applications of SU8 are the realization of moulds for electroforming of micro-mechanical components or the generation of templates for the replication of microfluidic devices in softer polymers (eg. PDMS). SU8 is now available in the form of dry film laminates which greatly simplify the processing allowing to circumvent many of the drawbacks of spin coated SU8 thus expanding the potential of this generic technological platform. The qualification vehicle presented below consisted in developing 20  $\mu\text{m}$  wide 100  $\mu\text{m}$ -high pyramidal microelectrodes arrays on CMOS wafers for brain research applications.

High aspect ratio photoresists up to thicknesses of a few hundred microns are widely used as moulds for electroplating of metallic structures or for the realization of microfluidic structures. Those resists are deposited by spin coating either in one or in several layers.

The main limitations encountered are the lack of thickness homogeneity of the coated layer which translate in a degradation of the critical dimension uniformity (CD) across wafer and from wafer to wafer during photolithography. Moreover, the processing requires, after each coating, long baking and cooling ramps to reduce internal stresses thus preventing cracking and delamination from the substrates. SU-8 resist is the most commonly spin-coated resist to achieve single-coat thicknesses of 20-200  $\mu\text{m}$  or more. With multi-steps coating, bake, UV-exposure and post-exposure bake, 3D structures have been obtained (Figure 1).

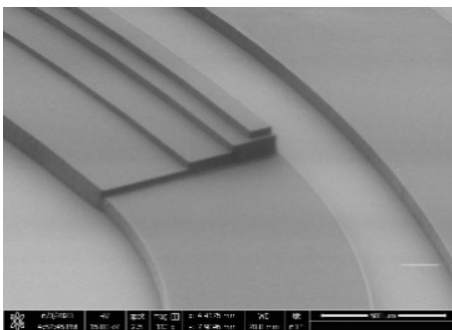


Figure 1: Five levels of SU8 for microfluidic applications.

The lamination of dry film resists (e.g. Ordyl, PerMX, SiNR, SUEX, TMMF, DF) is an interesting alternative to spin-coated resists. They offer the advantage of much shorter processing times and exhibit a very good thickness uniformity (e.g. 100  $\pm 2 \mu\text{m}$ ) up to the edge. Dry film can be used as for photolithography on pre-patterned wafers (e.g. holes, vias, ...) or as structural layer to bond two substrates together (e.g. Microfluidics applications). SU-8 dry films (SUEX) can be purchased in thicknesses ranging from 20 to 500  $\mu\text{m}$ . It is laminated at 70°C, exposed, baked, and developed in a few hours only. The results obtained after lithography and gold electroplating are repeatable, giving after stripping, structures with an aspect factor of 5 or more (Figure 3).

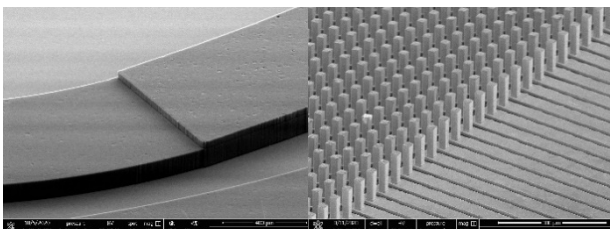


Figure 2: Two levels of SUEX (100  $\mu\text{m}$  + 50  $\mu\text{m}$ ).

Figure 3: 100  $\mu\text{m}$ -high electroplated gold pillars.

The SUEX can be used in multilayers, giving 3D structures in SUEX (Figure 2). An application examples is the fabrication of moulds for electroplating. As depicted in Figure 4, a SUEX layer is laminated on a wafer covered with a metallic seed layer, exposed, baked in oven then developed in a PGMEA solution (A). Then the SUEX mould is filled with electroplated gold and planarized (B). A second SUEX layer is deposited and patterned again by lithography (C). The second SUEX mould is then filled with gold by electroplating and planarized. The steps C and D can be repeated for higher and more complex structures. At the end, the SUEX resist and the seeding layer are etched, releasing the whole 3D gold structures (Figures 5 and 6).

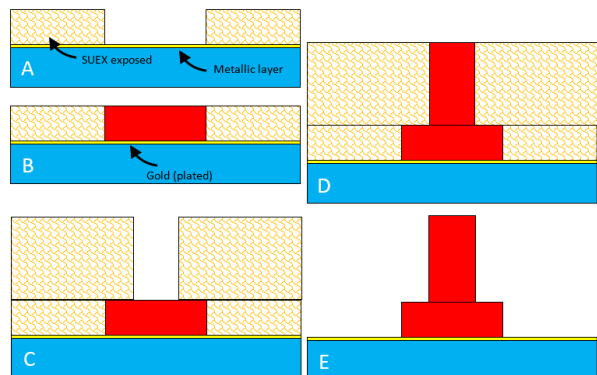


Figure 4: Process flow 2-level plating in dry film SUEX moulds.

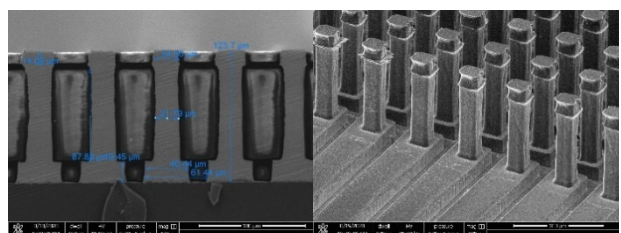


Figure 5: cross section of 3-level Au gold microprobes (20+90+15  $\mu\text{m}$ ) before stripping SUEX.

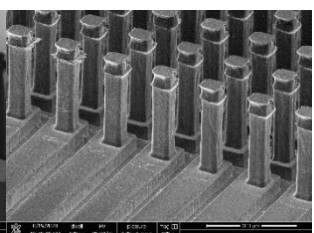


Figure 6: SEM view of 3-level Au gold microprobes (20+90+15  $\mu\text{m}$ ) after stripping SUEX.

# Advances in Microfabricated Electron Gun for Atomic Clocks

D. Faralli, F. Droz, M. Despont

A cold electron emitter has been fabricated as an alternative to standard hot-filament emitters. The device is a "Field Emitter Array" based on the known effect of the increase of electric fields in proximity of a sharp tip. A dense array of tips is fabricated using platinum silicide and integrated with a gate electrode done with the same material. The cold emitters will be used in the next generation of atomic clocks, where the use of hot filament emitters has several drawbacks. The samples have been assembled in a dedicated flange and tested for emissivity in a UHV system, down to  $10^{-6}$  mbar.

Atomic clocks using "trapped Hg ions" are being developed for the next generation of space and ground applications, due to their potential for superior stability [1]. An essential element of these clocks is the electron gun, which is used to ionize the Hg atoms. The standard "hot filament" electron guns have several drawbacks as: high power consumption, very slow switch on/off response, weight/volume, and power consumption.

Electron emission can be achieved at room temperature by using the "tip effect" i.e. the enhancement of electric field around sharp tips. The emitted current is given by a Fowler-Nordheim relation and depend mostly by the tip material work function, the tip sharpness and the gate geometry. Arrays of "field emitters" have been thus micro-fabricated to achieve emitted current around 1-10  $\mu$ A. In Figure 1 the cross section of a MEGA Field Emitter is shown. At a threshold voltage of  $\sim$ 80 V the emission starts and the electrons generated are collected by the anode, which is placed in the ion trap.

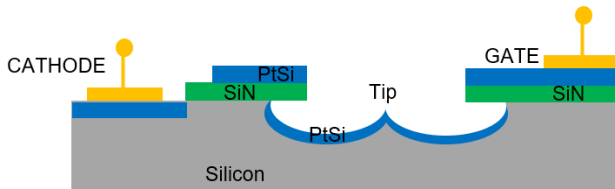


Figure 1: Schematic cross-section of a MEGA field emitter.

We use platinum silicide as material for the tips and for the gate electrode, due to its low work function and the excellent reliability and robustness properties. The tips are formed on the silicon substrate using an isotropic dry-etch process followed by thermal oxidation for sharpening. A platinum layer is sputtered and annealed @700C for silicide formation. The gate electrode is thus formed over an insulating SiN layer.

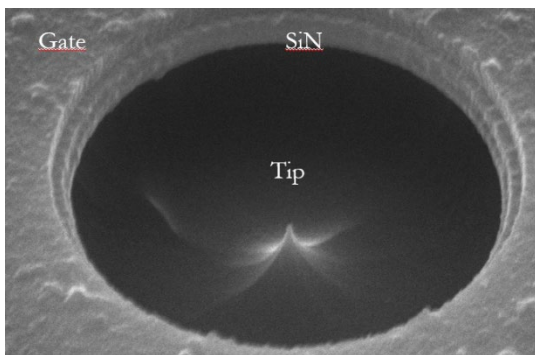


Figure 2: SEM picture of a tip from MEGA technology.

In Figure 3, an example of a micro-fabricated tip and gate electrode is shown. Arrays of different sizes and densities have been fabricated, ranging from 1.000 to 40.000 tips.

The device has been thus assembled in a dedicated vacuum flange (Figure 3) and mounted by the partner Spectratime in a UHV vacuum system to characterize the current emission as a function of the  $V_g$  voltage at pressures down to  $10^{-6}$  mbar.

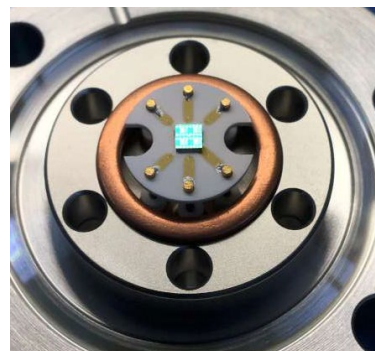
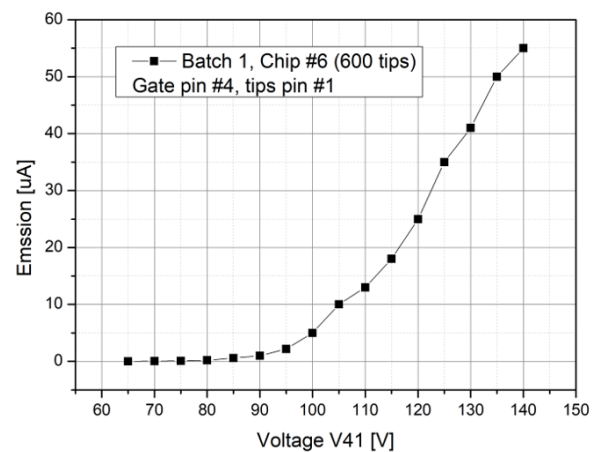


Figure 3: Picture of a Mega chip assembled in the dedicated flange.

The highest measured emitted current has been in the order of  $\sim$ 55  $\mu$ A @ $V_g$  =140 V from an array of 600 tips. At higher  $V_g$  the gate-cathode electrical breakdown is reached. The emission threshold has been measured @ $V_g$   $\sim$ 80 V.



The project has been supported by the MdP18 program, coordinated by the Swiss Space Center and funded by the Swiss Space Office of SERI (State Secretariat for Education, Research and Innovation). A new project together with the industrial partner Spectratime to improve the emitter fabrication yield and study its lifetime properties is under evaluation.

[1] <https://www.nasa.gov/directorates/heo/scan/engineering/technology/dsac>

# Wafer-scale in-plane Micro-optical Interconnects for Integrated Photonics Circuits (PICs)

A. H. Ghadimi, R. Krähenbühl, A. Luu-Dinh, R. Ferrini, M. Despont

Photonics packaging remains one of the most challenging steps in the PIC industry and therefore responsible for more than 80% of the total cost of a PIC product [1]. In this project, we present a novel wafer-scale packaging solution for interconnecting PICs and fibers. Our “plug-and-play” technology is based on 90-degree reflectors that are fabricated using the UV-casting process. Our wafer-level parallel replication process allows for fabrication of thousands of couplers at once and at very low costs and can significantly reduce the complexity and costs of packaging in PIC products.

In several markets relying on compact optical systems such as the telecom and data-com markets, metrology and photonics sensors, low-cost compact optical systems and devices are in constant demand to provide higher data rates, together with higher density and also to provide a high reliability in harsh environments. Integrated photonics circuits (PICs) profit from the increase in system integration and the substantial enhanced intensity by reducing the optical mode size.

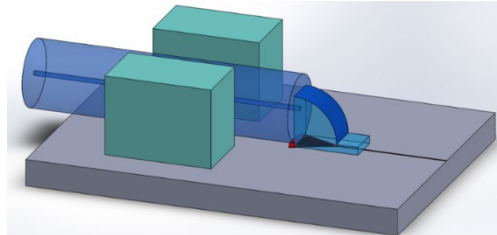


Figure 1: Schematic illustration of 90-degree Quadrature lens (Qlens) reflector that is fabricated on top of a grating coupler (red) and is used to coupling light from an optical fiber to the waveguide. The passive alignment structures (green blocks) are fabricated at the same time as the mirror, enable low-cost plug and play operation scheme.

However, a typical challenge associated to PICs is the ability to couple light in and/or out of the chip by an optical fiber or an optical fiber bundle. The conventional methods of coupling light from an optical fiber into a PIC such as edge-couplers or vertical couplers (e.g. grating couplers) requires active alignment in a serial process which is extremely time consuming and costly. Moreover, additional components are usually required (e.g. as fiber array bundles) that adds up to the complexity and cost of the packaging, as well as making the final product bulky. 3D printed micro-optical interconnects have recently emerged as an alternative solution for coupling of light from fibers into a PIC [2,3] in which a 3D printed micro-mirror or lens is fabricated on top of a waveguide or grating coupler thus removing the need for active alignment. These structures, however, are fabricated in a serial process (e.g. two-photon photolithography) which limits their scalability and cost.

In this project, we present a novel wafer-scale solution for interconnecting PICs and fibers. Our “plug-and-play” technology is based on 90-degree reflectors fabricated from reflowed quarter lenses (Qlens) [4]. The reflection enables a compact packaging solution where fiber is placed in-plane with respect to the chip. The reflow process also results in atomically smooth mirror walls, which is the key for low losses. In addition, our wafer-level parallel replication process allows for fabrication of thousands of couplers at once and at very low costs. This can significantly reduce the packaging costs of PIC products.

For this project, we used an internally developed SiN photonics platform to fabricate the grating couplers and waveguides

(Figure 3a). FEM simulations were used to optimize the design of the grating coupler at 1550 nm and the design of the Qlens reflector.

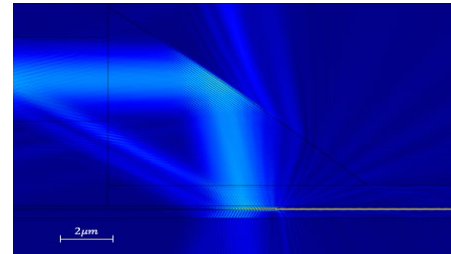


Figure 2: FEM simulation of Qlens reflector interconnect that illustrates its working mechanism based on total internal reflection. The input light from an optical fiber (inserter from the left) is reflected into the grating coupler and coupled into a waveguide. FEM simulations were used to optimize the grating coupler and the Qlens reflector.

The fabrication process of Qlens consist of two steps: First, the micro-optical structures are originated, and a “master” is fabricated, which is then used to produce the replication tool (mold). To create the master, a standard micro-lenses photolithography and a reflow process is used. Second, the micro-optical elements are replicated into a UV curable polymer (e.g. sol-gel) using the fabricated mold. Finally, a UV exposure is performed via a specifically designed photomask that cuts the extra parts of the micro-lens and define the final shape of the Qlens reflectors and the passive alignment structures. In addition to being low cost, wafer scale and fast, this process allows to fabrication of coupler arrays and allows several fibers to be coupled to PIC at the same time (Figure 3).

So far, optical measurements showed best transmission losses of around 12 dB in a singlemode (E9) to multi-mode (G50) fiber configuration without Qlens, and around 15 dB with the G50 fiber placed into an output Qlens indicating ~3dB excess losses.

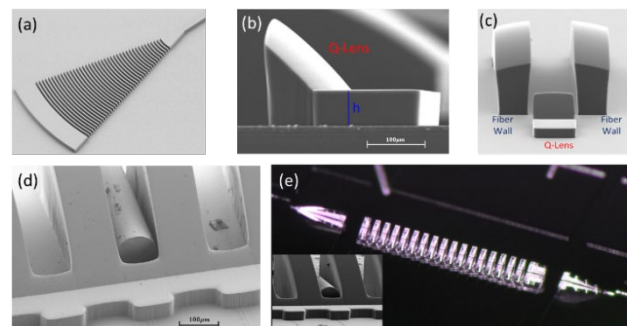


Figure 3: SEM and optical images of (a) grating coupler, (b) the Qlens reflector, (c) the Qlens and the two walls for passive alignment of the fiber (d) a completed device on top of the grating coupler and waveguide with a fiber inserted in position and (e) a Qlens array allow for multiple fiber couplings at the same time.

[1] E. Fuchs, et al., JLT, 2006, doi:10.1109/JLT.2006.875961

[2] H. Gehring, et al., Opt. Letters, 2019, doi:10.1364/OL.44.005089

[3] O. Gordillo, et al., Opt. Express, 2019, doi:10.1364/OE.27.020305

[4] R. Krähenbühl, et al., ECOC 2019, doi:10.1049/cp.2019.0916

# An Electro-optics Integrated Photonic Circuits (PICs) Platform based on Lithium Niobate

A. H. Ghadimi, H. Sattari, G. Choong, V. Brasch, Y. Petremand, O. Dubochet, S. Lecomte, M. Despont

Lithium niobate on insulator (LNOI) is one of the most promising emerging platforms for PICs that comprises a unique set of interesting optical properties: a high electro-optic (EO) coefficient, high intrinsic 2nd and 3rd order nonlinearities, and a large transparency window (350- 5500 nm). In this project, we developed the fabrication processes as well as the expertise and know-how to simulate, design and test PICs made from lithium niobate. The results of this project will pave the way for creation of the first European open PIC foundry for LNOI that will be available to all stakeholders in coming years.

Lithium niobate (LiN) has attracted a lot of attention since the 1970s as an electro-optics material, however, most of its industrial success in photonics domain has been so far limited to devices made from bulk crystals in the form of free-space or fiber-coupled components using ion-implanted waveguides<sup>[1]</sup>. Recent advancements in bonding of single crystal thin films of LiN onto silicon substrates (LNOI), opened a new avenue to explore the advantages of LiN in the context of PICs and benefit from the cost reduction, manufacturability and integration aspects offered by integrated circuits<sup>[2]</sup>. Here waveguides are fabricated using RIE etching in a LiN thin film which allows for significantly higher refractive index contrast ( $\Delta n \sim 0.7$ ) between the core and cladding compared to ion implantation technology ( $\Delta n \sim 0.02$ ) and thus more than  $\sim 100X$  reduction of mode volume. Such a tight confinement not only results in more efficient and faster modulators, but also significantly smaller bending radius and PIC footprint. This ultimately allows designing complex PICs with tens of components in small millimeters-sized chip.

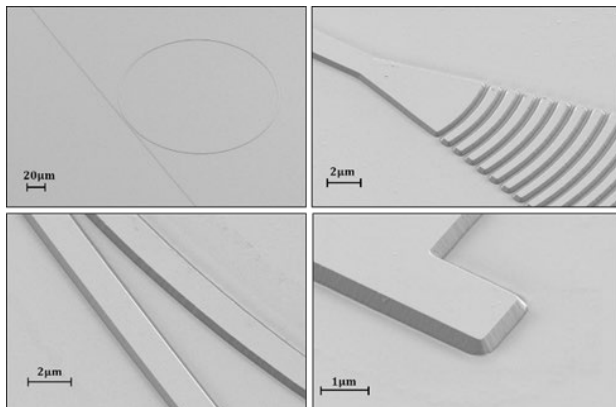


Figure 1: SEM images of LNOI devices fabricated at CSEM.

Due to its unique material properties a LNOI-based PIC platform can serve a vast range of applications including telecom, metrology, LiDAR, sensing and also making use of nonlinear photonics for signal processing, spectroscopy, quantum computing and other quantum technologies. LNOI is a platform that not only outperforms other PIC platforms in areas such as ultra-fast low-loss and efficient modulators, but also enables new functionalities that are currently beyond the capability of other PIC platforms. Examples for these novel functionalities are sum or difference frequency generation, second harmonic generation (SHG) and pure phase control at RF frequencies, which are needed for advancing novel quantum and sensing technologies.

However, outside of few academic labs around the world, there is no PIC foundry that offers LNOI as a PIC platform. CSEM is set to change that by developing the first industrial scale PIC foundry for LiN. Over the last year, an LiN etching recipe based

on ICP RIE Ar+ milling has been optimized at CSEM to achieve smooth sidewalls that are highlighted in Figure 1. Smooth optical sidewalls are the key to achieve low optical losses, which is extremely important for many applications. At CSEM, we have fabricated and measured the quality (Q) factor of ring resonators (similar to the ones illustrated in Figure 1) and demonstrated optical  $Q > 10^6$  at 1550 nm, corresponding to linear losses  $< 0.2$  dB/cm in uncladded waveguides.

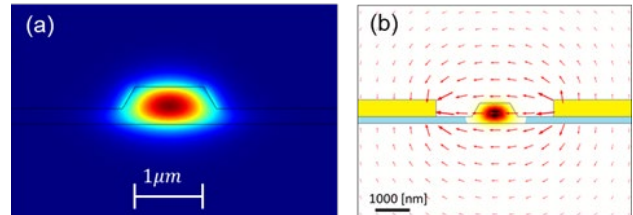


Figure 2: a) FEM simulation of an optical mode in a cross section of LiN waveguide. b) FEM simulation of the electric field distribution and the optical field that is used to calculate EO coupling in a phase modulator.

CSEM's LiN platform is based on commercially available LNOI wafers (purchased from NanoLN Co.) and the standard thin film layer stack consist of 600 nm single crystalline lithium niobate thin films on 4.7 μm of buried oxide (BOX). The waveguides are formed by etching 400 nm into the lithium niobate layer (see Figure 2a). 500 nm gold plates are patterned a few microns from the waveguides to provide efficient electro-optics control of the light within the waveguides (see Figure 2b). Finally, the LiN waveguides are protected by a 4 μm of SiO<sub>2</sub> cladding on top.

Thanks to such tight confinement, the optical intensity is high in the small waveguide mode volume, we were able to simulate phase shifter with EO coupling efficiencies below 15 mm.V and Mach-Zehnder modulators with efficiencies below 7.5 mm.V. This allows creation of CMOS compatible<sup>[3]</sup> EO modulators with  $V\pi < 1$  V. In addition, the tight confinement allows to achieve the threshold for optical nonlinear effects at low input power where for example we recently demonstrated supercontinuum generation<sup>[4]</sup> from a LiN waveguide with a 1550 nm input pump laser (Figure 3b).

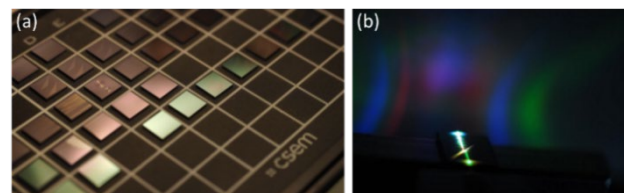


Figure 3: (a) Optical image of a batch of lithium niobate PICs designed and fabricated at CSEM. (b) Rainbow of colors generated from a 1550 nm laser in a LiN waveguide through optical nonlinear effects (supercontinuum generation).

[1] M. Fukuma, *et al.*, Applied Optics, 1980, doi:10.1364/ao.19.000591

[2] C. Wang, *et al.*, Nature, 2018, doi:10.1038/s41586-018-0551-y

[3] M. Zhang, *et al.*, Nature 2019, doi:10.1038/s41586-019-1008-7

[4] Y. Okawachi, *et al.*, Optica 2020, doi:10.1364/OPTICA.392363

# High Thermal Conductive Die Attach Material for High-power Semiconductor Devices in Space Applications

R. Jose James, G. Spinola Durante, M. Luetzelschwab, M. Fretz, K. Krasnopski, R. Limacher, I. Marozau, L. Murphy\*

High thermal conductivity of materials used for assembly of high-power semiconductors are becoming very important, as the power per unit area of these chips are increasing considerably. High power per unit area results in increase of junction temperatures, resulting in a considerable decrease in lifetime of these devices. To improve the conduction of heat away from the chip, high thermal conductivity silver sinter paste was studied as a replacement for AuSn solder for die-attach of GaN and silicon chips for space applications.

The wide band gap of Gallium Nitride (GaN) devices enables them to handle high breakdown voltages. They also show high charge capacity and high saturation velocity which enables them to handle high current loads. Due to these advantages and high-speed switching capabilities, GaN chips have become a choice for many RF applications like mobile communications infrastructure. On the downside, this causes high-power density which in turn results in high junction temperatures ( $>175^{\circ}\text{C}$ ). The lifetime of these devices decreases considerably with increase in junction temperature as shown in Figure 1. So, a reduction in channel temperature is critical for a long-term reliable operation.

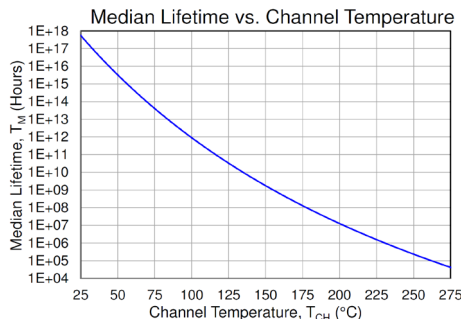


Figure 1: Decrease in lifetime with channel temperature [1].

There has been a lot of research on novel substrates consisting of high thermally conductive materials like different diamond composites and copper alloys. However, only few novel die-attach materials are being investigated. Silver sintering is a promising novel die-attach material for assemblies where high heat transfer is important. Silver sintering was studied as an alternative to Gold-Tin (AuSn) soldering, the main choice for die attach especially in space and photonics applications. This paper compares these two materials and outlines the applicability of silver sinter in space applications.

GaN HEMT transistors and silicon chips with integrated heating and temperature sensing elements were used for the study. Aluminum nitride DBC (direct bonded copper) substrates were used, to provide a good heat transfer away from the chip. 54 silicon chips and 28 GaN chips were fabricated of which half featured silver sinter and the other half AuSn. (Figure 2).

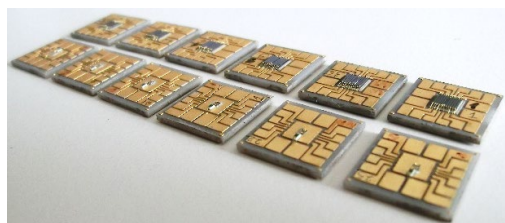


Figure 2: Silicon and GaN Samples after assembly.

\* ESTEC-ESA, Netherlands

Temperature measurements were conducted while powering up the silicon chip to different power levels, to compare the heat transfer in chip assemblies made using AuSn and silver sinter. As shown in Figure 3, silicon chip's surface temperature is ~10% lower for the silver sinter assembled chips compared to chips which were bonded using AuSn solder. This data is based on 27 chips each of solder and silver sinter bonded assemblies.

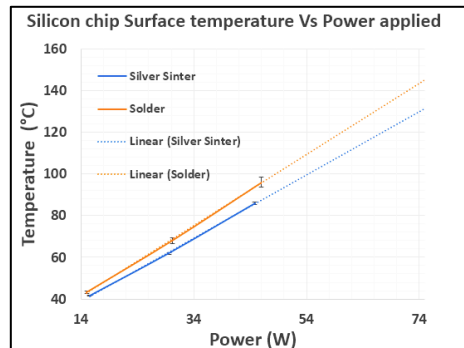


Figure 3: Surface temperature measured on the silicon chip.

It is thought that the lower temperature seen on the silver sintered samples can be attributed to 2 factors:

- Higher thermal conductivity of the silver sinter ( $>150\text{ W/mK}$ ) compared to AuSn solder ( $57\text{ W/mK}$ )
- The high amount of voiding in AuSn solder joints compared to the porosity in silver sinter which still needs to be accessed.

Silver sinter showed also other clear advantages compared to AuSn. The temperature required for silver sintering is much lower compared to AuSn soldering. The silicon chips assembled using AuSn showed a considerable change in characteristics due to the high temperatures incurred during the bonding process. The process time for silver sintering is not critical as in the case of AuSn, where a longer process time would be detrimental to the joint. The under-bump metallization surface quality and thickness is also less critical for silver sinter. For assemblies with low pitch and small feature sizes, AuSn will still be the preferred choice due to the deposition methods making it possible to produce small feature sizes enabling bonding of miniature chips.

As the next step, the assemblies will be reliability tested to check the applicability for space environment.

The project team acknowledges the funding provided by the ESTEC, European Space Agency (ESA).

[1] Datasheet TGF2023-2-01, '6 Watt Discrete Power GaN on SiC HEMT', [www.qorvo.com](http://www.qorvo.com), 2016.

# Advanced Packaging for Simultaneous Hermetic Lid Sealing and Chip Backside Heat Removal

G. Spinola Durante, R. Jose James, M. Luetzelschwab, E. Rutz, K. Krasnopski, A. Hoogerwerf

In the framework of the EU project Heatpack [1], we are exploring advanced packaging technologies for high power density components to improve state-of-the-art thermal management solutions. A new concept is presented here to remove the dissipated heat of a flip-chip mounted GaN chip, by physically connecting its backside to the package lid. The proposed solution utilizes a highly thermally conductive silver paste to both hermetic seal a transparent Silicon Carbide lid and connect the chip onto it. The bonding is based on a low-temperature laser diffusion bonding process (LADB) developed at CSEM [2].

The EU project Heatpack [1] aims to develop and validate critical technology building blocks for enabling transformative packages for space applications with very low thermal resistance. These thermal management solutions beyond state-of-the-art are necessary to fully exploit the potential of wide-bandgap technologies, which are now being considered as critical in numerous industrial sectors and, in particular, for space. The high thermal conductivity of the materials used for the assembly of high-power semiconductors is becoming very important, since the power per unit area of these chips is increasing considerably. Package miniaturization and increased functionality are driving the overall market of System-in-Packages (SiP) for Aerospace components. The high power per unit area results in an increase of junction temperatures. Benefits for a better thermal management solution will range from improved performance to increased components reliability and lifetime.

The cross-section of a SiP including a high-power GaN HEMT-based Solid State Power Amplifier and Electronic Power conditioner chip is shown in Figure 1. These components are assembled inside a ceramic package and sealed hermetically with a Silicon Carbide lid. The choice of the lid material and the low-temperature laser bonding are both crucial to reduce the stress to a minimum and to ensure the hermeticity of the lid and proper thermal connection to the back-side of the GaN chip, without compromising the structural integrity of the flip-chip bump interconnections.

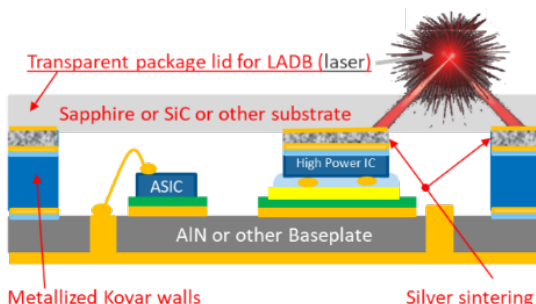


Figure 1: LADB (laser) hermetic sealing and back-side chip bonding on the lid to efficiently remove heat with silver paste sintering.

In a standard flip-chip configuration the heat is dissipated through the bumps and the underfiller. This is relatively inefficient due to the limited thermal conductivity of the underfiller materials (up to ten W/mK) and the large thickness and low surface area of the lead-free solder (~60 W/mK) bumps compared to the available chip surface. To exploit a larger surface for cooling we can

employ the chip's backside and connect it to a lid with a high thermal conductivity. This improves thermal management considerably, given that the chip substrate is a good thermal conductor compared to solder. Si or SiC substrates offer up to a factor 5 better thermal conductivity than SAC lead-free solder. To obtain a quantitative assessment of the proposed solution in terms of temperature values, thermal simulations were carried out and are shown in Figure 2. On the average, the maximum junction temperature is reduced by  $\Delta T_{\max} = (94.7 - 86.1^\circ\text{C}) \sim 9^\circ\text{C}$  for each chip dissipating 1 W. The effect scales linearly with dissipated heat.

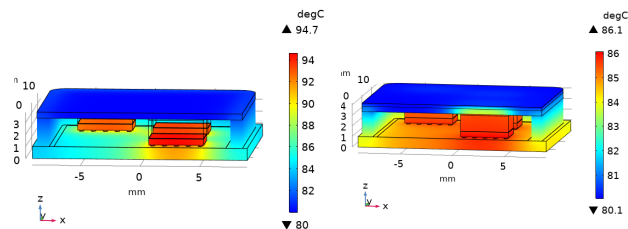


Figure 2: Temperature plot of chips dissipating 1 W each in flip-chip mount. Right: chip backside additionally connected to lid (SiC/Cu-D spacer + Ag paste).

The crucial aspect is to reduce mechanical stress by using a low-thermal expansion lid made of Silicon-Carbide and perform a low-temperature laser bonding process (LADB reached TRL 4 by ESA evaluation [2]), taking advantage of the partial transparency of SiC at the laser wavelength. SiC is preferred since it offers a very low thermal expansion (similar to GaN) and superior thermal conductivity, thereby ensuring better heat spreading. This technology has been developed and tested in the past for SiC-based MEMS pressure sensors [3].

Additional activities are carried out with the characterization of the thermal properties of silver paste as well as the thermo-optical model calibration for fine-tuning of the LADB process. Optimal parameters are needed for sintering the Silver paste according to the configuration shown in Figure 1. An independent task in the framework of this project is the development of micro-channels for removing heat from the SiC lid onto an external passive/active heat exchanger. This approach has the potential to be extended to general-purpose butterfly packages for high power optoelectronic components, where the Kovar lid could potentially be replaced by a Silicon carbide lid and connected to the component itself [4].

This work is supported in the framework of EU Project Heatpack.

[1] HEATPACK is an EU-Project Consortium developing "High thErmAl efficiency componenTs PACKages for space". <http://www.heatpack.eu/>

[2] R. Jose James, et al., "Radiation Hard Glass and Sapphire-based Miniature Hermetic Packages for Space Applications", CSEM Scientific and Technical Report (2019) 31.

[3] A. Hoogerwerf, et al., "Silicon carbide pressure sensors for harsh environments", Proceedings of Transducers Conference, Berlin (D), June 2019.

[4] G. Spinola Durante, et al., "Thermal Management Modeling of High-power Chips and Calibration with Experimental Data", CSEM Scientific and Technical Report (2019) 30.

# Photonic Multi-domain Integration Trends

S. Mohrdiek

Just recently "roadmapping" for future development in photonics and in particular photonic integration has gained a lot of momentum. CSEM is well positioned against the challenges to provide heterogeneous packaging and assembly solutions across a large variety of industrial applications.

Unlike mainly silicon-based electronics, photonic integration is characterized on one hand by a large diversity of material platforms used (Si, SiN, InP, GaAs, polymers) and on the other hand by wavelengths ranging from UV to the far infrared. In view of the difficulties to establish common, standardized platforms, heterogeneous integration continues to be a key element to drive new technologies and scientific advances for the next decade. The combination of heterogeneous functionalities with optical, thermal, electrical, fluidic, mechanical, and high frequency characteristics requires specialized materials and system integration (packaging and assembly) processes and equipment.

There is also a clear differentiation between large volumes of the same design in applications like datacenter transceivers, and low volumes usually with higher added value and a large variety of designs in e.g. aerospace, medical, biosensing and mechanical sensing applications. While the big data market, fueled by social media companies such as Google, Facebook, Microsoft, Amazon etc. is mainly challenged to get the production cost down, at lower volumes the cost for development and prototyping becomes critical.

RTOs like CSEM and a few companies are there to help bridging this valley-of-death between inventing and commercializing by providing prototyping services to enable SMEs and established companies alike to start seeding the market. On top of that the need is also recognized through EU funded pilot lines, with CSEM participating in the projects Mirphab, MedPhab and Phabulous.

A main feature in photonic roadmaps [1,2,3] is the quest to find packaging solutions for an increasing exposure of devices to an environment of higher temperature and humidity, which is also subject to corrosive elements across all application areas from datacenter to lidar and biophotonics, aerospace sensors and actuators. In addition to materials in demand for harsh environments, other common denominators in trend are flipchip assembly in micrometer range, thermal management concepts, long term hermeticity and small footprint packages.

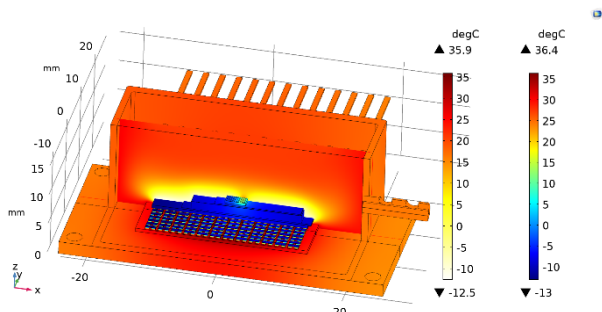


Figure 1: Thermo-electric FEM simulation of heat distribution from hot (red) to cold (blue).

The example in Figure 1 shows a typical optoelectronic Butterfly package design, demonstrating the use of a multiphysics FEM simulation program to assess thermoelectric performance including the pillars of a Peltier cooling element.

Other concepts include multiple properties, like the laser package in Figure 2 with a stabilization in the mK temperature range, featuring high frequency connections in GHz range.

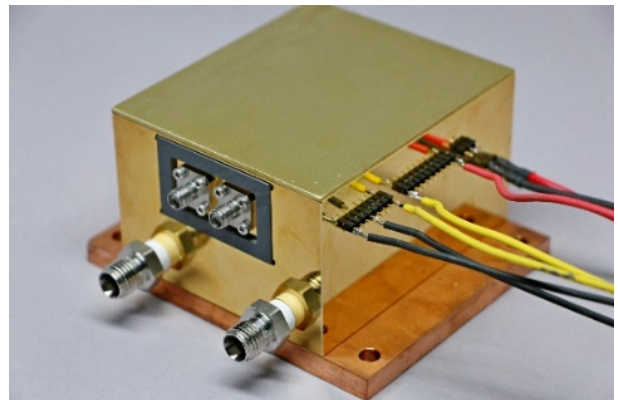


Figure 2: Water cooled temperature stabilized package with RF circuitry included.

Customized packaging solutions are developed at CSEM through conventional packaging and assembly processes as well as beyond state-of-the-art technology, in areas such as laser assisted joining processes and silver sintering for better heat dissipation.

Figure 3 shows a disposable biomedical sensor probe, which includes multifunctional properties like a mechanical function to generate pressure and optical sensing for measuring the blood flow in a very compact format.



Figure 3: Biomedical sensor probe with mechanical actuator.

CSEM's objectives are aligned with the global challenges as laid out in several photonic roadmaps, with a focus on development of new, affordable, compact and hybrid packaging solutions, including packages for harsh environments, thermal management solutions, and hermetic packages.

[1] Photonics21 Multiannual Strategic Roadmap 2021–2027, [www.photonics21.org](http://www.photonics21.org)

[2] Integrated Photonics Systems Roadmap (IPSR-I) <https://aimphotonics.academy/roadmap/ipsr-roadmap/>

[3] IEEE Electronics Packaging Society <https://eps.ieee.org/technology/heterogeneous-integration-roadmap/>

# SWaP—Smart Wall Pipes and Ducts

N. Hendricks, S. Lani, C. Manoli\*, J. Noël\*, P. Petagna\*

*Freedom of design, complex shapes, on demand production are few of the new possibilities that Additive Manufacturing (AM) is providing for many applications/fields. In particular, the field of thermal management systems is requiring more complex geometries to meet the increasing demands on thermal budgets. However, as systems become more complex so too does the measurement of fluid properties. Here, Smart Wall Pipes and ducts (SWaP) has developed revolutionary components with integrated sensing capabilities, which have been created by combined 3D printing techniques, to measure fundamental fluids properties of circulating fluids where the results are comparable to that of commercially available sensors.*

Thermal management is becoming ever more important due to increasing application demands in fields such as manufacturing (injection molds, tooling stamps), automotive (batteries, electric motors), and aerospace (engines, shielding). To meet these demanding requirements, Additive Manufacturing (AM) is being used to create parts with increased complexity to allow for more design freedom and, ultimately, more efficient thermal management. However, as the part complexity increases so too does the measurement of fundamental fluid parameters of thermal management systems. This intersection of part complexity and measurement of fluid parameters for thermal management systems, specifically hydraulic circuits used in cooling systems, is where the project focus of Smart Wall Pipes and ducts (SWaP) lies as a feasibility study [1].

The production process of the smart pipes consists of:

- Design of the smart pipe and generation of the printing file.
- Fabrication of the pipe, the electrical wires, electrical connectors, and fluidic interfaces by Laser Powder Bed Fusion (LPBF) by locally melting a powder layer with a laser and repeating this process until the part is finished. The used material is Stainless steel 17-4PH. After complete removal of the un-melted powder, an insulation layer, consisting of a UV-curable epoxy, is cast around the electrical wires to hold the wires in position as well as to create an electrical insulation layer on the inside of the cavity where the Resistive Temperature Detector (RTD) is printed.
- Removal of the pipes from the build platform by wire saw cutting and manual removal of the supporting materials. To reduce the leakage of the fluidic interfaces, the parts are electropolished.
- Finally, after a thermal treatment of the UV-curable epoxy, the RTD is deposited by Aerosol Jet Printing (AJP) using a silver-based nanoparticle ink. A thermal treatment is performed to sinter the nanoparticles together and to provide an electrical connection.

The fabricated pipe with integrated RTD sensor is depicted in Figure 1.

Different tests are carried on fabricated devices and consists of:

- Leak test with helium (He) and carbon dioxide (CO<sub>2</sub>) (up to 10 bars) and leak rate < to  $2 \times 10^{-10} \text{ mbar} \cdot \text{L} \cdot \text{s}^{-1}$  is measured, which is within the permissible range for hydraulic circuits.
- Thermal cycling tests from - 15°C to 5°C with a ramp rate of 2°C/min. where the sensor is demonstrating a very good repeatability.

- 
- CERN

- Calibration of the printed RTD (AJP sensor) with two temperature sensors attached to the outer surface of the pipe (TS1, TS2) and two temperature sensors integrated inside a PEEK tube embedded in a tee union (Probe1, Probe2). The sensor is demonstrating a linear behavior with a R<sup>2</sup> factor of 99.97%.
- Test with C6F14 liquid coolant to validate the performance of the sensor and its applicability to cooling systems. Figure 2 is depicting the result of a test with the liquid coolant and demonstrating similar performance to commercial temperature sensor (Pt100) but with a reduced mass and footprint.

In the future, pressure and flow sensors will be developed with a similar technology and deposited in the same structure as the RTD sensor to provide a cost effective, compact, and lightweight solution to integrate multiple sensors in a pipe for cooling systems.

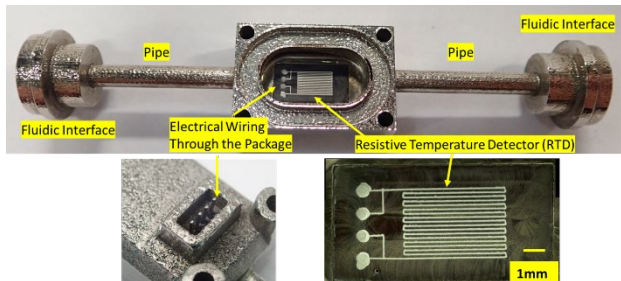


Figure 1: AM constructed pipe from LPBF with printed RTD sensor embedded.

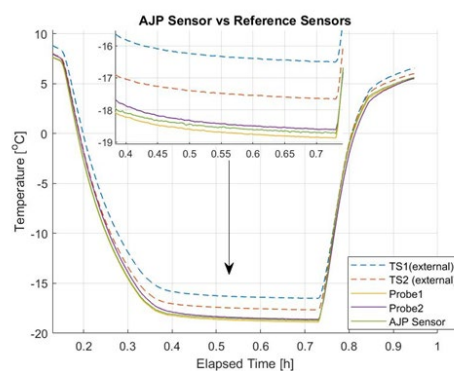


Figure 2: Comparison of AJP printed RTD sensor to that of commercially available Pt100 RTD sensors.

This project has received funding from the ATTRACT project funded by the EC under Grant Agreement 777222, in collaboration with CERN. CSEM would like to thank the Swiss Confederation for additional financial support.

[1] C. Manoli, N. Hendricks, J. Noël, P. Petagna, S. Lani, "Smart Wall Pipes and ducts", ATTRACT final conference, 2020.

# Development of Metal Matrix Composites by Laser Powder Bed Fusion

V. Pejchal, M. Bregeault, M. Dadras, O. Sereda

Metal Matrix Composites (MMCs) are materials that combine a continuous metallic matrix with a second reinforcing phase, typically made of ceramic, with a goal to produce a new material with properties superior to those of individual constituents. MMCs can thus combine high toughness, ductility and conductivity of metals combined with stiffness and wear resistance of ceramics [1]. An attractive class of MMCs are light metals such as aluminum reinforced with hard and stiff ceramic particles such as alumina providing stiff yet lightweight composites. One of the main drawbacks of MMCs is their poor machinability. Therefore, very near-net shape manufacturing techniques such as laser powder bed fusion (L-PBF) represents one of the potential ways of producing MMCs. In the recent development we demonstrated an aluminum based MMC with Young's modulus of 100 GPa and near 35 GPa.cm<sup>3</sup>.g<sup>-1</sup> specific modulus which is more than 30% improvement compared to traditional metals such as steel, titanium, and aluminium.

Laser powder bed fusion (L-PBF) system of Trumpf TruPrint 1000 was used to fabricate a AlSi12 matrix composite reinforced with 15vol.% of Al<sub>2</sub>O<sub>3</sub>. The feedstock powder was prepared by mechanical mixing of AlSi12 and Al<sub>2</sub>O<sub>3</sub> powders with 40 µm and 15 µm average size, respectively. A Design of Experiment approach considering several L-PBF parameters such as laser power, laser speed, hatch distance and rotation of adjacent layers was performed to study the influence of printing strategy on MMC fabrication and material samples in the form of 8x8x8 mm<sup>3</sup> cubes were fabricated (Figure 1a). Figure 1b shows the microstructure of one of the cubes manufactured with the laser parameters producing the lowest residual porosity. During the process, Al<sub>2</sub>O<sub>3</sub> particles melt and form bigger (several tens of micrometers) particles of irregular morphology. The residual porosity in the as-built samples was found to be in the range of 3 - 6% based on image analysis. Hot Isostatic Pressing (HIP) at 500°C and 100 MPa was performed to decrease the porosity. After HIP the porosity was found to decrease to 1 - 4% (Figure 1d).

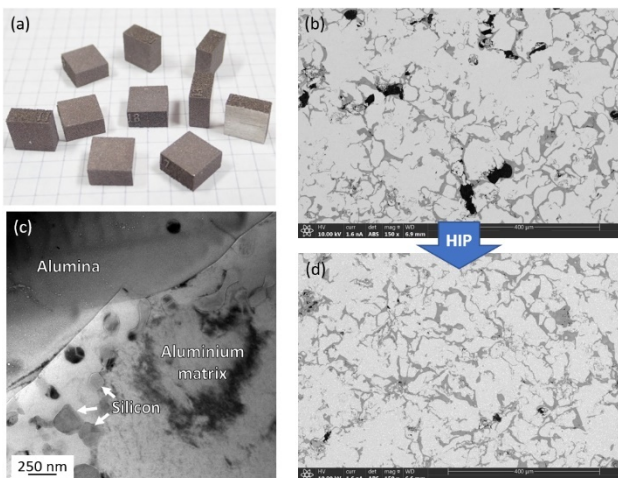


Figure 1: a) MMC material samples fabricated using L-PBF, b) SEM micrograph showing X/Y cross-section of as-built MMC sample, c) TEM micrograph showing a detail of the alumina-aluminium matrix interface, d) SEM micrograph showing X/Y cross-section of MMC sample after HIP post-treatment. In SEM micrographs light-gray represents AlSi12 matrix, dark-gray represents Al<sub>2</sub>O<sub>3</sub> particles, and black represents pores.

Transmission electron microscopy (TEM) was performed to closely examine the interface between the aluminium matrix and Al<sub>2</sub>O<sub>3</sub> particles (see Figure 1c). It shows that locally a good metallurgical bonding was achieved upon LPBF process optimization. TEM observation also revealed nanocrystalline silicon precipitates present in the aluminium matrix. The good

bonding between aluminium and reinforcing Al<sub>2</sub>O<sub>3</sub> particles is enabled by the so-called Maragoni convection that appears in the melt pool caused by local temperature gradient and chemical concentration difference [2]. A vigorous Maragoni convection disrupts the native oxide layer of AlSi12 particles and stirs Al<sub>2</sub>O<sub>3</sub> particles in the molten metal. Thus, due to the resultant capillary forces the liquid metal surrounds and wets Al<sub>2</sub>O<sub>3</sub> particles.

To evaluate the Young's modulus of the present MMC system, series of tensile samples were fabricated with near-net shape dimensions to test samples without need of machining. Along with MMC, tensile samples of the matrix material - AlSi12 were fabricated for comparison. The as-built tensile samples were HIP treated as described earlier. Figure 2 summarizes the results. Additively manufactured AlSi12 reinforced with 15vol% of Al<sub>2</sub>O<sub>3</sub> exhibits 100 GPa of Young's modulus compared to 72 GPa of non-reinforced AlSi12. Translated into specific modulus terms using the density measured by Archimedes method the present aluminium based MMC has near 35 GPa.cm<sup>3</sup>.g<sup>-1</sup> specific modulus which is more than 30% improvement compared to conventional metal alloys. The specific modulus of steel, aluminium and titanium alloys is for all near 25 GPa.cm<sup>3</sup>.g<sup>-1</sup>.

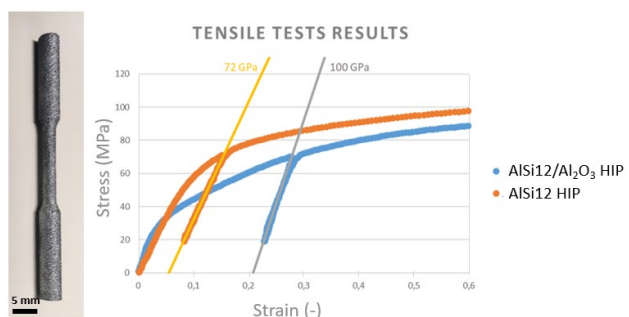


Figure 2: Tensile curves of as-built and HIP post-treated samples. Young's modulus was accurately determined by performing elastic unloading.

In conclusion, we show that L-PBF is a highly promising technology for manufacturing MMCs. With optimized printing strategy and HIP post-treatment aluminium based MMC with 15vol.% ceramic reinforcement and porosity below 4% was achieved. Mechanical characterization showed that improvement of specific modulus of more than 30% is attained. This result paves the way towards more lightweight and performant components with stiffness driven design. The further work focused on improving the strength and ductility of the resulting MMC is ongoing as well as exploration of new MMC systems.

[1] N. Chawla, K.K. Chawla, "Metal matrix composites", Springer, New York, 2006.

[2] J. Berthier, Micro-Drops and Digital Microfluidics, A volume in Micro and Nanotechnologies, Elsevier, 2013.

# 3D-printed Multi-material 3/2-way Valves for Soft Actuators

D. Bayat, F. Boudoire, S. Lani, S. Unterhofer, H. A. Sonar<sup>\*</sup>, J. Paik<sup>\*</sup>

Soft robotics and compliant actuators are emerging fields with applications in various sectors, from medical devices for rehabilitation to gaming/entertainment accessories. Additive manufacturing offers design freedom not achievable with conventional manufacturing processes. This project aims to investigate and design alternative pneumatic valves specifically applicable to soft robotic actuators. Our unique approach involves 3D-printed designs that can be easily adapted to the given robotic actuators' requirements. CSEM's 3D-printing group and EPFL's Reconfigurable Robotics Lab's collaboration brings together haptic devices and precision printing to achieve 3D-printed 3/2-way valves for soft actuators.

3D printing is gaining popularity in recent years, replacing conventional manufacturing methods. The emerging field of soft robotics and compliant actuators is also finding applications in a wide range of sectors, from medical devices for rehabilitation to gaming/entertainment accessories.

In this project, we aim to integrate valve designs that use 3D printing advantages such as monolithic fabrication and high precision stereolithography to design and fabricate 3/2-way valves that are adapted to the requirements of the soft robotic actuators manufactured by the Reconfigurable Robotics Lab of EPFL/RRL. The main advantages will be (1) flexible design, (2) improved reliability by reducing the assembly steps and the required variety of material, and (3) improved compactness.

In the first phase of this project, a proof of concept was successfully elaborated, simulated, built, and tested.

## 3D-printed valves and SPAs

One of the families of soft robotic actuators with excellent market potential is haptic feedback systems, which can apply vibrations, forces, or motions. These systems use Soft Pneumatic Actuators (SPAs) to provide feedback. Figure 1 shows fabricated actuators at EPFL/RRL and their exploded schematic view<sup>[1]</sup>.

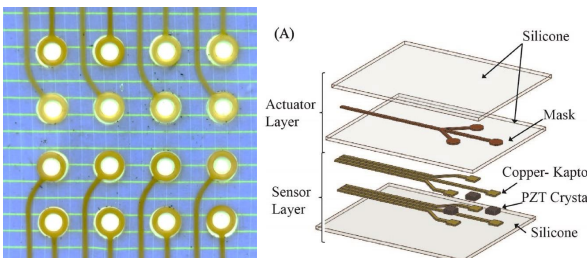


Figure 1: Soft actuator prototype (SPA-Skin) developed at RRL, EPFL, and its multiple component layers with integrated sensing layer<sup>[1]</sup>.

The schematics of the 2/3 valve is shown in Figure 2. Actuation is achieved by magnetic actuation with a moving-magnet, stationary-coil scheme.

The 3D-printed valves that are designed and printed at CSEM are shown in Figure 3 and Figure 4. The valve elements shown in Figure 3 consists of two separate parts which will be assembled together: one made with a flexible polymer (compliant structure) and one with a rigid polymer (casing). In addition, a micro-magnet (seen in Figure 3) is placed onto the flexible membrane after the printing step.

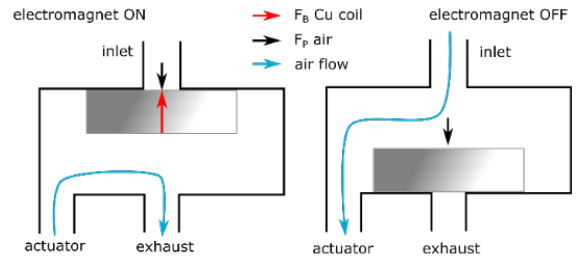


Figure 2: The two states of the valve actuation, allowing to fill and empty the SPA. current on: SPA is deflated. Current off: SPA is inflates.

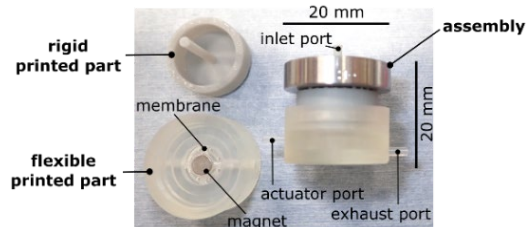


Figure 3: Prototype of printed multi-material soft valve: the rigid element and the flexible printed valve part with an integrated magnet.

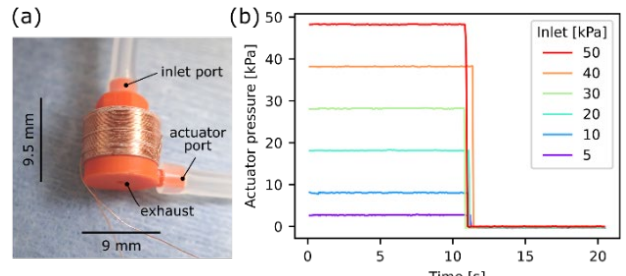


Figure 4: Prototype of printed monolithic valve with integrated magnet. a) the rigid actuator with the assembled coil. b) The plot of the actuator pressure in the open and close states.

Figure 4 shows a second valve with a monolithic design fabricated entirely from a rigid material requiring no assembly.

The magnet is directly integrated into the valve shown in Figure 4a during the fabrication process. Figure 4b shows the response of the SPA to the switching of the valve that can withstand pressures of 50 kPa.

These results show the advantage of 3D-printing in reducing the size and introducing design flexibility in the fabrication of fluidic systems and, in particular, pneumatic valves. In the future, the designs will be further optimized to reduce their footprint and power consumption.

CSEM thanks Innosuisse for the support and funding of this work.

<sup>\*</sup> Reconfigurable Robotics Lab (RRL), EPFL

<sup>[1]</sup> H. A. Sonar, "Interactive soft pneumatic actuator skin", IEEE/RSJ International Conference on Intelligent Robots and Systems, Vancouver, BC, Canada, September 24–28, 2017.

# SURFACE ENGINEERING

Helmut F. Knapp

The Surface Engineering program addresses controlling surface structure and composition (both topographical and chemical) and developing related manufacturing technologies that enable the fabrication of engineered surfaces, at large scales and competitive cost and applicable in an industrial environment. Topographical and chemical properties determine effects such as surface adhesion, wettability and friction, optical reflectivity and color, electrical conductivity, and (bio-) chemical affinity. In addition to elaborating scientific knowledge in the design and understanding of functional surfaces, the Surface Engineering program also develops higher-level integration pathways that enable CSEM to develop components or devices in which surface properties are a critical factor. Solutions for industry can be offered at all levels of this value chain.

Within the program the development and fabrication of nano-structured surfaces and nanoporous films with added functionality is addressed, as is the design and realization of nano-optical components based on nano-engineered surfaces. Furthermore, biochemical functionalized surfaces are developed for their use in (affinity) sensors, as cell and tissue support substrates, and for the development of microfluidic and sample handling instrumentation with improved functionality. Finally, a flexible and broad material and process technology base is established for the printing of components and hybrid systems for the fast and low-cost employment of flexible devices.

In short, the program focuses on research into and the development of engineered surfaces and interfaces by controlling their nano- or micro-structured topography and their surface composition using processes compatible with large-scale manufacturing, in order to design and optimize their (bio-) chemical, optical, and electrical properties to improve the performance of the respective components and integrated devices.

## Long-term objectives

The year 2020 sees the conclusion of the Surface Engineering program in its previous form. Starting in 2021, CSEM reorganized its research activities into the three priorities Precision Manufacturing, Digitalization, and Sustainable Energy, to better address the current needs of industry. These three priorities are each subdivided into "Focus Areas". The three activities of the former Surface Engineering program—that is, *Nano Surface Engineering*, *Bio Surface Engineering*, and *Printable Electronics*—still play a role in the new priority *Precision Manufacturing*. The *Bio Surface Engineering* activity is now more prominently positioned in the shape of the new Focus Area *Tools for Life Sciences*. Many of the optical aspects from the *Nano Surface Engineering* activity are incorporated into the new Focus Area *Photonics*, whereas the non-optical research from this activity makes up a major part of the new Focus Area *Functional Surfaces*. Finally, the *Printed Electronics* activity is incorporated into the new Focus Area *Additive Manufacturing*.

The Surface Engineering program is based on three activities:

The activity ***Nano Surface Engineering*** addresses manufacturing technologies for the cost-effective production of nanostructured surfaces, the development of functional nanocoatings with unique properties, as well as the engineering and production of micro- and nano-photonic components. While the first two topics remain focused on origination and up-scalable replication methods as well as sol-gel materials with controlled porosity and surface functionalization, the last topic has been broadened to encompass the production of small-scale optical components by printing and additive manufacturing. This includes the emerging field of free-form optics.

The activity ***Bio Surface Engineering*** aims to develop tools and integrated solutions for handling and monitoring samples and biological entities for life sciences, clinical diagnostics, and food and environmental monitoring. In biointerfacing, surface functionalization and structuring are optimized for their application in cell supports and other cell-handling components. The topic of biosensors addresses the biochemical sensing of a variety of application-relevant substances by electrochemical and optical methods, for applications in *in vitro* and *in vivo* diagnostics and environmental sensing. Finally, bio-instrumentation is being developed for the handling, treatment, and analysis of biological samples, by optimizing the corresponding liquid actuation and dosing systems, as well as filtration components.

The activity ***Printable Electronics*** addresses the development of materials and processes for the functional printing of layers and structures onto 2D and 3D substrates in order to generate functional components and to combine such printed components with conventional surface-mounted components into fully functional hybrid systems. A particular emphasis is put on flexible substrates and potentially large-scale printing processes including sheet-to-sheet and roll-to-roll printing.

These three activities have strong mutual synergies, including in the development of printed electrochemical sensors that are specifically functionalized for applications in environmental or biochemical sensing and for the development of cell culture supports with optimized surface topography and chemistry and integrated electrochemical sensors for monitoring.

Beyond that, the work carried out in the Surface Engineering program is a critical enabler for several projects in other research programs, including surface treatment for hermetic sealing solutions in functional packaging, the design of novel optical filters and masks that can be directly designed onto vision sensors, or surface roughness optimization in intermediate adsorption layers for increased conversion efficiencies in amorphous silicon PV cells.

## Highlights

The following reports describe some of the work elaborated within the last reporting period in the Surface Engineering program.

Specifically, the *Nano Surface Engineering* activity has progressed in UV imprint technology to produce high-efficiency grating or optical structures made from high-refractive-index materials. Furthermore, it has refined CSEM know-how in the construction of steel tools for injection molding, enabling the production of hierarchical micro/nano structures for the medical and watch industry and for the production of plastic parts with smartphone-readable, scrambled, and pixelated microstructures for part identification or brand protection. In the area of free-form optics, CSEM is building up expertise in design for manufacturing and appropriate characterization methods to efficiently manufacture free-form optical elements. This includes combining quality control data with machine learning methods to improve the actual production process. Finally, CSEM has been working on surface modification to improve the functionality of components in diverse applications. This includes methods for the silver electroless plating of 3D-printed plastic parts for improved RF performance and anti-corrosion properties, methods for the patterning of metal grids on solar cells to improve production costs, or understanding and improving water splitting efficiency on photoelectrodes.

The *Bio Surface Engineering* activity, in the biointerfacing domain, has been working on new materials for replacing PDMS with thermoplasts for industrialization purposes and porous materials for improving the sensitivity of lateral flow assays. Also, CSEM is participating in a European consortium working toward the reliable and reproducible construction of tissues using self-organized organoids. Also, a system for the automated screening of pharmaceutical compounds for musculoskeletal diseases using printed muscle tissues has been realized together with industrial partners. In the biosensors domain, CSEM developed new sensing methods for biomolecular analysis, including sensors based on carbon nanotubes, printed electrochemical sensors, molecular imprinted polymers, or plasmonic principles. Also, a platform for assessing the risks of nanoparticulate matter in a range of application fields was developed.

Last but not least, the *Printed Electronics* activity, as the youngest of the activities in the program, has continued working on inkjet-printed Pt-electrode arrays for in vivo neural recordings and the printing of a pressure-sensitive matrix on a flexible substrate suitable for assessing the wearing comfort of hearing aids or other earpieces.

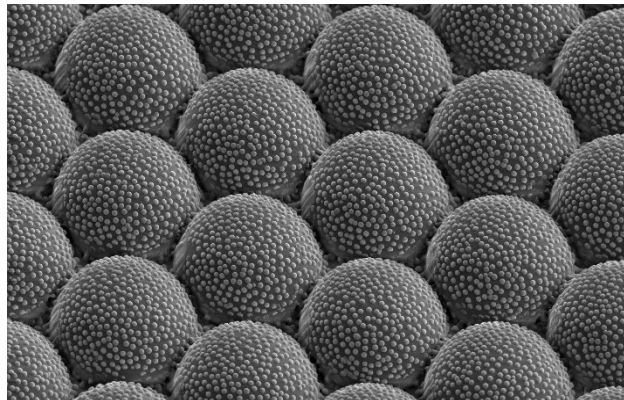


Figure 1: SEM image of the hierarchical surface structure of a self-cleaning plastic surface made using replication techniques.



Figure 2: Prototype device for the electrochemical urine analysis of 1–4 analytes.



Figure 3: Design for a micromirror/micro-prism array for realization by smart, laser-based manufacturing.

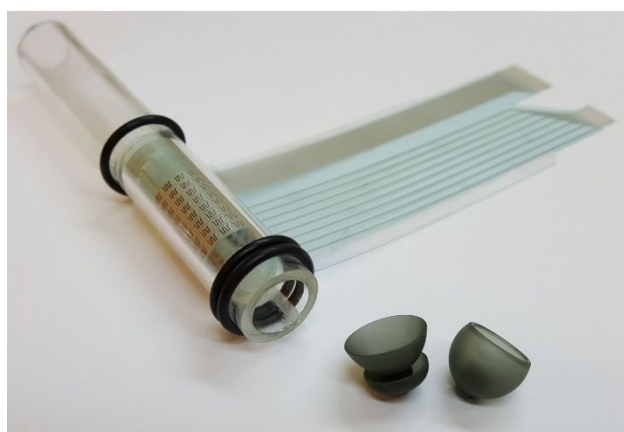


Figure 4: Ear canal model with integrated pressure sensor array for assessing the wearing comfort of earpieces.

# PLASMEX—Plasmonic Structures for Exosome Analysis

L. Driencourt, F. Kurth, F. Lütolf, R. Ferrini, S. Generelli

The clinical relevance of exosome analysis raised a significant demand in sensitive assays for the targeted detection of exosomal cargo and surface markers. This work presents polymer-based, nanostructured substrates for plasmonic signal enhancement and evaluates them for highly sensitive liposome detection using fluorescence microscopy. The presented fabrication strategy, compatible with large scale roll-to-roll-processes, has the potential to translate academic exosome analysis using plasmonic signal enhancement to the clinics.

Exosomes are actively secreted by mammalian cells, are present in nearly all body fluids and are thus optimal for the non-invasive clinical analysis by liquid biopsy. Optical detection of exosomes is however still lacking in sensitivity. Plasmonic structures expand analytical tools for exosome analysis, due to their ability to enhance the to-be-detected optical signal by multiple times [1]. Typical plasmonic substrates like nanohole arrays are fabricated with electron beam lithography, which limits their production scale and turnover for high throughput clinical diagnostics. This study applies for the first time nanostructured plasmonic polymer substrates formed by imprinting followed by gold evaporation for fluorescence enhancement. After further optimization, they have the potential to specifically target exosome fractions and thereby support diagnostics for personalized medicine (Figure 1).

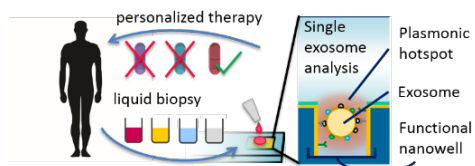


Figure 1: Liposomes are immobilized within the plasmonic field (right). The increased sensitivity can foster future exosome analysis and assist diagnostic devices for personalized therapy (left). A combination of different surface marker antibodies bound on the substrate can facilitate multiplexed analysis.

Gold substrates showing plasmonic near field enhancement were designed and simulated with surface integral equation with periodic boundary conditions [2]. One-dimensional trench patterns were optimized to excite strong near-fields at the maximum absorption or emission of the fluorescent dye DiD.

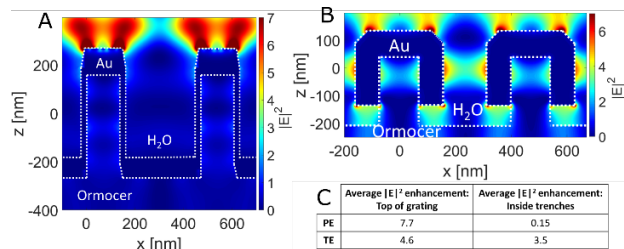


Figure 2: Simulated electric field intensity map for (a) perpendicular evaporation (PE) at  $\lambda = 640$  nm, and (b) tilted evaporation (TE) at  $\lambda = 660$  nm; c) Resulting field enhancement for both configurations.

We studied both nanostructures that can be fabricated with perpendicular (PE) or tilted (TE) gold evaporation. In case of the PE configuration, plasmonic near field focusing occurs only on the top of the grating (Figure 2a, c). In the case of TE, an

[1] H. Im, et al., Nat. Biotechnol. 32, 490-495, 2014.

[2] B. Gallinet, et al., J. Opt. Soc. of Am. A, 27 2261–2271, 2010.

enhancement occurs on the top of the grating and inside the trenches (Figure 2b, c).

The nanostructures were fabricated with UV nanoimprint lithography in Ormocer and subsequent evaporation of gold [3]. Characterization of the final substrates by SEM (Figure 3a) and specular reflectance measurements (Figure 3b) were performed to check the validity of the fabrication process. Liposomes were formed from brain lipid extract and, using sequential extrusion steps with a final pore size of 100 nm, tailored to a final diameter of about 114 nm. Cholesterol-PEG-thiol linkers were used to immobilize the liposomes on the gold substrates. SEM imaging was then used to visualize the immobilization location of the liposomes (Figure 3c).

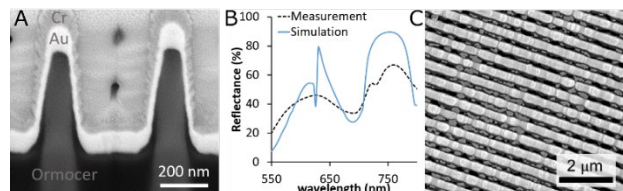


Figure 3: (a) SEM image of the PE-substrate obtained (focused ion beam cross section). (b) Polarized specular reflection of the gold PE-substrate. (c) SEM image of immobilized and fixated liposomes. Partial fusion of liposomes may have occurred during the fixation process.

Fluorescence microscopy (20x magnification) was conducted in two different spectral ranges: (i) R18 emission as negative control, and (ii) DiD as plasmonically-enhanced signal. The dyes R18 and DiD were bound to lipids and could thus be loaded into the liposomes' leaflets prior to imaging. Flat gold substrates served as negative control samples. The tested nanostructured substrates provided a plasmonic enhancement of the fluorescent signal for both design routes (Figure 4). The sample evaporated without angular tilt induced the strongest enhancement, indicating a strong contribution of liposomes located on the ridges.

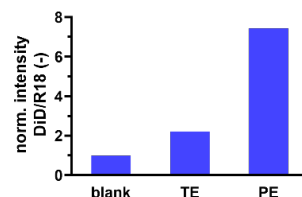


Figure 4: Comparison of the fluorescent ratios of the two tested nanostructured substrates normalized to a flat control substrate (blank).

This work is accepted for publication in ref. [4].

[3] F. Lütolf, et al., Nanoscale, 7, 18779-18187, 2015.

[4] F. Kurth et al., Proc. μTAS 2020, accepted.

# Modelling Optical Effects in Water Splitting Photoelectrodes

L. Driencourt, B. Gallinet, C. E. Housecroft\*, S. Fricke, E. C. Constable\*

In this work, we report a method for analyzing the contributions of optical effects to the incident photon to current efficiency (IPCE) of a water-splitting photoelectrode. The model is validated by comparing with published experimental data. This work will provide the opportunity for researchers to design optical elements for improving the solar to hydrogen (STH) efficiency of photoelectrodes

Hydrogen gas can be converted to electricity with a fuel cell. However, industrial dihydrogen is currently mainly produced in a non-sustainable way, by steam reforming of methane. This factor is so far limiting the use of dihydrogen as a fuel in e.g. transports. Solar water splitting with photoelectrochemical cells (PEC) has the potential of being a competitive and sustainable technology for hydrogen production. In such devices, one or two semiconductor photoelectrodes are immersed in an aqueous electrolyte and serve both as light harvester and catalyst of the water-splitting reaction. Metal oxide semiconductors are promising candidates for practical PEC water splitting thanks to their low cost and inherent stability in aqueous conditions. However, intensive research is still ongoing to develop high performance, inexpensive photoelectrodes that can operate for several years.

Optical effects such as plasmonics or light scattering have been widely studied for improving the STH efficiency of photoelectrodes by modifying the light absorption profile in the semiconductor. However, the distinction between optical and non-optical enhancement is not always clear, e.g. when the optical elements have also a catalytic effect.

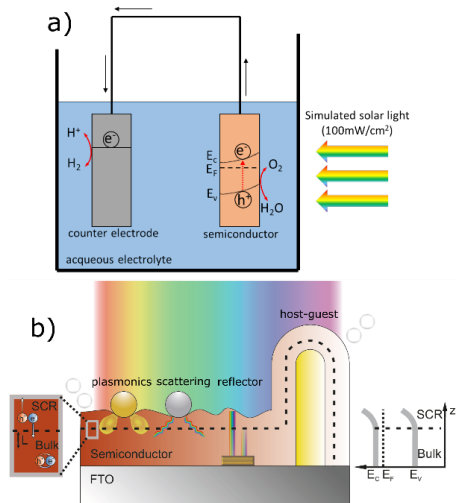


Figure 1: a) Scheme of a photoelectrochemical cell with a single semiconductor photoelectrode. b) Sketch of an illuminated photoanode and various optical effects previously studied for improving the solar-to-hydrogen efficiency. The inset on the left shows that separation between photogenerated electrons and holes can be achieved only in the space charge region (SCR) or close to it with respect to the minority carrier diffusion length.

We developed a numerical model to analyze and optimize the contribution of optical effects in water-splitting photoelectrodes [1]. The method can be applied to analyze various type of optical effects (some examples are shown in Figure 1b). The IPCE or external quantum efficiency (EQE) is modelled and can be compared with experimental measurements. Precise computation of the charge carrier generation power is performed with electromagnetic simulations, whereas the transport and transfer of photogenerated charges are treated semi-analytically, which limits the computational costs while enabling accurate description of the optical effects.

The model was validated by comparison with experimentally fabricated and measured photoelectrodes previously reported. Several metal oxide materials and types of optical elements (e.g. periodic and randomly distributed) were studied to demonstrate the broad scope of the method [1]. In Figure 2, the method is applied to a photoelectrode made of Fluorine-tin oxide (FTO) nanopillars periodically distributed with a square pattern on which a Ti-doped hematite (Ti:Fe<sub>2</sub>O<sub>3</sub>) layer was deposited. The simulated unit cell (Figure 2a) is designed according to the parameters extracted from a SEM image of the fabricated structure [2]. An excellent quantitative agreement between the measurement and the simulations is obtained (Figure 2b), demonstrating the accuracy of the method to describe this system. This shows that EQE enhancement provided by the nanostructured FTO scaffold is purely optical.

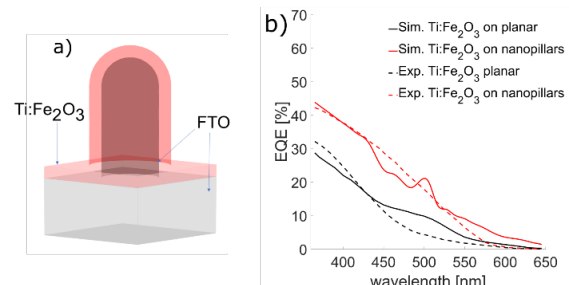


Figure 2: a) Sketch of the simulated unit cell. b) Measured and simulated EQEs for the flat configuration and the nanostructured scaffold.

This framework is therefore a powerful tool to analyze experimental results, as it enables to discriminate between optical and non-optical enhancement and identify the type of optical effect involved. In the future, it could be also used to optimize the optical enhancement in a photoelectrode.

This work was supported by the Swiss Nanoscience Institute PhD School (University of Basel).

\* University of Basel, Department of Chemistry

[1] L. Driencourt, et al., J. Phys. Chem. C, submitted.

[2] Y. Qiu, et al., Nano Letters, 14(4), 2014.

# Molecular Imprinted Polymer as a Sensing Layer for Various Analytes Detection

X. Bulliard, G. Voirin, X. Lefèvre, M. Crenna, M. Palmieri, R. Pugin

*Molecular Imprinted Polymer (MIP) deposited on a specific transducer is used as a sensitive and selective layer for the detection of a wide range of analytes. The different approaches for the fabrication and synthesis of the MIP layer and the compatibility of MIPs with different sensing platforms widen the number of possible targeted analytes and their range of detection. In current developments, MIPs are for example adapted to electro-chemical sensing, optical sensing and sensors based on Quartz Crystal Microbalance. The versatility of the technique broadens its field of applications. Our current researches focus on nicotine, melamine, and trypsin detection.*

Molecular Imprinted Polymer (MIP) is a promising approach for the detection of a wide range of target molecules, for example pollutants, contaminants, toxic gases, or biological markers. The general principle is to expose the MIP starting materials to the target analytes (or another molecule with similar shape and chemical composition). After polymerization, the target analyte is removed leaving cavities in the MIP material with a specific shape, size, and functionalities. The MIP material becomes therefore highly sensitive and selective when re-exposed to the target molecule.

For the MIP preparation, three different routes have been investigated at CSEM: (1) polymerization by heat and UV curing; (2) deposition of preformed nanoparticulate MIP; (3) electrodeposition and polymerization of monomers.

The MIP formation by polymerization is the most common route. In this case, a liquid solution composed of a monomer, crosslinker, solvent, and initiator is mixed with the target molecule. The mixture is deposited on the chosen transducer type, and after reticulation by heat or UV curing, the target molecule is extracted leaving cavities and specific surface chemical functionalities. For nanoparticulate MIP, nanoparticles are synthesized around the target molecules in gas or liquid phase. Here again the target molecule is then extracted. The MIP nanoparticles are collected and for example re-dispersed in a liquid before use. MIP by electrodeposition is an alternative way to polymerization. In this case conductive monomers are used and deposited on an electrode by cyclic voltammetry. This method allows for a precise control of the MIP materials deposited at the surface and hence of its thickness.

The specific MIP fabrication route and the choice of the transducer on which it is deposited depends on the target molecules. Currently three different transducer types are considered at CSEM: (1) Electrodes (electrochemical detection); (2) Quartz Crystal Microbalances (QCM); (3) Optical detection by WIOS (Wavelength Interrogated Optical Sensing).

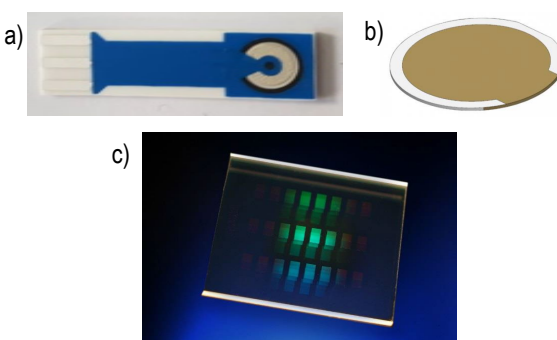


Figure 1: Three different transducers, on which the MIP layer can be deposited: a) electrode, b) gold QCM, and c) waveguide grating chip of the WIOS system.

For electrochemistry, electrodes composed of an active area, a working electrode, and a counter electrode are used (Figure 1a).

The MIP is deposited on the active area and signal changes are detected by Differential Pulse Voltammetry or Cyclic Voltammetry when the MIP layer is exposed to the target analyte. For QCM, a change in the properties of the deposited layer (i.e. its mass, density or the physical stress it exerts on the quartz crystals) is detected when the target analyte re-binds the selective MIP cavity (Figure 1b). Finally, WIOS is an optical MEMS device comprising a grated optical waveguide, on which the MIP layer is deposited. The system monitors the refractive index changes on top of the waveguide grating when the MIP layer comes into contact to the target molecule.

For electrochemical and optical detection, a thin MIP layer of a few 10ths of nanometer should be deposited on precise areas of the transducers. Pico Pulse Jetting composed of a piezo-actuated head of 100 µm can be used for that purpose. In the case of QCM, the amount of MIP should be larger and other dispensing techniques can be used.

In our research, the following molecules are tested as target analytes: nicotine, melamine, and trypsin. Figure 2 shows an example of detection of nicotine by electrochemistry using Fe(II)/Fe(III) as probe. Electrodes were functionalized by electrodeposition or by UV curing of a MIP layer deposited by picojet. Detection of nicotine on WIOS and QCM has also been confirmed.

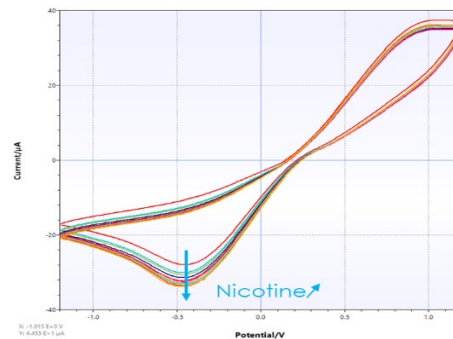


Figure 2: Detection of nicotine by MIP deposited on electrode.

For melamine and trypsin, QCMs have been chosen as transducer. In the case of trypsin, MIP nanoparticles are first synthesized and then deposited on the QCM by chemical grafting as a layer. As the layer can be quite thin, a relatively large molecule (trypsin for instance) is needed for the detection.

In summary, MIP can be adapted to a wide range of different transducers and detection platforms. The number of applications that can benefit of this approach is thus large, and comprises fields as wide as biomedicine, environment, chemical monitoring, and safety.

# Micro-nanostructuring of 3D Surfaces: on the Manufacturing of Functional Parts for the Medical and Watchmaking Industry

N. Blondiaux, M. Crenna, P. F. Chauvy\*, M. Diserens\*, B. Oudot\*\*, R. Pugin

We report on the main results of the Harissa project, which focused on the development of processes for the manufacturing of functional 3D plastic parts by injection molding. Steel surface structuring and injection molding processes have been optimized for the manufacturing of four demonstrators presenting unique properties based on surface micro-nanostructures.

The development of novel functionalities on plastic parts has been fostered during the last decade by the emergence of new micro- and nano-fabrication processes compatible with replication techniques. Several examples of planar devices embedding surface micro-nanostructures have been produced on an industrial scale in various fields of applications. However, one critical limitation to expand potential applications remains the processing of 3D surfaces, as it is the case for most injection-molded part.

In 2020, CSEM has completed the transnational Interreg project Harissa, which involved French and Swiss companies and research centers. This project focused on the development of new technologies for the manufacturing of functional 3D plastic parts by means of injection molding. The two major technical challenges that have been addressed were:

- The development of processes for the surface micro and nano structuring of 3D steel mold inserts (3D shapes, hierarchical structures) based on nanosphere lithography, laser ablation and electrochemical etching.
- The optimization of the injection molding process via the integration of new demolding concepts and the development of an injection compression module.



Figure 1: Photograph of a steel injection mold insert presenting 3 levels of surface structuring (dynamic optical effect: guilloche pattern & optically variable microstructure, opalescence: nanostructure).

To show the potential of the technologies developed, four industrial case studies were considered. The first focused on the manufacturing of watch magnifying glasses microstructured for customization purposes. Specific dynamic optical effects based on microstructures were designed and engraved on curved sections of the mold inserts and the elastomer part was injection molded (see Figure 2 right). In the same field of application, another demonstrator was a watch dial with tailored aesthetics (corresponding injection mold insert presented in Figure 1). In this demonstrator, the challenge was to fabricate surface nanostructures on a guilloche pattern presenting slanted

sidewalls at the milli and micrometer scale (3D microstructure). The resulting hierarchical structure leads to dynamic optical effects from the guilloche pattern and microstructure, superposed with an opalescence arising from the nanostructure. The third case study concerned the development of a medical device. The goal was here to replace the use of silicone oil lubrication by integrating surface nanostructures on the part. A real challenge addressed was the surface structuring of a large 3D part (150 mm long cylinder). As shown in Figure 2, the area treated on the mold insert was homogeneously structured.



Figure 2: (left) Photograph of the nanostructured steel insert of the biomedical device; (right) photograph of the injection molded microstructured watch magnifying glass.

The last case study focused on the development of self-cleaning surfaces based on the manufacturing of hierarchical surface structures. In this approach inspired by nature (lotus leaves), surface nanostructures were superposed on arrays of micro hemispheres (Figure 3), which allowed the manufacturing of superhydrophobic self-cleaning plastic surfaces made using replication techniques.

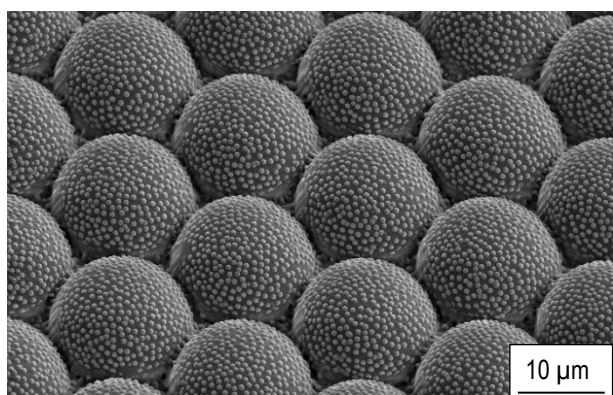


Figure 3: SEM image of the hierarchical surface structure of a self-cleaning plastic surface.

Harissa project has been supported by the Interreg France-Suisse 2014-2020 and funded by the European Regional Development Fund, and on the Swiss side by the OFES, the cantons of Neuchâtel, Bern and Vaud. CSEM thanks them for their support.

\* Micropat SA, Suisse, Renens, [www.micropat.ch](http://www.micropat.ch)

\*\* DNA plasturgie SARL, Suisse, Bienne

# Imprint of High Refractive Index Micro- and Nano-optical Structures

A. Luu-Dinh, F. Lütolf, F. Herzog, R. Krähenbühl, R. Ferrini, B. Gallinet

Materials for UV imprint lithography with refractive index ranging between 1.7 and 1.9 as well as related processes are reported. Such materials are recognized to have high potential for augmented reality applications as well as for on-chip replicated optical elements such as beam collimating microlenses on micro-LED or VCSEL arrays. Here, a diffractive waveguide combiner for augmented reality headsets is demonstrated.

High refractive index (HRI) materials for UV micro- and nano-imprint Lithography have a huge market potential for the manufacturing of micro-/nano-optical components for several application domains, notably for augmented/mixed reality (AR/MR) devices, whose market is foreseen to grow at high rate in the next few years. Aim of this project is to overcome these barriers for mass adoption of this manufacturing platform in order to bring it closer to industrial uptake by developing industrially validated UV imprint materials, formulations and processes for the fabrication of micro and nano-optical components with refractive indexes between 1.7 and 2.0 for AR/MR. Figure 1 shows a standard UV nanoimprint process which replicates the structure from a mold into a UV curable material. The mold can be fabricated using a variety of approaches, such as laser interference lithography or electron beam lithography. In this work, we developed a Ti-based hybrid polymer material for UV imprint on microlens arrays and diffractive gratings. This approach does not require a solvent formulation, thus enabling high residual layer thicknesses (so far up to 100  $\mu\text{m}$ ).

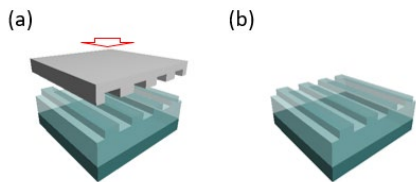


Figure 1: UV imprint process. a) A stamp is used to replicate micro- or nanostructures in a UV curable hybrid polymer. b) Structure after the stamp release.

After curing, the refractive index of the imprinted material was measured to be in the order of 1.75 in the visible range. This latter value can be further increased by applying calcination. While this process can induce shrinkage of the imprinted structures, we were able to limit this effect to less than 10% for a calcination temperature of 200°C with a significant increase of the refractive index up to 1.85-1.9. Higher temperatures have been tested, yielding a refractive index value up to 1.96. Figure 2 shows scanning electron micrographs of replicated micro- and nano-structures.

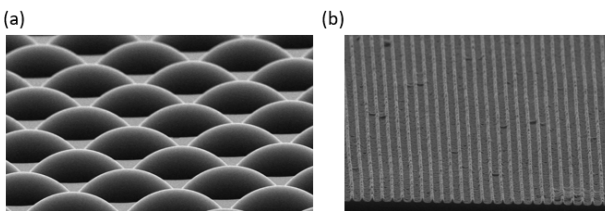


Figure 2: (a) Replicated microlenses with a refractive index of 1.7. (b) Replicated nano-gratings with refractive index in the order of 1.7-1.9 depending on the calcination temperature (here 200°C).

The materials and processes described above were applied for the fabrication of a diffractive waveguide system for AR (Figure 3a). Light projected by a miniaturized light engine is incoupled by a diffraction grating into a glass slab of refractive index 1.7. It is then outcoupled by another diffraction grating to reach the eye. The projected image is overlaid with the background, yielding an augmented reality experience for the user (Figure 3). In such a waveguide combiner, the field of view of the projected image that can be guided is directly determined by the refractive index of the waveguide. It is therefore of prime importance to increase it, while keeping the other optical performances (e.g. efficiency, light scattering) within the required device specifications.

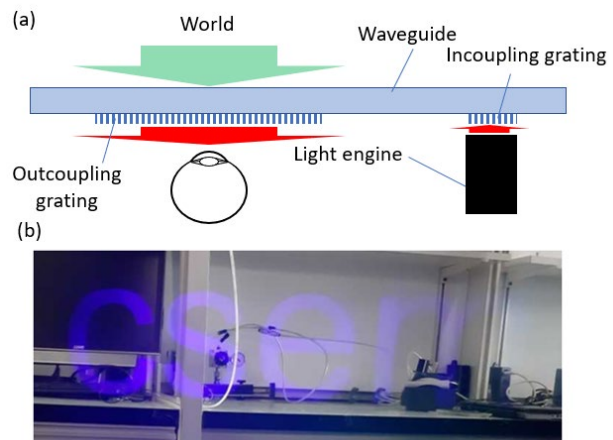


Figure 3: a) Functioning principle of a diffractive waveguide combiner for augmented reality. b) Image projected through the combiner and superimposed to the surrounding environment.

The gratings are imprinted on the waveguide substrate, and the incoupling grating is coated with a thin dielectric film to increase its efficiency [1]. In order to guarantee the incoupling of a full image in the waveguide, the refractive index of the imprint material must be matched with the one of the waveguide. Figure 3b shows a blue monochromatic picture projected through the waveguide and observed through the outcoupling grating. The projected image appears on the background.

In conclusion, solvent-free materials and processes have been developed for UV imprint lithography of micro- and nano-structures with a refractive index ranging between 1.7 and 1.9 in the visible range. A diffractive waveguide combiner with a refractive index of 1.7 and a field of view of 40° was fabricated. The fabrication of a diffractive waveguide combiner with a refractive index of 1.9 is planned as a next step in order to reach higher field of views. In particular, applications are foreseen in diffractive waveguides for augmented reality, as well as beam collimating microlenses for micro-LED or VCSEL arrays.

Funding from Innosuisse 38832.1 IP-ENG is gratefully acknowledged.

[1] F. Lütolf, et al., Optics Letters vol. 39, pp.6557-6560 (2014).

# Smartphone Readable Digital Scrambled Pixelated Microstructures for Part Identification and Brand Protection

R. Krähenbühl, D. Kallweit, C. Schneider, M. Schnieper

To prove the origin of products and to prevent them from being counterfeited, we developed pixelated (QR-code like) ordinary pictures incorporating copy-safe microstructures readable with a unique smartphone software application (app). Fabricated samples (embossed and injection molded) using steel tools incorporating diffractive optical elements (nanostructures in complex arrangements) showed good decoding and beam-shaping performance (projection of logos) for various colored PMMA and glass materials.

To allow a unique identification, steel tools (stamps, injection molding inserts) with appropriate scrambled pixelated picture designs were micro- and nanostructured. In parallel the distinct smartphone application that can read and decode such scrambled digital pictures was programmed and implemented. Finally, the transfer process of these tools into plastic (Figure 1) and glass material was developed and made ready for the industrialization.

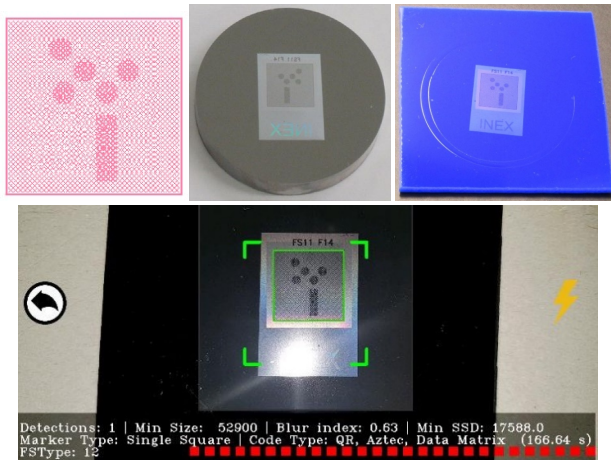


Figure 1: Pixelated picture design with logo, corresponding steel tool, a hot-embossed blue PMMA sample (from left to right), as well as the related excellent (blur index >>0.1) app-decoding (bottom).

To reach good pixel contrast ratios, different concepts of micro- and even nanostructures were considered, simulated, and evaluated (Figure 2). Among others, such as small (270 nm) and large (1900 nm) period gratings, Diffractive Optical Elements (DOEs) made of nanostructures in complex arrangements were found as best suited.

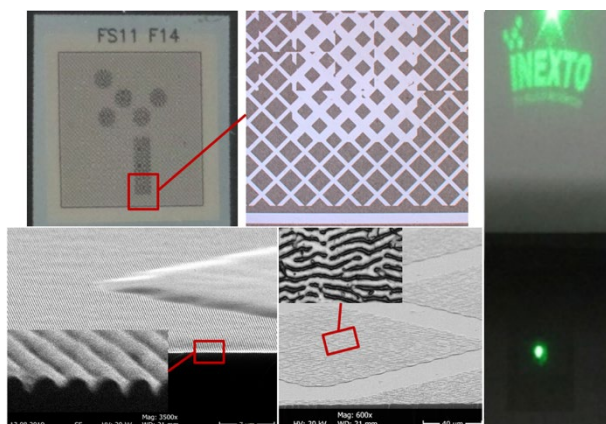


Figure 2: Photograph of the pixelated picture of a hot embossed sample (top left), microscope picture of a section (top middle), the SEM of a grating (bottom left) and a DOE nanostructure (bottom middle) responsible for the contrast enhancement. On the right: corresponding projection of the logo.

These DOE structures add a 2<sup>nd</sup> level in security feature, as they are capable to create output pattern with unique shapes and functionalities, such as projecting the INEXTO logo (Figure 2, right) onto a wall.

Evaluation of the reading performance proved, that samples embossed in different PMMA colors (except white) were good, and reasonably fast decodable with the smartphone at 5 to 15 cm distances and at angles between 0 and 20 degrees, thereby successfully fulfilling the targeted requirements.

To prove the industrialization, steel tool inserts were realized, and injection molding runs carried out (Figure 3 left).

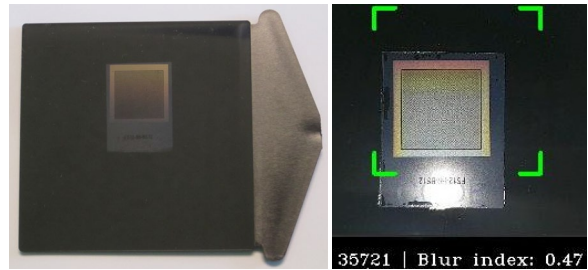


Figure 3: One of the injection molded samples (left), as well as the related excellent (blur index >>0.1) app-decoding.

The smartphone readability (Figure 3 right) showed no measurable degradation for the over 500 produced samples. This was expected, as injection molding using structured steel tools typically allows producing several hundreds of thousands up to over two million pieces (depending on the process and material).

Finally, the above DOE based picture was used to develop the transfer process into glass. Several decodable pictures on glass wafers were produced (Figure 4).

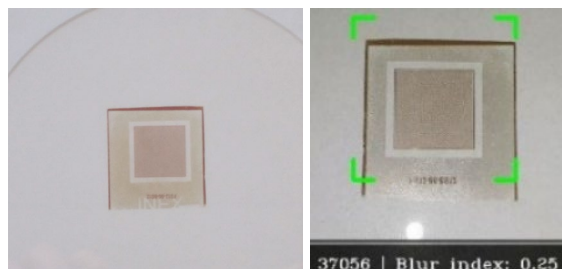


Figure 4: One of the pictures incorporating DOE nanostructures transferred to a glass wafer (left), as well as the related good (blur index >>0.1) app-decoding.

With this new technology platform, Inexto will be able to address new markets with innovative products, increase revenue and create jobs throughout the whole value chain.

The authors would like to thank INEXTO and Innosuisse for their financial support (PhoMiPro\_34956.1 IP-ENG).

# High-efficiency Gratings at 1.55 μm Fabricated by UV Imprint

F. Lütolf, F. Herzog, I. Zhurinsky, J. Disser, G. Basset, R. Ferrini

*High-efficiency gratings are used as building blocks in many classical and emerging optical applications like spectrometers, photonic integrated circuits, lasers, etc. Unfortunately, high efficiencies usually require very accurate shape control and can only be achieved for deep gratings and/or specific coatings. We present high-efficiency gratings fabricated by UV imprint, which achieve 92% first order transmittance in Littrow configuration at 1.55 μm.*

In the photonic community, gratings are well-known commodities produced by several specialized companies around the world. State-of-the-art transmission gratings can achieve efficiencies in the range of 97% or higher, but they can be very expensive. The main driver for their cost is the elaborate and time-consuming manufacturing process as well as the often relatively low yield. The most common fabrication process relies on holographic recording of a grating in a photoresist and subsequent transfer of the structure into a robust material (e.g. quartz) by plasma etching. Any inaccuracy in this process directly affects the grating efficiency. Finally, the glass interface typically reflects >4% of any incoming light, which diminishes the efficiency. The industry standard to reduce the reflection is the evaporation of a multilayer of high- and low-refractive index coatings. This process is again delicate and prone to manufacturing inhomogeneities.

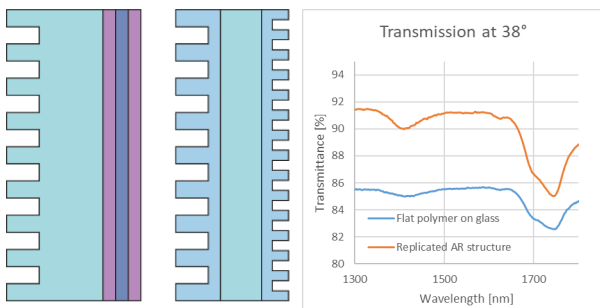


Figure 1: Sketches of a state-of-the-art grating composition (left) and the layout of our high-efficiency grating developed in the framework of the NanoArgovia project "UltraNanoGRACO" (center) together with (right) the optical performance of a replicated anti-reflective structure.

In the framework of the NanoArgovia project "UltraNanoGRACO", we developed and fabricated high-efficiency gratings using UV imprint, a polymer-based replication process mastered at CSEM for micro- and nano-structuring. The process is precise, reliable, cost-efficient and hence well-suited for the manufacturing of such gratings. Figure 1 compares the layout of a typical state-of-the-art grating (left) to our solution (center). First, the anti-reflective (AR) multilayer coating on the backside was replaced by an anti-reflective nanostructure. AR structures can easily be replicated as they usually do not require deep shapes. Here, a 2-D "egg-box" shaped nanostructure was used (Figure 2a, blue box). The structure enables a 5-6% increase in transmittance in the final illumination geometry when compared to a glass coated with a flat polymer layer (38° angle of incidence and TE polarized light). Note that the polymer does not show any significant absorption bands in the 1.55 μm wavelength range. The refractive index of the glass substrate was chosen to match the one of the polymer in order to avoid reflections at their interfaces.

The design of the high-diffraction grating is similar to state-of-the-art gratings. The challenge resides in the combination of suitable materials and replication processes that must reach the high aspect-ratio (height of a structure in comparison to its width) required for obtaining high diffraction efficiencies. This necessitates a specific mold material that is neither too rigid (i.e. impossible to demold) nor too soft (i.e. the structures could

collapse). Gratings with >2 μm depth, 1.25 μm period, and an aspect ratio above 3 were directly replicated with the semi-soft mold on a 5-inch wafer area. An aspect ratio of 3 was determined to be the best compromise in terms of diffraction efficiency and manufacturing yield. To reach higher aspect ratios (e.g. 4-5), the process would require additional development and testing.

An alternative manufacturing process was developed to further improve the diffraction efficiency while still avoiding the repetition of the challenging holography step for each produced grating. It consists in replicating a lower aspect ratio grating and subsequently etching it to the desired depth in the polymer instead of using a deep mold, which would bring challenges e.g. in demolding. This process is still very reliable due to the very accurate combination of replication and etching, while offering two major advantages at the expense of an additional etching step: First, the replication process becomes much easier and could even rely on standard master materials instead of the semi-soft stamp. Second, much higher aspect ratios can be achieved through this process: an aspect ratio in the order of 4.5 was eventually achieved on an entire 5" wafer (Figure 2a & b).

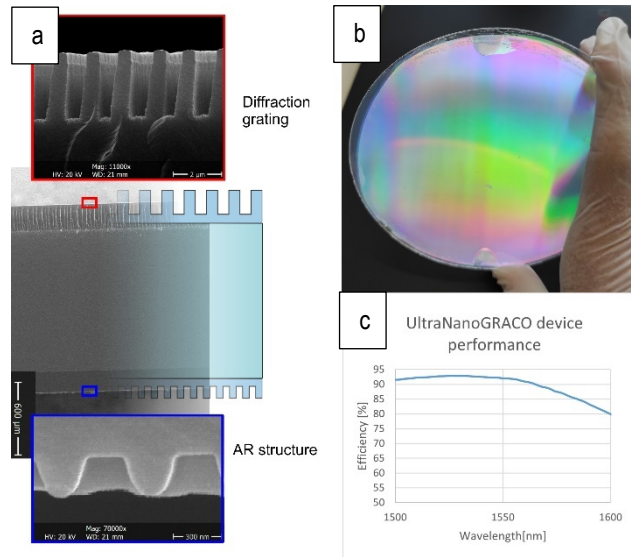


Figure 2: a) SEM images of the full device with zooms on the main grating (red) and the anti-reflective structure (blue); b) Picture of the structures fabricated on a full 5-inch wafer; c) Final device's optical performance.

After application of the AR nanostructure, an efficiency of 92% was measured (Figure 2c), a value very close to the maximum efficiency of 97% that was simulated for the binary geometry. Note that, while the grating master structures still need to be fabricated with standard processes like holography, it needs to be done only once for a full production batch.

Funding from Nano Argovia for the project 14.19 "UltraNanoGRACO" together with FHNW and Menhir Photonics AG is gratefully acknowledged.

# Freeform Micro Optics: Design, Manufacturing, Characterization

O. Fernandez, T. Aderneuer, T. Offermans, R. Ferrini

The successful manufacturing of freeform micro-optical solutions demands for advanced design analysis. Specifically, the format conversion from point clouds or polygon meshes or from analytical expressions to CAD standard NURBS surface description as well as for accurate surface benchmark against manufacturing limitations. On the other hand, the surface profile of the manufactured freeform microlens arrays, FMLAs, needs to be compared to the nominal designs, for which it needs to be precisely measured. In the framework of the PHABULOU $\mu$ S Pilot-Line, CSEM is developing design-for-manufacturing tools and exploring innovative surface characterization strategies and technologies.

Freeform microlens arrays, FMLAs, combine the design freedom offered by non-symmetric (aka freeform) optical surfaces with the microscopic nature of microlens arrays. In the last years, several FMLA-based solutions have been proposed that predict new functionalities or substantial performance boosts, thereby raising a considerable scientific and industrial interest. However, their demonstration in real devices is rather infrequent due to the severe manufacturing limitations. The PHABULOU $\mu$ S Pilot-line will prove highly advanced & robust manufacturing technologies for optical free-form micro-structures.

**Design kits for manufacturing** - In the initial phase CSEM has focussed on developing design-for-manufacturing tools to a) validate customer optical designs for manufacturability, b) quantify expected manufacturing deviations and c) predict the associated performance degradation. Such tools will enable customers to de-risk decisions and the Pilot Line to speed up the manufacturing process.

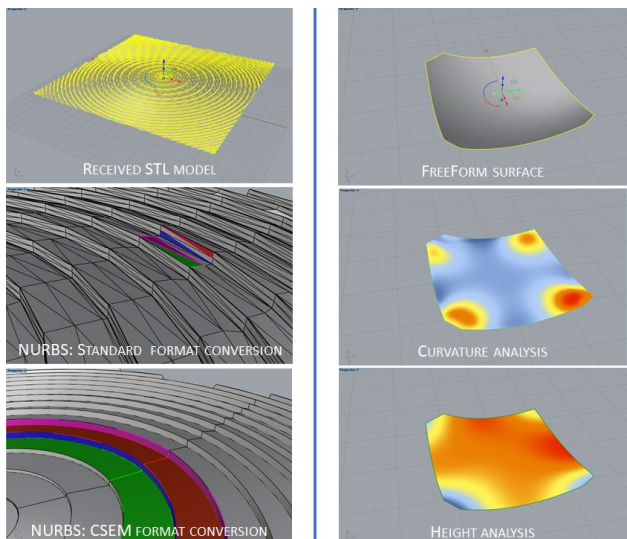


Figure 1: Example of an STL-to-NURBS conversion by CSEM (left). Example of a NURBS surface analysis by CSEM (right).

a) Surface representation is an important aspect of the design and manufacturing of FMLAs. Whereas point clouds and polynomials are widely used in the design phase, NURBS (Non-Rational Radial B-Splines) is standard in CAD/CAM and optical simulation tools. This asymmetry demands for efficient and accurate conversion tools. CSEM is developing such tools which, contrary to standard approaches, can identify the (manufacturing) relevant features (Figure 1; left).

b) Surface analysis is an important tool to quickly assess the manufacturability of nominal FMLA designs. Combining commercial CAD software tools and custom-made scripts CSEM can extract relevant properties of the FMLAs including, but not limited to, height and/or surface curvature maps (Figure 1; right).

**Characterization:** The manufactured FMLAs must be characterized to assess their compliance to customer

specifications. CSEM has recently developed a characterization method based on ray-traceable 3D CAD models of the manufactured FMLAs (see our article *Customized Illumination enabled by Freeform Optics* in this report). Such models are based on accurately recorded FMLA surface profile using e.g. Confocal Laser Scanning, White Light Interferometry, Atomic Force microscopy, etc. (Figure 2).

However, these instruments have limitations with steep angles. SEM, with much better resolution is an interesting alternative especially with 3D surface reconstruction algorithms.

CSEM's preliminary results with such tools show that they are not yet sufficiently developed for the purpose in question (Figure 3).



Figure 2: 3D profile of CSEM micro-pyramid using a Keyence VK-1100 confocal microscope.

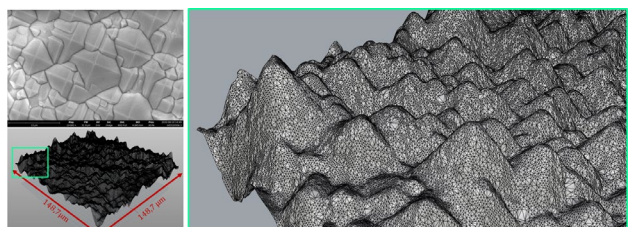


Figure 3: SEM picture (top left) and extracted 3D profiles (bottom left and right) of CSEM micro-pyramids using a ThermoFisher PHENOM GL2 SEM microscope with 4-quadrant surface reconstruction capabilities.

## Acknowledgements

This project has received funding from the European Union's Horizon 2020 research and innovation programme under grant agreement No 871710, project PHABULOU $\mu$ S. For more information visit [www.phabulous.eu](http://www.phabulous.eu).



PHOTONICS PUBLIC PRIVATE PARTNERSHIP

[www.photonics21.org](http://www.photonics21.org)



# Freeform Microlenses for High-quality Lighting

T. Aderneuer, O. Fernandez, R. Ferrini

Freeform micro-optical structures are designed with no symmetry constraints to increase design freedom and ultimately to effectively achieve non-symmetrical light distributions. As a flip side, the additional complexity introduces additional manufacturing and characterization challenges. Here we focus on the latter and report on preliminary results towards standardizing characterization procedures for freeform microlens arrays.

Freeform micro-optical components have recently raised considerable scientific and industrial interest. On the one hand, they enable optical systems with lower number of components, smaller size, improved optical performance and higher efficiency. On the other hand, freeform microlens arrays can foster system miniaturization even further and are compatible with large area manufacturing.

However, new fabrication technologies are required to originate such complex freeform micro-structures as standard processes used for microlens arrays (e.g. thermal reflow) cannot be applied due to the non-rotational symmetric shape of the targeted freeform micro-optical elements.

On the other hand, characterization methods are also necessary that can assess the quality of the manufactured components both in terms of the (micrometer level) form accuracy and the (nanometer level) surface roughness, both paramount for the optical performance. The characterization of freeform microlens arrays is not yet standardized. A main objective of CSEM in the domain of freeform micro-optics is to propose characterization methods that can eventually be adopted by the freeform microlens community.

Here we report on preliminary results in this activity exemplified by means of two commercially available freeform microlens arrays based on: a) de-glaring micropyramids (Polyscale GmbH & Co. KG) and a randomized freeform microlenses (Thorlabs EDS50).

**Manufacturing.** Two-photon absorption (TPA) is a tool free, laser-based technology with writing resolution of ca. 0.1 micron. It is compatible with the manufacturing of complexly shaped freeform microstructures.

The two selected freeform microstructures were manufactured using TPA (by INKA) and compared to their commercial counterparts.

**Form accuracy.** The surface topology of the TPA microstructures was characterized with a confocal laser microscope (Keyence VK-1100). Confocal microscopes provide high resolution and sufficient field of view (to capture complete microfeatures). Despite the writing parameters were optimized for maximum form accuracy, differences between the TPA samples and the commercial counterparts can be easily spotted (see Figure 1).

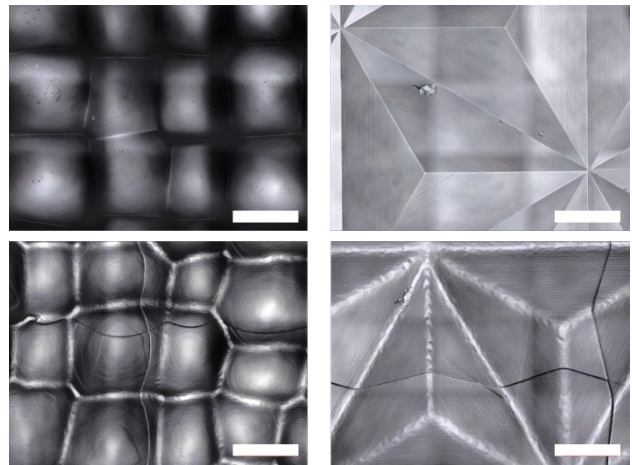


Figure 1: Surface characterization with confocal laser microscope of left: a micro-optical diffuser (curved shapes) and right: de-glaring film (pyramid shapes). All images show measurements obtained with a 150x magnification objective. (scale bars 50 µm). The upper images show the commercial samples and lower ones the samples fabricated by TPA.

**Surface roughness.** Less evident from Figure 2 is the surface quality. Indeed, confocal laser microscopy does not provide the lateral resolution required for roughness characterization (nanometer resolution) and Atomic Force Microscopy (AFM) was used instead.

All corners and multiple center locations were (AFM) measured to ensure a broad distribution and therefore a representative evaluation of the complete surface. The AFM results on the TPA samples indicate a surface roughness of  $S_a < 10 \text{ nm}$  (profile roughness defined by Ra (ISO 4287), and areal roughness by Sa (ISO25178)).

**Conclusion.** The combination of two different technologies for the characterization of freeform microlens arrays in the micro- and nano-scale domain allows an easy identification of form deviations and surface quality of manufactured samples.

Moreover, by selecting representative areas of the sample, time-consuming inspection of the complete area can be avoided, while still capturing sufficient information on the surface topology and quality, a first step towards standardization.

**Acknowledgements.** This work was done in the framework of the Innosuisse project 30049.1 together with the Fachhochschule Nordwestschweiz, School of Engineering Institute of Polymer Nanotechnology (INKA).

# Smart Laser-based Manufacturing for Precision Industry 4.0

D. Kallweit, R. Ferrini

In the Innosuisse Impulse project Smart Laser Manufacturing for precision industry 4.0 (SLAM 4.0), the combination of highly configurable ultra-short pulse (USP) laser source, online optical quality inspection and machine learning will allow the acceleration of the process optimization and manufacturing cycles, thus enabling more flexibility and ensuring the highest level of product quality. CSEM participates in the development of the USP laser and supplies the design of freeform optical elements and micro-mirror / prism arrays for lighting applications, where the limits and peculiarities of the manufacturing processes are considered or compensated.

When it comes to generating arbitrary (non-symmetric) light distribution, standard components such as lenses, mirrors, etc. quickly reach their limits. Diffractive optical elements (DOEs) such as computer-generated holograms are in principle able to virtually generate any type of light distribution, but are limited to monochromatic, partially coherent light. Micro-mirror / -prism arrays are not subject to these restrictions since they are not based on the principle of refraction instead of diffraction. However, their fabrication is currently not straightforward, since precisely aligned 3D micrometer structures must be originated. This is due to the fact that the projection angles of the individual image points are not given by the diffraction angle, but by the tilt angle of the micro-mirror/ prism surfaces.

As a first test case, a 20x20 array of tilted and in-plane rotated 500 µm micro-prisms was designed. A 3D sketch is shown in Figure 1.



Figure 1: Designed micro-mirror / micro-prism array.

Since the number of array elements was limited in this first test structure, a simple target projection was used. Figure 2 shows the simulated projection of such a micro-prism array working in transmission at 532 nm. The design is based on collimated light but can also handle divergent light sources.

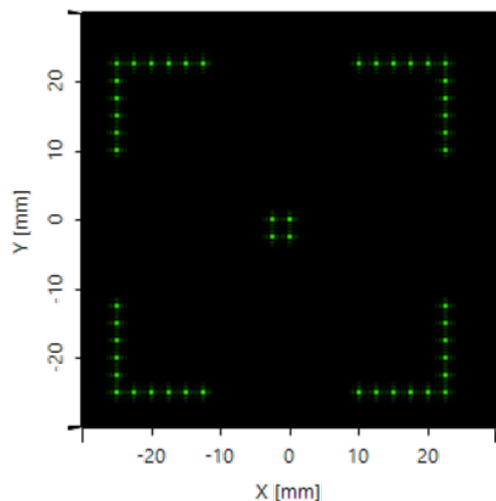


Figure 2: Target projection of the 20x20 micro-prism array.

To realize more sophisticated projections, a design with 100x100 (and more) optical elements were also made. The result of such a design, when illuminated with white light, is shown in Figure 3.

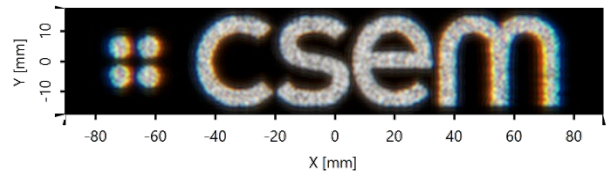


Figure 3: Projection of the CSEM logo with white light.

Based on this first design, a steel master was manufactured by at the Bern University of Applied Sciences (see Figure 4).

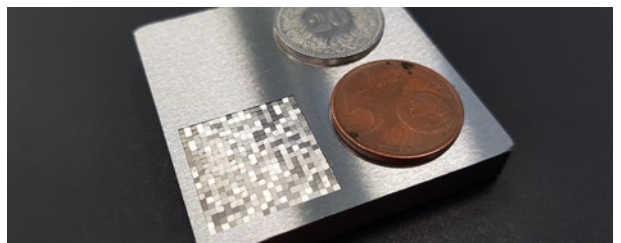


Figure 4: Fabricated steel master with the designed micro-prism array.

Limitations of the laser process such as maximum tilt angle or the minimum size of the individual array elements can also be considered in the design process.

In order to test the usability of the steel master for manufacturing, a replica was made by UV casting (see Figure 5), while in the future such test masters will be also tested with injection molding. The evaluation and optimization of the laser process is still in progress.

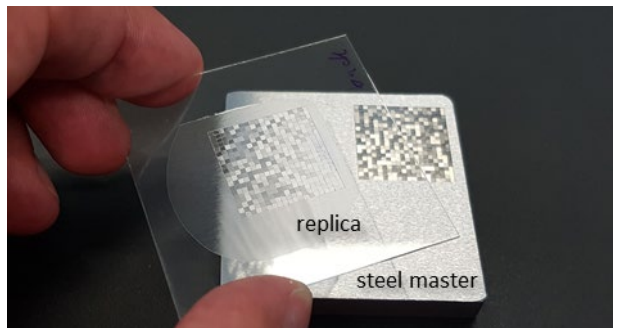


Figure 5: Photograph of the master and the replica on glass.

The first samples produced are currently being characterized and the production process is refined (exactness of the angles, surface quality, size and number of array elements). The optical structures made in steel will ultimately be replicated using injection molding.

The authors acknowledge Innosuisse for the financial support of this project (SLAM 4.0, no. 35148.1 IP-ENG).

# Silver Electroless Coating of 3D-Printed Parts

G. Andreatta, A. Grivel, P. Blanc\*, M. Billod\*

The industry standard for radiofrequency (RF) products in the aerospace industry are aluminum machined parts combined with silver electroplating to ensure high RF performance and anti-corrosion properties. However, the shape of RF products usually contain a large amount of internal cavities that cannot be machined into one piece and are hence split into a large number of sub-components that are produced separately and then silver plated through galvanic processes. Additive manufacturing done at SWISSto12 allows for the building of such complex internal cavity products in one piece, thereby not necessitating assemblies. This feature offers great advantage in terms of the reduction of number of parts, the performance, and the weight of the products. But this technology is not compatible with galvanic silver plating processes. CSEM and SWISSto12 are developing jointly an electroless silver coating process which is tailored to the 3D-printed materials used in SWISSto12 products.

SWISSto12 pioneers the development and industrial supply of radiofrequency (RF) antenna, waveguide and filter products based on additive manufacturing (AM), also known as 3D-printing. This approach gives SWISSto12 products unique benefits such as flexibility of design, reduced waste, reduced lead times and low weight, the latter being critical in the aeronautics and space industries.

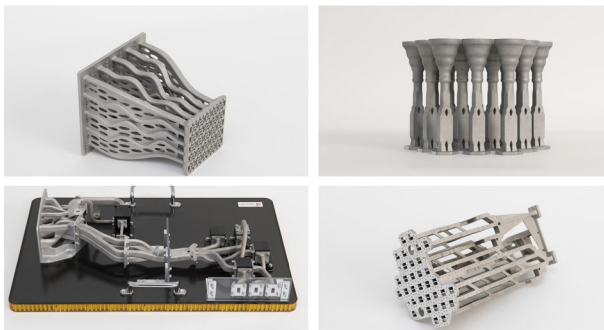


Figure 1: 3D printed RF designs by SWISSto12.

Once the design is fixed and the products are 3D-printed out of advanced polymers or lightweight metals, their surface must be treated by metal plating. There are various methods of plating known in the art, including electroplating and electroless plating. Using electroless plating over electroplating gives the ability of plating a uniform metallic coating onto a substrate having an irregular shape. Electroless plating involves the deposition of a metallic coating from an aqueous bath onto a substrate by a controlled chemical reduction reaction which is autocatalyzed at the surface once the process is initiated. Unfortunately, current standard electroless plating of silver is not a commercially available process due to its lack of stability.

The bath composition was first determined on plastic substrates with a palladium-based catalyst. The bath is stable for several hours and depending on the bath conditions, up to 10 µm of silver could be deposited conformally onto the substrate with high crystallinity. Figure 2 shows the effect of the bath temperature on the silver deposition. The stability of both 30°C and 50°C baths was several hours.

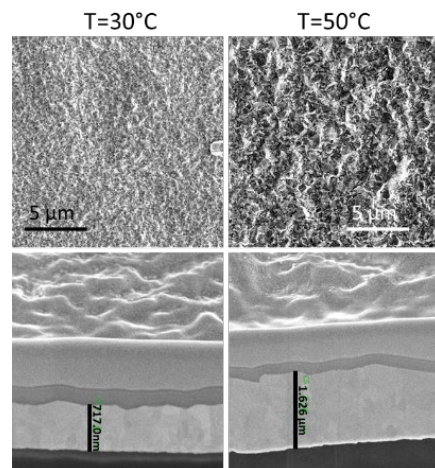


Figure 2: Silver metal deposited by electroless plating on polyethylene surfaces. Top two images are scanning electron micrographs and bottom pictures show cross sections of the silver layers.

The same process was then applied to surfaces obtained by selective laser melting (SLM) 3D-printing process at SWISSto12. The SLM surface is significantly rougher than that of the plastic samples used for optimization, yet a highly conformal silver layer was obtained.

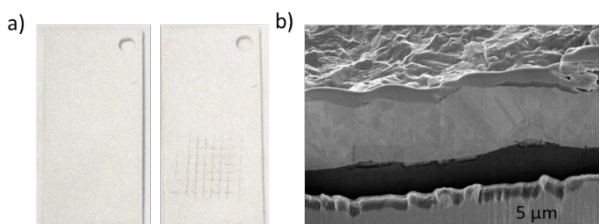


Figure 3: Silver metal deposited by electroless plating on SLM surfaces after a chemical polishing treatment; a) adhesion test of the silver layer and b) cross-section of the silver layer showing its polycrystallinity and conformality to the surface.

The process was then adapted to increase its lifetime from several hours to several days while keeping the high quality and high rate of silver deposition, including several tests for replenishment cycles. We are also actively working on upscaling the silver bath to work on larger parts and more complex structures obtained by SLM printing.

CSEM and SWISSto12 would like to thankfully acknowledge the financial support of Innosuisse during this project.

\* SWISSto12 SA, Avenue des Baumettes 19, 1020 Ecublens, Switzerland

# Patterning Metal Grids on Heterojunction Solar Cells using Self-assembled Monolayers

G. Andreatta, A. Lachowicz, N. Blondiaux, A. Faes, C. Alleb  

The metal grids for heterojunction solar cells are typically made with dedicated screen-printed silver paste, resulting in significant costs compared to standard homojunction solar cells. Copper plating is thus seen as an interesting alternative to screen-printed silver. Being a highly conductive material and hundred times cheaper than silver, copper is a promising candidate to boost solar cell efficiency while reducing material costs. We propose here a novel concept based on self-assembled monolayers (SAMs) to obtain patterned copper lines on transparent conductive oxides (TCOs). Since SAMs utilize an extremely small amount of material, this approach could achieve plating selectivity with ultra-low costs.

While silicon-based homojunction solar cells still dominate the solar industry, silicon hetero-junction (HJT) solar cells have the intrinsic qualities to overthrow this domination: low surface recombination losses, high operating voltages, simple structure fabricated at low temperatures, with a native bifaciality [1] and with low manufacturing cost potential particularly attractive if silver paste consumption is reduced or suppressed.

CSEM is developing a novel, simple and cost-effective method for patterning transparent conductive oxides (TCO) to form solar cells metal grids by electro-plating [2]. Self-assembled monolayers (SAMs) are prepared by dipping substrates in or spraying TCO with perfluorinated and alkylated phosphonic acid solutions [3]. The investigated chemistry and explored deposition parameters on indium tin oxide have resulted in highly hydrophobic surfaces with exceptional coverage of the TCO by the SAMs. The resistance of the deposited layers to acidic plating conditions has been challenging but SAMs at optimized processing conditions have demonstrated masking properties for nickel electroplating.

The process flow for production of HJT solar cells requires a first layer of nickel to be electroplated on the TCO to provide sufficient adhesion for the copper lines. Results discussed presently correspond to nickel plating tests. Figure 1 shows the patterned nickel lines obtained in a mild ( $\text{pH}=4.4$ ) sulphamate nickel electroplating bath. Patterning using oxygen plasma combined with a hard mask removes the SAMs selectively. Prior to the electroplating step, one sample edge is dipped in concentrated sulfuric acid to remove the SAM and to allow contacting.



Figure 1: Pictures of three samples after nickel electroplating on the n-side using a SAM as resist. Unpatterned sample placed in plating solution (left); Sample patterned on the n-side using a silicon hard mask by a directional RIE O<sub>2</sub> plasma during 15s (middle); Sample patterned on the n-side during 30s (right).

[1] A. Descoeuilles, C. Alleb  , N. Badel, L. Barraud, et al., "Low-temperature processes for passivation and metallization of high-efficiency crystalline silicon solar cells", Sol. Energy 175 (2018) 54–59.

[2] Patent filed

The unpatterned sample shows that the plating is selective, and that the SAM works as a resist. On the patterned samples, nickel lines are well-defined, and the plating limit shows little blurring.

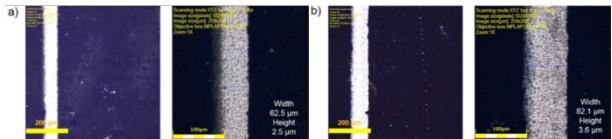


Figure 2: Scanning confocal microscopy images taken on samples shown in Figure 1. a) images taken on the thinnest line of the sample patterned during 15s. Some parasitic plating is evidenced. b) images taken on the thinnest line of the sample patterned during 30s. Some of the phosphonic acid layer may have been damaged by the hard mask as evidenced by the white dots on the masked part.

Depending on the time span of the plasma patterning step, the thinnest conductive lines observed varied in width and length. Therefore, the nanolayer formed by the phosphonic acid molecules allows the electroplating of  $\mu\text{m}$ -high Ni lines (Figure 2). However, the patterning has not been optimized. These first tests were done with a simple home-made mask produced by laser engraving silicon wafers.

Laser patterning of the SAM was also tested, and we obtained promising results. With the right parameters, the solar cell underlayers are not damaged by the laser patterning and high-resolution patterns can be obtained (Figure 3).

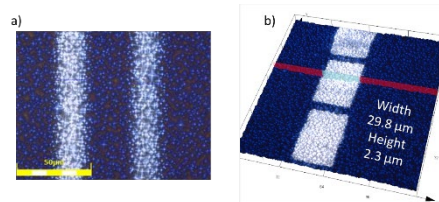


Figure 3: Solar cell precursor after nickel electroplating using laser-patterning of the SAM resist: a) continuous nickel lines, and b) nickel square patterns.

We plan to improve the quality of the SAMs, patterning and to use to SAMs for copper electroplating in the future. In this process, the extremely low amount of material including solvents used for the SAM spraying makes our process cost-effective and eco-friendly.

We would like to thank CEA-INES for providing substrates and the Swiss National Science Foundation for its financial support.

[3] G. A. L. Andreatta, A. Lachowicz, N. Blondiaux, C. Alleb  , A. Faes, "Patterning solar cell metal grids on transparent conductive oxides using self-assembled phosphonic acid monolayers", Thin Solid Films 691 (2019) 137624-137629.

# PDMS Replacement in Organ-on-Chip Systems and in vitro Assays

S. Boder-Pasche, S. Heub, D. Migliozi, G. Weder

Whereas most Organ-on-Chip (OoC) systems are currently based on polydimethylsiloxane (PDMS), they suffer from several drawbacks during their industrialization. They are not compatible with large-scale fabrication techniques. We therefore aim at exploring alternatives with soft thermoplastic elastomers that combine the elastomeric properties of PDMS with thermoplastic processing.

OoC is a microfluidic-based device containing living engineered tissue structures in a physiological micro-environment that recapitulate functions of an organ *in vivo* [1]. OoC has broad applications in precision medicine and pre-clinical testing in drug discovery.

Following the trends in precision medicine by considering individual gene variability, CSEM has started the proprietary concept YOU-ON-CHIP™. Design, materials selection and fabrication techniques for manufacturing OoC platforms are not trivial tasks (Figure 1). The perfusion of the biological tissues as well as the integration of complex components to mimic organ-level functions involve the integration of hard and flexible biocompatible materials [2].

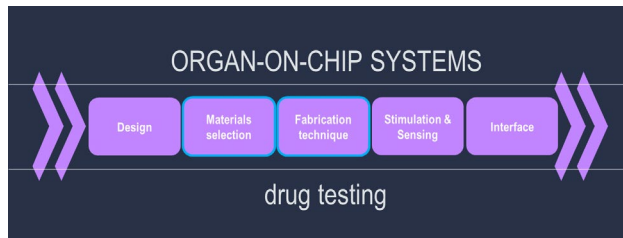


Figure 1: Materials selection and fabrication technique are technology building blocks of CSEM roadmap for the development of OoC systems from concept to biovalidation.

Materials selection and fabrication techniques are mutually joined. Both thermoset plastics and thermoplastics (TP) are widely used for OoC devices with pros and cons. Silicone-based polymers, such as polydimethylsiloxane (PDMS), are widely used for prototyping and small-scale fabrication using thermoset curing process. PDMS is easy to mold, biocompatible, gas permeable, optically transparent and bonds well to several materials: a perfect candidate for prototypes with cells.

For industrialization, PDMS suffers from several drawbacks including low resistance to organic solvents, acids and bases, sorption of (bio)molecules, leaching, and channel deformation. In addition, long curing time and difficult handling are impeding costs rationalization and large-scale industrial processes.

Developed in collaboration with CSEM, the new high-density 3D microelectrode array Khiron chip from 3Brain [3] is integrated in brain-on-chip and retina-on-chip systems (Figure 2). The reservoir is made of polycarbonate. Despite attractive benefits into the scale-up of the manufacturing process, these thermoplastics do not offer elastic properties provided by PDMS for flexible components and membranes. Instead, thermoplastic elastomers (TPE), such as styrenic block copolymers, constitute interesting candidates combining both mechanical flexibility and

high-throughput thermoforming potential. TPE bridge the gap between silicones and thermoplastics.

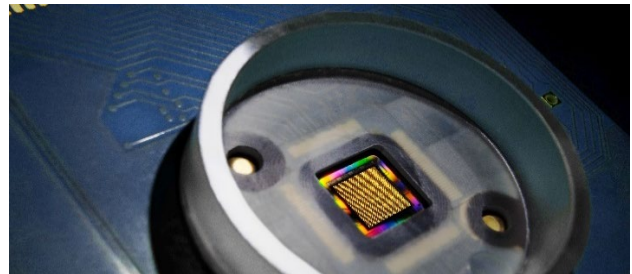


Figure 2: The Khiron chip, a commercial PDMS-free OoC system integrating a 3D microelectrode array for brain and retina diseases modeling.

In this context, we are exploring the potential of Flexdym™ for OoC systems and in vitro assays, a thermoplastic elastomer material that recently came to the market [4]. With similar elastic properties than PDMS, it offers faster microfabrication capabilities at lower costs making it an ideal candidate for both prototyping and industrial production. Other advantages include high performances of self-sealing, transparency for microscopy, stable hydrophilization and sorption properties, as well as excellent mechanical and bonding performances to various substrates.

The production of films down to 100 µm thick has been performed. They are being tested in pneumatic Quake multilayer microvalves without PDMS. Several designs were produced to optimize the bonding with thermoplastics and the permeability of the deformation of the wall (membrane) between the two networks.

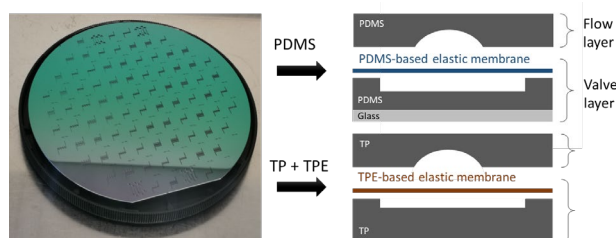


Figure 3: Design optimization of PDMS-free Quake valves for bonding and closing performances using Flexdym™ and thermoplastics.

Keywords of the next-generation OoC systems are standardization and parallelization for high throughput testing. Thanks to its ability to integrate biological assembly in the microfluidics fabrication process, Flexdym™ brings clear benefits for OOC systems. As other thermoplastic materials, Flexdym™ is compatible with high-volume manufacturing processes.

[1] <https://euroocs.eu/organ-on-chip>

[2] J. Hoeng, et al., "Organ-on-a-chip", 1st Edition Engineered Microenvironments for Safety and Efficacy Testing, 2019.

[3] [www.3brain.com](http://www.3brain.com)

[4] <https://eden-microfluidics.com/flexdym>

# Organoid Technology Platform for Tissue Engineering

S. Boder-Pasche, T. Valentin, J. Goldowsky, V. Revol, G. Weder

Organoid technology has emerged to play a central role in tissue engineering applications. Based on stem cells, the potential of each cell to self-organize provides three-dimensional tissue cultures that mimic *in vivo* counterparts. The transition from bench to clinic requires standardized protocols with operator-independent culture microsystems that are compatible with automation platforms. In this context, CSEM is developing tools to produce, sort, assemble, mature, monitor and analyze organoids on a large scale.

As in the embryonic development, self-assembling stem cells produce discrete units that self-organize and create mini organs called organoids. Such organoid models have therapeutic potential for tissue engineering, where they are used as building blocks to engineer organs.

Standardized large-scale production of organoids along with sorting, assembling and maturation are current technological limitations.

Within the research activities of organoid technology, CSEM has established a roadmap towards tools for tissue engineering (Figure 1). In this context, CSEM is coordinating a European consortium to develop an automated and standardized tissue engineering platform capable of generating a liver construct: ORGANTRANS<sup>[1]</sup>. The platform is based on autonomous self-assembly to provide personalized liver tissues, using organoids as building blocks. Tissue architecture (biomimicry) is replicated using bioprinting with three-dimensional positioning and assembling of the organoids in a biomaterial within a vascular network (Figure 2).



Figure 1: CSEM roadmap on organoid technology for regenerative medicine.

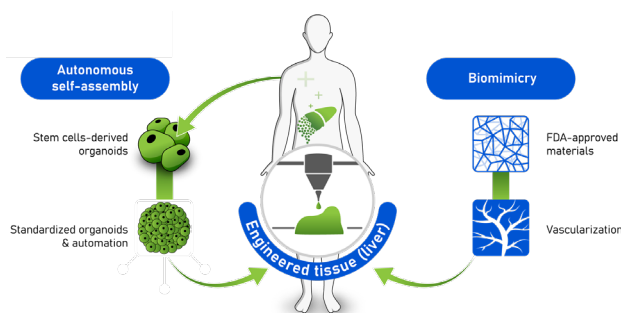


Figure 2: Overview of the ORGANTRANS' process combining autonomous self-assembly and biomimicry for liver tissue engineering.

[1] [www.organtrans.eu](http://www.organtrans.eu) (grant agreement No 874586 funded by the EU Horizon 2020 research and innovation program)

[2] [www.kugelmeiers.com](http://www.kugelmeiers.com) (ORGANTRANS' consortium partner)

[3] S. F. Graf, et al., "Image-based fluidic sorting system for automated Zebrafish egg sorting into multiwell plates", *J Lab Autom.* 2011;16(2):105-111.

Tissue manufacturing starts with the production of large-scale uniform organoids<sup>[2]</sup> followed by meticulous sorting based on deep learning algorithms<sup>[3]</sup>. The system is composed of a handling module to harvest and sort organoids without clogging. The imaging module acquires high-resolution video sequences that serve as inputs for the classification module with learnt quality criteria. This precise sorting enables prediction and elimination of the risk for tumorigenesis.

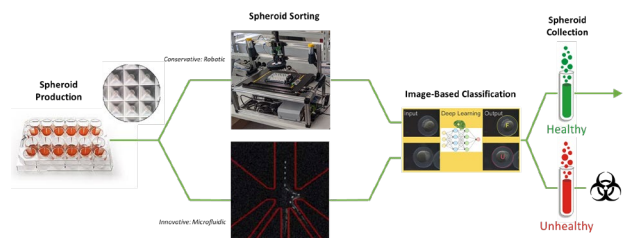


Figure 3: Automated processing of large biological entities (zebrafish eggs, organoids, etc.) based on self-learning vision algorithms to eliminate the cells showing risk of tumorigenicity.

The assembly of tissue is performed using bioprinting<sup>[4]</sup> followed by maturation of the liver construct in a physiological microenvironment. The perfusion of the tissues is based on a smart lid approach, which is compatible with a multi-well plate format, and enables automated medium circulation to facilitate standardization. In addition, optical oxygen sensing technology<sup>[5]</sup> allows for monitoring of the oxygenation in each well without risks of contaminations.

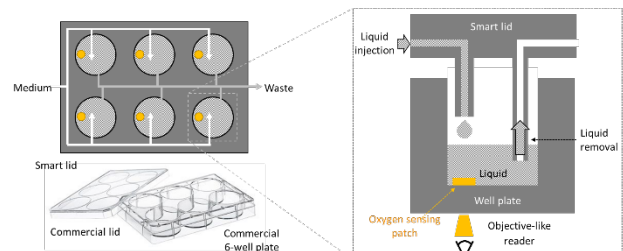


Figure 4. Smart lid approach for the continuous and automated perfusion of biological tissues in standard 6-well plate format.

ORGANTRANS aims to develop a disruptive alternative to donor organs for patients with chronic or end-stage liver diseases who still have healthy residual tissue by isolating autologous liver stem cells. The platform uniquely combines autonomous self-assembly and biomimicry for tissue engineering.

[4] [www.regenhu.com](http://www.regenhu.com) (ORGANTRANS' consortium partner)

[5] S. Heub, et al., "Non-invasive Optical Oxygen Sensing for Life Sciences and Environmental Monitoring" CSEM Scientific and Technical Report (2019) 45.

# MUSTANG—Automated Screening Platform for Skeletal Muscle Contractility Assays

J. Goldowsky, M. Kirschmann, V. Revol

The novel screening platform 'MUSTANG' (Muscle Tissue Analyzer Gear) is a first-of-its-kind automated solution capable of measuring the contractility of 3D printed micro-muscles via electrical pulse stimulation. Developed for Novartis by CSEM, Life Imaging Services, Weidmann Medical Technology and the Zurich University of Applied Sciences (ZHAW), the apparatus is set to enhance the reliability and robustness of drug development for Musculoskeletal Diseases. Compact in size, 'MUSTANG' can analyze 3D bioprinted human muscle tissues within a 24-well plate. After undergoing maturation and differentiation, electrodes stimulate the micro-muscles, mimicking the biological functionality of the tissues (e.g. force and fatigue). All the while, the differences in the way these tissues contract and react in the presence of different drugs or compounds such as caffeine (a well-known muscle stimulant) are automatically and optically monitored by an advanced algorithm developed at CSEM.

Located under the term Musculoskeletal Diseases (MSD), muscle-related diseases are a major contributor to disability worldwide, with their prevalence rising even further with aging populations. To date, new therapies and drugs for MSD have been limited by a lack of high throughput assays to assess the efficacy of novel compounds onto skeletal muscle tissues. As of today, there is no automated solution on the market for combined electrical stimulation and force readout that allows the efficient use of 3D printed muscle tissue models in drug screening.

Based on recent 3D bio-printing achievements it is now possible to bioengineer human skeletal muscle tissue into a 24-well plate format. Figure 1 shows such a 3D printed muscle tissue into a single well. Printed onto an injection-molded insert with flexible posts, the contractility of the muscle tissues can be assessed and compared by measuring the deflection of the posts while the muscle tissues are stimulated with an electrical field.



Figure 1: 3D muscle tissue printed around the posts of the specialized well plate insert.

The post position is observed from its top and is computed with the help of image analysis. By running the ORB (Oriented FAST and rotated BREIF) based image analysis on the systems graphics processing unit, the cameras high resolution images are processed up to 30 Hz in real time. By that the user has instant feedback of the muscle's contractility.

Figure 2 shows the measurement result of a muscle tissue stimulated with 5 pulse trains which are repeated at 0.2 Hz, each pulse train consisting of 8 bidirectional pulses of 80 mA current and 1 ms duration. The measurement shows precise and repeatable response of the tissue to the stimulation. The measurements noise is below 2  $\mu\text{m}$  rms, giving an excellent signal to noise ratio. The measurement was then repeated right after adding 10 mM of caffeine and show a strong reaction of the muscle tissue in terms of contractility (+33%) and relaxation time.

The system further includes a stage top incubator and a temperature control, custom designed by Life Imaging Services. This allows to keep the muscle tissues under incubation conditions throughout the experimental procedure. Thus, experiments of several hours or days can be performed without degrading the tissues performance.

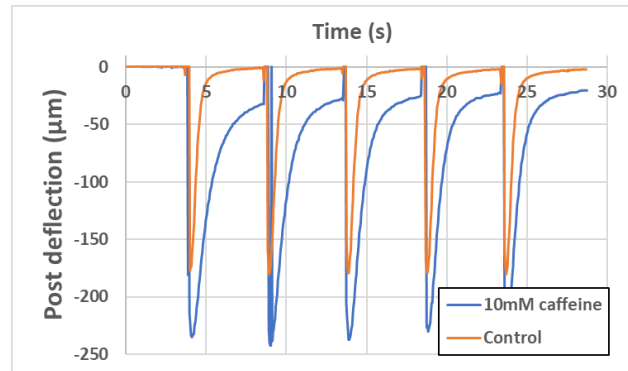


Figure 2: Contractility measurement of 3D printed skeletal muscle tissue stimulated by pulse trains (pulse train consists of 8 single bi-directional pulses of 1 ms duration with 200 mA current) repeated with 0.2 Hz. The orange curve shows the control measurement while the blue curve is obtained right after adding 10 mM of caffeine.

Figure 3 shows a picture of the system installed in the laboratory of University of Applied Sciences ZHAW in Wädenswil.

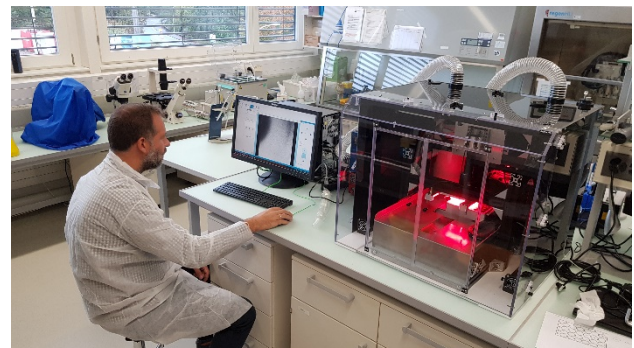


Figure 3: Automated screening platform for skeletal muscle contractility assays, including the computer, stage-top-incubator, electrical stimulation electronics, camera and positioning system.

Two prototypes of the system are in operation at ZHAW and Novartis. The project know-how has been transferred to Life Imaging Services who are responsible for sales and distribution.

"Thanks to the precise and accurate nature of this data collection, the 3D tissue analyzer platform will be able to test new drugs for MSD more efficiently, hopefully leading to novel therapies for patients," says Hansjoerg Keller, Senior Principal Scientist at Novartis. "In the not-too-distant future we would like to extend the platform to cardiac muscles enabling us to address an even broader range of pharmaceutical applications," he adds.

We thank Innosuisse for their support.

# Calibration-free Air Flow-rate Sensor for Monitoring Dispensing Systems

N. Schmid, J. Goldowsky, O. Follonier, V. Revol

Microliter and nanoliter dispensing of liquids are used in a broad range of applications, such as laboratory instrumentation or production technologies (e.g. adhesive or grease dispensing). Controlling the exact amount of liquid dispensed is key in many critical dispensing processes. Pressure driven nano-dispensing systems are used widely but are typically missing a feed-back system and are sensitive to changing conditions such as temperature, clogging and bubbles. Monitoring the dispensing cycle from the gas phase which is pressurizing the dispensing reservoir allows such systems to become calibration free - regardless of the properties of the liquid dispensed.

## Key facts

- Calibration-free pneumatic dispensing (up to 8 bar)
- Non-contact sensing, independent of liquid properties
- Measurement of droplet volume and flow rate
- Measurement of cartridge volume
- Easily scalable to different volumes and flow rates

CSEM has developed process control solutions by observing the properties and behavior of the pressurized gas in time pressure dispensing systems, previously [1,2]. Such indirect measurement methods are beneficial since the measurement is contactless and independent from the liquid's properties.

For the process to work reliably, an optimized connection between sensorbox and cartridge was developed. This was accomplished by developing a high-closing-force lever cap (Figure 1, right) replacing commercially available twist caps.

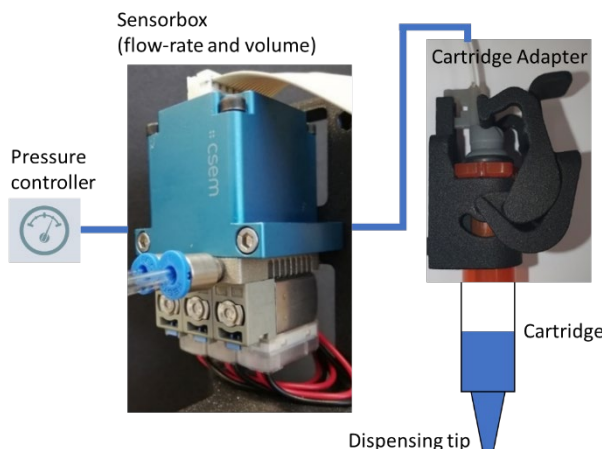


Figure 1: Sensorbox (center) to meter flow rate and droplet volume.

The air flow-rate sensor (sensorbox, Figure 1, center) has been adapted to measure  $\mu\text{l}$ -per-minute flow rates (Figure 2) as well as nanoliter-droplets (Figure 3) by using sensitive pressure sensors. At the same time, it allows unobstructed high milliliter-per-second flow rates through the sensorbox by integrating a smart valving mechanism. Thanks to this feature, dispensing flow rates can be instantaneously increased, reduced and even stopped at will. This allows to operate the system using inexpensive, disposable components only (e.g. cartridge, valves) without needing a (costly and difficult to clean) valve in the liquid path.

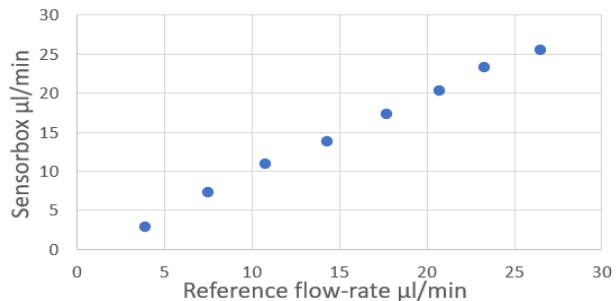


Figure 2: Measuring of  $\mu\text{l}/\text{min}$  flow rates.

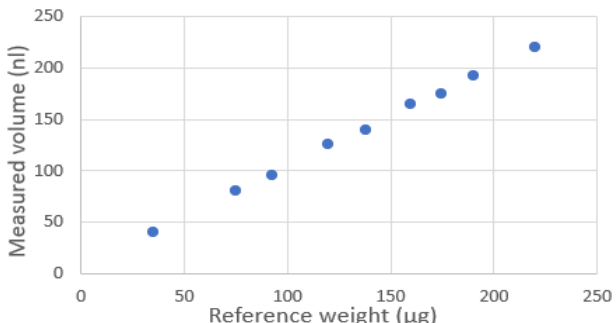


Figure 3: Dispensing of nanoliter-droplets.

In Figure 4 the difference between smart valving engaged and disengaged is shown. When this feature is applied, there is no measurable lag between the pressure increase (blue curve) and the flow rate (orange curve) measured with a reference flow-rate sensor placed after the dispense tip. In addition, it has an integrated vent valve, allowing immediate flow-stops without needing to adapt the inlet pressure to the sensorbox.

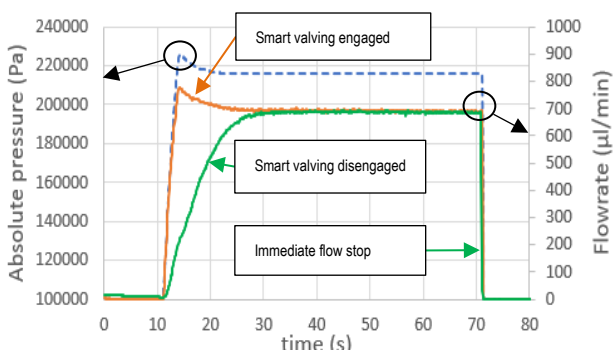


Figure 4: Smart valving to immediately react to pressure changes.

This work is supported by the Cantons of Central Switzerland.

[1] J. Goldowsky, et al., "Calibration-free Liquid Dispensing of Microliter Volumes", CSEM Scientific & Technical Report (2018) 47.

[2] T. Volden, et al., "Portable Systems for Metered Dispensing of Aggressive Liquids", SLAS Technology 2018, Vol. 23(5), 470-475.

# DropWatch—High-speed Volumetric Measurement System for Nanoliter Droplets in Flight

P. Cristofolini, S. Cattaneo, P. Jokic, H. R. Graf, J. Hilti\*, J. Rast\*, H. P. Romer\*

A dual camera high-speed imaging system for dispensed droplets was developed. It can measure the volume of nanoliter-sized droplets and the trajectories of droplets as small as 20 picoliters in flight. It is used as an accurate R&D tool to analyse dispensing systems and has the potential to be employed as a new quality control and calibration method for liquid handling robots.

Automatic liquid handling robots are the backbone of modern clinical and pharmacological laboratories. Their ability to reliably dispense precise microliter quantities of liquid on demand is of paramount importance in today's high throughput lab routines and needs to be checked at regular intervals. The volume of dispensed droplets is traditionally measured via the droplet mass with a high precision weighing scale. For even smaller nanoliter droplets, this measurement method is reaching its limits because the evaporation rate of the droplet on the scale is high enough to influence the weighing process. The measured droplet mass is too small since some of the water has evaporated in the time the balance needs to settle for the exact mass reading.

Hamilton AG in Bonaduz GR, one of the leading manufacturers of such liquid dispensing machines, is continuously improving the dispensing accuracy and droplet fire rate of their systems. Thanks to technological breakthroughs the most recent evolution, Hamilton's newly developed "MagPip" system can dispense droplets with volumes of only a few hundreds of nanoliters at an unprecedented fire rate, making it necessary to develop a new in-flight measurement and calibration system for nanoliter-sized droplets.

In collaboration with Hamilton AG, CSEM has developed a versatile new optical measurement tool for in-flight droplets based on high-speed imaging. The "DropWatch" system consists of two synchronised highspeed cameras positioned at 90 degrees to each other. The "FastEye" cameras (Figure 1b) are developed completely by CSEM and offer 2'000 frames per second at 1.3-megapixel resolution with 10-bit image depth. The optical system has a field of view of 36 x 33 mm and features telecentric illumination and imaging optics for measurement-grade images with excellent contrast. The exposure time of 50 microseconds eliminates motion blur during the fast dynamics of droplet tear-off, oscillation and inflight clashes of droplets (Figure 1a). Thanks to the camera's small footprint and folded telecentric optics, it was possible to encase the measurement system in a 40 x 40 x 14 cm box, meeting Hamilton's demanding optical requirements and size constraints (Figure 1c).

"DropWatch" is capable of volume measurement of droplets in the range from 1 nanoliter to several microliters and trajectory tracking of droplets as small as 20 picoliters. High-speed video sequences are recorded from two orthogonal directions and buffered on the two "FastEye" cameras for many consecutive dispensing events. A graphical user interface allows to control both cameras, set recording parameters, inspect and save the recorded image sequences. A sophisticated piece of software developed by Hamilton analyses the video sequences to extract the droplet position and shape. It then reconstructs a 3D model

of the oscillating droplet as it flies from the pipette tip to the collection vessel, also yielding an accurate measurement of the droplet volume.

Each "FastEye" camera is equipped with a powerful FPGA with an embedded programmable neural network. This allows the "DropWatch" system to analyse droplet events in real time. In the future advanced functions like onboard volume and trajectory calculation, object recognition, image segmentation, image thresholding and automatic recording control (no synchronisation between dispensing system and camera necessary) can be implemented. The "DropWatch" system has considerable miniaturisation potential when targeted towards a specific application.

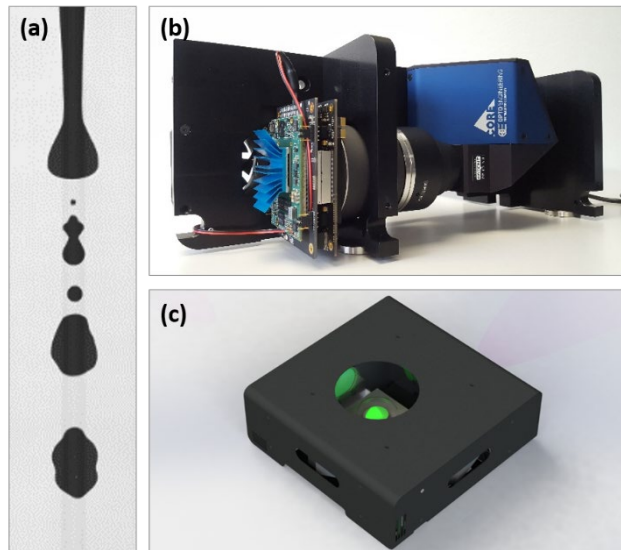


Figure 1: a) Image from a highspeed sequence, freezing the fast dynamics of several droplets detaching from the pipette tip. b) "FastEye" (left side) with telecentric optics (right side) mounted on the main frame. c) View into the heart of the "DropWatch" setup with green collimated light illuminating the measurement region.

The most challenging aspect of the project was to translate Hamilton's requirements and size restrictions into a well-balanced optical system that delivers the required resolution, image quality and frame rate in a volume small enough to fit inside Hamilton's pipetting robots. In the future it is envisaged to explore the miniaturisation possibilities and the new FPGA processing functions, with the goal to build a portable quality control tool for liquid dispensing systems. Furthermore, optical calibration methods are in development, to ensure absolute volume measurement accuracy for instrument calibration in production lines and in the field.

\* Hamilton Bonaduz AG

# Development of Digital Droplet Nucleic Acid Amplification Platform for Field-deployable Diagnostics

Z. Halvorsen, V. Revol, H. Knapp

A high throughput microfluidic device to produce monodisperse microbeads has been developed. Hydrogel beads with a narrow size distribution can be used as a massive partitioning tool for biological applications in diagnostics and drug discovery. The method is demonstrated for pathogen detection in a resource-limited setting using loop-mediated isothermal amplification.

Antimicrobial resistance (AMR) in bacterial infections kills more than seven hundred thousand people per year; a number predicted to rise to ten million by 2050<sup>[1]</sup>. Methicillin-Resistant Staphylococcus Aureus (MRSA) is one of the most prevalent AMR pathogens with persistently high morbidity and mortality<sup>[2]</sup>. Rapid, simple, and effective detection, in hospitals and health care centers, is necessary. Targeting the genetic material of pathogens in clinical samples using nucleic acid amplification tests allows for versatile in vitro diagnostics.

We developed a point-of-care (POC) in vitro diagnostic device based on digital droplet loop-mediated isothermal amplification (LAMP). A 10<sup>9</sup>-fold amplification is obtained in less than 30 minutes in the droplet without requiring thermal cycling nor complex instrumentation.

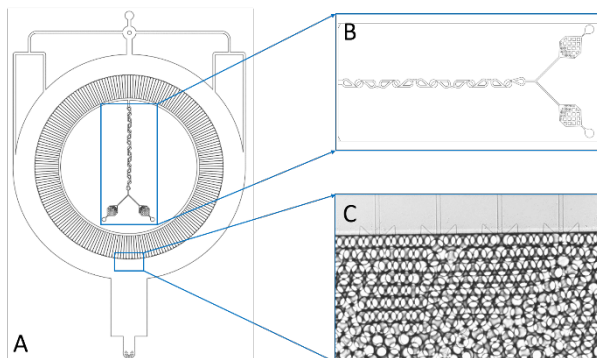


Figure 1: a) Schematic view of the emulsification device with (b) integrated mixer and (c) close-up of the nozzles and droplets.

The membrane emulsification device is illustrated in Figure 1 and was realized with conventional lithographic techniques. It allows to generate massive water in oil emulsions with a narrow size distribution, as illustrated in Figure 2.

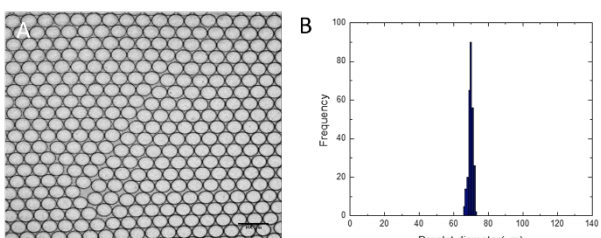


Figure 2: a) Highly monodisperse water in oil droplets with size around 70  $\mu\text{m}$ . b) Histogram of the droplet size distribution demonstrating exceptional monodispersity.

[1] WHO Global action plan for the prevention and control of noncommunicable diseases 2013-2020. World Health Organizations: 2013.

[2] D. A. Emge, R. L. Bassett, M. Duvic, A.O. Huen, "Methicillin-resistant Staphylococcus aureus (MRSA) is an important pathogen

Water in oil droplets containing polyacrylamide monomer were then converted to solid hydrogel beads by incubation at 65°C for 12 hours while immersed in oil phase containing 1% Tetramethylethylenediamine (TEMED). Washed hydrogel beads were then immersed into a LAMP master mix, DNA template, polymerase, and SYBR green for 15 min. The solution was finally compartmentalized by adding HFE 7500 oil with surfactant and vortexed for 30 s. After vortexing, the compartmentalized hydrogels were incubated in a real-time PCR machine to investigate the amplification signal. As shown in Figure 3, the positive results of 100 ng/ $\mu\text{L}$  of the *mecA* gene showed bright fluorescence green beads under fluorescence microscopy, indicating that dsDNA templates were amplified, while the negative control does not show any amplification. Furthermore, the same method was applied to other common bacteria and demonstrated its excellent selectivity.

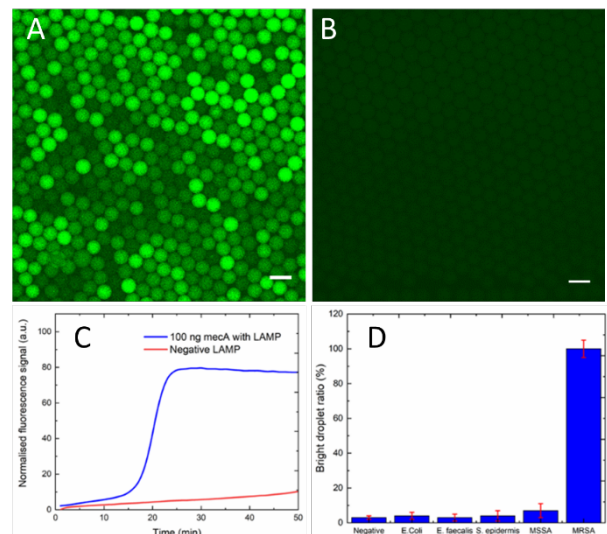


Figure 3: Images of (a) positive (100 ng/ $\mu\text{L}$ ) and (b) negative (0 ng/ $\mu\text{L}$ ) LAMP reaction using hydrogel beads, incubated at 60 °C for 60 min (scale bar 150  $\mu\text{m}$ ). c) Time-dependence fluorometric signal of positive and negative LAMP reaction. d) selectivity study with several pathogens.

The developed HD-LAMP holds a great promise for rapid and cost-effective POC devices with excellent analytical performance, i.e., sensitivity, accuracy, and enabling precision analysis in the field of digital biology. Compared to other digital PCR assays<sup>[3]</sup>, it is more specific and can be integrated into field-deployable diagnostics devices.

in erythrodermic cutaneous T-cell lymphoma (CTCL) patients." Archives of dermatological research 2020, 312 (4), 283-288.

[3] M. N. Hatori, S. C. Kim, A. R. Abate, "Particle-templated emulsification for microfluidics-free digital biology." Analytical Chemistry 2018, 90 (16), 9813-9820.

# Optical Sensor for Glucose Monitoring in Cell Cultures

V. Zubkovs, G. Oravez, L. Burr, E. Rutz, H. Chai-Gao, I. Stergiou, S. Beyer\*, F. Betschon\*, A. A. Boghossian\*\*, S. Cattaneo

The unique optical properties of single-walled carbon nanotubes (SWCNTs) make them a versatile platform in fluorescence-based sensing applications. The inherent photostability of SWCNTs promises to extend the lifetime of the fluorescence-based sensors, enabling longtime continuous monitoring of various analytes. Currently, CSEM is working on the development of an optical sensor for continuous glucose monitoring in cell cultures based on this innovative technology. In the future, this platform could be extended to multi-analyte sensing.

Glucose is the main source of energy for living organisms and it is commonly used as the nutrient in cell culturing. To sustain normal growth and minimize the risk of development pathologies in the cells, it is critical to control the concentration of glucose in cell culture media and maintain it within the physiological limits. As glucose is consumed by living cells during their proliferation its concentration should be monitored and maintained constant during the process. This calls for miniaturized, continuous monitoring devices, which can be integrated into cell culture incubators and bioreactors. Despite significant strides made in development of continuous glucose monitoring sensors, current commercial devices must be frequently recalibrated using off-line methods. Therefore, there is still a demand on the market for an autonomous sensor which could enable effortless monitoring of glucose in cell cultures with minimal effort.

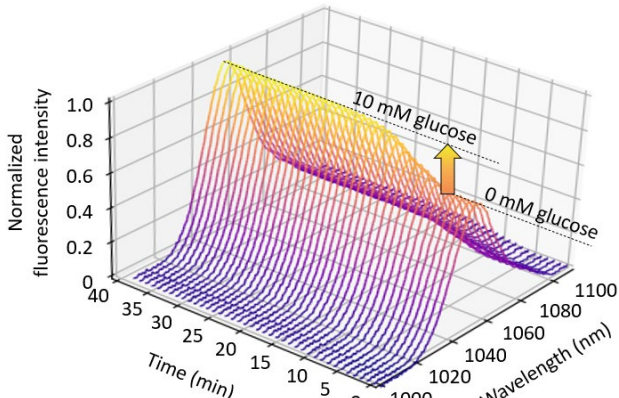


Figure 1: Fluorescence spectra of the SWCNT-based glucose sensor measured after addition of 10 mM glucose solution. A laser at 660 nm (1 mW) is used for excitation, and the spectra are recorded with one-minute intervals.

Semiconductive SWCNTs are used as optical transducers, due to their fluorescent response and inherent photostability. A SWCNT-based glucose sensor was developed at EPFL [1]. The researchers have demonstrated a method for cross-linking a bio-engineered glucose selective protein and an amphotolytic linker molecule, which serves as an anchor to the SWCNT. An increase in fluorescence intensity is triggered when a glucose-containing solution is in contact with the SWCNT-based sensor (Figure 1), and the emission intensity returns to its initial level when the glucose concentration decreases to zero. This method has enabled a site-specific immobilization of the proteins onto the

SWCNTs, thereby enhancing the response of the sensing material [2]. This sensor technology has the potential to significantly extend the life cycle of protein-based sensors for continuous glucose monitoring.

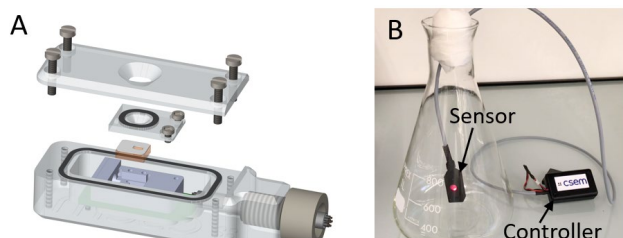


Figure 2: a) CAD drawing showing the main components of the SWCNT-based sensor reader device and the waterproof packaging. The optical sensor material is immobilized on an optical waveguide, integrated into a custom optoelectronic board. b) A photograph of the sensor and the controller board of the device, showing its possible application in laboratory flasks.

In the laboratory environment, fluorescence response of SWCNT sensors is monitored using near-infrared microscopes or tabletop setups. The large dimensions and high cost of these devices limit the use of the sensors outside the laboratory settings. That creates an urgent need for a miniaturized and easy-to-use SWCNT fluorescence reader.

CSEM is developing a compact and cost-effective device, which enables to monitor near-infrared fluorescence of the SWCNT-based sensors (Figure 2a). The miniaturization was achieved by designing a customized optoelectronic layout integrating optical waveguide technology developed in collaboration with Vario-Optics AG. The sensor board is enclosed in an impermeable packaging which allows monitoring glucose in cell culture flasks (Figure 2b).

The versatility of the SWCNT has the potential to enable contactless monitoring of multiple analytes in a multiplexed sensor array. For example, optical SWCNT-based sensors were demonstrated for the detection of other analytes such as insulin, dopamine, nitric oxide, hydrogen peroxide, and micro-RNA molecules [3]. This allows developing a multi-analyte sensor platform with a single optical reader. This revolutionary technology has the potential to open a new page in bio-sensing applications.

- Vario-Optics AG, Heiden
  - École Polytechnique Fédérale de Lausanne (EPFL), Lausanne
- [1] V. Zubkovs, N. Schuergers, B. Lambert, E. Ahunbay, A. A. Boghossian, "Mediatorless, reversible optical nanosensor enabled through enzymatic pocket doping", *Small* (2017).
- [2] V. Zubkovs, S.-J. Wu, S. Y. Rahnamaee, N. Schuergers, A. A. Boghossian, "Site-specific protein conjugation onto

fluorescent single-walled carbon nanotubes", *Chemistry of Materials* (2020).

[3] J. Pan, F. Li, J. H. Choi, "Single-walled carbon nanotubes as optical probes for bio-sensing and imaging", *Journal of Materials Chemistry B* (2017).

# ACEnano—New Tools for Nanomaterials Risk Assessment

D. Schmid, L. Burr, S. Cattaneo

Risk assessment for nanomaterials (NM) is still lagging considerably despite their widespread use in countless fields, from car tires, to pharmaceuticals, to batteries. The goal of the European research project ACEnano is to introduce confidence, adaptability and clarity into NM risk assessment by developing a widely implementable and robust tiered approach to physicochemical characterization that will simplify and facilitate the development and use of new materials with respect to their hazard and exposure risk. As part of a conceptual toolbox to achieve this goal, CSEM has developed new methods and instruments to determine the hydrophobicity, the solubility, and the reactivity of NM.

The European research project ACEnano strives for analytical and characterization excellence in NM risk assessment through a tiered approach: Benchmarked toolbox building on guidance and decision trees, and data warehouse building, enabling easy access to relevant data and training for the academic and industrial community<sup>[1]</sup>. As part of this toolbox, CSEM developed new methods and instruments to assess the hazard and exposure risks that are related to 3 key properties of nanomaterials, hydrophobicity, surface reactivity and solubility, for which there is a substantial lack of techniques for reproducible measurement.

Hydrophobicity is a crucial parameter in nanodrugs development as well as for nanotoxicity assessment. CSEM investigated two novel approaches for determining the hydrophobicity of nanoparticles, based respectively on hydrophobic interaction chromatography (HIC) with elution investigation in hydrophobic columns (3D structure) and on 2D surface analysis with CSEM's waveguide interrogated optical sensor (WIOS) instrument<sup>[2]</sup>. It was shown, that with both surface-based methods, hydrophobicities can be characterized and compared, which in turn can be used to develop a qualitative comparison chart for nanoparticles. Figure 1 below shows hydrophobic interaction chromatograms of native and differently functionalized polystyrene beads: Native 100 and 50 nm, carboxyl, and amine functionalization both on 100 nm particles. Hydrophobic NPs are retained longer due to hydrophobic interactions with the HIC column. The ratio of particles retained over the total amount of particle injected (indicated in Figure 1 as retention %) also showed a similar behavior.

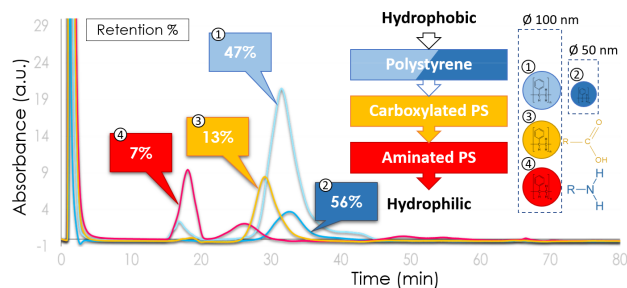


Figure 1: Hydrophobic interaction chromatograms for surface-functionalized PS beads with different hydrophobicity showing good correlation with retention time.

[1] [www.acenano-project.eu](http://www.acenano-project.eu)

[2] J. Adrian, S. Boder-Pasche, J. Diserens, S. Sánchez-Baeza, H. Gao, M. Marco, G. Voirin, "Waveguide interrogated optical immunosensor (WIOS) for detection of sulfonamide antibiotics in milk, Biosens. Bioelectron. 2009, 24, 3340-3346.

For reactivity assessment, CSEM developed a compact and affordable optoelectronic system for monitoring of 24 samples in parallel (MINCA). The instrument can be used for a colorimetric assay, developed by the consortium partner Wageningen Food Safety Research, where the catalytic reactivity of NMs correlates with the optical absorption of a dye at a specific wavelength.

The approach uses differential two-wavelengths monitoring to measure static and dynamic changes in absorbance, which allows to quickly screen for the possible presence and reactivity of nanoparticles in samples. It was shown that, unlike current analytical methods, CSEM's solution does not require highly trained personnel, nor expensive instrumentation and time-consuming sample preparation, is easily transportable and can be used for tests in the field. The system has been validated and reproducibility has been shown in comparison to a manual cuvette-based method. Figure 2 below shows a validation measurement with 50 nm Ag particles at different concentrations and the instrument MINCA in use.

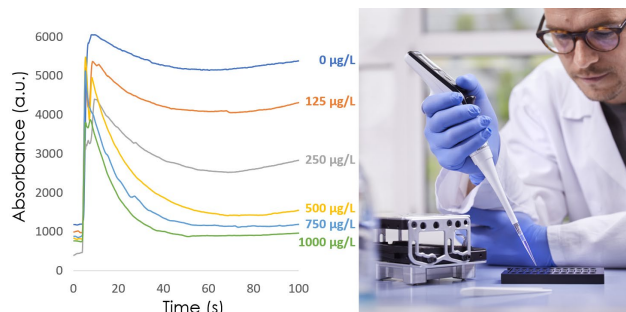


Figure 2: (left) Absorbance of methylene blue in the presence of different concentrations of 50 nm citrate stabilized silver nanoparticles measured with CSEM's portable reader. (right) Operation of CSEM's MINCA instrument.

For solubility monitoring, CSEM's automated sample preparation system has been presented in the STR 2019<sup>[3]</sup>. It is currently being validated in an interlaboratory comparison by CSEM's consortium partners.

The ACEnano project is a collaboration between 28 European, Chinese and Korean consortium partners ([www.acenano-project.eu](http://www.acenano-project.eu)) and received funding from the European Union's Horizon 2020 research and innovation program under grant agreement No. 720952. CSEM thanks them for their support.

[3] D. Schmid, L. Burr, P. Cristofolini, F. Kurth, G. Oravec, S. Cattaneo, "ACEnano—Hydrophobicity, Solubility and Reactivity Monitoring of Nanomaterials", CSEM Scientific Technical Report (2019) 61.

# NIIDS—Digital Urine Analysis with Printed Electrochemical Sensors

N. Glaser, D. Migliorelli, M. Zinggeler, L. Burr, K. Petropoulos, H. Gao L. Mühlbach, R. Junuzovic, N. Schmid, F. Geister, S. Fricke, S. Paoletti, C. Abongomera\*, D. Paris\*, S. Generelli

There is a need for developing new solutions that enable rapid diagnostic tests in low resource settings. CSEM is working on the development of a hand-held fluidic cartridge, containing an array of printed electrochemical sensors for the digital recording of urinary glucose and pH. The system is being developed for the Swiss Tropical and Public Health Institute (Swiss TPH) to assist clinical decision making in low-resource settings such as refugee camps.

Clinical decision making in low-resource settings is often based on limited diagnostic information. Inaccurate treatment of febrile illnesses (e.g. by broadband antibiotics) is often the consequence. The Swiss TPH ([www.swisstph.ch](http://www.swisstph.ch)) aims to develop a diagnostic tool for the most common pathogens and febrile illnesses, to fight migrant diseases. Nowadays, basic urinalysis is done with urine paper dipsticks with color indicators. These results are prone to misinterpretation and need to be manually recorded in most cases.

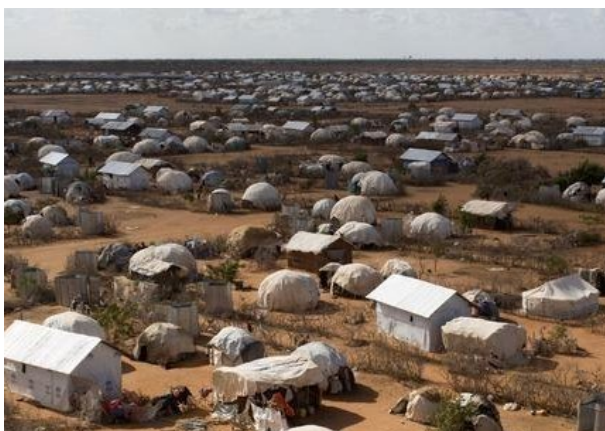


Figure 1: In collaboration with the Swiss TPH we study in Switzerland and Ethiopia the use of new tools for better decision making in low-resource settings such as refugee camps like these.

We have developed a digital sensing device to detect important ions and metabolites in urine. Among these are pH, sodium, lactate and glucose. Sensors for glucose and pH have been realized on the device and showed good results in first urine tests.

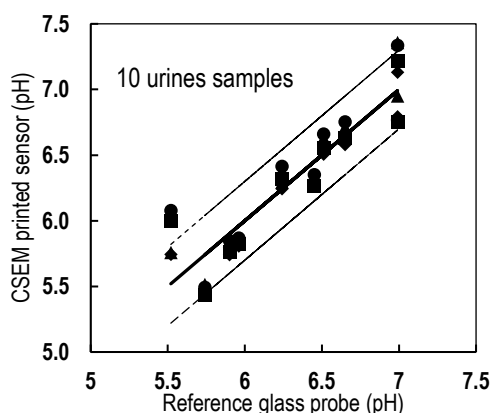


Figure 2: Results of 4 printed pH-sensors (round, square, triangle and diamond) in 10 human urine samples. Zero deviation from the reference sensor is indicated by the solid line and +/- 0.3 pH units by the dashed lines.

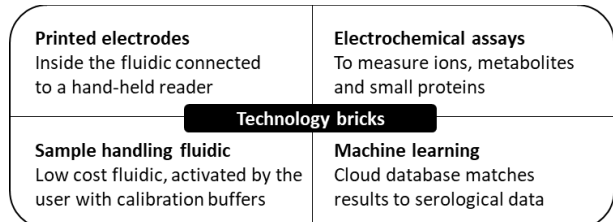


Figure 3: The technologies at CSEM to develop a urine sensor.

Our printed pH sensors show excellent agreement with the reference system and very good sensor reproducibility (Figure 2). Glucose (data not shown here) can be measured with higher sensitivity compared to urine dipsticks, which may allow to detect diabetes at an early stage. Later, sensors for additional analytes, such as lactate and sodium, will be added to the device array.

A fluidic cartridge is developed with integrated printed electrodes and pre-stored buffers for sensor calibration. These cartridges will be interfaced to a hand-held reader and provide results within 5 minutes. The device shown in Figure 4 incorporates a sensing chamber for pH and glucose and two additional analytes to be added later. In the next phase of the collaboration, we aim to add sensors to detect small proteins in urine.

Our device provides quantitative data, which is going to be uploaded to a cloud-based database. Within the NIIDS project of the Swiss TPH (PI: Prof. Dr. med. Daniel H. Paris), results will be collated from blood analyses (serological and molecular data), reference diagnostics and complemented with our urine data. By means of a learning database, the Swiss TPH aims to assist low-resource clinics with point of care tests and cloud-based data analysis procedures.



Figure 4: Prototype device for the electrochemical urine analysis of 1-4 analytes.

Acknowledgement: We thank the Stanley Thomas Johnson foundation for funding.

# Multiplex Photonic Sensor Platform for Plasmonic-based Detection of Contaminants in Milk

D. Kallweit, E. Haenni, J. A. Lahera Perrez, G. Banderet, P. Chervet, A. Falhi, M. Frosio, M. Correvon

In the European project MOLOKO CSEM and its partners are developing a self-managing and automatic miniaturized integrated photonic sensor to be used for fast response on-site monitoring of security and quality analytes within the milk supply chain. As part of the project, CSEM takes on optical simulation, tolerance analysis and optimization of the complete opto-plasmonic chip. Furthermore, CSEM develops the control electronics and software for the operation of the entire sensor platform as well as the processing and storage of the data (track and trace via cloud service).

In the MOLOKO project we are developing a highly integrated mobile label-free biosensor based on the principle of Surface Plasmon Resonance (SPR). The sensor chip consists of two main parts: a) the optoplasmic sensor, and b) the micro-fluidic module as shown in Figure 1.

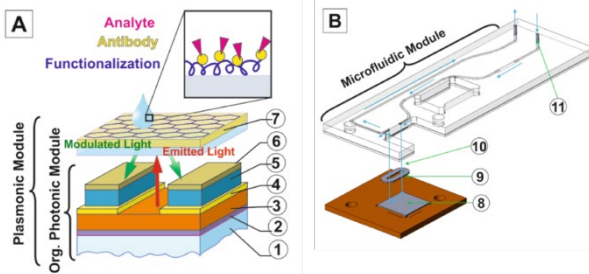


Figure 1: Illustration of the opto-plasmonic MOLOKO sensor.

The measuring principle is based on the modulation of the reflected light when the refractive index changes at the boundary to the microfluidic channel. Thereby a monolithic approach is followed: The entire excitation and detection optics are integrated in one chip. That means there are no external light sources, detectors, or optics such as prisms, lenses, or polarizers. However, several microfluidic cells can be read out using multiplexing and different analytes can thus be detected in parallel.

In the design phase the complete opto-plasmonic chip was simulated by CSEM. Due to its subwavelength features, the 3D plasmonic grating had to be simulated rigorously, which is quite time consuming. Thus, to significantly speed up simulations, the subwavelength grating was described by a lookup table, which includes its angular spectral response. The resulting simulation principle is illustrated in Figure 2.

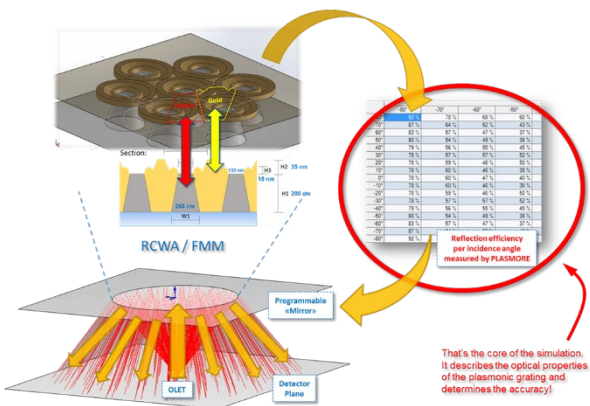


Figure 2: Illustration of the 3D optical simulation setup.

With that approach we were able to efficiently simulate the complete optoplasmic sensor by means of wave optical simulations considering amplitude, phase, polarization, and wavelength. Also, the spectral power density of the organic light source was considered, and the sensor sensitivity was optimized

through positioning and dimensioning of the individual elements. The simulated resulting sensor signal when going from pure water to a 2% ethanol solution is shown in Figure 3. The influence of the x-dimension of the organic photodiode (OPD) is shown on the abscissa.

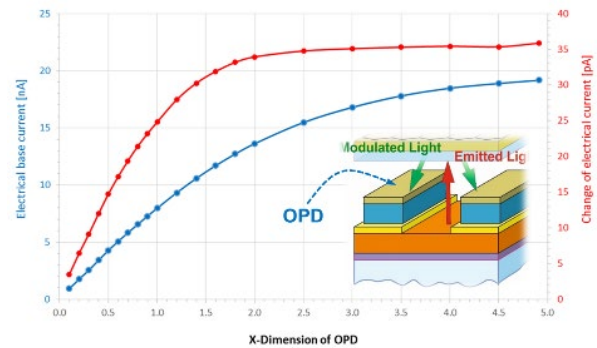


Figure 3: Simulated response of the MOLOKO sensor.

Due to the low power of the light sources, the electronics must be able to resolve variations in the photoelectric current of a few pA, while the base current is around 2uA. There are therefore high demands on the electronics for the OLED and OPD transimpedance amplifiers in terms of noise and temperature control. A complete analog front-end (AFE) was developed as well as a digital front-end to control the different actuators of the microfluidics, to drive the AFE, and to communicate the results to the user.



Figure 4: MOLOKO controlling electronics developed at CSEM.

A simple but useful and intuitive graphical user interface was developed in Python to control and read-out the data acquired by the optical sensor. A dedicated firmware running on a STM32F777 was written to coordinate the whole system.

The first laboratory tests with analytes of interest (lactoferrin, κ-casein, streptomycin) have been carried out successfully. Tests in an industrial environment are planned for 2021.

The authors acknowledge the European Commission for the financial support of this project ("MOLOKO", Grant Agreement number: 780839).

# Porous Material Assisted Lateral Flow Immunoassay (LFIA) for Improved Sensitivity and Detection Limit

Y. Tang, H. Chai-Gao, F. Kurth, K. Petropoulos, D. Migliorelli, S. Generelli

This study reports a new strategy to increase the sensitivity of lateral flow immunoassays (LFIA) by first time integrating porous material in a LFIA and tested for the detection of mouse IgG. Compared to a conventional LFIA strip, the modified LFIA strips exhibited a noticeable extension of the reaction time between detection antibody and analytes of interest, an improvement in sensitivity, a broader dynamic range, and a lower limit of detection. In the future, the porous material assisted LFIA is expected to be applied in the quantification of biomarkers of interest for medical diagnostics.

Lateral flow immunoassays (LFIA) are employed as medical diagnostics tools. One of the major limitations of LFIA is that it only provides qualitative and/or semi-quantitative analysis with low sensitivity compared to quantitative enzyme-linked immunosorbent assays (ELISA). One of the reasons for these major drawbacks is the short reaction time between the detection antibody and the analytes of interest.

The sensitivity of a LFIA usually depends on an efficient binding between the detection antibodies and the analytes, which increases with longer incubation times. This reaction time is limited by one of the key parameters in the design of lateral flow assays, namely the time the fluid mixtures need to flow through the lateral flow strip. But especially this time tends to be minimized and is thus not a typical parameter for optimization.

This work reports the development of a porous material assisted LFIA strip for the quantitative detection of IgG. The porous material was integrated between the conjugation pad and the nitrocellulose pad of a conventional LFIA strip (Figure 1). The novel material insert delays the sample fluid propagation in the lateral flow strip and thus increases the reaction time between the analyte (IgG) and the detection antibodies prior reaching the test and control lines.<sup>[1]</sup>

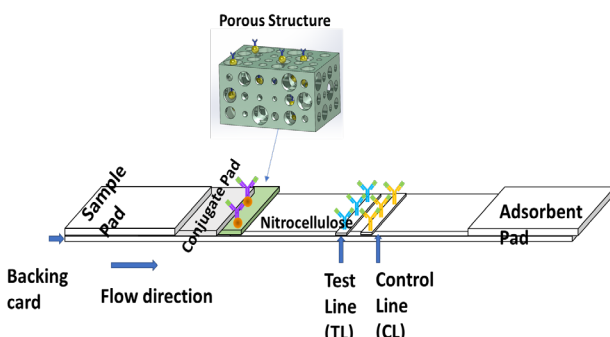


Figure 1: Schematic illustration of the porous material assisted LFIA.

To evaluate the effect of the integrated porous material on the fluid flow in the LFIA strip, we measured the propagation of phosphate buffer solution dispensed on conventional and modified LFIA strips at different time points (Figure 2). The buffer reached the absorbent pad after 180 seconds in conventional LFIA strips, while the integrated porous material caused a delay of about 90 seconds and 120 seconds for aerogels of 3 mm and 4 mm length, respectively, indicating a prolongation of the reaction time of about 50% to 60%.

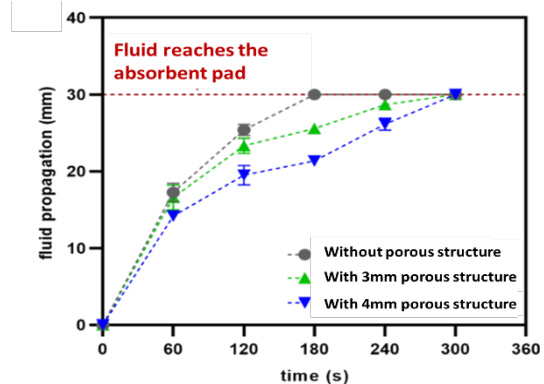


Figure 2 Analyzed time-lapse fluid propagation in the three different LFIA settings tested.

Different LFIA strips were tested with different concentrations of mouse IgG (0.01 ng/ml to 1000 ng/ml) spiked in PBST buffer containing 1% BSA. Signals were recorded by a mobile phone camera after 20 minutes and gray values of the test and control lines analyzed using ImageJ. The calibration curves were obtained by plotting the gray value ratios (test line/control line) as a function of the different mouse IgG concentrations. The dash line in the Figure 3b is the fitting curve ( $y = 1.8787 \ln(x) + 81.947$ ) of the quantification range (0.01 ng/ml – 100 ng/ml) of the porous material assisted LFIA for detection of mouse IgG.

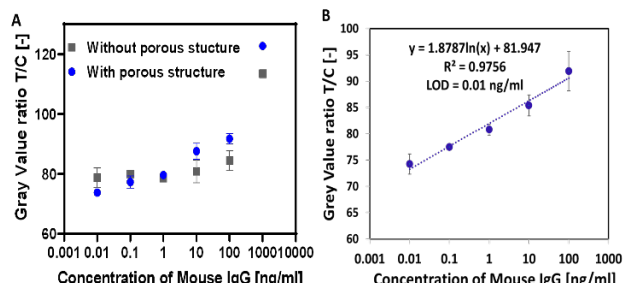


Figure 3: a) Comparison of the calibration curves of the LFIA with (red) and without (blue) aerogel (n=6 per group). b) Fitting curve of the quantification range of the porous material assisted LFIA for mouse IgG detection in buffer.

While the limit of detection (LOD) of the conventional LFIA is 100 ng/ml, the aerogel modified LFIA has a LOD of 0.01 ng/ml. The expected quantification range of the modified LFIA strips is between 0.1 ng/ml and 100 ng/ml. With such a sensitivity increase of about 1000-fold compared to the conventional LFIA, the porous material modified LFIA strips reached comparable sensitivity as commercial ELISA kits.

[1] Gasperino, et.al. (2018), "Improving Lateral Flow Assay Performance Using Computational Modeling". Annual Review of Analytical Chemistry 11: 219–244.

# Inkjet Printed Pt-electrode Array for in vivo Neural Recordings

N. Marjanovic, J. Schleuniger, F. Lütolf, A. Lücke, S. Fricke

Microelectrode arrays (MEAs) are typically interfacing an electroactive tissue with the bioelectronic systems. Printing techniques, such as inkjet and screen printing, are attractive methods for the manufacturing of a customized MEAs because they allow flexible, low-temperature, scalable, and cost-effective fabrication processes. CSEM fabricated all-printed electrocorticography arrays by inkjet printing of platinum electrodes and screen printing of polyimide as a passivation layer. Herein, the mechanical and electrochemical characterizations of the printed MEAs is reported. The printed MEAs were proven not to be cytotoxic. The printed MEAs were used at EPFL for in vivo recording of a visually evoked cortical potentials in rabbits upon flash stimulation. Altogether, the results open a path for using of printed MEAs for neurological applications.

Microelectrode array (MEA) devices are essential to interface with electroactive tissues, such as the nervous system and muscles. Several biomedical devices rely on microelectrodes to deliver electrical stimuli or to record electrical activity from the tissue. Medical-grade MEAs are mostly relying on clean-room processes. However, these are limiting the size of MEAs to the wafer dimension and the number of possible layouts due to expensive lithographic masks. On the other side, printing technology easily overcome the above-mentioned issues since it is based on low-temperature, flexible, cost-effective, and large-area processes.

In this study, platinum based MEA arrays were inkjet printed using a commercial platinum precursor ink (16512, Ceimig Limited) on 60  $\mu\text{m}$  thick polyimide foils (PI; Kapton HN, DuPont). The choice of PI as a substrate material relied mainly on its flexibility, a crucial feature when designing medical MEAs to interface soft tissues such as the brain. Each MEA consists of 16 square electrodes of 450  $\mu\text{m}$  in size with a pitch of 1120  $\mu\text{m}$ . Electrodes, tracks, and pads were inkjet printed with a single scan resulting in a mean line thickness of 130 nm. The mean line width was 250  $\mu\text{m}$ .

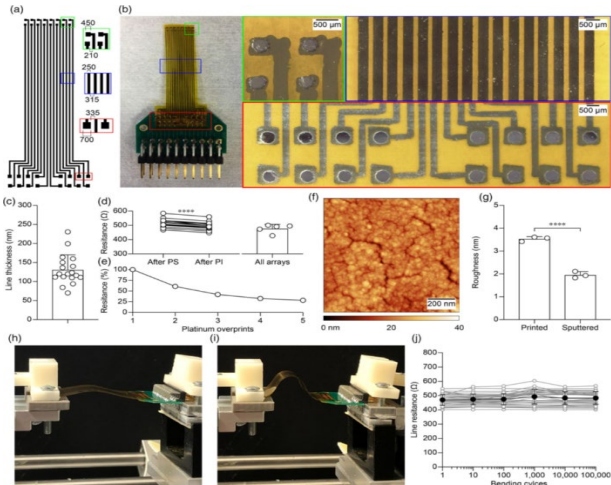


Figure 1: Printed and characterized platinum based MEA electrode array. Figure published in Ref [1].

Therefore, photonic sintering (PulseForge 1300, Novacentrix) was performed to decrease the line resistance by a factor of 2.5 [1]. The array was encapsulated by screen printing of PI (HP-1000G2, Hitachi Chemical). The electrode and pad openings in the encapsulation layer were 300  $\mu\text{m}$  and 530  $\mu\text{m}$ , respectively. The thickness of the screen-printed PI encapsulation was 4.4  $\mu\text{m}$ . The peak to valley roughness of the printed platinum electrodes was 3.5 nm, which is 1.8 times higher than the sputtered (reference) platinum electrodes (Figure 1). For this application,

higher surface roughness is beneficial and should provide more intimate contact with the tissue and therefore better electrochemical performance. We also tested the mechanical robustness of the printed arrays upon cyclic bending. Printed platinum based MEAs were stable upon 100'000 cycles of flexions (Figure 1). The line resistance was monitored over cycles, and no statistically significant change was observed. In vitro cytotoxicity test was performed by an accredited company (Medistri SA). The test was conducted according to the requirement of ISO 10993-5 [1]. Results on the printed platinum based MEA arrays showed a 100% viability.

In vivo validation of the printed MEAs was performed at EPFL (here we acknowledge Prof. Diego Ghezzi and his group). The printed array was placed in the visual cortex of an anesthetized rabbit and visually evoked potentials were recorded upon flash stimulation of the eye contralateral to the recording hemisphere (Figure 2) [1].

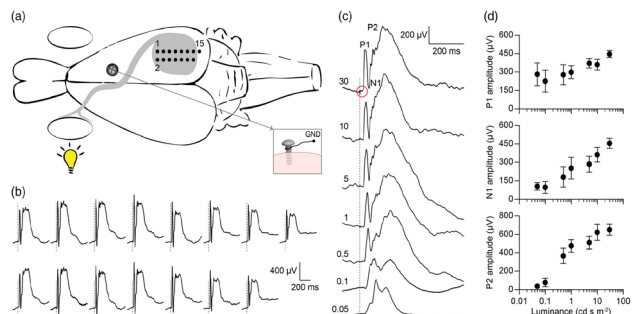


Figure 2: Recordings of visually evoked cortical potentials with the printed MEAs array. Figure published in Ref [1].

Recordings show the appearance of the classical peaks of the visually evoked potentials with an amplitude modulated by the stimulus luminance.

The performed all-printed platinum-based MEAs study showed clear advantages of the printing compared to the clean-room microfabrication processes. Among others those advantages are:

- Low-temperature processes
- Flexible and large-area substrates
- Cost-effectiveness

These aspects are relevant for future production of medical-grade and customized MEAs. In this work, exclusively commercially available materials were used, which is another advantage for a faster clinical translation to printed MEAs.

We acknowledge EPFL Lausanne and Wyss Center for Bio and Neuroengineering, Genève, for their financial support.

[1] E. Borda, et al., Adv. Eng. Mater. 2020, 22, 1901403.

# Artificial Ear Canal with Integrated Pressure Sensors

M. Zinggeler, N. Glaser, J. Disser, F. Geister, A. Lücke, C. Seitz, S. Fricke

Unsatisfactory wearing comfort of earpieces, which are placed in the ear canal, is a major reason for not wearing hearing instruments. In order to address this problem, a better understanding of the contact pressure of earpieces and its distribution is needed. In this project, we have developed a custom-made research setup for the company Sonova AG. The system is based on a printed, highly sensitive pressure sensor matrix on foil, which was integrated into an ear canal model using a simple roll up procedure.

Around 15% of adults suffer from some degree of hearing impairment. However, only about 20% of affected people in developed countries are wearing a hearing instrument. One of the top three reasons why people are not wearing it, is unsatisfactory wearing comfort (source: Sonova internal report). The contact pressure and the contact pressure distribution of the earpiece, which is placed deep in the ear canal of the patient, has been identified as one of the key factors influencing wearing comfort. However, little is known so far about the underlying biophysics. In order to address this shortcoming, we have developed a custom-made research instrument for Sonova.

We realized a pressure sensitive matrix on foil with a total thickness of about 250 µm using screen-printing. The matrix consists of 96 (12 x 8) pressure sensitive pixels with a size of 1.8 mm x 1.8 mm (Figure 1). The pixels show a pressure dependent electrical resistance (i.e. resistance between silver fingers contacted by a carbon pad) and their design was optimized to enable contact pressure measurements in the low millibar range.

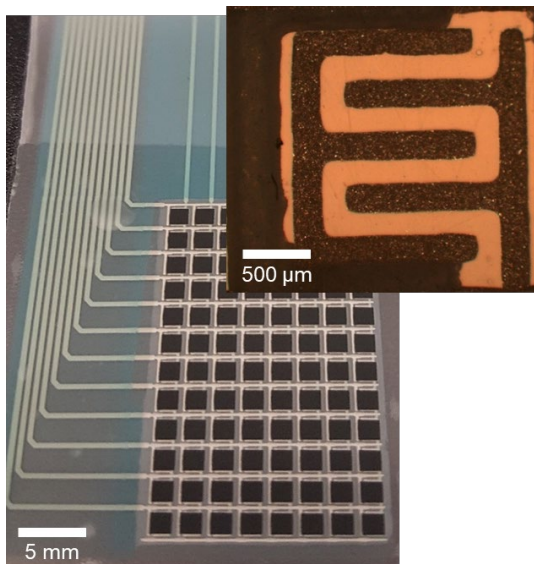


Figure 1: Photograph of the fabricated pressure sensitive matrix on foil (bottom image) and micrograph showing the inner workings (i.e. silver fingers) of a single pixel (inset).

The flexible matrix was rolled up and inserted into a PMMA tube with 11 mm inner diameter resembling a simple ear canal geometry (Figure 2). The electrical connections were passed through a slot opening which was sealed with silicone. Hard- and software for electrical read-out was developed and the system was calibrated using controlled air pressure.



Figure 2: Photograph of the developed ear canal model with integrated pressure sensors.

The system enables real-time pressure mapping and was tested using different silicone earpieces from Sonova, both in static (i.e. no movement of earpieces) and dynamic (i.e. moving earpieces) experiments. An example of a dynamic test is shown in Figure 3.

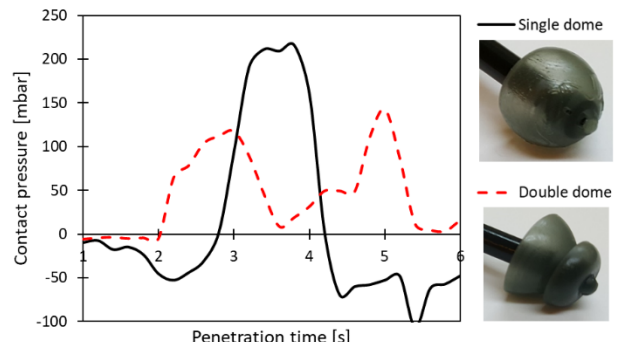


Figure 3: Real-time contact pressure responses of a selected pixel for different silicone earpieces (single vs. double dome) passing through the system. While positive pressure readings show the contact pressure of the different domes, negative pressure readings are indicative for shear stresses.

Our printed pressure sensor technology enables the fabrication of custom-made pressure mapping systems on flexible substrates. The design of the systems can readily be adapted to cover the targeted pressure range (mbar to bar). The low thickness and high flexibility of the pressure sensitive foils greatly facilitate system integration. This capability was successfully demonstrated in this project by the realization of an artificial ear canal with integrated pressure sensors for the company Sonova.

We thank Dr. Markus Müller, Paul Wagner, Dr. Petra Gunde and Dr. Erwin Kuipers from Sonova AG for a great collaboration.



# PHOTOVOLTAICS & ENERGY MANAGEMENT

Christophe Ballif

To curb and finally suppress CO<sub>2</sub> emissions, a fast transition of the energy system is required. In the most realistic and cost-effective scenarios, it should take place through a massive deployment of photovoltaics and wind energy, and by a major shift from fuel to electricity for transport and heating. This should be accompanied by increased penetration from electrochemical storage systems and by the selective use of biomass and of hydrogen for applications that require high energy density or longer-term storage (e.g., long-distance transport, heat for industrial processes, or wintertime electricity generation...). The 25% of total CO<sub>2</sub> emissions that are linked to agriculture also need to be addressed, for example by significantly improved management of soils and forests to recapture increased quantities of CO<sub>2</sub>. Figure 1 shows—with regard to electricity—what such a scenario would mean for the power sector in Europe, with an important increase in wind and solar electricity production, with a grid regulated and controlled, in large part, thanks to pumped-hydro and batteries. Storage will also ensure both the security and the continuity of the energy supply, facilitate exchange, and enable both local and global grid stability. This “e-transition” will need the support of technologies to forecast, control, and distribute electricity and energy. Hence, the three *Ds*—decarbonization, decentralization, and digitalization—are becoming core topics of discussion across all industries, including in Switzerland, leading all to question how best they can transition toward a more renewable and digitalized energy system.

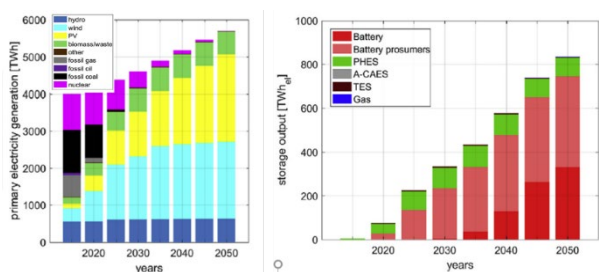


Figure 1: Example of a decarbonized scenario for the power sector in Europe—batteries combined with pumped-hydro storage (PHES) are used to manage, based on hourly simulation, the increasing amount of electricity from wind and solar. The global cost of electricity is reduced by ~20% compared to today. (Child et al., Renewable Energy 139, 2019, in the “area connected” scenario). A full energy system decarbonization scenario is presented in [1].

Switzerland is a country with a remarkably rich network of solar and cleantech industries, start-ups, and research entities. It has long been a provider of high-level deep tech and digital solutions, which are used locally or worldwide. Moreover, with its dense electrical grid and general electricity infrastructure (including

pumped-hydro), it can play a leading role in demonstrating the field application of novel solutions and in implementing them effectively at an impactful scale.

## Photovoltaics and energy management at CSEM

The program deals with three major activities—*Emerging PV and Thin-Film Devices*, *PV Cells and Modules*, and *Energy Systems*—and has close links with EPFL in Neuchâtel. It is based on unique technology platforms, illustrated in Figure 2, with over 2500 m<sup>2</sup> of high-tech facilities, with additional infrastructure shared with BFH on battery storage and a partnership with SUPSI on module testing. CSEM’s Photovoltaics & Energy Management program has built a strong technical team with expertise spanning multiple disciplines, from “new solar cells” to “the control of entire energy systems”. Access to CSEM’s established activities in the fields of system design, low-power electronics, coatings and surfaces, and printing technology constitutes an additional, unparalleled knowledge base for all multidisciplinary projects.

Today, CSEM’s diversified technology and patent portfolio in the PV&E program includes, for instance, the realization of advanced solar cells and modules with related processes and manufacturing equipment (with over 1.4 GW of production lines operating or under construction, directly linked to Swiss companies working with CSEM). CSEM has several new cell designs, based on crystalline silicon or tandem devices, approaching the industrial phase, and offers support to numerous Swiss customers who are looking for novel ways of integrating PV into the building envelope—including by using our colorizing solutions (such as white or terra-cotta active building elements)—or into mobility and stratospheric solutions based on our proprietary lightweight modules. Metrology tools, energy yield simulators, or weather forecasting algorithms are developed for multiple partners. Solar cells and small-size energy scavengers for the Internet of Things (IOT), with integrated low-power electronics, are now entering the market, including within the new Tissot T-Touch Connect Solar, whose solar dial is manufactured by CSEM. All this is completed by novel algorithms and hardware for battery performance prediction, predictive maintenance algorithms validated for, for example, wind turbines, and intelligent valves for the heating systems installed in many buildings.

Several of the technologies developed in the CSEM sustainable energy (SE) priority are also valuable in other applications, and these include coatings for medical applications, for greenhouses, or for special power-electronic components.

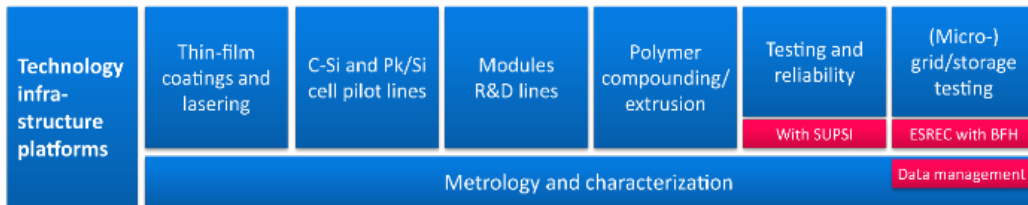
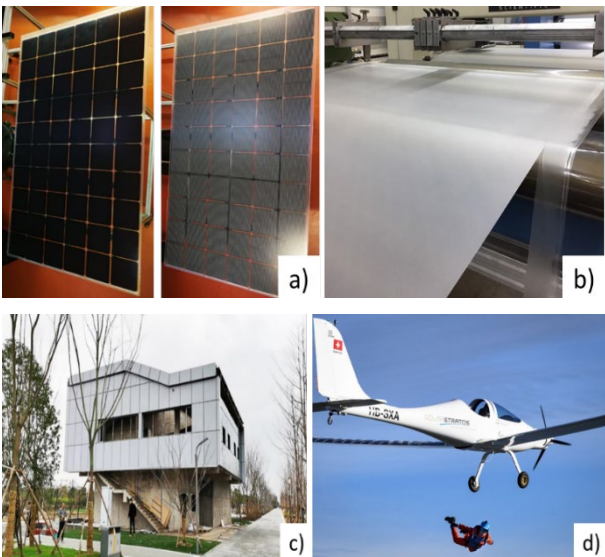


Figure 2: CSEM’s unique PV&E technology platform attracts many Swiss and international customers, for instance for the development of niche market, higher-value PV applications, including watches, solar boats or planes, solar blinds, and building elements, or for greenhouse heat management. Infrastructures include extensive testing facilities for reliability (in partnership with SUPSI) and electrochemical storage (in partnership with BFH) as well as software platforms for the digital grid focus area or for energy management (see, e.g., our [Maestro](#) software).

### The three core activities

The **Emerging PV and Thin-Film Devices** activity is divided in two major topics. In the first, we focus on new materials with applications for photovoltaics or power electronics, with a particular focus on perovskite materials and perovskite-based solar cells. In the second topic, we pilot the operation of a platform for the manufacturing of a new generation of small energy scavengers for use in IoT products such as wristbands, watch dials, and autonomous sensors, including high-solar-performance integrated generators or photodetectors. The platform offers the possibility to design and produce quickly devices from the mm<sup>2</sup> to cm<sup>2</sup> scale using unique tools for glass cutting or drilling, laser ablation, and printing conductive or protective layers, as well as advanced functional and decorative coatings. In joint internal or industrial project, high-value mobile or sensoric applications are targeted, relying on adding the expertise of CSEM in low-power electronics, communications, and data treatment.



*Figure 3: Some selected highlights of the Cells and Modules activity. a) First sixty-cell modules with CSEM patented IBC heterojunction technology (in partnership with Meyer Burger). CSEM achieves 25.4% efficiency on 25 cm<sup>2</sup> cells. b) Extrusion of CSEM high-quality PO foils for specialty PV applications and higher reliability. c) First white solar building, incorporating the white foils developed by CSEM and Solaxess. d) First solar sky diving, by Raphael Domjan, from the Solarstratos airplane with a new set of ultra-lightweight high-performance PV modules.*

In the **PV Cells and Modules** activity, a first focus is on the development of higher-performance crystalline PV cells, such as solar cells with high or low temperature passivating contacts, or back-contacted cells. A second focus is on the design of metallization (printing, plating) and corresponding module packaging to deliver solutions that extend lifetime and reliability, increase efficiency, and lower costs. We thus also support the development of new manufacturing hardware or metrology solutions, such as advanced solar testers. In a third focus, CSEM develops solutions for specific applications, in particular the design and realization of multifunctional PV elements—for example, for building applications—with which many companies in Switzerland and Europe deal. In particular, CSEM has developed several colorization and imaging PV technologies, which allow a number of customers to commercialize “invisible” PV modules, fitting roofs and facades with the best possible level

of architectural integration. A final focus is the design and realization of customer specific solutions for larger-scale mobile PV application. Lightweight, highly reliable modules find applications in mobility—for cars, planes, boats, drones, spacecraft, or stratospheric objects—or even in specialty building applications. Across these topics, we ensure that all related materials and processes, as well as the development of specialty in-house polymers for packaging, are fully mastered and controlled.

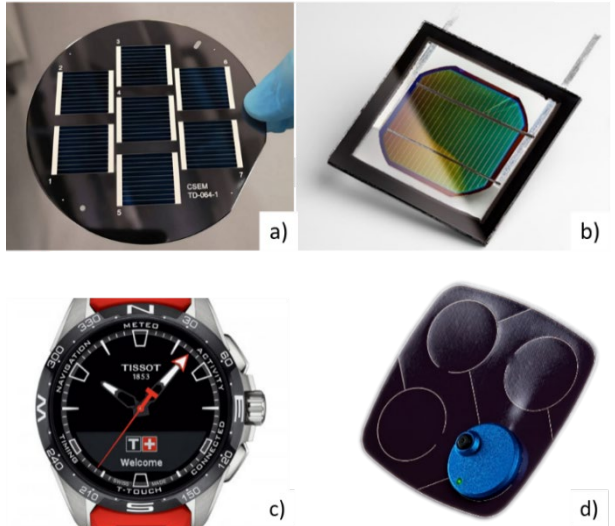


*Figure 4: Emerging PV and Thin-Film activity. a) Screen-printed perovskite-heterojunction solar cells reaching >26.5% on full wafers, with industry compatible processes. b) Improved reliability of perovskite silicon tandem with dedicated packaging on full 4" wafer size. c) Fully integrated, black solar dial designed and manufactured at CSEM incorporated into the new Tissot T-Touch Connect Solar. The dials are produced on the CSEM energy scavenger processing platform. d) PV flexible substrate for an ultra-low-power autonomous smart camera. The sticker can be glued on any surface and perform non-stop operation, without any external energy supply.*

In the **Energy Systems** activity we focus on two topics: In the Digital Grid topic, dedicated software and AI solutions are developed to interconnect energy vectors and control increasingly distributed energy resources. The global challenge CSEM contributes to meeting is how to best integrate these mixed energy generation sources with the wider grid, considering their intermittency and stochastic nature. This area draws on global research in data science and artificial intelligence to address specific challenges across energy applications—data efficiency, scalability, and reliability. The outcomes include solutions for autonomous, fast-learning control of buildings, and PV production forecasting outperforming existing solutions, as well as predictive maintenance of energy assets such as wind turbines and hydro or photovoltaic assets. In the Storage and Energy Management topic we deal with subjects primarily related to electrochemical and thermal storage. First, we address, through a combination of heavy battery testing and electro-physical models, the design of advanced models for battery degradation. Second, we consider the development of software and hardware for advanced battery management systems, including on-the-fly electro-impedance spectroscopy (EIS), which allows for a more accurate measurement of the state of charge and state of health of batteries. Finally, we deal with the optimal management of storage systems at local and district levels (e.g., our Maestro software). This includes thermal storage (e.g., heat pumps), electrochemical storage (batteries), and

electrical vehicles. Seasonal storage based on power-to-gas is also addressed. CSEM is also an initiator and founder, with BFH, of the [iBAT](#) Association, which promotes battery-based innovation in Switzerland.

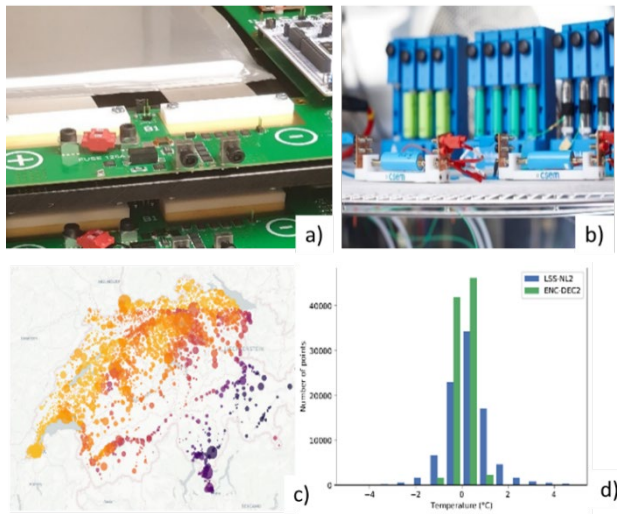


*Figure 5: Selected highlights of the Energy Systems activity. a) Cell-based battery monitoring incorporating in situ measurement of state of health and state of charge by impedance spectroscopy. b) Characterization and modeling of high-energy-density automotive batteries, allowing for enhanced battery lifetime and performance. c) Snapshot of rooftop PV production time series over Switzerland, allowing various high-precision forecasts and predictive failure identification. d) Reduced distribution of error of temperature prediction in a building: recurrent neural networks (green) or a linear state-space model (blue). The CSEM models allow for faster learning and adaptation of heating and cooling conditions in various types of buildings.*

---

[1] 100% Renewable Europe: How To Make Europe's Energy System Climate-Neutral Before 2050 (<https://www.solarpowereurope.org/100-renewable-europe/>).

# Deep Black Solar Cells for Energy Harvesting

J.-W. Schüttauf, E. Favre, M. Benkhaira, J. Brossard, C. Denizot, D. Dominé, P. Häfliger, J. Bailat

Aesthetics and visual appearance are particularly important for solar cell designs that are integrated in small-scale consumer applications such as watches, wearables, calculators and cell phones. More specifically, the ability to fabricate uniform, deep black appearing solar cell surfaces is especially desired by watchmakers. To this end, we have developed an n-type semiconductor layer that has a narrower optical bandgap than the principal absorber material of the solar cell. The n-layer absorbs the lower bandgap photons for which the base of the solar cell is optically transparent. This intentional parasitic absorption leads on the one hand to a slightly reduced power output, but on the other hand to a strongly reduced red color appearance. Furthermore, two different anti-reflective coatings are added that improve both the power output and reduce the reflection over a relatively wide wavelength range. Combining both approaches leads to a strongly enhanced deep black color appearance of our solar cells and dials.

The integration of photovoltaic solar cells in small-scale devices such as watches, wearables, calculators and cell phones can strongly improve their power autonomy, and even make the application fully independent of external power sources<sup>[1]</sup>. For such energy harvesting applications, the aesthetics and visual appearance of the integrated solar cells are particularly important. Standard amorphous silicon thin-film solar cells are often deemed too red to be integrated in a final product. The red-brownish color is the result of the high bandgap of the absorber material, making it transparent for (infra)red photons.

We have developed a simple, elegant and effective manner to fabricate thin-film silicon-based solar cells with a deep black color appearance using an n-type amorphous silicon-germanium (a-SiGe:H) layer with a high (infra)red photon absorption due to its lower optical bandgap, combined with two different types of anti-reflective coatings on the front side of the device<sup>[2]</sup>. a-SiGe:H has usually been applied in thin-film silicon solar cells as a low bandgap absorber layer in multijunction devices<sup>[3,4]</sup>. In the case of an n-layer, the intentional parasitic absorption leads to a reduced current density for longer wavelengths. However, it also leads to a strongly reduced red color appearance (see Figure 2). Additionally, two different types of anti-reflective coatings are applied on the front side of the device to (i) further improve the deep black appearance, and (ii) slightly enhance the photogenerated current density.

In Figure 1, the wavelength-dependent reflectance of four different device structures is shown: (1) our standard a-Si:H solar cell, (2) our standard a-Si:H solar cell with anti-reflective coatings, (3) a cell with our novel n-type a-SiGe:H layer, and (4) a cell with our novel n-type a-SiGe:H layer with anti-reflective coatings. In Table 1, the color parameters  $L^*$ ,  $a^*$ ,  $b^*$ , as well as the short circuit current density and cell efficiency are shown. In the CIELAB color space, the parameter  $L^*$  indicates the lightness (100 = white, 0 = black), whereas  $a^* > 0$  indicates the redness of the sample.  $b^*$  ranges from blue (negative) to yellow (positive).

In summary, we observe that applying the n-type a-SiGe:H layer strongly decreases the red color appearance, while adding the anti-reflective coatings strongly reduces the lightness ( $L^*$ ) of our

solar cells. A combination of both approaches is thus a very effective manner to strongly improve the black color appearance of our solar cell devices, making them very suitable for integration in a wide range of products for energy harvesting applications.

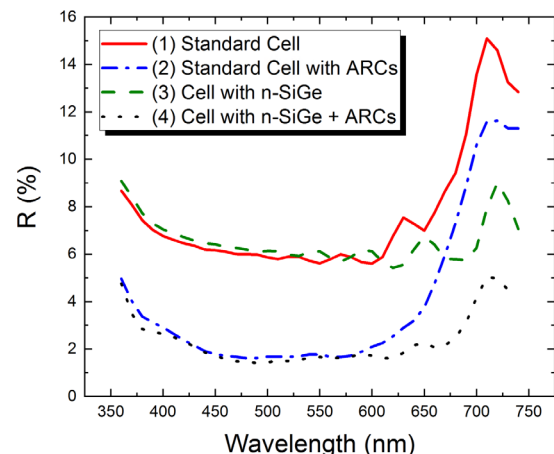


Figure 1: Wavelength dependent reflectance of the four different device structures.



Figure 2: Photograph of the four different color tones, displayed in increasing order from left (1) to right (4).

Table 1: Color parameters  $L^*$ ,  $a^*$ ,  $b^*$  (CIELAB color space, D65, SCI), as well as short circuit current density and efficiency for the four different device structures.

Cell Type	$L^*$	$a^*$	$b^*$	$J_{sc}$ (mA/cm <sup>2</sup> )	Eff (%)
1	29.3	2.3	-1.0	14.5	9.1
2	14.8	6.0	0.1	14.9	9.4
3	29.4	0.2	-1.8	11.9	7.4
4	13.4	2.9	-1.4	12.2	7.7

[1] Developed in collaboration with CSEM: TISSOT T-TOUCH CONNECT SOLAR: <https://www.tissotwatches.com/en/t1214204705101.html>

[2] J. Bailat, et al., "Black-Coloured Photovoltaic Device", Patent Publication No. WO/2020/169789 (2020).

[3] B. Yan, et al., J. Vac. Sci. Technol. A 30 (2012), 04D108.

[4] J.-W. Schüttauf, et al., Sol. Energy Mater. Sol. Cells 133 (2015), pp. 163-169.

# From an Internal Research Project to a Product: The Wear-a-Watt Project and a Production Platform for IOT Energy Harvesters

C. Aeby, J. Bailat, C. Ballif, R. Barbey, M. Benkhaira, G. Bergonzi, S. Bogdanovic, J. Brossard, C. Denizot, D. Dominé, O. Dubochet, E. Favre, M. Ferrara, O. Fetticha, P. Häfliiger, S. Hallinger, L. Maire, L. Re, K. Schürch, J.-W. Schüttauf, M.-J. Tschudi

We summarize here the outcome of a multi-interdisciplinary project called Wear-a-Watt and how this study evolved into an industrialization and a production project with an impact on the whole value chain in Switzerland.

In 2015, CSEM initiated the 'wear-a-watt' project where the objective was to assess how much energy can be harvested on average over a year by solar cells integrated in the dial and the wristband of a wristwatch. The prototype watch could therefore measure, store temporarily and finally transmit via Bluetooth the data through a gateway – a smart phone or a tablet – which were finally collected into a database hosted on a server.

The goals were to evaluate the amount of energy one can collect, to understand the use cases that PV technology could open for wearables and finally to understand the key factors to optimize new PV solutions for wearables.

To produce the solar cells, we used the technology based on thin film silicon solar cells, also called "amorphous silicon". The key reason to use this technology for this application was the ease it provides for the integration in a tight space and the multiple possibilities to pattern and shape the cells. What's more it is known for its efficiency under low or artificial illumination (up to 20% efficiency under indoor lighting) and for the possibility for monolithic interconnection - the manufacturing of several individual cells on the same substrate and interconnecting them electrically in series during the production process without having to stack or solder them after their manufacturing.

One of the results of the 18 months study showed that for a significant proportion of the bearers most of the energy comes from the few moments outdoor where the cell is powered by the strong sunlight instead of artificial or low indoor light.

When making bespoke PV dials for this project we observed that the thin film silicon cells on the market for watch applications show usually a fairly high series resistance which hinders the power produced at high illumination compared to the potential of the technology, unless the solar cells are patterned as "mini-modules" which shows then strong optical marks. This is not a practical issue since those cells are usually hidden under a decorative watch dial for aesthetic reasons, and because of the typical low energy requirements of watches with basic functions. However, were these cells to be used directly without decoration, they would not be able to benefit to the full extent from the stronger light conditions.

In the wear-a-watt approach, we used very low series resistance transparent contacts which allowed us to design a single-cell PV watch dial that benefited from stronger light conditions. Combined with an aesthetics surface, the cells do not need to be hidden under a decorative semi-transparent dial anymore. Combining better cell aesthetics and better outdoor performance, CSEM thin film solar cells can tap into the few moments outdoor when a lot of energy is available, delivering more power for the application, while still providing enough energy for basic functions for "indoor" users.



Figure 1: Top left and clockwise. The T-Touch Solar Connect Solar incorporating CSEM PV watch dial, the first wear-a-watt prototype dial, the visual inspection of PV watch dials produced on CSEM's PV platform.

Both aesthetics and performance are related to the fact that the substrate used for the processing of the amorphous solar cells resides in a glass substrate. This is not a new approach in the field of PV but what is new is the use of single-cell glass substrate based solar cells in a watch.

The hurdles that were overcome in the development phase for an industrial production of the watch dial were multiple. For instance, we had to adapt and develop various techniques for the precise drilling of the center hole and for the dicing of the PV dial, keeping the tolerances required by the application (including resistance to shocks, absence of marks or residual dust), while preserving the properties of the solar cells. Several solutions were developed with local partners, one of them being the Bienné based company Posalux, who develops a new technology for dicing glass without taper angle.

The industrialization involved several other local partners and suppliers and the support from the customer, a collective effort that involved many companies across the value chain.

The expertise and efforts developed in the project, allows now CSEM to manufacture small size products in significant quantities. The platform put in place for this project enables the fast development and the launch of fabrication for new autonomous products in the field of sensors, IOT and of course watch related application, supporting many companies in Switzerland and creating jobs all along the value chain. The efforts put in place to produce the dials were also rich in learnings and further enhance the capacity of CSEM to help its customers in their industrialization phase.

# Optical Coating for Fluorescence-based Diagnostics and Advanced Microscopy

R. Barbey\*, J.-W. Schüttauf, N. Descharmes \*\*, J. Bailat

Fluorescence-based analyses are widely spread in the fields of life sciences and medical diagnostics. The use of light-emitting dyes enable the detection, visualization and localization of molecular species in biological samples otherwise undetectable with conventional microscopy methods. This technique is at the heart of technologies such as next generation sequencing, high content screening, or protein or antibody microarrays. The amount of detectable fluorescence signal constitutes the ultimate limitation in terms of sensitivity and reliability of this type of measurements.

Whether in medical diagnostics or life sciences, it is common practice to use fluorescent molecular probes to reveal the presence of biomarkers in biological samples. These biomarkers can be, for example, antibodies, DNA strands, proteins, etc. The capacity to detect minute amounts of light emitted by low abundance markers is thus of the greatest interest, in particular in the view of detecting severe pathologies at an early stage. Many fluorescence-based analyses are performed on glass or plastic labware such as microscopy slides or Petri dishes. Unfortunately, this approach turns out to be quite inefficient since a large part of the emitted fluorescence remains trapped within the labware and thus cannot be detected during the analysis.

In collaboration with the Laboratory of Photovoltaics and Thin Film Electronics (PVLAB) of EPFL, the CSEM has developed a silicon based optical coating that is capable of strongly improving the detection of fluorescent species located in its vicinity. Fluorescence signal enhancements greater than one order of magnitude have been achieved on a broad range of wavelengths (colors). Figure 1 demonstrates this effect and shows how the nanostructured surface can amplify the signal for three fluorescence channels (488 nm, 532 nm, and 647 nm) simultaneously.

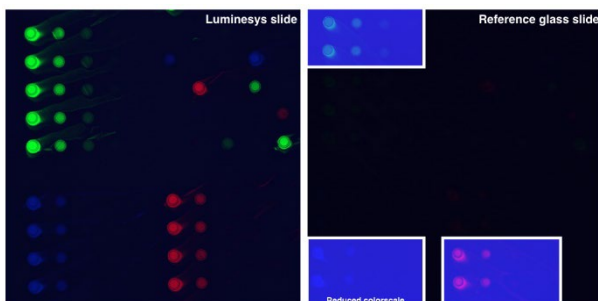


Figure 1: Comparison of fluorescence images for spots of three different fluorescently-labelled proteins deposited on the engineered slide (left) and a standard microscope slide (right). Identical imaging conditions.

The coating can be deposited on a variety of substrates. In its current implementation, the technology is being provided to pilot customers and users in the form of coated microscope slides. The slides are produced in batches of 100 following a chemical vapor deposition, with an excellent uniformity of the enhancement effect and enabling us to reach a high production yield.

We have demonstrated that these slides can be used, for example, to decrease the limit of detection of a protein microarray (Figure 2). The signal to noise ratio is improved by a factor of 25,

allowing faster and more sensitive testing. The slides have also been used successfully to decrease the acquisition time of multichannel immunofluorescence analyses of biopsy microsections when recorded with a Whole Slide Imager (Figure 3). These results have been confirmed by our pilot partners. Exciting results have also been achieved in other applications such as enhanced Raman spectroscopy and high-contrast dark-field imaging.

The optical coating that we have developed holds great promises for the medical diagnostics and life sciences domains in general. By acting directly on the light-emission properties of the analyte, we demonstrate that a whole new field of performance and functionalities is at hand. A start-up company, Luminesys, is being founded to exploit the results of this research.

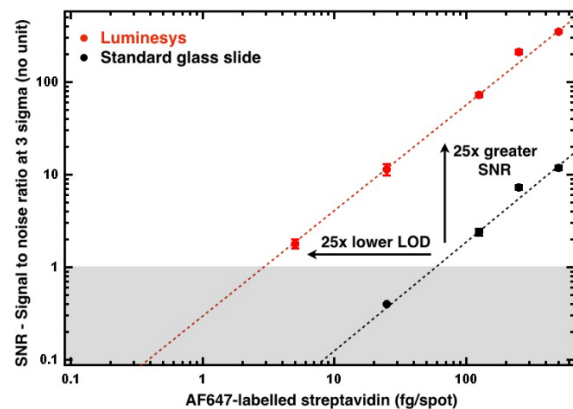


Figure 2: Signal-to-noise (SNR) as a function of labeled protein concentration. Comparison between the engineered slide (red) and a standard microscope slide (black), showing a 25x enhancement of the SNR, which directly translates in a reduction of the limit-of-detection (LOD) by a factor 25.

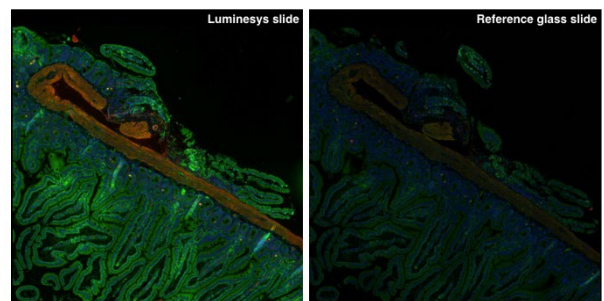


Figure 3: Four-color immunofluorescence staining of intestine tissues. Comparison of fluorescence images obtained in identical conditions on the engineered slide (left) and a standard microscope slide (right).

\* Creator of the « GoBeyond » project, co-founder of Luminesys  
[www.luminesys.com](http://www.luminesys.com)

\*\* EPFL, Institute of Microengineering (IMT), Photovoltaics and Thin Film Electronics Laboratory (PV-Lab), Neuchâtel, Switzerland, and creator of the « GoBeyond » project, co-founder of Luminesys.

# DIPPS—Upscaling of Perovskite/Silicon Tandem Cells

B. A. Kamino, B. Paviet-Salomon, A. Descouedres, L. Lauber, P. Wyss, L. Ding, S. Nicolay

Perovskite/Silicon tandem solar cells have the potential to push solar panel efficiency significantly beyond its current limits. However, moving these devices beyond small laboratory samples towards cells that resemble standard PV products requires the integration of industrially compatible processes into their process flow. By combining the process toolsets of an industrial partner along with several internal developments, CSEM has demonstrated an efficient, large-area tandem solar cells deposited using a number of scalable processes.

As the leveled cost of electricity for photovoltaic (PV) installations continues to fall, the industry is continually looking for new technologies to continue pushing this value ever lower. The most effective way to do this is to increase the conversion efficiency of cell within the panel. However, current cell technologies are quickly reaching their thermodynamic limits and new paradigms are required to continue this growth. Perovskite/Silicon (PK/Si) tandem solar cells are a very promising avenue to accomplish this goal with laboratory devices of over 29% efficiency being published and significant potential for even higher efficiencies.

Despite this remarkable efficiency, current known processes for fabricating PK/Si tandem solar cells are largely limited to small research sized samples ( $\sim 1 \text{ cm}^2$ ). For these device types to eventually reach the market, low-cost deposition processes that are compatible with standard 6-inch PV wafers and the unique stability requirements of perovskite solar cells need to be developed. Of the many new processes required, the most prominent include preparation of compatible bottom silicon solar cells, large-area deposition of the perovskite layer, low-temperature metallization, and encapsulation.

The DIPPS project seeks to meet these challenges by partnering with Meyer Burger Research (MBR) within the framework of an Innosuisse project. By leveraging the production experience of MBR along with their large-scale toolsets, industrially compatible bottom cells for large area PK/Si tandem solar cells were produced. In parallel, large-area perovskite deposition techniques were developed within CSEM.

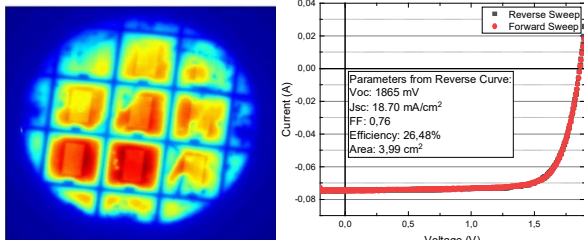


Figure 1: (left) photoluminescent image of Si wafer damaged by old tandem integration process (right) LIV curves from a small PK/Si cell with printable metallization and an improved tandem integration process.

The first challenge of this project was improving the base efficiency of PK/Si tandem process at CSEM. It was found that paying careful attention to handling and process integration was critical in avoiding damage to the silicon bottom cells. These improvements along with developments in low temperature Ag pastes allowed the demonstration of small tandem devices of up to 26.5% efficiency (Figure 1). Turning towards scaling up of this architecture, a standard sized silicon bottom cell adapted for tandem integration was needed. Such cells for small laboratory sized cells typically use mechanically polished wafer surfaces. Due to the large cost of these wafers, an inexpensive wet-chemical approach must be found for industrialization. To this end, a chemical polishing step was developed to provide a

microscopically smooth surface compatible with a solution processed perovskite layer. By transferring contact layer processes from CSEM to MBR's production level equipment, silicon cells ready for tandem integration could be realized. In order to coat a perovskite layer on top of these cells, a deposition method which inexpensively deposits perovskite layers over at least a 6-inch wafer was needed. To accomplish this, a meniscus coating-based approach was developed at CSEM. Key to this approach is an innovative perovskite ink formulation. Unlike most perovskite inks, we have developed an ink which allows the deposition of state-of-the-art perovskite compositions without the use of highly toxic solvents. Additionally, we demonstrate that such inks can tolerate high coating speeds allowing the coating of a standard PV wafer on the order of 1-2 s.

Bringing all of these developments together, a large area perovskite/silicon tandem solar cell ( $100 \text{ cm}^2$ ) on a standard PV wafer format (M2) was produced. Initial results show promising efficiencies of over >22% (Figure 2). More importantly, it is demonstrated that by carefully controlling the silicon surface can result in a perovskite layer without any significant coating defects leading to shunts. Optimization of the contact layer materials on the perovskite cell and further improvements to the passivation of the bottom silicon cells are expected to push these efficiencies up to 25%. Work in encapsulating these samples is on-going and initial tests indicate that standard glass-glass lamination is largely compatible.

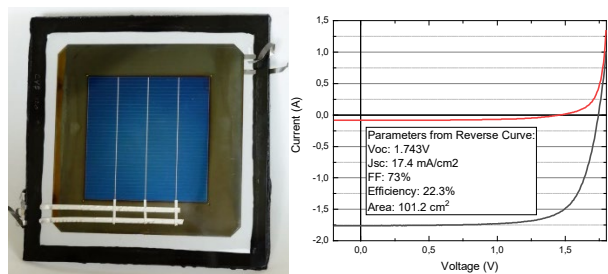


Figure 2: (left) an encapsulated large-area PK/Si tandem solar cell based on an M2 wafer (right) LIV curves from a large-area PK/Si cell. Black and red curves represent the cell output at 1 and 0.05 suns, respectively.

Through this project, we have demonstrated a potentially viable process flow towards large area PK/Si tandem cells. This feat places CSEM as only one of two institutions in the world to demonstrate this. As well, the technology transferred to the industrial partner will significantly improve their knowledge base in developing this device type. The knowledge built in this project should provide a robust base with which to further extend this technology towards other silicon solar cell technologies.

# Development of Sputtered Passivating Contacts for Industrial, High-efficiency Silicon Solar Cells

J. J. Diaz Leon, A. Ingenito, P. Wyss, C. Alleb  , S. Nicolay

Current Si-based industrial solar cells suffer from high-surface recombination at the contacts between the absorber and the metal electrodes. The introduction of passivating contacts avoids this detrimental effect by physically separating light absorption and current extraction. In this work, we show the development of high-temperature compatible passivating contacts deposited by sputtering, which will pave the way for the industrialization of high-efficiency solar cells.

Passivating contacts (PCs) compatible with high-temperature processing have recently seen a renaissance<sup>[1]</sup> in Si-based solar cells and achieved very high efficiencies up to 24.8% in industrially relevant devices<sup>[2]</sup>. These devices are based on a thin interfacial oxide ( $d < 2$  nm) covered by a doped polySi layer and activated during a thermal process. PCs passivate the full area of the device while enabling selective charge extraction. This combination in turn allows for an increased open-circuit voltage of the device and a higher solar cell efficiency. The most common integration approach replaces the backside of a standard PERC/PERT device (Figure 1a/c) with a doped polySi layer at the rear (Figure 1b/d, respectively).

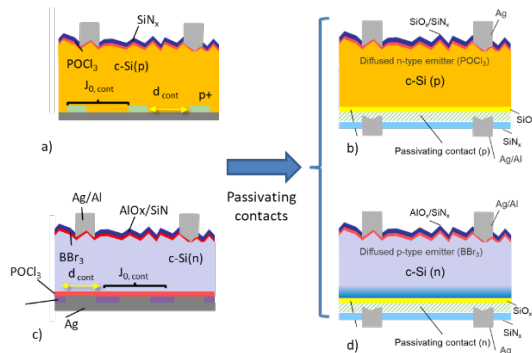


Figure 1: Current a) PERC and b) PERT solar cell architecture upgraded with (b) p-type polySi or d) n-type polySi on the rear side.

Even though there is a clear advantage when applying PCs to solar cells, their integration is still unclear. Low-pressure chemical vapor deposition (LPCVD) is typically used for the deposition of the polySi layer; however, LPCVD suffers from "wraparound" at the cell edge and requires thick ( $d > 150$  nm) polySi layers, making this process cumbersome. Recently, ANU has developed a polySi deposition process based on sputtering with an impressive device efficiency of 23%<sup>[3]</sup>. Sputtering is a very attractive deposition technique for PCs, given its low cost, high-throughput, its ability to deposit truly single-side, and the lack of toxic gases used in the process.

At CSEM, we are developing passivating contacts based on sputtering using DC-magnetron sputtering, a scalable deposition technique. Furthermore, our work is focused on metallizing these structures using a combination of dielectric deposition for layer hydrogenation, screen printing of metallic fingers and subsequent fast firing, as it is done today for PERC devices industrially. Figure 3 shows our current structure for n- and p-type sputtered PCs (Figure 2a and c, respectively) along with photoluminescence (PL) images of these passivating contacts

once metallized (Figure 2b and d for n- and p-type PCs, respectively). These PL showcase the lack of metallization damage on the screen printed fingers (not visible in the image), with only some damage present when the metallization area is largely increased to more than 50% in the case of polySi(p). (top left in Figure 2d). The n-type polySi is doped via an ex-situ process, while the p-type contacts are doped in-situ (sputtering a mixture of Si and B).

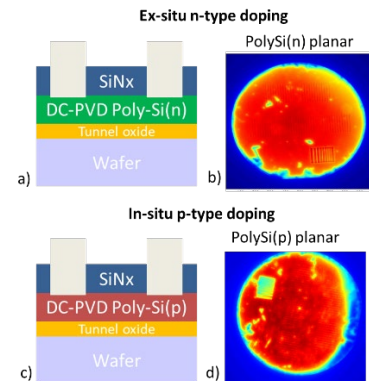


Figure 2: Sputtered PCs metallized using screen printing and firing. a) and c) show a schematic of the p.

Table 1 shows the best passivation (implied voltage  $iV_{oc}$  and surface recombination current  $J_0$ ) and contacting results (contact resistivity  $\rho_c$ ) achieved on symmetrical structures with sputtered PCs developed at CSEM. As it can be seen, this solution presents a combination of very high surface passivation with low contact resistivity, which make them ideal candidates for their integration into high-efficiency solar cells. Currently, CSEM is working on developing solar cells implementing either one or both-polarity sputtered PCs, keeping in mind a lean process integration route.

Table 1: Passivation and contact resistivity results achieved on symmetrical structures at CSEM using sputtered PCs.

	$iV_{oc}$ [mV]	$J_0$ [fA.cm <sup>-2</sup> ]	$\rho_c$ [m��.cm <sup>-2</sup> ]
PolySi(n) planar	742	5	36
PolySi(n) textured	726	9	11
PolySi(p) planar	718	14	16

[1] A. Richter, et al. Solar Energy Materials and Solar cells 173, 96 (2017).

[2] Online announcement: <https://ir.jinkosolar.com/news-releases/news-release-details/jinkosolar-large-area-n-type-monocrystalline-silicon-solar-cell>

[3] D. Yan, et al., Applied Physics Letters 113, 061603 (2018).

# AMPERE—Silicon Heterojunction for High-performance Photovoltaics

B. Paviet-Salomon, A. Descoeuilles, J. Zhao, L.-L. Senaud, G. Christmann, J. Geissbühler, A. Faes, A. Lachowicz, C. Allebé, N. Badel, G. Nogay, J. Champliaud, P. Wyss, J. Levrat, D. Petri, G. Cattaneo, H. Li, J. Escarre, S. Nicolay, M. Despeisse, C. Ballif.

In the frame of the H2020 project AMPERE<sup>[1]</sup>, CSEM is fostering the installation of a fully automated 200 MWp pilot production line of silicon heterojunction solar cells and modules in Europe. The main tasks covered by CSEM are the qualification of n- and p-type silicon wafers, the development of tailored wet-chemistry recipes and advanced TCO materials to increase the conversion efficiency of SHJ devices, as well as several key contributions to ensure the 25-year reliability of SHJ modules.

The silicon heterojunction (SHJ) technology is considered as one of the most serious challengers to take over the mainstream PERC technology in the near future. Indeed, SHJ solar cells uniquely combine high power conversion efficiency, with best-in-class SHJ devices reaching >25% efficiency in industrial environments, along with fewer production steps than PERC-like devices. Moreover, the SHJ technology features a low temperature coefficient (< -0.3%/°C) as well as high bifaciality (>90%), which foster a high energy yield for bifacial SHJ modules in the field, hence decreasing the levelized cost of energy. Furthermore, owing to its stress-free symmetric structure and to its high level of passivation, the bifacial SHJ technology ideally benefits from the current industrial push towards the integration of thinner silicon wafers.

Along these lines, CSEM and 13 other European stakeholders joint their efforts to foster the transition of PV manufacturers towards the SHJ technology in the frame of the H2020 AMPERE project (2017 – 2020). The AMPERE<sup>[1]</sup> project – short for "Automated photovoltaic cell and Module industrial Production to regain and secure European Renewable Energy Market" – aims at supporting the installation and ramping-up of a fully automated 200 MWp pilot production line of SHJ solar cells and modules in Catania, Sicily, in the premises of the company Enel Green Power.

In the frame of this project, CSEM conducted dedicated studies with p-type CZ wafer materials to check its compatibility with high efficiency SHJ solar cells manufacturing. CSEM demonstrated that by a proper selection of p-type materials specifications and adapted SHJ processes, excellent SHJ devices can be achieved on p-type wafers, with efficiencies on par with those obtained on n-type materials (see Figure 1). Remarkably, SHJ devices on p-type wafers demonstrated up to 23.6% efficiency and high-performance stability over the whole ingot length. This is an important leap towards a wider acceptance of the SHJ technology, as p-type materials still represent the larger part of the total silicon wafers production.

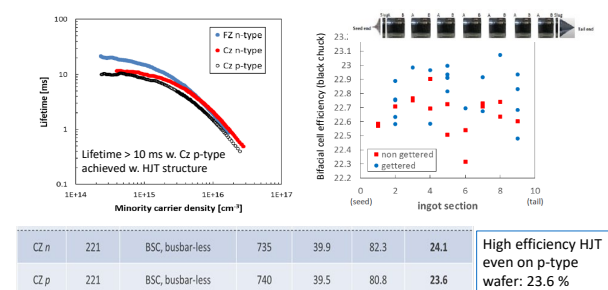


Figure 1. Lifetime curves (top left), efficiency along the silicon ingot length (top right), and best results (bottom table) for SHJ solar cells on p- and n-type silicon wafers.

In addition, CSEM tested a new commercial texturing additive to decrease the pyramids size to 2-3 µm with enhanced batch-to-batch stability in pyramid size distribution, wafer reflectivity and cell electrical parameters. Such properties were compared with the CSEM reference additive. The new additive creates much smaller pyramids with a sharper distribution in size, as illustrated in Figure 2. Consequently, a 0.1 mA/cm<sup>2</sup> gain in J<sub>sc</sub> was obtained by using the new texturing additive owing to the lower wafer reflectivity with small pyramids.

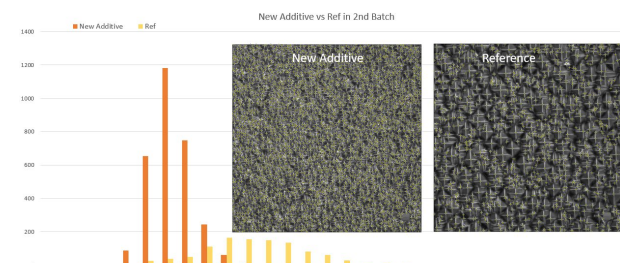


Figure 2. Pyramid size distribution and confocal microscopy images of wafers textured with the reference and the new additives.

CSEM also developed advanced TCO materials to replace the standard ITO. Here, IWO was demonstrated to provide higher carrier concentration and mobility, resulting in lower series resistance losses, hence higher FF, together with higher transparency, resulting in higher J<sub>sc</sub> (see Figure 3). The gains have been estimated to be 7 to 8 W for a 72-cell module. Importantly, encapsulated IWO SHJ cells were demonstrated to pass 500h of damp heat test without major degradation.

	Thickness (nm)	[N] carrier density (cm <sup>-3</sup> )	$\mu$ (cm <sup>2</sup> /(V.S))	Rsheet (ohm/sq)
ITO	100	1.2E20	26	209
IWO	115	1.9E20	70	41

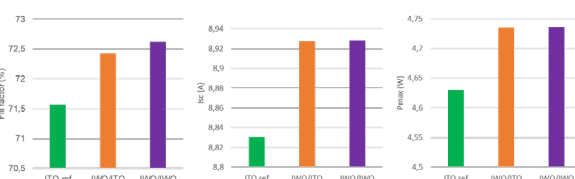


Figure 3. Properties of IWO compared to ITO (top table) and results once integrated into SHJ devices (bottom graphs).

CSEM further contributed to several other key developments to boost the efficiency of SHJ modules, as well as ensuring their 25-year reliability as requested by the IEC norms. As a major result of the whole AMPERE project, the Enel Green Power's fully automatized 200 MWp SHJ production line was ramped-up in due time, routinely producing high efficiency SHJ solar cells.

[1] H2920 AMPERE project, [www.ampere-h2020.eu](http://www.ampere-h2020.eu)

# Finding the Best Models for Model Predictive Control in Buildings

B. Schubnel, R. E. Carrillo, P.-J. Alet, A. Hutter, T. Gorecki

As a complement to thermal renovation, integration of intelligent controllers in buildings can significantly reduce the CO<sub>2</sub> footprint of heating and cooling systems by increasing their usage efficiency. Within the European project SABINA, CSEM investigated what could be the best machine learning architecture to represent and control complex buildings. Representation power does not go hand in hand with controllability, and our results suggest that linear state space models with simple non-linear regressors give better control results than RNN architectures for model predictive control. The best architecture found in our study has been deployed on the CSEM site in Neuchâtel.

Deep learning architectures have been increasingly popular to model non-linear physical systems. They are known to provide a net gain in prediction accuracy as compared to state of the art (linear state space models). However, if deep models are used within an optimization problem, their non-convexity creates issues, and their higher accuracy does not necessarily translate into a net gain for optimal controllers built on top of them. Energy management in buildings is a representative example of systems where such models can be used, as recent technical equipment (heat pump, HVAC) or low-level control loops are a source of non-linearities.

CSEM recently investigated deep architectures called recurrent encoder-decoder networks (or "seq2seq" models), that show very good representation power on a large set of physical systems. We have shown [1] that they could effectively be used as models to control complex physical systems, in particular large building facilities, using as controllers neural networks trained with state-of-the-art reinforcement learning (RL) algorithms. Using model-based RL algorithms for optimal control is a promising path for such non-linear architectures but is still in its infancy for industrial applications due, notably, to sample inefficiency and difficulties in reward shaping.

In our recent work [2], we investigated how encoder-decoder models were performing with respect to linear state space models coupled with non-linear regression (LSS-NL), in the case were traditional optimization techniques (here sequential quadratic programming, SQP) rather than RL are used to solve the optimal control problem. Our study was made on a simulated building with four apartments, eight thermal zones and solar panels on its roof (Figure 1).

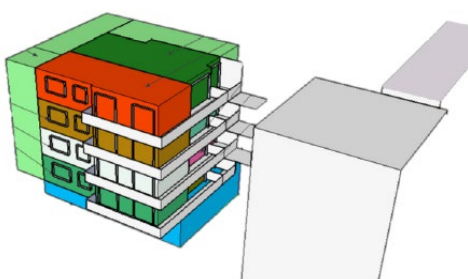


Figure 1: Overview of the test building with its four floors.

[1] B. Schubnel, R. E. Carrillo, P.-J. Alet, A. Hutter, "A Hybrid Learning Method for System Identification and Optimal Control," IEEE Transactions on Neural Networks and Learning Systems (2020) [doi:10.1109/TNNLS.2020.3016906].

The simulated building incorporated two main sources of non-linearities. Its first source is a geothermal heat pump that provides heat to the living spaces and the hot water tanks; see Figure 2. Its second source is a low-level control loop (that cannot be changed, as often in real buildings) that triggers the opening of the thermostatic valves and the on-off cycles of the pump, based on the room temperature setpoints.

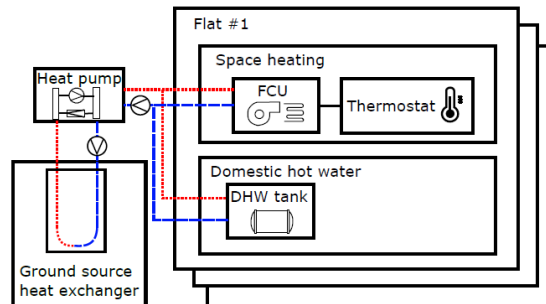


Figure 2: Schematic view of the heating and distribution system.

The purpose of the optimal controller was to respect the temperature constraints in the building (the zone temperatures had to stay between 19°C and 23°C) while minimizing the energy exchanged with the grid (i.e., consuming as much as possible its own PV production). Both architectures were used to solve the same optimization problem under the same conditions with SQP.

As expected, encoder-decoder architectures need more samples to carry out proper system identification but are more accurate once enough data are used. More surprisingly, the objective minimization with SQP was best performed with the simpler architecture, even if it slightly underperformed on the comfort constraints. Even if we tried to optimize the computation time with the encoder-decoder, and performed gradient computation with the GPU, we could not achieve the same computation time as with simpler models.

Based on these results, CSEM has developed a library for model predictive control with the LSS-NL architecture and deployed it successfully in the CSEM building ("Ecrivain" and "Dessinateur" meeting rooms).

This project has received funding from the European Union's Horizon 2020 research and innovation program under grant agreement no 731211, project SABINA.

[2] B. Schubnel, R. E. Carrillo, P. Taddeo, L. C. Casals, J. Salom, Y. Stauffer, P.-J. Alet, "State-space models for building control: how deep should you go?," Journal of Building Performance Simulation 13(6), 707–719, Taylor & Francis (2020) [doi:10.1080/19401493.2020.1817149].

# A Software Solution to Manage Local Energy: from the House to the District

T. Gorecki, A. Hutter, R. Langou

The local management of energy systems will be a key enabler in the future of a power grid incorporating more and more decentralized resources. CSEM has developed a software solution to manage energy at the district scale that focuses on energy cost reduction. It implements a predictive control approach where weather forecasts are used in combination with prediction models for the district subsystems to determine in real time the best strategy to store, produce and consume energy. This solution was deployed in several buildings' energy managers in partnership with a consortium of startup led by Soleco.



Buildings are increasingly being outfitted with solar panels, heat pumps, electric batteries, electric vehicles (EVs) charging stations and other means of producing and storing energy, all of which interconnect with the electrical grid. At the level of a neighborhood, these decentralized energy sources form a complex network.

Managing these multi-energy systems and optimizing energy costs raises several questions. Should energy be consumed when it is produced, sold to the grid, or stored for later use? And how should energy sources be distributed if there are groups of consumers generating their own energy? In the framework of the European project PENTAGON, CSEM has developed smart, predictive software capable of providing real-time answers to these questions. Designed for non-specialists, it uses weather forecasts, data from local infrastructure, residents' consumption habits and market energy costs. As its name indicates, Maestro is like an orchestra conductor that automatically manages resources and keeps costs down. An online simulator, based on a building with eight family apartments, has been developed to demonstrate its potential and is accessible on the CSEM website.

The software is easy to use and can be flexibly adapted to different neighborhoods. To start with, parameters such as solar panel size, buildings' surface area, battery storage capacity and user preferences and priorities are fed into a configuration file. The system combines state-of-the-art control algorithms, namely mixed-integer linear model predictive control, and forecasting algorithms to calculate minimum cost operation strategies. Production data from energy installations, provided by sensors, are collected, and then sent to the cloud, where Maestro automatically compares possible consumption decisions and identifies the most cost-effective one, considering both energy power consumption peak costs. Instructions are sent back to a

local gateway computer, which carries them out on site. Through a feedback loop, the plan is updated every 15 minutes in response to new events (such as an electric vehicle arrival).

Maestro can incorporate boilers, heat pumps and EV charging stations, as well as electric batteries, renewable energy sources such as solar panels, power-to-gas facilities, thermal storage tanks, and more.

Competitor systems on the market are designed for single-family homes and often apply a simple strategy: increase consumption when photovoltaic energy is produced. This can lead to over-consumption of energy and as a result to very marginal cost savings, if any<sup>[1]</sup>. Maestro does not use predefined rules but calculates the best use of energy at any point in time, based on weather forecasts and energy costs. In addition, it integrates new elements such as EVs, heating & cooling of the house, etc. With Maestro, cost savings will vary from home to home and user to user. A preliminary study on the first house running Maestro revealed an approximately 20% reduction in heating costs alone.

Maestro works for individual buildings, but it could also prove very useful for a prosumer community, where renewable energy sources are shared across several buildings. In 2018, Soleco, based in Maur in the canton of Zurich, won CSEM's Digital Journey Award together with its partners Geminise and Vela Solaris. The award came with CHF 100,000 in technical assistance for the development of a digital project. The teams have developed an energy management system which integrates the Maestro software and have installed it in two single-family homes and an apartment building. With this deployment, several practical challenges were addressed, from interfacing to different technical equipment reliably, comparing local and on-the-cloud deployment, to dealing with equipment failures and forecast errors.

A proof-of-concept simulation was run to demonstrate the ability of Maestro to manage consumption peaks for this district, served by a district heating system with several large heat pumps. New challenges will have to be tackled in deploying Maestro at this scale, from user interfaces to data management and computational issues, but the experience and data currently gathered in the field help us make Maestro more and more deployable and reliable. A future development is the integration of learning elements that improve the performance of the controller over time in an automated fashion.

Maestro was presented at the IFAC World Congress in Berlin.<sup>[2]</sup>

[1] A. Hutter, N. Koch, Y. Stauffer, T. Gorecki, "Augmenter l'efficacité des prosommateurs," bulletin.ch, vol. 8/2019, Jan. 08, 2019.

[2] T. T. Gorecki, W. Martin, "Maestro: A Python library for multi-carrier energy district optimal control design," presented at the

# Integration of Advanced Diagnostic Capabilities in Battery Management Systems

E. Namor, C. Brivio, E. Le Roux, D. Piguet, A. Hutter

Within the BATMAN project, CSEM developed an innovative battery management system (BMS), capable of carrying out online electrochemical impedance spectroscopy (EIS), a battery diagnostic technique capable of determining the state of health (SOH) of Li-ion cells precisely and in a regular manner. Moreover, the prototype integrates a power switching architecture to bypass individual Li-ion cells in a battery. This architecture enhances the performance of battery packs in electric vehicle and stationary storage systems through more precise SOH estimation and improved cell balancing.

The performance of battery energy storage systems, both in electric vehicles and for stationary applications, is highly dependent on the battery management systems (BMS). These, among other tasks, must estimate the SOH of each Li-ion cell in the battery pack and determine their balancing strategy. The computation of SOH typically requires dedicated time-consuming off-line tests that can be carried out only occasionally. The absence of a reliable online SOH estimation method forces the designers of battery packs to make conservative choices to ensure pack safety, increasing the pack weight and volume. Moreover, different cells in a pack may degrade with different pace. Since the operation of a pack is limited by its weakest cell, this has a detrimental effect on the pack performance.

Within BATMAN, CSEM designed, fabricated and tested a set of cell management boards tackling these issues by introducing three innovations: 1) the capability to carry out EIS on each cell during pack operation, in order to get real-time information about the cells' degradation; 2) the capability to bypass individual cells within a battery module for increased reliability and smarter balancing (i.e. balancing optimizing battery lifetime); 3) the development of supervisory electronics at cell level rather than centralized, i.e. a "cell management system" (CMS) concept. Figure 1 shows a detail of such prototype. It consists of a small module composed by 8 200Wh NMC pouch cells, each equipped with its own CMS. Each CMS is composed of a custom PCB hosting an ST Nucleo board equipped with an STM32 microprocessor. The latter embeds the firmware developed to carry out conventional BMS tasks (such as voltage and temperature measurement and safety checks) as well as implementation and control of the mentioned features.



Figure 1: BATMAN prototype.

## Online EIS

The EIS is carried out by subjecting the battery to a sinusoidal excitation signal spanning from 1 kHz to 10 mHz. Frequencies in the sub-Hertz domain contain important information about the degradation of the battery and are therefore relevant for estimating the SOH. The impedances at the highest frequencies can instead be exploited to estimate the internal temperature of the cell. Figure 2 shows the results of EIS testing carried out with the BATMAN CMSs. The results were compared with reference impedance values collected on the same cells with a Biologic BCS815 battery tester. Although a resistive shift of about 1.5 mOhm is present, the impedance curve shows the expected general behaviour. Moreover, the results show good consistency over repeated tests, confirming the reliability of the

measurements. For frequencies up to 100 Hz, the average coefficient of variation of the measurements is of about 2%.

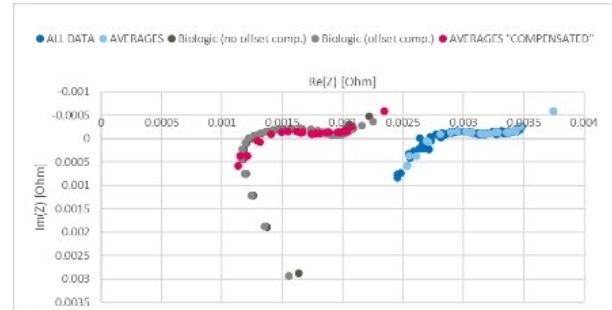


Figure 2: EIS results.

## Cell bypass and lifetime balancing

The bypassing capability is achieved by integrating, in each CMS, MOSFET transistors that can insert the cell in the high-current path or bypass it. It has been validated for currents up to 45 A. Switching delays have been calibrated to avoid harmful cell conditions and minimize voltage and current transients.

Such switching feature will be exploited in future developments of the platform in order to demonstrate the concept of lifetime balancing: individual cells within the module carrying its electrical load for fractions of the operating time that are related to their SOH. By this modulation, it will be possible to maintain a uniform level of degradation within a string and avoid a shortened module life due to one "weak" cell.

## CMS concept

The features 1. and 2. are enabled by moving of the intelligence of the battery management from a centralised BMS to management entities integrated in every cells. This offers several advantages. It enables the integration of an increased number of sensors without a corresponding increase in system complexity. Secondly, it simplifies the repurposing of individual cells in second-life applications since all information relevant to their usage is now stored on the cells themselves. This solution is particularly suited for pouch cells with high capacity (>200 Wh), which are being deployed more and more frequently in battery packs. The existing drawbacks are in the cost and communication requirements, which are being tackled by ongoing development projects.

The BATMAN prototype will serve as platform for testing and developing in a realistic setup further aspects of battery management such as model-based state-of-charge (SOC) estimators, charge and lifetime balancing strategies. Further developments of this CMS platform will be carried out within the MIP project ROBIN (development of power line communication) and EU project SPARTACUS (integration of further sensors).

The BATMAN project was funded by Innosuisse under the project number 34738.1 IP-EE.

# Multi-site PV Forecasting using Spatio-temporal Machine Learning Models

J. Simeunović, R. Carrillo, B. Schubnel, P.-J. Alet

Accurate photovoltaics forecasting is essential to integrate renewable energy sources into the power grid. CSEM developed data-driven methods for forecasting PV production over a large area with fine temporal and spatial resolution using graph-based methods. These methods outperform the state of the art for horizons up to six hours.

Accurate time-series forecasting of renewable power generation is vital for the improvement of electricity management, power system scheduling and trading on the electricity market<sup>[1]</sup>. However, photovoltaic power production is dependent on weather conditions, which makes forecasting challenging.

The focus of the project was on intra-day multi-site PV forecasting since it is key to grid scheduling and planning. State-of-the-art methods within this temporal horizon use numerical weather predictions (NWP). However, NWP has a coarse resolution. Therefore, we have not relied on weather data, only on the past PV data and geographical information. However, due to limitations in the data collection and transmission, real-world data usually contains missing values.

CSEM developed a robust solution for time-series PV forecasting. Figure 1 depicts the solution, where the gap reconstruction and pre-processing module is applied to the data, before the forecasting module. Input data are past PV data, which are denoised, normalized, de-trended and imputed. Furthermore, these historical data are passed to the graph model learning module to learn graph embeddings, as well as to the forecaster.

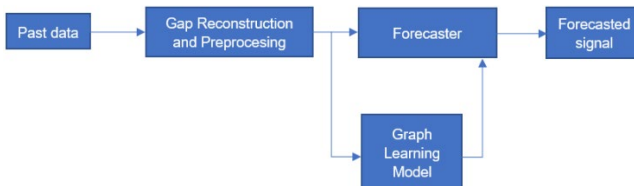


Figure 1: Block diagram of the proposed approach for robust PV production forecasting.

For the forecasting itself, we chose to model spatio-temporal correlations in multi-site PV data with graph structures. PV stations are modelled as nodes and the observed PV production data as signals on the graph.

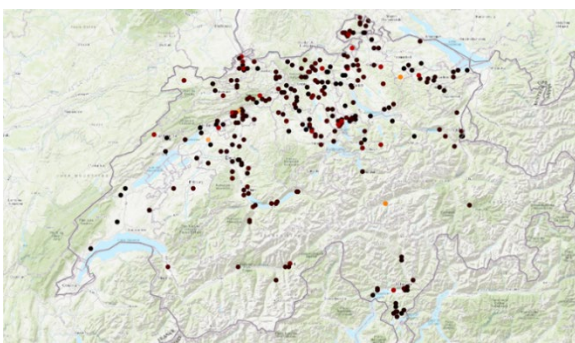


Figure 2: Spatial distribution of the evaluation dataset. Colors indicate the peak production at each site.

One linear and three nonlinear graph-based methods have been developed to capture spatial and temporal correlations between time series. Our models find the nodes which are the most informative and important when making a forecast. The developed non-linear methods use state-of-the-art neural network models that rely on combination of recurrent, graph convolutional, and attention structures. We have compared our graph-based models to the state-of-the-art combination of machine learning (here: support vector regression, SVR) and NWP for two single sites: Bern and for Bätterkinden. To validate our approaches, we have used 300 spatially distributed PV stations across Switzerland (Figure 2). Models were trained on the data from the year 2016 and evaluated on the following year.

Figure 3 shows the evolution of normalized root mean square (NRMSE) error over forecasting horizon. The developed methods outperform methods based on the numerical weather forecast and prove the intuition that graph-based methods can capture nonstationary and stochastic behaviors of the data, by jointly capturing spatial and temporal correlations. What is more, graph-based methods have shown to be powerful in the reconstruction of the missing and noisy data. As a result, the full forecasting pipeline proved very robust against faulty data.

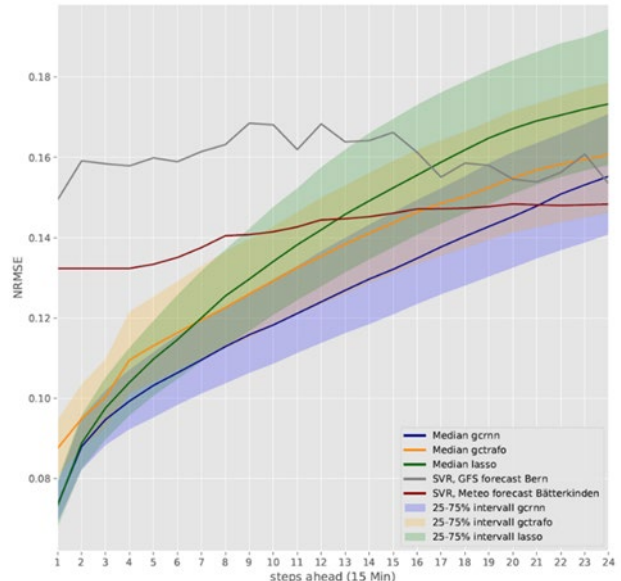


Figure 3: Forecast NMRSE for the real dataset. The forecast horizon is 6 hours in steps of 15 minutes.

Part of this work was carried out on behalf of and with the support of the Swiss Federal Office of Energy (research contract SI/501803-01). The authors are solely responsible for the content and conclusions of the paper. The authors also thank BKW AG for their support.

<sup>[1]</sup> P.-J. Alet, et al., "Forecasting and Observability: Critical Technologies for System Operations with High PV Penetration," in Proceedings of the 32nd European Photovoltaic Solar Energy

Conference and Exhibition, pp. 1444–1448, Munich (2016)  
[doi:10.4229/EUPVSEC20162016-5DP.1.3].

# DC Distribution in Low-energy Buildings with Innovative, Compact Hybrid Storage System

N. Koch, P.-J. Alet

Building on its experience in design and control of direct current (DC) distribution, CSEM is developing and manufacturing an improved version of its electric system in the scope of the HYBUILD project. This enhanced system will enable innovative and compact hybrid (i.e., thermal and electric) storage system for low-energy buildings. It is compliant with safety standards and will be evaluated in real operations at three sites across Europe.

Supplying buildings with locally-produced heat and electricity from renewable sources is a central element of energy policies in Europe. To optimally manage the resulting energy flows the Horizon 2020 project HYBUILD<sup>[1]</sup> aims at developing an innovative, compact, hybrid storage system for low energy buildings.

## Hybrid system architecture

On top of implementing solar thermal and photovoltaic generation and state-of-the-art heating and cooling systems (district heating and cooling, dry cooler, and heap pump), the hybrid system proposed in the HYBUILD project (Figure 1) aims to store energy in two different forms: electricity and heat. Electricity is stored in high-performance lithium-titanate batteries, and heat in latent storage made of phase change materials (PCM). With the heat pump (HP) being the interface between the two energy vectors, this solution offers a high flexibility in terms of optimization of the energy flows inside the building.

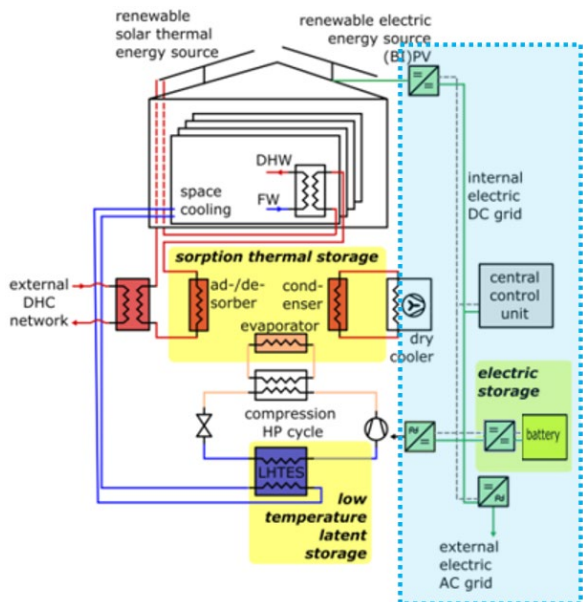


Figure 1: General topology of the hybrid system proposed in the HYBUILD project; CSEM's scope of activities is highlighted in blue.

In this architecture, CSEM is in charge of developing the electric subsystem (highlighted in blue in Figure 1) with a focus on the interconnection, control and supervision of the electric components to guarantee their safe, reliable and optimal operation. The electric system is articulated around an internal DC bus linking together the PV field, the battery, the HP and the AC distribution grid thanks to suitable conversion units.

## Direct current distribution

With most components in this architecture natively running in direct current, opting for a DC bus for the electricity distribution increases the overall efficiency<sup>[2]</sup>. Indeed, a reduced number of conversion stages are needed, and those stages are generally more efficient compared to their AC counterpart.

## Demonstrators

CSEM's main contribution is the delivery of three electric demonstrators (Figure 2), one for each demonstration site. The related activities focus on the following aspects:

- Development of a hardware platform with high efficiency and commercially available conversion units, a safe protection circuit and a reliable internal communication network;
- Development of a software platform for the control and supervision of the subsystem's internal components, and communication layer for integration in the system;
- System integration in a compact and plug-and-play cabinet and draw up of a complete documentation.



Figure 2: Front (left) and top (right) view of the demonstrator embedded in a cabinet.

The system has been designed in compliance with the IEC/EN 60204-1 standard, making it ready for safe deployment in operational environments.

## Outlook

The demonstrators have been successfully tested in-house and will be commissioned at the demonstration sites by the end of 2020. They will then be intensively tested in real operation for one year. The data acquired in this process will allow to experimentally validate the system operation and help further refining its design.

The HYBUILD project has received funding from the European Union's Horizon 2020 research and innovation programme under grant agreement n° 768824.

[1] [www.hybuild.eu](http://www.hybuild.eu)

[2] U. Boeke, M. Wendt, "DC power grids for buildings," in IEEE First International Conference on DC Microgrids (ICDCM), pp. 210-214, IEEE, Atlanta, GA, USA (2015)  
[doi:10.1109/ICDCM.2015.7152040].

# A Building Model Library for Simulation and Control of Energy systems

M. Boegli, P.-J. Alet

The Energy Strategy 2050 calls to reduce net greenhouse gas emissions to zero by 2050 in Switzerland. A positive environmental impact depends on climate-change mitigation and prevention of air pollution. In buildings, in addition to proper envelope isolation, the replacement of oil-based heating systems with heat pumps coupled to PV panels contribute to reduce both greenhouse gas emissions and local air pollution. Moreover, efficient penetration of intermittent renewable energy is greatly improved by the adoption of energy management system to deal with energy flows between production, consumption, and storage. In this work, a model-based simulation platform coupled to energy management control strategies is developed to help assess the energy balance of consumption and production units in buildings.

The adoption of renewable solar energy, i.e. PV electricity and solar thermal panels, coupled to storage facilities for both electricity and heat requires dedicated simulation platforms for the development and performance assessment of energy management systems.

The considered typical single-family house does include a heat pump system, either air-to-water or brine-to-water connected to a ground source heat exchanger. The heat pump supplies heat to thermal storage tanks for domestic hot water and space heating, where space heating demand is determined by occupancy, ambient conditions and building envelope. Solar photovoltaic systems supply electricity to the heat pump while solar thermal systems directly supply heat to storage tanks. Various model combinations, as shown in Figure 1, can be configured by using Modelica modeling language framework.

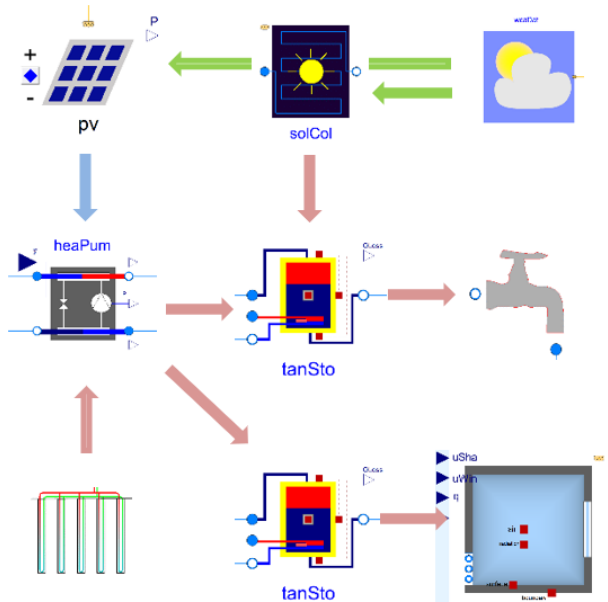


Figure 1: Modelica model template with connected system components and energy flows: i.e. solar irradiance in green, heat in red and electricity in blue.

Modelica [1] is an object-oriented, declarative, multi-domain modeling language for engineering systems including building envelopes, thermal and electrical energy systems. Advantages of Modelica include the availability of comprehensive existing

open-source libraries of building envelopes and energy system components, and the simplicity to adapt model fidelity to the assessment requirements. The development of the here presented benchmark library for building envelope and technical device models relied on complete and well documented Modelica libraries, such as the extensive buildings library from Lawrence Berkeley National Laboratory [1].

The optimization of building energy flow between production, consumption, and storage is orchestrated by an energy management system as shown in Figure 2.

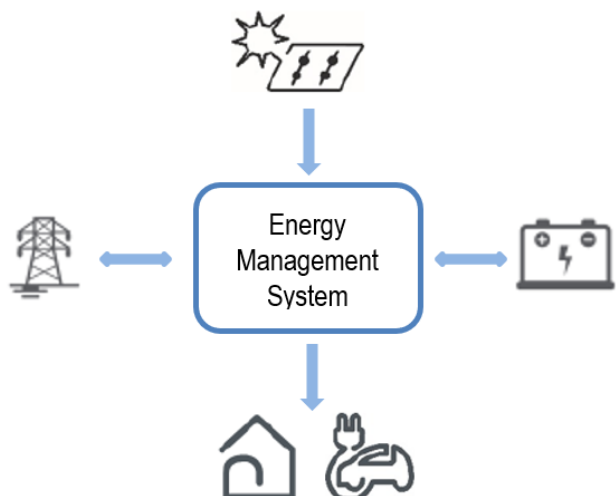


Figure 2: Energy management system with bidirectional energy flow connection to the grid and internal battery storage, and directional energy flow from PV panels and to internal consumption.

Self-consumption and autonomy are maximized by cleverly distributing the PV generated electricity between heat-pump, electric vehicle charger and the in-house battery. The battery mainly act as a buffer to transfer excess PV energy to periods in which PV production is lower than the demand. Yet, the battery can also be used for peak shaving, i.e. for peak power reduction to or from the grid, which would otherwise result in extra cost.

The building model library framework was developed within the CTI project MODECORES (project number 26'565.2 PFIW-IW) in collaboration with the SME Eturnity [2] and EMPA. Within the project the library was used to develop a customized simulation platform for rapid prototyping of building energy assessment [3].

[1] "Modelica Building Library", from the Simulation Research Group of the Lawrence Berkeley National Laboratory (LBNL)  
<https://simulationresearch.lbl.gov/modelica>

[2] Eturnity AG, <https://eturnity.ch/en/home-eng>

[3] J. Allan, M. Boegli, A. Bollinger, P.-J. Alet, M. Wiget, "Speed-Optimized Simulation Models for Rapid Performance Evaluation of Heating and Energy Management Systems" in the Proceedings of the 16th Building Simulation 2019 (BS2019) conference of the International Building Performance Simulation Association (IBPSA), pp. 3668-3675,  
<https://doi.org/10.26868/25222708.2019.210997>



# SYSTEMS

Jens Krauss

The Systems research program vision is to promote micro-technological innovations and new product concepts along the three application domains of (1) *Scientific Instrumentation*, (2) *Automation*, and (3) *Medical Device Technology*. Our *Scientific Instrumentation* research activities aim at meeting coming demands in the fields of astrophysics, space exploration, space-based systems, and watchmaking, as well as meteorology and industrial instrumentation. Within our *Automation* research activities, we develop technologies for enhanced manufacturing and process flexibility, as well as smart Industry 4.0 solutions to support the objective of keeping manufacturing activity within Switzerland. The *Medical Device Technology* research activity ranges from innovative sensing technologies for monitoring human vital signs to bio-signal processing and active medical device technologies.

## Long-term objectives

**Scientific Instrumentation:** For the last 30 years, CSEM has been developing strong expertise in the design, simulation, manufacturing, integration, and testing of high-precision micro-mechatronic systems based on compliant structures. CSEM expertise in high-precision mechanisms, leveraged with new findings within its strategic activity in MEMS (and MOEMS), has paved the way to a number of new space exploration and science missions, with spillover effects in the (Swiss) watchmaking domain and medical applications. CSEM supports the Swiss Space Policy along the technology axes of high-precision mechanisms, atomic clocks, photonics, and scientific instruments. Similarly, the watch industry is pivotal for Switzerland and CSEM is dedicated to leveraging its Flextec heritage, with its long-standing track record in MEMS and microsystems manufacturing. The use of CSEM's competences in the design, simulation, development, and testing of complex, miniature, hybrid, precision systems has led to quantum leaps in performance compared to existing systems. The resulting advantages include highly precise and reproducible motion patterns, a far smaller number of movable parts enabling easier production at lower cost, and the absence of friction and premature wear. This increases longevity and reduces maintenance requirements, which is key for the (Swiss) space and watchmaking industries.

**Automation:** Maintaining industrial manufacturing activity is essential for the future prosperity of the Swiss economy. For a high-labor-cost country such as Switzerland, this can only be achieved by high-end products in combination with smart production processes. Industry 4.0 addresses this optimization of industrial processes and impacts the whole value chain from handling, robotics, and quality control to logistics and new business models. Successful implementation of Industry 4.0 relies heavily on data acquisition, smart algorithms (deep learning), and adaptive concepts (life-long learning) to deliver smart and highly adaptive processes, machines, and equipment. CSEM is mainly active in three fields. First, industrial quality control or process optimization, often based on machine vision algorithms. Second, the state of industrial equipment is addressed by monitoring and predicting its status for optimum operating efficiency. Third, we develop human-centric

automation strategies because long-term efficiency in industrial processes will only be achieved when equipment supports humans without demotivating or deskilling them.

**Medical Device Technology:** The current COVID-19 pandemic is highlighting the challenges Western industrialized countries are facing in guaranteeing their populations—which are undergoing demographic change—access to an optimal, operational healthcare system by limiting the rapid increase in healthcare expenditures. Digitalization and efficient digital healthcare technologies offer patients and caregivers new solutions that increase the standard of care and reduce costs, with a focus on prevention and public health, patient empowerment, and out-of-hospital care. While wearables have flooded the sports and fitness market in recent years, today we are seeing a steady increase in consumer wearables with medical features, along with medical devices becoming more wearable. Specifically, remote patient monitoring systems are a driving force of medical wearables, with a focus on patient empowerment, enabling disease self-management and improving the lives of patients and caregivers. Starting with wearable technologies 20 years ago, CSEM has accumulated an important patent portfolio and considerable know-how regarding both hardware (including ASICs) and software (including algorithms). CSEM is ISO13485-certified and works closely with the Swiss university hospitals, including Inselspital in Bern, in order to maximize its added value to medical customers, hence positioning itself closer to the targeted use case and the final product development phases.

## Highlights

**Scientific Instrumentation:** Among the many highlights related to high-precision space mechanisms, we report the successful delivery of the flight model of the Re-Focus Mechanism (RFM) to be integrated into the CLose-Up Imager (CLUPI): this high-precision, compliant mechanism will equip the Mars Rover, to be launched in the framework of the Exomars mission by 2022 onward. Moreover, CSEM will reinforce—with the ESA research project Large Angular Flexible Pivot (LAFF)—its Flextec solution portfolio for future space applications with high-angular flexible pivots, and during the reporting period we successfully delivered the first prototypes. Our research activities in the so-called FlexMEMS domain are focusing on the simulation and design of novel mechanical resonators and escape mechanisms compliant with the thermal and shock environment restrictions of modern high-quality mechanical watches. A major research highlight during the last reporting period is the integration, testing, and characterization of our proprietary Siloscape watch mechanism, which allows the power reserve to be increased by a factor of three. Another important focus area of the *Scientific Instrumentation* research activity is the photonics domain. In the framework of the European Flagship Project macQSim, CSEM as a coordinator continues to deploy huge efforts in maintaining and advancing its long-standing track record in MEMS based Miniature Atomic Clocks (MAC). Regarding our LiDAR research activities, we report the successful close-out of the REMOVE-Debris space mission, for which our Flash LiDAR served as the vision-based-navigation (VBN) sensor for testing the different

debris capture technologies. Thanks to this successful mission, CSEM is also involved in the future mission ADRIOS, with the Swiss start-up ClearSpace.



Figure 1: Focus mechanism flight model for the Close-Up Imager (CLUPI) in the framework of the Exomars mission (launch in 2022).

**Automation:** Here, development and research activities are driven by three industrial requirements: quality control and process control, traceability, and flexible production. Smart concepts of Industry 4.0 and deep learning algorithms form the basis of our application-oriented achievements. CSEM develops tools to bridge latest results in artificial intelligence to real-world applications, especially production sites.

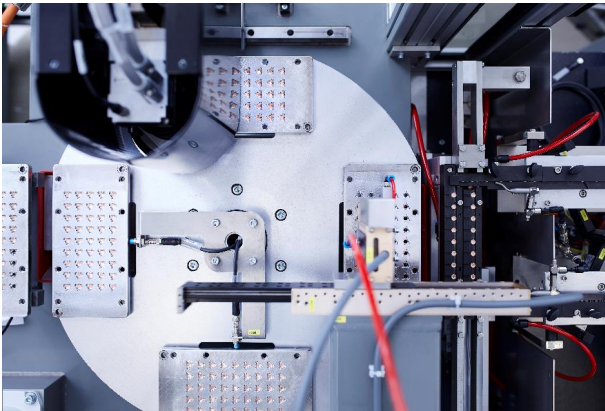


Figure 2: In-line quality control with high-speed 3D lightfield technology powered by deep learning, fully deployed in a production line (Renata).

Calculation power is widely available but efforts with regard to data acquisition, annotation, and deployment are still very high. Assisted labelling tools and the synthetic generation of training data are promising paths to overcoming this issue. The first successful implementations have been realized in the domain of bin picking for small objects and the in-line quality control of injection molding parts. The modular PC-based software environment CSEM VISARD (Vision Automation Robotics Designer) is designed to deploy full processing pipelines and to integrate version control for neural networks (CSEM ModelStore) and is optimized for usability. This framework runs across multiple industries: the watch industry, MEMS inspection, lab automation, production, agriculture, geospatial, and service maintenance. One of the key research topics is predictive

maintenance. Beside identifying an issue on a machine, the goal is to determine the root cause of the failure already after short training period and small datasets. Such an approach is particularly important for special-purpose machines, which are usually individual and unique.

**Medical Device Technology:** A major research highlight of the reporting period is the improvement of the accuracy of CSEM's oBPMTM technology—the so-called optical blood pressure monitor, a patented sensing technology that is capable of estimating blood pressure values in humans from optical signals. Through collaborations with the Swiss start-ups Ava, Biospectral, and Aktiia, this clinically proven technology has overcome all the limitations of traditional inflatable cuffs for blood pressure monitoring in humans, in various form factors including smartphones, bracelets, armpods, finger clips, and textiles, and many more (see Figure 3, below).



Figure 3: CSEM start-up Aktiia, commercializing our proprietary optical blood pressure monitoring technology oBPMTM with a medical certified smart wrist device for which market launch is planned in Q2-2021.

Another digital health research highlight is CSEM's proprietary cooperative sensors technology (CST), a disruptive approach to measuring biopotentials and bio-impedances and allowing a radical simplification of cabling requirements. CST is ideal for the next generation of wearables featuring imaging and sound capabilities. During the last reporting period, we found solutions to remotely powering the sensors, without adding more wires and in compliance with medical standards regarding current leakage. These new solutions have been prototyped for EIT devices (Electrical Impedance Tomography) and combined with a stethoscope function. A major challenge for these medical wearables remains data ownership, (data) integration into the current health system, and regulatory boundaries. In this context, we are investigating new technologies that ensure data privacy and security, including privacy-preserving ML algorithms and distributed AI.

# A Stable Mode-locked Laser as Local Oscillator for a Photonics-based Radar

N. Torcheboef, L. Giriens, S. Droz, S. Kundermann, D. Grivon, L. Karlen, S. Lecomte

Mode-locked lasers are oscillators with exquisitely low-noise properties that are key to unleash the unique capabilities of photonics-based radars. In the H2020 project Roborder, CSEM developed a compact and rugged high-repetition rate 1560 nm femtosecond diode-pumped solid-state oscillator and its driving electronics. In particular, the developed laser assembly technology has shown to lead to reliable lasers and can be adapted to the manufacturing of cost-effective and rugged solid-state lasers as well as other optical systems.

Photonics-based radars open up new possibilities and capabilities to improve the resolution and coverage of traditional microwave radars. In the H2020 project Roborder<sup>[1]</sup>, the CNIT in Pisa, Italy, will build such a photonics-based radar that will have at its core a mode-locked laser as local oscillator. This unique radar will perform a demonstration at the Livorno harbor by detecting and imaging incoming ships.

The radar local oscillator is based on a high-repetition rate mode-locked laser. The technology of choice to realize such a laser is diode-pumping of a passively mode-locked solid-state laser. In particular, the repetition rate is 600 MHz and the center wavelength shall lie in the telecom C-band for low-loss fiber distribution of the oscillator light. Importantly, the selected technology is inherently low-noise thanks to the low-loss cavity and high intracavity power of the laser. Indeed, such technology offers the best oscillators physics gives us.

In order to have a reliable and rugged device, the design and construction of the laser are essential. Sub-micron level misalignment of optical components detrimentally affects the laser performance. At the same time, the components shall be precisely positioned prior to fixation. The fixation shall not move the component and the component has to stay in position for the system lifetime. It is important to pay particular attention to the material stress after manufacturing and to the thermal expansion of the different materials.

CSEM performed the design according to specifications. Several laser units were manufactured and integrated. The engineering tasks started by a careful cavity design aiming at minimizing alignment sensitivity. Then the selection of the materials was performed to ensure long term dimensional stability, compliance with thermal cycling and robustness against vibrations and shocks. An assembly technology based on gluing and manual positioning was also developed such that the different components can be put in place within the  $\mu\text{m}$ , fixed, released without displacement and kept in position for system lifetime (15 years) of the laser. The overall design was also based on low-outgassing components and on achieving a compact form factor. Finally, the selected materials and technologies are cost-effective.

In Figure 1, top, a picture of the oscillator is shown. The dimensions are 149x270x41 mm<sup>3</sup>. A dedicated validation campaign was performed. The laser emitted 37 mW out of a

polarization maintaining fiber (polarization extinction ratio of 24 dB) with an optical spectrum centered at 1561 nm and a FWHM of 12 nm. The soliton pulses have a duration of 213 fs. As requested by the photonics-based radar, the laser has a pulse repetition rate of 600 MHz.



Figure 1: Picture of the packaged laser (top).

To have a turn-key system, the laser oscillator was mounted in a 19" rack with its drive electronics. For operation, the electronics needs to be powered (220 V AC) and the laser switched on via a single switch. In Figure 2, a picture of the rack containing the laser and the electronics is shown.



Figure 2: Picture of the rack containing the laser oscillator and its electronics for turn-key operation.

The manufacturing of rugged and reliable solid-state lasers is notoriously known to be tricky while essential for industrial products. The technology developed by CSEM will be proposed to laser manufacturers to improve their production yields and product reliability. Finally, such a laser will be internally used as frequency comb stabilized to a high-finesse ultra-stable optical reference cavity and to an active hydrogen maser. It will be used for the metrology of the lasers to be developed in the frame of the LISA mission<sup>[2]</sup> of the European Space Agency (ESA).

[1] <https://roborder.eu>

[2] [https://www.esa.int/Science\\_Exploration/Space\\_Science/LISA](https://www.esa.int/Science_Exploration/Space_Science/LISA)

# MEMS Cells for High Stability Miniature Atomic Clocks

S. Karlen, J. Haesler, T. Overstolz, J. Gobet, L. Balet, F. Droz, S. Lecomte

CSEM together with its industrial partner Orolia Switzerland SA demonstrated state-of-the-art long-term frequency stability with a miniature atomic clock including microfabricated atomic vapor cells.

Atomic clocks are timekeeping devices which achieve extreme performance in terms of stability and accuracy. Behind this name, hides a variety of different systems for different applications with a variety of sizes and complexities. Of particular interest for CSEM are the miniature atomic clocks, devices that squeeze the atomic interrogation in a limited size and allow for a reduced power consumption. The extreme miniaturization of these devices makes them direct competitor to high-performance quartz oscillators and allows for the exploration of new applications with more stringent requirements.

At the heart of a miniature atomic clocks are the atomic vapor cells. These components, traditionally fabricated by glass blowing, are used in a large variety of other applications ranging from quantum sensor to quantum light source, including atomic spectroscopy and quantum memory<sup>[1]</sup>. In order to reduce the size and power consumption of atomic clocks, microfabrication (MEMS) techniques are used by CSEM for their wafer-level fabrication.

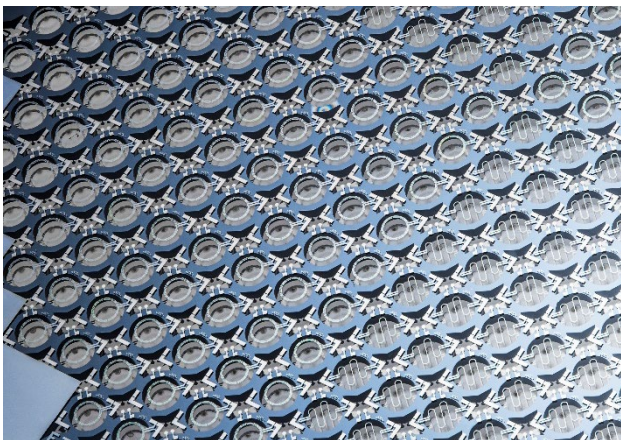


Figure 1: Wafer-level view of CSEM MEMS cells.

Cells fabricated with MEMS techniques are typically composed of a Si-etched cavity and closed at both ends by a borosilicate glass window (see Figure 1). The cavity is filled with an alkali metal (here rubidium) and a buffer gas mixture (here nitrogen and argon). CSEM cells are filled with rubidium by a patented RbN<sub>3</sub> UV decomposition method which allows to generate both the rubidium and the nitrogen inside the cell cavity at low cost. The cells include an aluminum oxide coating to enhance the cell lifetime<sup>[2]</sup> as well as patented gold microdisks. This last feature

allows for condensation of the alkali metal droplets on specific areas of the cell cavity, preventing them to interfere with the light path of the laser used for frequency interrogation of the atoms. It thus increases the miniature clock frequency stability<sup>[3]</sup>.

Recently, MEMS atomic vapor cells produced by CSEM were tested in a commercial miniature atomic clock system developed by the company Orolia. In these devices, the atomic frequency is interrogated by the so-called double-resonance method: a radiofrequency field is applied to an atomic transition of the alkali atoms. The absorption of the atomic ensemble is then detected in the optical domain with a resonant laser and serves to stabilize the radiofrequency field and hence the clock output.

The test devices, measured by Orolia, demonstrated for the first time in Europe state-of-the-art ultra-low frequency drift performances with MEMS cells, equaling world best miniature atomic clocks. After 3 months of continuous operation, cells delivered by CSEM and integrated in these devices showed frequency drifts compatible with the requirements expressed by the European Space Agency (ESA) i.e. below 1E-11 per day (1  $\mu$ s/day). The measurement results are presented on Figure 2 together with the asymptotic frequency drifts performances.

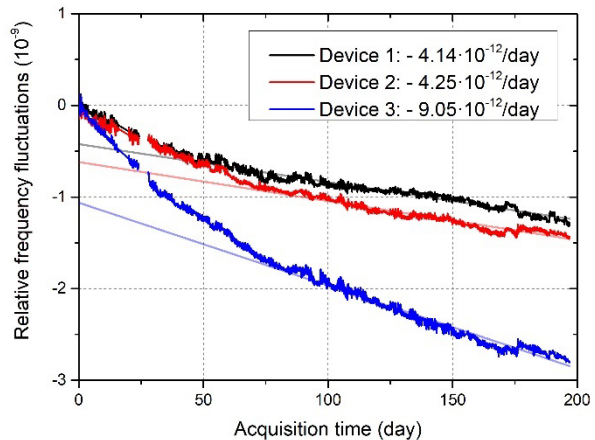


Figure 2: Frequency stabilities and asymptotic drift values measured by Orolia Switzerland SA on three different miniature atomic clocks including CSEM MEMS atomic vapor cells.

Based on these promising results, CSEM is now working together with Orolia to develop a more compact and power efficient commercial atomic clock device including MEMS cells as a baseline for ground and space applications.

[1] J. Kitching, "Chip-scale atomic devices", Applied Physics Reviews, 5(3), 2018.

[2] S. Karlen, J. Gobet, T. Overstolz, J. Haesler, S. Lecomte, "Lifetime assessment of RbN<sub>3</sub>-filled MEMS atomic vapor cells with Al<sub>2</sub>O<sub>3</sub> coating", Optics Express, 25(3), 2017.

[3] S. Karlen, T. Overstolz, J. Gobet, J. Haesler, F. Droz, S. Lecomte, "Gold microdisks as alkali preferential condensation spots for cell clock long-term frequency improvement", European Frequency and Time Forum (EFTF), 2018.

# macQsimal—Towards Reliable Miniature Quantum Sensors

J. Haesler, S. Karlen, L. Balet, T. Overstolz, G. Bergonzi, F. Droz, S. Lecomte

As a project under the Quantum Technologies (QT) Flagship of the European Commission, macQsimal is at the forefront of European efforts to push the boundaries of quantum technologies. The project, coordinated by CSEM, develops advanced prototypes for enhanced applications in various fields such as communication, navigation, and medical imaging.

macQsimal [1] develops miniaturized advanced quantum-enabled sensors with outstanding expected sensitivity to measure physical observables in five key areas: magnetic fields, time, rotation, electro-magnetic radiation and gas concentration.

Five different types of miniaturized quantum sensor prototypes are under development: optically pumped magnetometers (OPM) for brain activity imaging, atomic clocks (MAC) for communication and space applications, nuclear magnetic resonance gyroscopes (NMRG) for autonomous cars driving, atomic GHz/THz sensors and imagers, and lastly, Rydberg-based gas sensors. The common core technology for these sensors is formed by atomic vapor cells realized as integrated microelectromechanical systems (MEMS).



Figure 1: MEMS atomic vapor cell fabricated at the wafer-level for: OPM (left), GHz/THz (middle), and MAC (right) applications.

Fabricating such MEMS atomic vapor cells at the wafer-level<sup>[2]</sup> allows for high-volume, high-reliability and low-cost deployment of miniaturized and integrated sensors, critical to wide-spread adoption. 6-inch wafers, with up to 744 cells per wafer, were already fabricated (Figure 1), and promising world-class low-drift performances have been measured<sup>[3]</sup>, opening the path towards the first European commercial miniature atomic clock by our partner Orolia Spectratime in Neuchâtel. CSEM, thanks to more than 12 years of development towards reliable, well performing and cost effective MEMS atomic vapor cells, will thus be the provider of one of the core element of such a commercial clock.

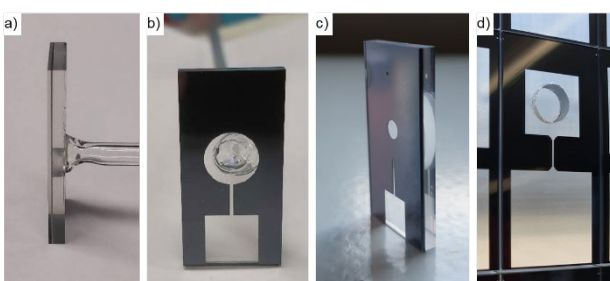


Figure 2: MEMS atomic vapor cell fabricated at the wafer-level for: a,b): gas sensing (with a stem attached by the University of Stuttgart), c): GHz sensing and imaging and d): THz imaging.

Wafers of customized dual-cavity cells (Figure 2) for GHz/THz applications were also successfully fabricated. Such cells show

specific features like: i) compensation cavities, ii) filling stem for very low-pressure applications, iii) thin reflective inner walls for beam shaping and iv) very thin side walls for enhanced resolution.

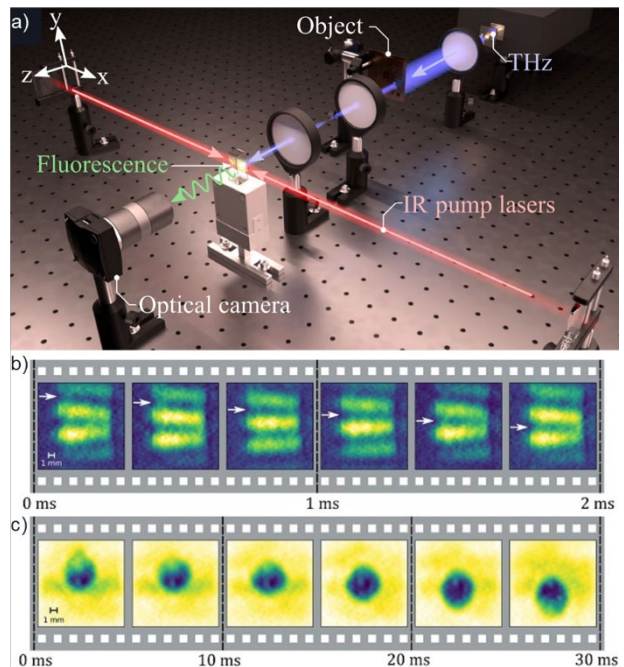


Figure 3: Fast 2D THz imaging demonstration by the University of Durham. a) lab setup, b) chopper wheel imaged at 3'000 frames per second, and c) falling water drop imaged at 500 frames per second.

THz imaging systems, one pillar of macQsimal, illustrates another big potential of such MEMS vapor cells. These systems have applications in security scanning, biomedical imaging, and non-destructive testing. This is due to the non-ionizing and penetrating nature of THz radiation. To circumvent the limitations of current THz imaging systems (low frame rate, low THz power and low THz detector sensitivity), colleagues at the University of Durham use an alkali vapor in a standard cubic glass cell that converts terahertz-frequency photons into easily detectable optical-frequency ones. They recently reported on a 2D THz imaging system (Figure 3) capable of fast and low noise full-field imaging<sup>[4]</sup>, with frame rates two orders of magnitude higher than the current state of the art in THz imaging.

MEMS atomic vapor cell fabricated at CSEM will allow to further improve the THz imaging system performances by reducing interferences existing in the current cubic glass cell and thus improving the optical signal characteristics of the system.

macQsimal is funded by the European Union's Horizon 2020 research and innovation program under grant agreement No. 20393.

[1] [www.macQsimal.eu](http://www.macQsimal.eu)

[2] CSEM patent n°US8906470 (B2)

[3] S. Karlen, J. Haesler, T. Overstolz, J. Gobet, L. Balet, F. Droz, S. Lecomte, "MEMS Cells for High Stability Miniature Atomic Clocks", CSEM Scientific and Technical Report (2020) 76.

[4] A. Downes, et al., Phys. Rev. X, 10, 011027 (2020).

# LiDAR Use in Sunlight: Pathway to New Opportunities

A. Pollini, D. Nguyen, C. Pache

Capable of acquiring 3D images of a scene in a single snapshot, flash imaging LiDAR is considered as a key enabling technology for applications such as autonomous navigation (e.g. airborne, space), mapping (e.g. geology, underwater) and objects detection. So far, flash imaging LiDARs developed at CSEM were highly sensitive to sunlight background, preventing their use in daylight. In the frame of a project for the European Space Agency (ESA), the robustness against sunlight was dramatically improved, enabling to demonstrate the applicability of flash LiDARs in broad daylight. The final objective was to assess the technology potential for terrestrial applications. In this view, this development opens doors to further opportunities in the above-mentioned domains.

Over the past 7 years, CSEM has been benefiting from the support of the European Space Agency (ESA) to develop and mature a flash imaging LiDAR technology, conceived for autonomous landing on celestial objects and on-orbit automatized operations for landing applications. A flash imaging LiDAR generates 3D images of the target in a single snapshot, which confers the following advantages over a traditional scanning architecture: better integration (i.e. miniaturization), longer lifetime (i.e. no mechanical fatigue), no compromise on angular resolution, measurement rate or platform stability.

## Diversification towards terrestrial applications

Based on a matrix detector with single-photon direct time-of-flight capability, the resulting prototype offers a range precision below 5 cm over 200 m, within a 4° field-of-view. The frame rate is equal to 8 Hz and the image resolution is 128x128 pixels. These excellent performances opened doors to complementary terrestrial applications for which a snapshot acquisition is key. Therefore, the following proof-of-concept studies were carried out: all-weather helicopter navigation for REGA, (Swiss Air-Rescue Association) geodesy (i.e. rockslide monitoring) with SLF (Swiss institute for avalanches), and underwater imaging with the archeological service of Neuchâtel and the Laténium museum. This latter demonstration paved the way towards two additional European collaborations to demonstrate the potential of the technology for bathymetry (i.e. underwater imaging) from autonomous platforms (i.e. water surface and airborne autonomous vehicles).

## Night operation

Despite its interesting performances, the system suffered from a major limitation: its high sensitivity to background light completely precluded its use in daylight, forcing all demonstrations to be performed at night. Such a limitation was clearly identified as detrimental for any future real application. To overcome this shortcoming, the aim of the current ESA project, consists in investigating and validating solutions to work in daylight.

## Like night and day

The system is based on active illumination by a pulsed laser, emitting light at a wavelength of 532 nm (green). Hence, the challenge consists in reducing the sensitivity to background light characterized by a broad spectrum, while maintaining a high efficiency for the wavelength of interest. The approach includes three different steps and their combination.

First, the bandwidth to the optical bandpass filter was reduced to the maximal extent possible. Designed for collimated light, interferential bandpass filters suffer from an intrinsic shift of their transmission bandwidth dependent on the incidence angle. This shift was carefully characterized over a range of ±20° for different filter bandwidths: 1, 3 and 10 nm. Measurements are

first fitted to generate synthetic data with a high sampling rate, as illustrated in Figure 1.

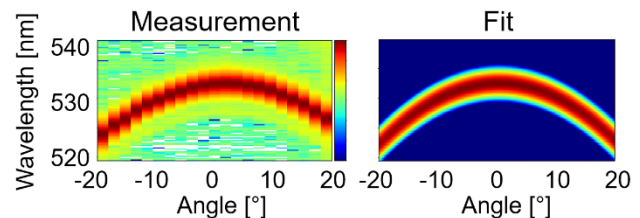


Figure 1: Raw measurements and synthetic data obtained after fitting.

Based on the resulting data, it's possible to select the minimal bandwidth without compromising the transmission over the entire field-of-view, i.e. maintain a constant transmission.

The second step consists in fine-tuning the laser wavelength to precisely align it to the spectral peak transmission of the procured filter. This is made possible by the laser manufacturer, that allowed the access to certain laser parameters.

Finally, a motorized iris was integrated into the system to allow adapting the photon collection efficiency to any situation. In practice, the iris diameter and laser power are continuously adapted depending on the illumination conditions and targets, with the aim of maximizing the signal-to-background ratio. Figure 2 demonstrates the potential of the technology for objects detection. In this test, images of a flying drone are recorded with the LiDAR and a classical camera. In comparison to the camera, not only the LiDAR provides the third-dimension information, but also does not suffer from contrast perturbations such as shadows created by the trees, thanks to its active illumination.

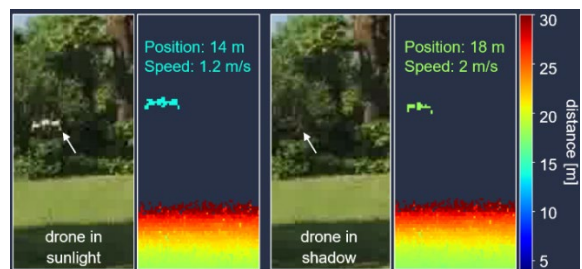


Figure 2: Classical camera VS flash LiDAR on a flying drone.

In conclusion, the realized improvements result in a versatile instrument that can be employed over a large range of illumination conditions and target distances. Clearly, overcoming the "night operation" limitation will tremendously facilitate measurement campaigns and will allow tackling several applications for which a day use is required.

We thank the European Space Agency for its financial support and Lumibird for their support on tuning the laser wavelength.

# PULSAR—Development of a Mirror Tile Prototype for Future Large Telescopes Robotically Assembled in Space

F. Cosandier, D. Nguyen, J. Rouvinet, V. Schaffter, A. Verhaeghe

The PULSAR project consists in developing demonstrators illustrating the construction of telescopes in orbits, with primary mirror diameters up to 35 m. CSEM developed single mirror tile demonstrators capable of adjusting the mirror position to compensate for robotic assembly induced inaccuracies. This tripod mechanism is composed of three actuation stages and three transmission stages including flexible elements. The mirror position is controlled along the mirror piston axis and tip/tilt rotations. The piston stroke is  $\pm 3$  mm with 1  $\mu\text{m}$  resolution and 5  $\mu\text{m}$  repeatability while the tip/tilt strokes are  $\pm 1^\circ$  with 4  $\mu\text{rad}$  resolution and 20  $\mu\text{rad}$  repeatability.

The H2020 PULSAR<sup>[1]</sup> (Prototype for an Ultra-Large Structure Assembly Robot) development objectives are to create three demonstrators that will pave the way for the assembly of large structures in orbit. The study case considered in PULSAR is the assembly of a segmented primary mirror for the next generation of 35 m space-based telescope. This problematic is answered by a large consortium of actors of the space industry: Magellum, Graal Tech, DLR, DFKI, Space Application Services, Onera, Thales Alenia Space France and CSEM.

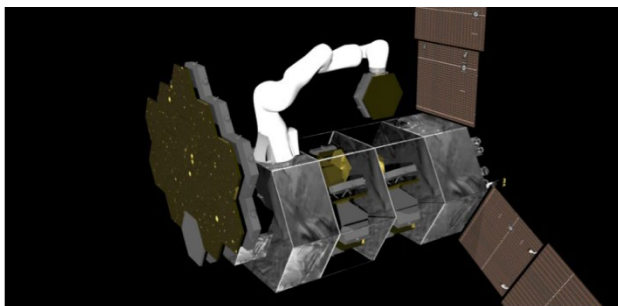


Figure 1: PULSAR study case - a robotically assembled primary mirror of a space telescope.

To reach this goal, the consortium is developing three demonstrators, each of them addressing one aspect of the problematic.

- The dPAMT demonstrator aims to demonstrate the precision capability of a robotically assembled structure.
- The dLSAFFE demonstrator aims to demonstrate the extended mobility concept of the robotic assembly and is taking place in a zero buoyancy facility.
- The dISAS demonstrator aims to simulate the complete robotic assembly and will also be used as a development tool for future mission scenario.

In the frame of this project, CSEM is developing single mirror tile demonstrators (SMT) for the dPAMT demonstrator. These tiles host a positioning mechanism capable of adjusting the position of the hexagonal mirror tile to compensate for inaccuracies generated by the robotic assembly. This mechanism is based on a tripod architecture. It is composed of three linear actuators and of transmission stages, made of a flexible pivot and a gimbal.

This mechanism allows for controlling the mirror position along three degrees of freedom (piston translation, tip and tilt rotations). The piston stroke is required to be  $\pm 3$  mm with a resolution of 1  $\mu\text{m}$  and a repeatability better than 5  $\mu\text{m}$  while the tip/tilt strokes are  $\pm 1^\circ$  with 4  $\mu\text{rad}$  of resolution and 20  $\mu\text{rad}$  of repeatability.

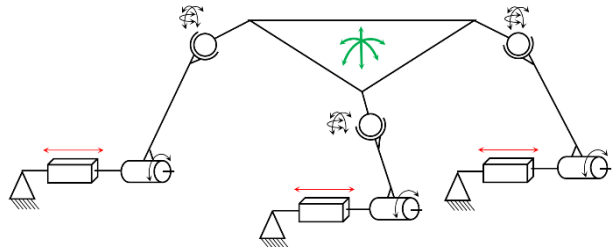


Figure 2: Kinematic diagram of the dSMT positioning mechanism.

The tile design benefits from CSEM's extensive experience in compliant mechanisms and in additive manufacturing applied to the domain of scientific instrumentations for space application.

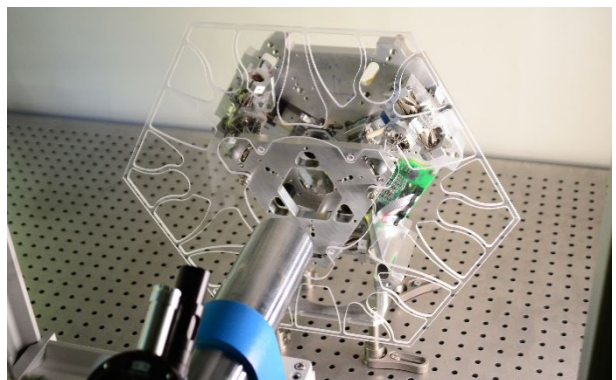


Figure 3: Tripod mechanism of a PULSAR mirror tile in calibration.

A total of 6 tiles are manufactured to serve as elemental brick of the demonstration assembly. Four of these tiles are passive and two of them are equipped with a positioning mechanism.

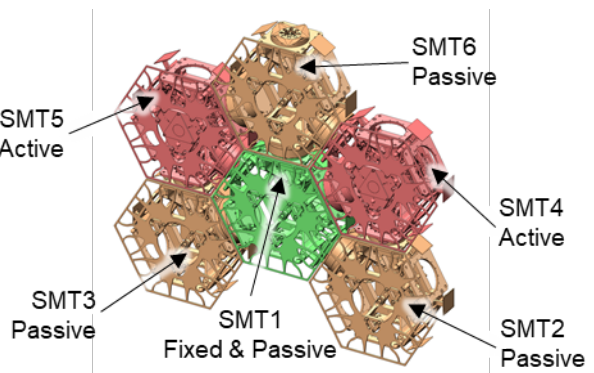


Figure 4: dPAMT tile assembly.

Tiles have been manufactured and are currently being calibrated. Preliminary evaluation shows that the performance requirement should be met with a margin factor of 2.

[1] H2020 PULSAR website: <https://www.h2020-pulsar.eu/>  
Call H2020-SPACE-2018 — EU Project ID 821858

# SMARTES—Slip Ring Assemblies based on Additive Manufacturing for Space Applications

H. Saudan, L. Kiener, D. Novo, S. Lani, M. Miler\*, M. Henry, D. Cerutti, D. Bilbeau

CSEM and RUAG Slip Rings SA (RSSR) are developing a new generation of Slip Ring Assembly (SRA) rotors based on Additive Manufacturing. The design and manufacturing concept proposed by CSEM enables significant improvements which shall allow RSSR to reach its objective to meet the requirements of the space industry 4.0 regarding SRAs. From 2016 to 2018, the concept was developed up to TRL4 in the frame of the project AMAR funded by the Swiss Space Office. In the current project SMARTES, funded by ESA within its ARTES program, CSEM is consolidating the design of the rotor towards RSSR's latest requirements and the two partners are optimizing the whole manufacturing and post-process sequence. Later in the project, RSSR will qualify the rotor at SRA level up to TRL7 in order to validate its performances.

Slip Ring Assemblies (SRAs) are continuity devices whose function is to transfer electrical signals from a stationary member to a rotating member. In space, SRAs are part of many satellite sub-systems such as Solar Arrays Drive Mechanisms (SADM), Antenna Pointing Mechanisms, Control Momentum Gyroscopes and others<sup>[1]</sup>. To date, the physical architecture of SRA rotors relies on a delicate manufacturing and assembly sequence involving many operations. Notably, each conductive ring is manually soldered to a cable (see Figure 1), itself manually routed and connected to a terminal block. Furthermore, stacking conductive and insulating rings implies a long tolerance chain which makes it mandatory to achieve high dimensional precision for each component. As an example, a 30 channels SRA rotor involves the stacking of 60 rings. Considering a ring thickness tolerance of  $\pm 10 \mu\text{m}$ , the overall track pitch deviation increases to  $\pm 600 \mu\text{m}$ , causing obvious design, machining and assembly issues.

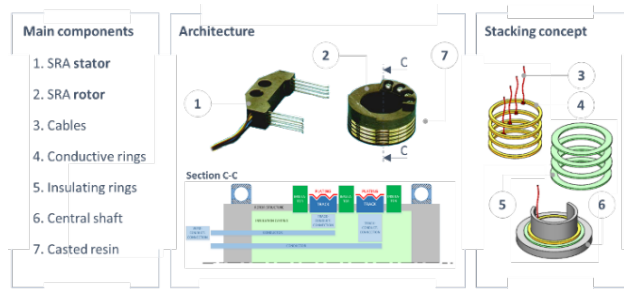
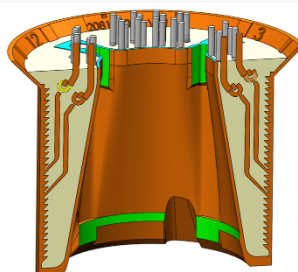


Figure 1: Architecture and assembly of conventional SRA rotors.

To avoid the use of cables and reduce the number of components, a novel design concept based on an Additive Manufacturing (AM) process was applied to the SRA rotor and validated by means of electrical performances and lifetime testing<sup>[2]</sup>. The concept enables the design of metallic structural parts which include conductive wires. Hence, for a rotor featuring 30 electrical channels, the new architecture enables a reduction of the number of components from more than 90 parts to a single one. The design of this single part can be adapted to customer requirements much more easily compared to the dozens of parts to be produced when the conventional approach is followed. With the new concept, the final function of the rotor is achieved by means of four subsequent steps which follow the initial additive manufacturing, namely (1) cables soldering, (2) resin casting, (3) re-machining and (4) gold plating.

Early in the SMARTES, the whole shape of the rotor was re-adjusted to match RSSR's latest requirements, leading to challenging geometries for the AM step. Following a detailed trade-off analysis carried out with RSSR, CSEM implemented the final geometry of the wire terminations. Those are now shaped as pierced terminals allowing the soldering of up to two wires per terminal, an advantage when high current is running in the conductors (see Figure 2). The design is such that up to three rotors can be stacked together on a central shaft.

Rotor after cables soldering and resin casting



Rotor after machining

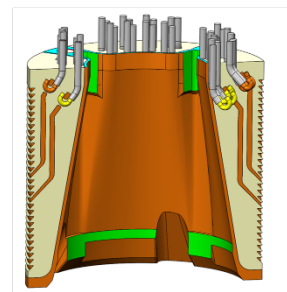


Figure 2: Cross section of the new rotor before and after re-machining.

To validate the feasibility, CSEM carried out an AM technology trade-off including the most promising technologies and their associated materials, namely (1) Binder Jetting of bronze in a stainless-steel matrix, (2) Investment Casting based on additively manufactured polymer patterns and finally Laser Powder Bed Fusion (LPBF) of (3) bronze and (4) pure copper. The options (1) and (2) were discarded since the manufacturing tolerances could not be reached. The competition is still ongoing between LPBF bronze and copper which must now prove their compatibility with re-machining and gold plating. The best material candidate will be used to manufacture the qualification models to be integrated to the complete SRA and qualified up to TRL7.

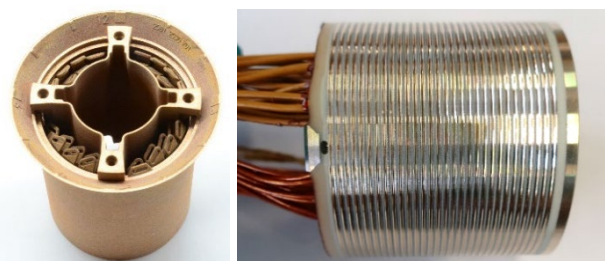


Figure 3: Bronze rotor printed by CSEM and post-processed by RSSR.

\* RUAG Slip Rings SA (RSSR)

[1] P. L. Conley, 1998, Wiley, Space vehicle mechanisms: elements of successful design, ISBN: 978-0-471-12141-1.

[2] H. Saudan, L. Kiener, F. Cochet, S. Liberatoscioli, "Redesign, manufacturing and testing of a slirring rotor for space applications based on Additive Manufacturing", CSEM Scientific and Technical Report (2018) 75.

# Compliant Mechanism built by Additive Manufacturing

L. Kiener, H. Saudan, F. Cosandier, G. Perruchoud, A. Verhaeghe

The development of compliant mechanisms made by Additive Manufacturing (AM) leads to innovative designs and significant improvements in the field of high-precision positioning systems. In the frame of the European Space Agency COMAM project (Compliant Mechanism based on Additive Manufacturing), new and innovative architectures have been built and are now tested intensively to assess their precision performance. The space market is anticipating the performance requirements to further push the limits for such kind of mechanisms within future satellite instruments.

CSEM has been mandated by the European Space Agency (ESA) in the frame of highly innovative research frame to develop Compliant Mechanisms (CM) made by Additive Manufacturing (AM). This is the recognition of a heritage of more than 30 years in the development of compliant mechanisms where high precision and long lifetime are required to move optical payloads. In parallel, CSEM has investigated over the last years the use of AM for such applications, to overcome the current limitations of costly machining and lengthy assembly of hundreds of parts to build a reliable compliant mechanism. With the COMAM project it is proposed to build a CM in one part.

## Challenging the additive manufacturing rules to build new compliant mechanisms

Since CMs demand long and thin flexure blades for certain movements, the classical AM design rules shall be drastically challenged. For example, AM equipment providers recommend avoiding thin structures or to machine the flexures afterward for a smooth surface. Such limitations are not compatible with flexure applications, which make it mandatory to improve the process iteratively to obtain functional parts. The performance in terms of mechanical strength, including fatigue behavior, are as of today dictated by the requirements relative to space applications. CSEM focuses on improving geometrical accuracy to increase the motion guiding performance.

## The non-existence of the right software tool to design CR built by AM

The design of a monolithic compliant mechanism imposes new challenges. For example, no commercial software can simulate and optimize these structures, which are an assembly of flexible volumes (to allow the movements) and rigid volumes (the fixation interfaces and the links between the flexures). To overcome this major limitation, CSEM is developing its own optimization tools for flexures, in parallel with the use of commercial topology optimization software Altair Optistruct™ for rigid part design. The results are shown in Figure 1 with the Compliant Rotation Reduction Mechanism (CRRM) developed for ESA.

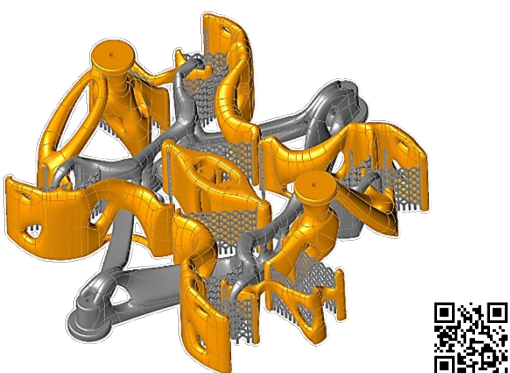


Figure 1: Compliant Rotation Reduction Mechanism (CRRM) after topology optimization. The CRRM offers a 1:10 rotation reduction ratio.

The patented concept of interlocked lattice flexures blades applied to the CRRM was also successfully applied to the re-

design of a flexible pivot which made it possible to reduce the number of parts from seven, for the commercial product, to a single one, as shown in Figure 2.



Figure 2: Interlocked lattice flexible pivots developed and built at CSEM.

## Manufacturing of the CRRM

After several iteration loops between multiple software tools (interface design, topology optimization, surface smoothing, structural finite element modeling), the CRRM was ready for the additive manufacturing process. The use of the manufacturing process simulation software, Amphyon™, helped reducing the deformations due to the AM process. The monolithic mechanism built by Laser Powder Bed Fusion (LPBF) is shown in Figure 3.

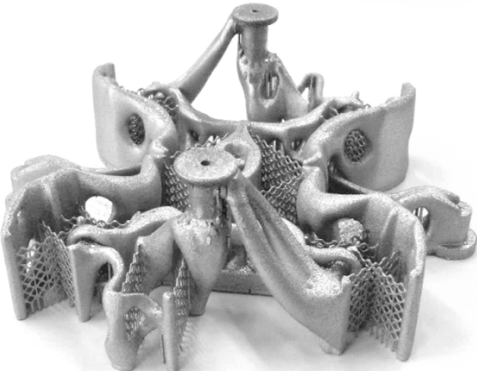


Figure 3: Compliant mechanism built by Additive Manufacturing.

The material, a high-performance stainless steel (17-4PH), was selected for its high fatigue limit. This aspect was intensively tested with representative samples to ensure that the mechanical performances are in line with conventionally machined parts.

This compliant mechanism is currently being tested to assess its guiding, stiffness, and fatigue performances.

We would like to thank the European Space Agency for its technical guidance and supervision, the Swiss project partners 3D Precision and Almatech for the constructive cooperation and the Swiss Space Office for the funding.

# CITCOM—Automated 3D Quality Control of MEMS

M. A. Kirschmann, F. Crivelli, P. A. E. Schmid

Miniaturized sensing and actuating devices are found in smartphones, cars, and medical devices. Latest micro-electro-mechanical systems (MEMS) have complex 3D shapes. This property makes optical quality control challenging. Within the European Union funded project CITCOM a solution is being developed that combines a plenoptic 3D camera with state-of-the-art computer vision algorithms, to automate this task.

MEMS miniaturize sensing and actuating functions such as acceleration measurements, ultrasound transduction, and optical switching. This makes them ideal for many application fields including smartphones, automotive, IoT, and medical. Compared to purely electrical integrated circuits (IC), MEMS can have highly three-dimensional topography. During production of MEMS, quality control is crucial for cost-effective manufacturing. Optimally all production defects should be detected early before defective specimens are integrated with other components. Currently, optical quality control is performed by human specialists manually assessing MEMS with microscopes as highly topographical structures are incompatible with the instruments used in the non-MEMS IC industry.

One goal of the European-Union funded project CITCOM<sup>[1]</sup> is to automate this challenging task of optical quality control of highly-three-dimensional MEMS. To achieve this goal, an electric wafer prober was retrofitted with a plenoptic 3D camera by consortium partner (CP) Raytrix<sup>[2]</sup> in collaboration with CP aixACCT<sup>[3]</sup>, (see Figure 1).

The plenoptic camera is controlled by a workstation running CSEM Visard<sup>[4]</sup>, responsible for image acquisition and analysis.

The integrated plenoptic camera has two big advantages: a submicron planar ( $0.7 \mu\text{m}$ ) and axial ( $0.4 \mu\text{m}$ ) resolution, and an extended depth-of-field by more than factor 30 compared to a conventional camera. This allows for single-shot acquisition of MEMS with up to  $50 \mu\text{m}$  extension in depth.

The camera software reconstructs two image types on GPU, fully focused images, and a depth-map. Based on these images types two CSEM Visard modules were developed and deployed to find defects and outliers: A Deep-Neural-Network (faster R-CNN Inception v2 COCO) model was trained to detect debris and other defects such as cracks or broken edges together with CP Brunel Innovation Centre<sup>[5]</sup> (see Figure 2). Secondly, a metrology module can measure intensities and heights based on user-defined locations in reference to a MEMS template. These measurements are compared with measurements of defect-free MEMS and outliers are flagged as potential defects.

Finally, inspection results from both modules are saved. The user can display the images with inspection results on the workstation controlling the wafer prober. Communication between both computer systems is implemented via REST APIs.

Final testing of this system will start at CP Microchip<sup>[6]</sup> in September.

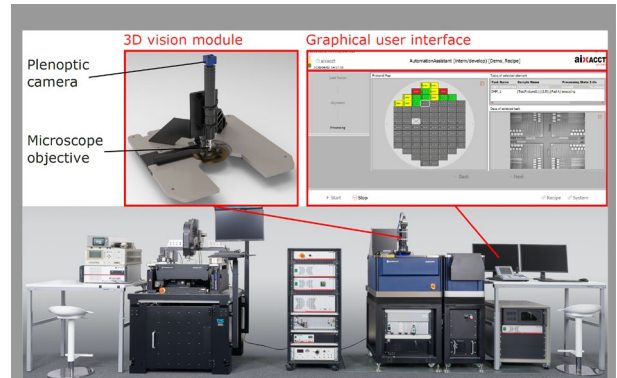


Figure 1: CITCOM optical inspection system, plenoptic camera integrated into wafer prober system.

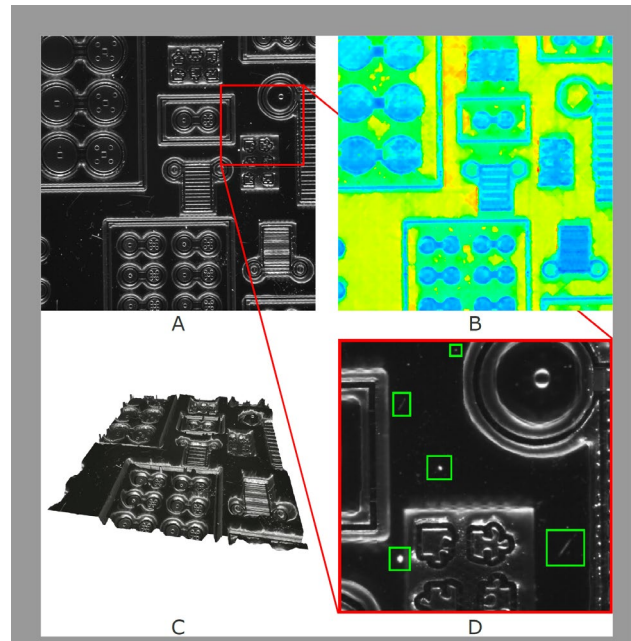


Figure 2: a) Total focus images of a MEMS (CP Philips<sup>[7]</sup>), image area  $7.8 \text{ mm} \times 7.8 \text{ mm}$ ; b) Depth map; c) Rendered 3D view; d) Crop on box from sub-image (a) with highlighted defects: Three particles and two scratches marked by green bounding boxes.

This work is supported through the Horizon 2020 grant agreement No. 768883 and by the Cantons of Central Switzerland.

<sup>[1]</sup> www.citcom.eu; This project has received funding from the European Union's HORIZON 2020 research and innovation program under Grant Agreement no. 768883.

<sup>[2]</sup> Raytrix GmbH, Schauenburgerstraße 116, D-24118 Kiel, Germany.

<sup>[3]</sup> aixACCT Systems GmbH, Talbotstr. 25, 52068 Aachen, Germany.

<sup>[4]</sup> <http://www.visard.ch/>

<sup>[5]</sup> Brunel Innovation Center, Granta Park, Great Abington, Cambridge, CB216AL, United Kingdom.

<sup>[6]</sup> Microchip Technology Inc., Phase 2, Castlegate Business Park, Unit 4, Caldicot, Monmouthshire, South Wales, United Kingdom.

<sup>[7]</sup> Philips Electronics, Boschdijk, Eindhoven, Netherlands.

# AI-based Generic Machine Health Monitoring

S. Widmer, M. Russi, L. Biggio, P. A. E. Schmid

Maintenance of industrial assets is usually performed at fixed time intervals, often leading to either unnecessary interventions or missed service operations resulting in downtime and increased costs. To cope with these downsides, the past and current data of the industrial component are continuously analyzed by a 1D convolutional autoencoder neural network, in order to detect eventual anomalies. To keep the algorithm as generic and easy deployable as possible, training is only performed with data describing the normal operating condition of the application since these are in general significantly more abundant than anomalous ones.

These days, maintenance operations of industrial assets are typically carried out at fixed time intervals. While the idea behind this approach is to reduce the amount of application downtime and the occurrence of catastrophic failures, the difficulty lies in properly scheduling those. If they are too large, the risk increases that the application reaches a high level of degradation, leading to potentially serious damage and downtime. If they are too short, unnecessary costly operations are performed and the downtime is increased accordingly. In order to avoid these downsides, predictive maintenance employs data-driven techniques to assist technicians to efficiently set times for service operations. The benefits are clearly in performing maintenance only when it is needed, reducing downtime of the application and avoiding damage to it. While most predictive maintenance algorithms are tailored to a specific application, the work of 'Industry 4.0' focuses on generic approach. As a result, the network architecture shall be the same for all types of applications and the algorithm should be easy to deploy: no downtime of the application, no additional sensors, no need of recording provoked defects.

For collecting data to train and evaluate our algorithm, the lab-setup consisted of a SCARA-robot picking up electrical fuses from a feeder, moving them into the fuse-test-bench, where the heating up of the fuse is checked with a thermal camera and then moved into the feeder with two conveyor belts. Both, process control and health data acquisition were implemented with CSEM VISARD [1]. With the lab-setup, healthy as well as un-healthy machine process data was collected. The un-healthy data was generated by introducing artificial defects, such as vacuum or pressure leakage or change in speed of the conveyor belts.



Figure 1: Lab-Setup.

In total, 8 different defects were simulated, each with a duration of 60 min. The data acquisition process was fully automatized. The user only had to select the specific artificial defect and the test duration before starting the application. The whole test run was labelled based on the selected defect. To deal with all the aforementioned requirements, a 1D convolutional autoencoder was trained with healthy data only. In particular, the goal of this neural network is to output a signal, which is as close as possible to its input. The rationale is that, since the autoencoder is trained on healthy data, the reconstruction error it provides should be higher for data it has never seen before, such those associated with anomalies. Threshold values are then calculated for each sensor based on the 99-percentile of the reconstruction error obtained on validation healthy data. At inference time, if the reconstruction error associated with a certain sensor exceeds the threshold calculated at training time, an alarm is raised [2,3].

The first results showed that the algorithm provides satisfactory anomaly detection performance on the majority of the test cases analyzed (7 out of 8). For each sensor an anomaly score based on the reconstruction error is shown and compared with the reference values calculated on the healthy data (Figure 2).

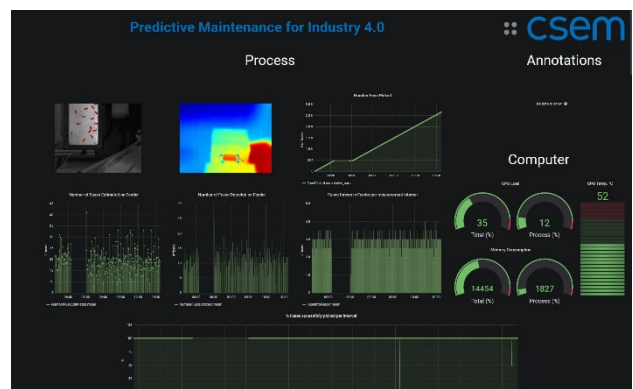


Figure 2: Online Graphana visualisation of the acquired data. Once an anomaly is detected by the autoencoder. A trigger is being raised and a notification is sent out to an external device.

The future work consists of making the step from health data monitoring to real predictive maintenance, where not only the status of the application is monitored, but also predictions are made.

CSEM thanks AUROVIS AG, maxon motor ag, Schurter AG & KNF Flodos AG for their valuable support.

This work is supported by the Cantons of Central Switzerland.

[1] [www.visard.ch](http://www.visard.ch)

[2] X. Liu, Q. Zhou, J. Zhao, H. Shen, X.; Xiong, "Fault Diagnosis of Rotating Machinery under Noisy Environment Conditions Based on a 1-D Convolutional Autoencoder and 1-D Convolutional Neural Network", Sensors 2019, 19, 972.

[3] L. Eren, T. Ince, S. Kiranyaz (2019), "A Generic Intelligent Bearing Fault Diagnosis System Using Compact Adaptive 1D CNN Classifier", Journal of Signal Processing Systems, 91, 179-189.

# CSEM Visard Enables AI for Industrial Quality Control

I. Kastanis, M. Höchemer, T. Schöpe, P.A.E. Schmid

Artificial Intelligence for industrial quality control plays an important role in Industry 4.0. The availability of appropriate tools that are industry-ready is still scarce. In particular, tools that are mature enough to be used in production lines are limited and do not offer the full potential of modern AI capabilities. On the other side, state of the art libraries are too complex to be used directly in the industry. CSEM with its long experience in both areas of AI and industrial systems has developed and deployed tools to bridge this gap and bring the latest advancements on AI-based quality control in a simple to integrate package.

One of the main goals of Industry 4.0 is to decentralize the decision-making process and make machines as autonomous as possible. Artificial Intelligence technologies provide the means for machines to be able to handle a variety of situations without the need for extensive human intervention. Quality control is an essential element of industrial production. Within Industry 4.0 quality control should be automated and thus reduce the need for human involvement in repetitive and monotonous tasks of controlling parts manually. So far, the automation of industrial quality control consisted of designing algorithms for solving very specific problems. While this approach removes the need for manual inspection, it is laborious to implement such systems, it requires expert knowledge and it is typically difficult to adapt to variants of the inspected system. AI aims to overcome exactly these difficulties, by providing flexible systems that can perform tasks without human expert knowledge.

Typically, in many academic works as well as industrial applications, AI systems are designed to run within a specific scope defined by a fixed data set. The AI-based method is implemented and then applied as is without the ability to further modify it in a simple manner. This static approach addresses only partially the issues of the classical approach where algorithms are designed by experts. For AI to realize its full potential, systems need to be modifiable after the original design and deployment. The non-expert user of the system needs to have control in his hands to adapt to the system.

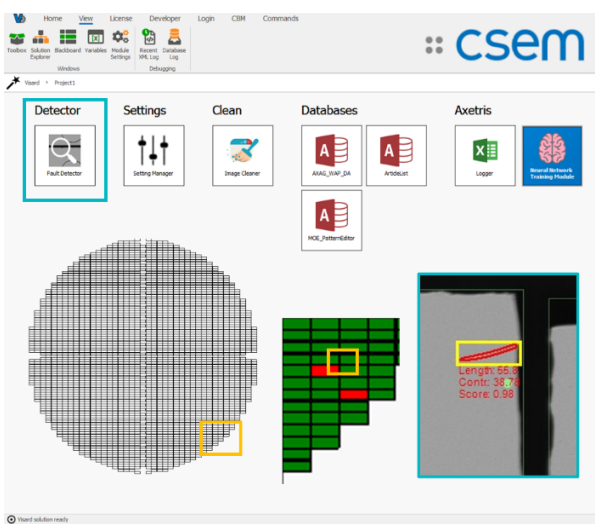


Figure 1: Visard used for defect detection on optoelectronic components.

CSEM has developed Visard<sup>[1]</sup> to address the design of Industry 4.0 automation systems in a highly efficient manner. Visard offers

[1] M. Höchemer, I. Kastanis, P. A. Schmid, "VISARD —Vision Automation Robotics Designer", CSEM Scientific and Technical Report (2016) 95. [www.visard.ch](http://www.visard.ch)

[2] <https://opcfoundation.org/about/opc-technologies/opc-ua/>

a variety of communication protocols ranging from TCP/IP to OPC UA<sup>[2]</sup>, widely adapted in the industrial domain, and gRPC. To cover the needs of modern industrial quality control Visard integrates AI technology. AI-based solutions can be executed natively within Visard but can also be linked with external applications to offer increased flexibility. Currently, the most popular programming language for AI is Python. Visard can communicate with Python programs directly and easily exchange information. This ability enables developers to drastically shorten the road from prototyping to deployment.

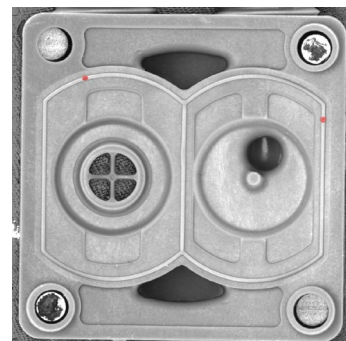


Figure 2: AI-based defect detection (red marks) on a pump part.

Visard based solutions have already been deployed in the industry for the purpose of quality control. Users can tune their AI models to improve the performance of the control system, to adapt it to newly observed phenomena, and even to create models for new product variations. This enables the user to work independently without requiring any programming nor the need of an AI expert, to maintain the quality of the production on a high level and to efficiently introduce new variations in production. Two examples of applications are: inspection of optoelectronic components realized with Axetris AG (Figure 1) and pump assembly with KNF Flodos AG (Figure 2).

To cover the needs of these complex data pipelines CSEM has developed a complete ecosystem<sup>[3]</sup> for managing labels and AI models, advanced visualization of complex data, and smart labeling tools. This ecosystem is designed with traceability, modularity, and repeatability in mind. While it covers a range of applications out of the box, it is flexible and allows customization for the specific needs of each production line. CSEM Visard lowers the hurdles for implementing dynamic AI-based solutions and facilitates companies to integrate advanced quality control in their production lines.

This work is supported by the Cantons of Central Switzerland.

[3] I. Kastanis, M. Höchemer, P. A. Schmid, "Life-long learning: Handling the complete data pipeline", CSEM Scientific and Technical Report (2020) 89.

# Pignosis—Hierarchical Time Series Forecasting using Multiple Machine Learning Methods

D. Kohli, I. Kastanis, M. Höchemer, P. A. E. Schmid

This report describes a study that was conducted to investigate the accuracy of prediction of livestock trading data using deep neural networks. CSEM machine learning expertise was successfully applied to time-series of trading data. Deep Neural Networks demonstrated the potential to outperform classical time series analysis algorithms in this application. This procedure can potentially be applied to similar business data.

Forecasting multivariate time-series is a standard problem in the field of data science, with many well-established tools to solve it. However, these standard algorithms sometimes fail to produce satisfying results. For example, when working with non-continuities or complex higher-order interactions in the data. Besides, classical tools are not always able to leverage the potential of big data sets. In such cases, Deep Learning methods can pose a viable alternative.

Livestock production, specifically for pigs, in Switzerland, is divided between specialized farmers over the lifecycle of the animals. Trade and logistics are carried out by separate companies. CSEM is developing a framework to forecast those trades for Anicom AG<sup>[1]</sup>, a large Swiss agricultural trading company.

The study described hereafter aims to answer the question, whether trades of living pigs by Anicom AG can reliably be forecasted using Machine Learning for data preprocessing and specifically Deep Learning for the modeling part.

The main challenges to be solved are the following:

- Non-continuity of the time-series data
- High input dimensionality
- Making predictions over several production steps
- The training data provides no exact ground truth about the underlying process but contains high variation induced by unobserved factors.

The potential of state-of-the-art Machine Learning methods was exploited on a dataset where classical algorithms did not produce sufficient results. Starting with an SQL database of animals trading data containing multiple features and millions of data points, forecasts of trading volumes that outperformed classical time series analysis models were produced. Different machine learning methods allow to reduce the complexity of the raw data and capture the complicated dynamics. Building custom models using modern Machine Learning and Deep Learning algorithms allow to incorporate domain knowledge not only in the preprocessing part of the analysis but also model building itself.

First, the data were clustered according to some features using several hundred logistic regression models and analyzing the parameters. Data is transformed into machine-readable time series for hundreds of clusters individually. Database operations at this scale required significant computing time. Loading the relevant datasets in entirety into memory was not feasible. Using the Dask<sup>[2]</sup> library, the data was stored on disk and manipulated

in parallel, which accelerated manipulation of the data by orders of magnitude.

Then, models could be trained specifically for individual clusters. The first experiments with a multilayer perceptron showed promising results. Improving these first results, convolutional deep neural networks were able to capture patterns in the input data and reduce dimensionality for subsequent layers. Later, these layers will be connected to probabilistic output layers using the growing TensorFlow probability<sup>[3]</sup> library that maps the inputs to specific distributions of the outcome. The used distributions include Poisson distribution for count data or normal distribution for the weight of the animals. This allows to predict a whole outcome distribution in addition to the point forecast and make consistent statements about the uncertainty of the predictions.

The time series at hand has a hierarchical structure in the time granularity as well as in production stages. Forecasts will be made at different hierarchies with specifically trained models at each step and the results will be combined to improve consistency and accuracy, as shown in Figure 1.

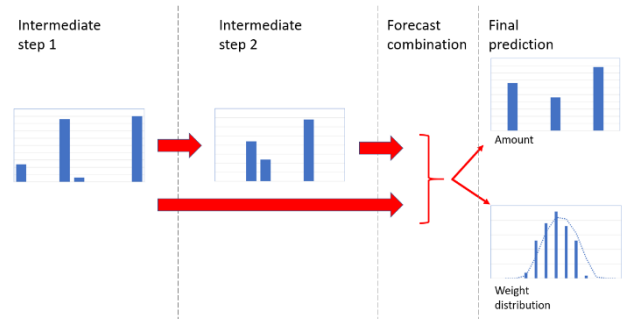


Figure 1: Prediction steps (red arrows) for an example cluster. Each arrow corresponds to a separately trained model.

In the end, predictions should be made for hundreds of individual players in the value chain at the same time. The output involves estimates of time of the trade, the number of traded animals, and the weight of the animals for different time points. The goal of the finished framework is to enable easy analysis of single farms, clusters, and the whole market. In this study, predictions with average error rates between 5% and 10% per week were achieved, depending on the counterparty of the forecasted trade. More importantly, the variation in time of the true series was well described by the forecast.

This analysis shows that CSEM Deep Learning and Software Engineering expertise for industrial machine data and image processing can be successfully transferred to other types of data that appear in large businesses and trading companies.

[1] Anicom AG, Eichenweg 4, 3052 Zollikofen

[2] <https://dask.org/>

[3] <https://www.tensorflow.org/probability>

# Metal Working Fluid Monitoring for Industry 4.0

D. Schmid, K. Petropoulos, S. Cattaneo, S. Generelli, I. Hourani<sup>\*</sup>, W. Kratz<sup>\*</sup>, P. Schmid

Together with Swiss-based Axino Solutions AG, CSEM is developing the cutting fluid monitoring solution of the future. CSEM's electrochemical sensors technology and Axino's IoT solution build the core of tomorrow's real-time quality and safety monitoring for the metal working industry.

Remote machine monitoring is becoming a cornerstone in efficient, automated and connected industry 4.0. Metal working fluids (MWF) must cool and lubricate both tools and materials to ensure optimal processing performance. However, such liquids can deteriorate over time, thus causing loss in quality and also a potential threat to the health of operators; bacteria and fungal spores as well as processing by-products can contaminate the cutting fluid and reach the skin or enter the respiratory tract through aerosol formation during machining. Hundreds of cases of diseases due to occupational MWF exposure are reported each year in Switzerland alone [1].



Figure 1: Machining with water-oil emulsion-type metal working fluids enables high quality surface finish and extended tool lifetime but may cause a risk to human health through contaminated aerosols.

Prevention of degradation by frequent exchange, actually applied by the majority of industries operating in the sector of CNC machining, has important economic drawbacks (costly product and machine down times).

Main challenge in today's approach of managing MWF is the classical way of determining the contamination in the MWF by sampling it and testing it in a laboratory.

For such tests, bacteria and fungal spores have to grow over a time of 24-48 hours to be determined. This kind of classical monitoring is not compatible any more with the speed needed for Industry 4.0. That's why a lot of companies tend to exchange the cutting fluid before the end-of-life cycle which in turn has an environmental impact.

CSEM is developing a multi-sensor approach, based on its technology platform for low-cost disposable electrochemical sensors, in order to monitor MWF in terms of cooling efficiency, lubrication capacity and biological contamination.

Preliminary results are promising: CSEM's sensors work reliably and with high sensitivity in these complex water-oil emulsions. Monitoring of pH and other parameters show significant differences between fresh and used/degraded cutting fluids. However, due to the vast differences in MWF compositions, a

common absolute threshold value cannot be set, but must be adapted specifically for each type of MWF.

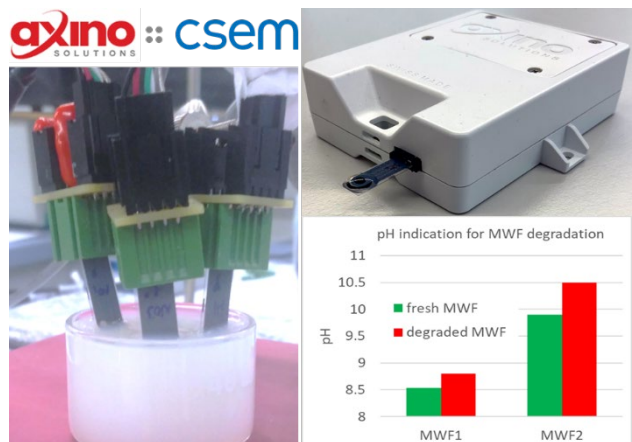


Figure 2: Testing of CSEM's disposable screen-printed sensors with both laboratory instrumentation and Axino's read-out system in real cutting fluids. Significant signal difference for fresh and degraded samples were observed.

Besides pH, additional chemical parameters are currently being validated for a reliable monitoring of biological contamination.

Remote monitoring via LoRaWAN network through Axino's expertise in IoT applications offers a new continuous and data-driven solution for real-time control in the metal working industry – in accordance with the industry 4.0 concept, quality process and health and safety regulations. This novel cutting fluid monitoring solution aims at lowering the need for manual intervention on the control and maintenance process, while at the same time extending safely the usage lifetime of the fluids. The continuous monitoring of the contamination ensures a sound health and safety environment for workers. The small and cost-effective innovative automated system is interfaced with fully customizable cloud-based backend. Data is analyzed in real-time and a possible warning signal is sent to the backend control room within minutes.

Work is ongoing for further characterization of real and spiked MWF samples as well as for sensor fabrication optimization towards large scale production. Axino is developing an error algorithm based on statistical quantities (variance, dynamics) using different methods in machine learning (simple recurrent network SRN, long-short term memory network LSTM). The further optimization of the predictive maintenance will be validated by training and testing the system in real-time industrial settings.

The authors would like to thank Innosuisse Solutions and Axino Solutions AG for their financial support (Project No 35163.1 IP-ICT).

\* Axino Solutions AG, 4500 Solothurn, CH

[1] M. F. Koller, C. Pletscher, S. M. Scholz, P. Schneuwly, "Metal working fluid exposure and diseases in Switzerland", *Intl. J. Occup. Environ. Health*, 22 (2016), 193.

# Solving the Data Problem: Deep Learning based Image Synthesis for Industrial Applications

E. Ntavelis, I. Kastanis, P. A. E. Schmid

The evolution of generative adversarial networks has permitted the generation of realistic fake images which, in some cases, are indistinguishable from the real ones. Many recent works in image generation focus on learning internal image statistics via training only on a single natural image. While natural images exhibit variability in their attributes, industrial images are often acquired in a controlled environment following a specific structure. In this work, the state-of-the-art single image generation method was extended to handle a handful of well-structured industrial images. Deep Learning plays an important role in Industry 4.0 manufacturing lines and multiple ML-based image processing products are currently on the market. To be able to tackle a variety of problems where image acquisition is costly and a time-consuming data generation is a promising approach.

The field of Image Generation has produced a vast plethora of works since the introduction of Generative Adversarial Networks (GANs)<sup>[1]</sup>. Yet only a small fraction is dedicated to industrial images, which differ from natural images in a significant manner. Natural images contain a variety of different objects, structures, and colors. In industrial images, manufactured objects are encountered, with simpler appearances and well-defined structures, material, and positions. Thus, industrial images require methods that can handle them differently than natural images.

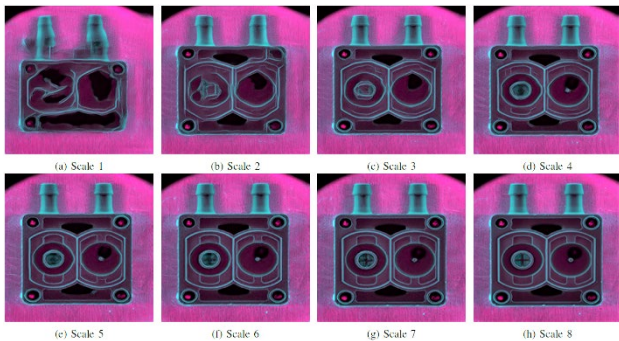


Figure 1: Changing the scale we input a real image to the network creates a trade-off between variation and structural integrity in the output.

Generative Adversarial Networks have promising applications in the industrial sector. In low data regimes, GANs can be used to augment a dataset by generating new samples or synthesizing defects on top of healthy ones. However, a standard GAN requires an abundance of data to train.

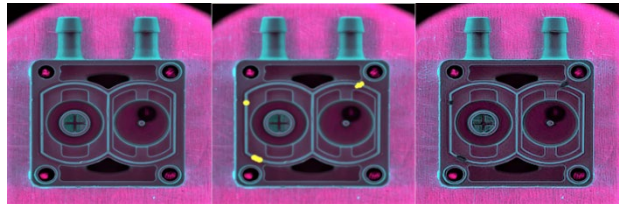


Figure 2: With our proposed solution the user can draw over the industrial part to dictate where the network will create the defects.

The proposed method, Same Same but Different GAN (SSD-GAN)<sup>[2]</sup>, is trained only on a handful of industrial images, utilizing their structured nature, and offers image manipulation capabilities at the inference time. Like SinGAN<sup>[3]</sup>, eight pairs of generators and discriminators are trained hierarchically. The network starts by synthesizing low-resolution images from noise at the coarser scale and every additional pair increases the resolution, focusing on the finer details of the synthesized image. A novel loss is introduced that can handle more than one image in the latent space: the Same Same But Different Loss. This loss is aiming to bring every synthesized image at each scale of the network closer to the two most similar training images to it, while at the same time it tries to push away the one that it differs from the most.

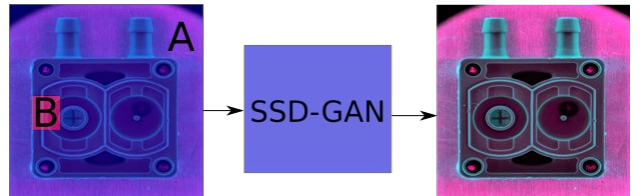


Figure 3: Patch B featuring a defect is extracted from Part B and stitched on top of part A. Our SSD-GAN harmonized the resulting image.

When the training is finished, the generator can be used to augment the small input dataset with defected pixels. Firstly, instead of generating the images based on random noise inputs, a real image is introduced at a different resolution scale and the network synthesizes a similar sample from it. As we can see in Figure 1, the earlier we input the image the more variability we observe in the output of the latest scale, but we lose structural integrity. Using the trained generator we can generate samples with defects. Figure 2 shows how we can draw over an image and dictate where the network will synthesize defects on the output. Another approach is to use the CutMix<sup>[4]</sup> method, where one patch/defect of one image is placed on top of another image. The result of this collage can create discontinuities, which can be fixed by SSD-GAN, in the process shown in Figure 3.

This work is supported by the Cantons of Central Switzerland.

[1] I. J. Goodfellow, J. Pouget-Abadie, M. Mirza, B. Xu, D. Warde-Farley, S. Ozair, A. C. Courville, Y. Bengio, "Generative Adversarial Nets", NIPS (2014).

[2] E. Ntavelis, I. Kastanis, L. Van Gool, R. Timofte, "Same Same but Different: Augmentation of Tiny Industrial Datasets using Generative Adversarial Networks", 2020 7th Swiss Conference on Data Science (SDS).

[3] S. Tamar Rott, T. Dekel, T. Michaeli. "SinGAN: Learning a Generative Model from a Single Natural Image", 2019 IEEE/CVF International Conference on Computer Vision (ICCV) (2019).

[4] S. Yun, D. Han, S. Joon Oh, S. Chun, J. Choe, Y. Yoo. "CutMix: Regularization Strategy to Train Strong Classifiers with Localizable Features", 2019 IEEE/CVF International Conference on Computer Vision (ICCV) (2019).

# Detecting the Source of Defects in Condition-based Maintenance

L. Biggio, I. Kastanis, P. A. E. Schmid

In condition-based maintenance (CBM), data-driven approaches are employed to extract relevant patterns from sensor data and guide subsequent maintenance interventions. However, often, these techniques are not designed to provide information about the origin of a certain alarm, leaving the search for this source of failure to the user. Furthermore, they often need to "see" several instances of anomalous data to recognize a failure at test time. In this report, we describe a residual-based approach based on a convolutional autoencoder (AE) which copes with the two shortcomings of standard approaches in CBM. The proposed technique is flexible and can be utilized in a wide range of CBM applications.

Currently, the most popular approaches to maintenance can be divided into two categories, namely reactive maintenance, and scheduled maintenance. The first implements maintenance operations immediately after a system failure occurs (Reactive Maintenance), whereas the second is based on scheduling maintenance operations at regular time intervals (Scheduled Maintenance). These strategies naturally introduce significant extra costs due to machine downtime, component replacement, or unnecessary maintenance interventions. CBM differs from the previously described types of maintenance strategies in that it employs data-driven techniques to assist technicians to efficiently set times for maintenance activities. In CBM, whenever an anomalous behavior is detected, an alarm is raised and maintenance takes place. These three different approaches are illustrated in Figure 1.

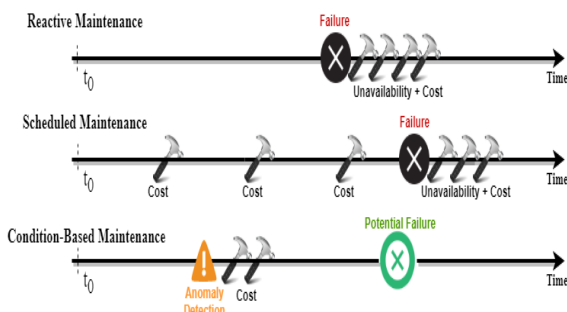


Figure 1: Different types of maintenance strategies and associated costs.

A traditional class of approaches to perform anomaly detection in the context of CBM is represented by the so-called residual-based techniques. These methods learn an internal representation of the data describing the nominal operating conditions of a certain machine and measure the distance of a new data instance from the previously learned "healthy" representation. If the distance is above a pre-specified threshold, an alarm is raised. AE architectures are particularly well-suited for this kind of approach<sup>[1]</sup>. An AE is a neural network whose output is the reconstruction of its input. The idea is that, if the AE is trained to reconstruct "healthy" data, whenever an "unhealthy" observation appears, the network will be unable to precisely reconstruct its input. Alarm thresholds can then be defined by considering the 99-percentile of the reconstruction error on the validation ("healthy") data. Our methodology is based on

calculating such validation thresholds for each sensor, allowing us to customize each alarm to the specific sensor behavior (see Figure 2). Most importantly, our AE is trained with "healthy" data only. This is particularly useful in all those cases where failures correspond to rare events and collecting large anomalous datasets is difficult or even impossible. Initial effort for a new machine remains at a minimum.

Most of the time, in the context of industrial applications, sensor data come in the form of time series. Therefore, it is important to design Machine Learning algorithms capable of extracting and processing temporal correlations. To this purpose, similarly to [2], we replace the standard feed-forward layers of the traditional AE with one-dimensional convolutional modules. The inputs of the resulting AE are therefore multi-dimensional time series chunks of fixed length, each representing a different sensor reading. Besides their enormous success in Computer Vision, Convolutional neural networks have demonstrated excellent performances also in the context of time series analysis [3].

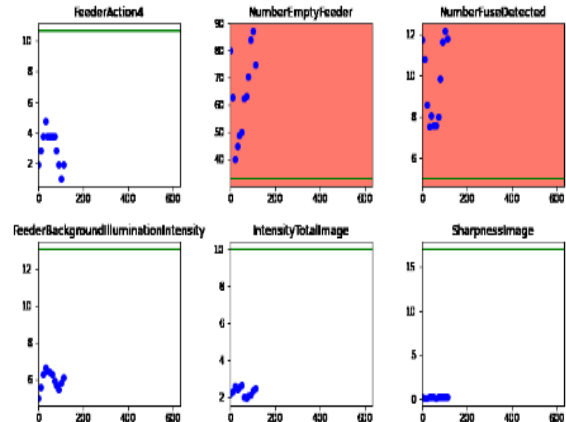


Figure 2: Convolutional autoencoder anomaly detection. Red panels represent anomalous sensors. For them, the reconstruction error lays above the corresponding threshold (green line).

The algorithm shows excellent anomaly detection performances and has been included into the online data acquisition pipeline based on CSEM Visard<sup>[4]</sup>. Future work will focus on retraining the model with more data and exploring more advanced architectures based on the same principle.

This work is supported by the Cantons of Central Switzerland.

[1] R. Chalapathy, S. Chawla, "Deep learning for anomaly detection: A survey", arXiv preprint arXiv:1901.03407 (2019).

[2] X. Liu, Q. Zhou, J. Zhao, H. Shen, X. Xiong, "Fault Diagnosis of Rotating Machinery under Noisy Environment Conditions Based on a 1-D Convolutional Autoencoder and 1-D Convolutional Neural Network", Sensors 2019, 19, 972.

[3] H. I. Fawaz, et al., "Deep learning for time series classification: a review", Data Mining and Knowledge Discovery 33.4 (2019): 917-963.

[4] M. Höchemer, I. Kastanis, P. Schmid, "VISARD—Vision Automation Robotics Designer", CSEM Scientific and Technical Report (2016) 95.

# Life-long Learning: Handling the Complete Data Pipeline

I. Kastanis, M. Höchemer, P. A. E. Schmid

The promise of Artificial Intelligence: systems that evolve in time while adapting to changing conditions. While this is theoretically possible currently, various hurdles need to be overcome before such systems get deployed in real-world applications. This report describes the required infrastructure for life-long learning applications. CSEM has developed an ecosystem of tools that enable SMEs to easily overcome the obstacles during the integration of advanced AI technology.

One of the reasons why AI has become so popular with both technical and mainstream audiences is its promised ability to adapt to new situations without the need for explicit human intervention. Life-long learning approaches have been researched and implemented in academic work, but they have not yet reached the industry. The reason for this is that there is a strong need for appropriate infrastructure. The complexity of such systems is an order of magnitude higher than static solutions. One has to consider the complete development process of a life-long learning system and not only the final application. The infrastructure has to provide tools to analyze the system at any timepoint and detect potential faults. For this purpose, the following three aspects have to be addressed:

- Traceability
- Reproducibility
- Transparency

CSEM has developed software frameworks that support the construction of complex data pipelines in dynamic scenarios. CSEM ModelStore<sup>[1]</sup> is a framework for managing machine learning models. It provides the means to clearly identify each model, trace its origin, and build it again from scratch. CSEM LabelStore is designed upon similar principles as ModelStore, with the purpose of connecting data to labels. Labeling is considered as a dynamic process, where different strategies are used, be it through AI or human effort. Tracking of these labeling strategies is essential as they are typically incompatible with each other. LabelStore is a lightweight tool that focuses on the meta-information regarding the data and is agnostic to the underlying data source.

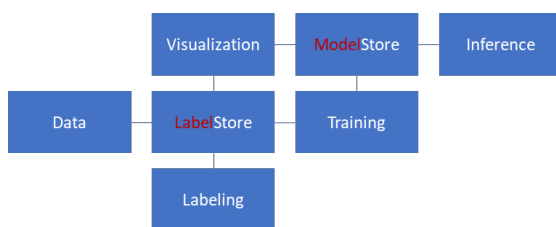


Figure 1: Diagram of a lifelong learning application.

Frameworks for managing data and models are only the foundations for life-long learning applications, it is human intelligence that must be injected in the system, through data selection and annotation. This has to be done in a highly efficient way to allow large collections of data to be processed. To achieve this goal CSEM has developed advanced visualization tools. This allows multi-dimensional data to be projected on two dimensions and to be grouped together according to automatically selected

features from an underlying machine learning model. It further offers the user the ability to overlay additional information and, in this manner, analyze data extensively. The visualization tools facilitate the cleaning of the data and smart selection for labeling. Outliers are easily found without the need to use handcrafted rules that typically require a fair amount of time. In this manner, each group can be sampled according to its proximity to other groups. Through the smart selection, the data to be labeled by the user is significantly reduced. It also avoids the mundane task of repeatedly annotating simplistic data and drives the focus in the most interesting cases on the boundaries between groups of different characteristics.

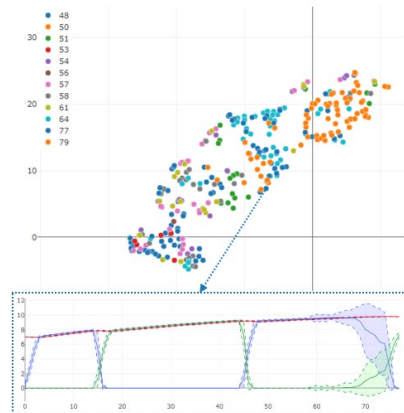


Figure 2: Visualization of multidimensional data using automatically extracted features and t-distributed Stochastic Neighbor Embedding<sup>[2]</sup>.

The final step of the data pipeline is actual labeling. It is here where the intelligence of the human expert is required. Beyond the smart selection, CSEM designed tools to make labeling as efficient as possible. Algorithms ranging from classical signal processing to advanced neural networks are deployed in an assistive manner. These tools ease the annotation process by making suggestions and by simplifying the interaction with the software.

The development of life-long learning applications requires an ecosystem of tools that can be combined flexibly. Machine learning has to be viewed not only as a final decision maker, but also an analytical tool that helps in transitional stages. Ultimately the application is a dynamic and evolving system, where changes, such as the updating of a model, have to be transparent and reproducible. CSEM has developed a versatile ecosystem of tools that are already deployed in the industry. This facilitates the creation and efficient integration of advanced data-driven methods even in SMEs that are not data specialists.

This work is supported by the Cantons of Central Switzerland.

[1] I. Kastanis, et al., "ModelStore-A Lightweight System for Storing Neural Network Models", CSEM Scientific and Technical Report (2019) 88.

[2] L. van der Maaten, G. Hinton, Geoffrey (2008), Visualizing data using t-SNE. Journal of Machine Learning Research. 9. 2579-2605.

# Machine Learning Approaches for PPG-based Blood Pressure Monitoring: Validation against Invasive Arterial Line Measurements

J. Jorge, M. Proen  a, C. Aguet, J. Van Zaen, G. Bonnier, P. Renevey, A. Lemkaddem, P. Schoettker\*, M. Lemay

Arterial blood pressure is a physiological parameter of major importance to medical applications. CSEM has developed pioneering techniques for blood pressure estimation based on optical signals such as photoplethysmographic pulse wave analysis (known as oBPM®), which enable continuous non-invasive blood pressure monitoring. Recently, CSEM explored data-driven approaches using machine learning to enhance the performance of these techniques. The novel methods were tested in the clinical setting and found to outperform previous approaches by up to 15%.

Photoplethysmography (PPG) could provide a novel approach for continuous, non-obtrusive blood pressure (BP) monitoring, comfortably integrated in wearables and smartphones. CSEM has conducted extensive work in this domain, developing the oBPM® technology for PPG-based BP monitoring [1]. As part of our continued efforts to boost the accuracy, robustness, and applicability of oBPM®, we have explored machine learning (ML) techniques in this framework, motivated by the increasing availability of labeled PPG datasets for supervised learning.

In this work, we developed a novel hybrid approach that pre-processes PPG signals and extracts physiological features using our well-established and clinically validated oBPM® library, and then performs BP estimation via data-based ML models (Figure 1). ML methods capable of automatic feature selection were used to identify the most meaningful features. The selected feature sets were then used to develop higher-accuracy estimation models. For this work, the estimation was focused on systolic (Sys) BP.

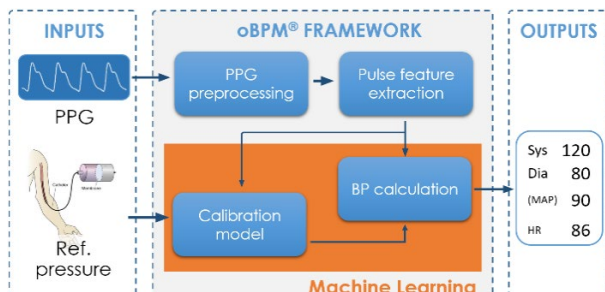


Figure 1: Outline of the novel hybrid approach explored in this work, combining modules from CSEM's oBPM® with novel ML models.

The method was explored on PPG data collected from clinical patients undergoing general anesthesia induction, which caused strong variations in BP over time [2]. Concurrent traces of Sys BP were obtained invasively (catheter) and served as reference.

The PPG data were segmented in 20-second segments, which were grouped in pairs to model a situation where a calibration measurement was previously made (PPG + gold-standard reference), and a second, PPG-only measurement is performed for which Sys BP is to be estimated (Figure 2). The patient group was split into a training and test sets, with each patient contributing to only one set. Three ML models were explored: LASSO regression, Gaussian process regression (GPR), and support vector regression (SVR). A Control model was also included where the Sys BP estimate is equal to the reference Sys BP of the calibration segment, thus assuming no BP variations.

\* Lausanne University Hospital and University of Lausanne, Switzerland

[1] M. Proen  a, J. Sol  , M. Lemay, C. Verjus, "Method, apparatus and computer program for determining a blood pressure value," Patent Application WO 2016/138965 A1, Sep. 2016.

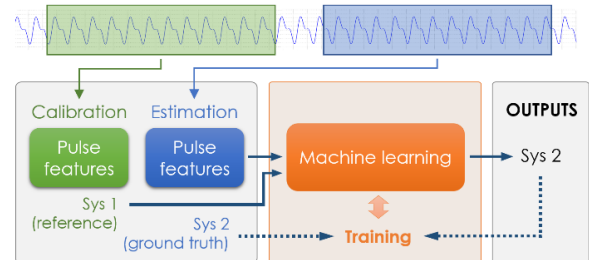


Figure 2: Learning approach to estimate systolic (Sys) BP at a given time (blue) in the presence of calibration information (green).

After training, all models performed substantially better than the Control, and the ML models were found to outperform oBPM® as well, reducing the standard deviation of the estimation error by approximately 9–15% in the test set (Figure 3). This indicates a very favorable performance in this clinical setting, with the potential to expand oBPM®'s accuracy under AAMI standards to a larger range of applicability [2]. Moreover, models like LASSO presented comparable computational costs to oBPM®, and are therefore well suited for embedded estimation as well.

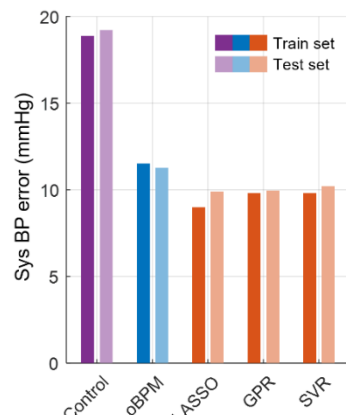


Figure 3: Sys BP estimation performance for different Sys BP estimation models. The Control model is a simple approach where the value of the reference BP in the calibration is used directly as the estimate.

Overall, these results suggest that ML techniques, namely LASSO, GPR, and SVR, are highly promising for non-obtrusive BP monitoring, leveraging CSEM's previous experience in model-based BP estimation with new predictors learned directly from the data. These insights may prove extremely valuable to pursue the challenging goal of BP monitoring using wearable technology and measured in different points of the body.

[2] M. Proen  a, Y. Ghamri, G. Hofmann, et al., "Automated Pulse Oximeter Waveform Analysis to Track Changes in Blood Pressure during Anesthesia Induction: A Proof-of-Concept Study," *Anesth Analg*, 2020, 130(5).

# Blood Pressure via Smartphone Camera: Validation against Auscultatory Measurements

M. Proen  , G. Bonnier, A. Lemkadem, J. Degott\*, G. Hofmann\*, R. Schorer\*\*, U. Christen \*, J.F. Knebel \*, A. Wuerzner \*\*,  
M. Burnier \*\*, G. Wuerzner \*\*, P. Schoettker\*, M. Lemay

Hypertension, or chronically high blood pressure, is the leading risk factor for cardiovascular diseases, which constitute the main cause of death worldwide. With close to 1.5 billion hypertensive individuals globally, the need for accessible and accurate means of screening and monitoring blood pressure is key in fighting this epidemic. Smartphones, which are widely available, could play a leading role, provided that their ability in providing accurate blood pressure measurements is demonstrated. We present hereafter a validation study performed on 85 patients of a hypertension clinic where our pulse wave analysis algorithm oBPM® estimated blood pressure from optical signals acquired at the fingertip of the patients via a smartphone camera. The results, compared to auscultatory measurements, demonstrate compliance with the ISO 81060-2 standard for non-invasive sphygmomanometers.

High blood pressure (BP), or hypertension, is the main risk factor for cardiovascular diseases and the root cause for approximately ten million deaths each year. By 2025, the number of people suffering from hypertension is expected to reach 1.5 billion. Early detection, prevention, and management of hypertension are essential, but require accessible and accurate measurements.

Smartphones represent a widespread, readily available device for mobile health, with over one third of consumers owning one worldwide. With the potential to measure a photoplethysmographic (PPG) signal at the fingertip using the phone's camera and the recent advances in PPG-based BP monitoring [1], the potential of smartphones for hypertension prevention, diagnosis and management is obvious.

We have recently validated our patented optical blood pressure monitoring algorithm [2], oBPM®, during general anesthesia induction using PPG signals from a standard pulse oximeter [3]. In the present study, our aim was to assess the accuracy of oBPM® applied to smartphone-derived PPG signals acquired via a dedicated app (OptiBP®).

The study [4] consisted of two arms (ClinicalTrials.gov identifier: NCT03875248). In the first arm, the parameters of the algorithm were trained using the data of 51 patients scheduled for an elective surgery necessitating general anesthesia and invasive arterial BP monitoring at the Lausanne (CHUV) or Geneva University Hospitals. The choice of general anesthesia induction was motivated by the fact that it causes large BP variations, which allows a proper training of the sensitivity of the algorithm. In the second arm of the study, the BP values estimated by the algorithm on 85 patients scheduled for an elective visit at the outpatient hypertension clinic at CHUV were compared to reference auscultatory measurements obtained by two independent observers using a double stethoscope. A total of

seven pairs of measurements were obtained for each of the 85 patients of the validation group. An initial calibration procedure—consisting in an offset correction—was applied for each patient. Unreliable BP estimates were automatically rejected.

The accuracy of the BP estimates was evaluated against the reference auscultatory measurements following the metrics of the ISO 81060-2 standard for non-invasive sphygmomanometers, which requires the cohort-wise mean error to be within  $\pm 5$  mmHg, and the standard deviation of the error no greater than 8 mmHg. Because auscultatory measurements only provide systolic and diastolic BP values, reference mean BP values were obtained as 2/3 diastolic + 1/3 systolic. Table 1 shows the results obtained and whether the compliance with the ISO 81060-2 standard was met for each BP value.

Table 1: Accuracy (mean error and standard deviation of the error) of the smartphone-derived BP values estimated by the oBPM® algorithm compared to reference auscultatory measurements.

BP	Mean error (mmHg)	SD of error (mmHg)	Compliance with ISO 81060-2
Systolic	0.5	7.8	YES
Mean	0.5	4.4	YES
Diastolic	2.0	4.8	YES

Improving the accessibility of BP measurements at a worldwide scale is key in reducing the mortality and morbidity associated with hypertension. Smartphones, because of their widespread use—including in third world and low-income countries—are an ideal solution to this issue if a clinically accepted accuracy is met. This has been demonstrated in our study on 85 patients where our BP estimates are compliant with the ISO 81060-2 standard.

- Department of Anesthesiology, Lausanne University Hospital and University of Lausanne, Switzerland
- Department of Acute Medicine, Geneva University Hospital and University of Geneva, Switzerland
- \* Biospectral SA, Lausanne, Switzerland
- \*\* Service of Nephrology and Hypertension, Lausanne University Hospital and University of Lausanne, Switzerland
- [1] M. Proen  , P. Renevey, F. Braun, et al., "Pulse Wave Analysis Techniques". In: J. Sol  , R. Delgado-Gonzalo (eds) The Handbook of Cuffless Blood Pressure Monitoring. Springer, Cham, 2019.

[2] M. Proen  , J. Sol  , M. Lemay, C. Verjus, "Method, apparatus and computer program for determining a blood pressure value", WO 2016138965 A1, 9th of September 2016.

[3] M. Proen  , Y. Ghamri, G. Hofmann, et al., "Automated pulse oximeter waveform analysis to track changes in blood pressure during anesthesia induction: a proof-of-concept study", Anesthesia & Analgesia, 130(5):1222-1233, 2020.

[4] P. Schoettker, J. Degott, G. Hofmann, et al., "Blood pressure measurements with the OptiBP® smartphone app validated against reference auscultatory measurements", manuscript in prep., 2020.

# Wearable Multiparametric Monitoring System with Embedded Intelligence: towards Seamless Atrial Fibrillation Detection

J. Lahera, H. Sigurthorsdottir, R. Delgado-Gonzalo

Low-power sensing technologies, such as wearables, have emerged in the healthcare domain since they enable continuous and non-invasive monitoring of physiological signals. Nowadays, data-driven methods, such as deep learning, offer attractive accuracies at the expense of being resource and memory demanding. In this context, CSEM has developed an edge-computing solution to address atrial fibrillation detection based on the inference of neural networks running in microcontrollers and low-power processors which wearable sensors and devices are generally equipped with. CSEM has successfully fulfilled key aspects of (medical) edge devices in terms of size and real-time execution with a memory footprint of 213 KB, and a throughput of 33.98 MOP/s.

The recent developments in the field of Deep Learning (DL) have given an important boost to the field of Digital Healthcare by outperforming classical hand-crafted algorithms. DL-based algorithms are characterized by their flexibility as well as their large computational requirements. Thus, the adoption of such solutions in wearable technology has been systematically hindered by hardware limitations (e.g. computational power, memory, and battery life). Today, new edge computing devices emerge bringing data processing closer than ever before to the data acquisition source. The advantages of processing into the device itself are threefold: (1) **latency**: without the need of the data to be processed on the cloud, the DL algorithms can react instantly; (2) **power consumption**: wireless transmission of raw sensor signals is energy demanding; thus, local processing drastically reduces the power consumption; and (3) **data privacy**: there is no data leakage since the data does not leave the device.

CSEM endowed a multiparametric wearable sensor device developed in-house with DL algorithms for detecting and classifying cardiac arrhythmias, that is, cardiac irregularities of heart beats that can lead to severe health complications. Our development extends our previous work<sup>[1]</sup>, a convolutional-Recurrent Neural Network (RNN) architecture for atrial fibrillation detection, trained on the Electrocardiogram (ECG) dataset provided for the 2017 Computation in Cardiology Challenge.

We used CMSIS-NN, a subset of CMSIS HAL library with an Application Programming Interface (API) for deploying Neural Networks (NN) on ARM Cortex-based microcontrollers. We implemented a quantization with 2 integer bits and 5 fractional bits through CMSIS-NN (noted Q2.5) in order to minimize the memory footprint and to maximize the speedup heavily relying on Single Instruction Multiple Data (SIMD). We structured the real-time data processing by windowing the ECG input signal and feeding them into our embedded neural network. In particular, each window is first processed through a sequence of 7 convolutional layers of size 5, each followed by an average pooling layer with size and stride equal to 2. The number of channels is kept multiple of 8 to exploit the speedup from the optimized convolutional kernels of CMSIS-NN. A global averaging pooling layer is applied after the last layer. The output of the convolutional part is a set of 128-dimensional tensors, one for each window, which is then fed into a Gate Recurrent Unit (GRU) with 64 hidden units.

This embedded neural network was deployed on a previously developed wearable system at CSEM measuring human vital

signs such as ECG and photoplethysmography (PPG), as shown under Figure 1. The system is driven by the nRF52832 SoC from Nordic Semiconductors. It is powered by an ARM Cortex-M4 microcontroller clocked at 64 MHz and equipped with 64 KB of RAM and 512 KB of FLASH memory.



Figure 1: CSEM's wearable sensor device with four ECG electrodes and a PPG module where the neural network has been deployed.

The accuracy metrics of the original neural network and the wearable system are equivalent in terms of sensitivity, specificity, and F1 score<sup>[2]</sup> when validating for the following classes: normal rhythm, atrial fibrillation, noise, and other. CSEM's techniques of filter quantization, network compression, knowledge distillation and deployment using CMSIS-NN provided a memory footprint that allowed the neural network to make effective predictions in real time (Figure 2).

Performance Metric	Value
Execution Time/Window [s]	0.0948
Throughput [OPs]	33.98 M
Power (Network execution) [mW]	20.65
Power (idle) [mW]	15.4
Power (sleep mode) [mW]	0.56
Power Efficiency [OPs/W]	1.64 G
Size on FLASH (KB)	213
Size on RAM (KB)	9.8

Figure 2: Performance metrics measured on the wearable platform.

In conclusion, the accuracy and deployment performance obtained with this wearable device open the door to a transfer of knowledge from the DL community to resource constrained systems. Several DL-based algorithms in the medical domain can similarly be compressed and deployed without the need of cloud infrastructure.

[1] J. Van Zaen, et al., "Classification of cardiac arrhythmias from single lead ECG with a convolutional recurrent neural network", Proc. BIOSTEC 2019.

[2] A. Faraone, et al., "Convolutional-Recurrent Neural Networks on Low-Power Wearable Platforms for Cardiac Arrhythmia Detection", Proc. IEEE AICAS 2020.

# Pulse Oximetry and Respiration Rate Assessment at the Wrist: towards the Unobtrusive Detection of Sleep Apnea

F. Braun, P. Renevey, P. Theurillat, M. Proen  a, A. Lemkadem, D. Ferrario, K. De Jaegere\*, C. M. Horvath\*, C. Roth\*, A. K. Brill\*, M. Lemay, S. R. Ott\*\*

Polysomnography (PSG) or home sleep apnea testing (HSAT) are the current standard diagnostics for sleep apnea. These systems require a multitude of sensors and are obtrusive and thus not suited for long-term monitoring. Recent advances in optical heart rate monitoring at the wrist give promise for low-cost wearable devices suitable for the early detection and ambulatory monitoring of sleep apnea. Even though not expected to completely replace PSG or HSAT, such devices could allow for a reliable pre-screening over several nights in larger populations. We investigated the feasibility of replacing important PSG measurements (oxygen saturation, respiratory rate and cardiac interbeat intervals) using CSEM's proprietary wearable device.

Sleep is an important part of our life since each of us spends about 27 years of his or her lifetime asleep. Yet, the importance of sleep is often neglected, and sleep disorders are highly prevalent in the general population but remain poorly identified. As an example, obstructive sleep apnea (OSA) affects an estimated 9 to 38% of the general population. In the US for instance, 80% of the individuals affected with OSA remain undiagnosed which adds up to an estimated economic burden of 150 billion USD per year. Patients suffering from sleep disorders often have a decreased quality of life and are more prone to accidents. To improve this situation, the present project investigates the use of an unobtrusive, wrist-worn wearable device (such as CSEM's smartwatch) for the early screening of OSA in ambulatory environment. We investigated the accuracy of our system in estimating oxygen saturation ( $\text{SpO}_2$ ), respiratory rate (RR), and cardiac interbeat intervals (IBI), which are three important measurements included in PSG.

We compared our smartwatch against PSG on 66 subjects (27 healthy volunteers and 39 patients with sleep disorders) in a clinical study (NCT03823105) at the Sleep-Wake-Epilepsy-Center of the Neurology Department of the University Hospital of Bern (Inselspital), Switzerland. In parallel to an overnight PSG, accelerometric and photoplethysmographic signals were acquired using a CSEM smartwatch. From these signals,

$\text{SpO}_2$ <sup>[1]</sup>, RR<sup>[2,3]</sup> and IBIs<sup>[2]</sup> were estimated and compared to PSG-derived reference measurements in terms of RMS error (for  $\text{SpO}_2$ ) and mean absolute error (for RR and IBI).

Watch-based  $\text{SpO}_2$  estimates showed an RMS error of 3.2% (after the automatic rejection of 15.8% data with insufficient signal quality by our algorithm<sup>[4]</sup>) which is compliant with the ISO 80601-2-61:2017 standard and FDA guidance for reflectance type sensors. Figure 1 shows the temporal evolution of overnight  $\text{SpO}_2$  estimates for two representative subjects. In both examples the watch-based estimates closely follow the fingertip-based  $\text{SpO}_2$  reference. Periodic desaturations caused by reoccurring apnea events due to severe OSA were detected by the watch (see Figure 1, bottom). Moreover, RR and IBI were estimated with a subject-wise mean absolute error of  $1.55 \pm 1.04$  breaths/min and  $6.54 \pm 5.41$  milliseconds, respectively.

The present results show promising performances for watch-based estimation of  $\text{SpO}_2$ , RR, and IBIs during sleep. Limited by a rather small dataset, this approach should be confirmed in a larger population, especially on patients with moderate to severe OSA. Future work will focus on combining  $\text{SpO}_2$ , RR, and IBI estimates to provide a low-cost solution for the early detection and long-term ambulatory monitoring of OSA.

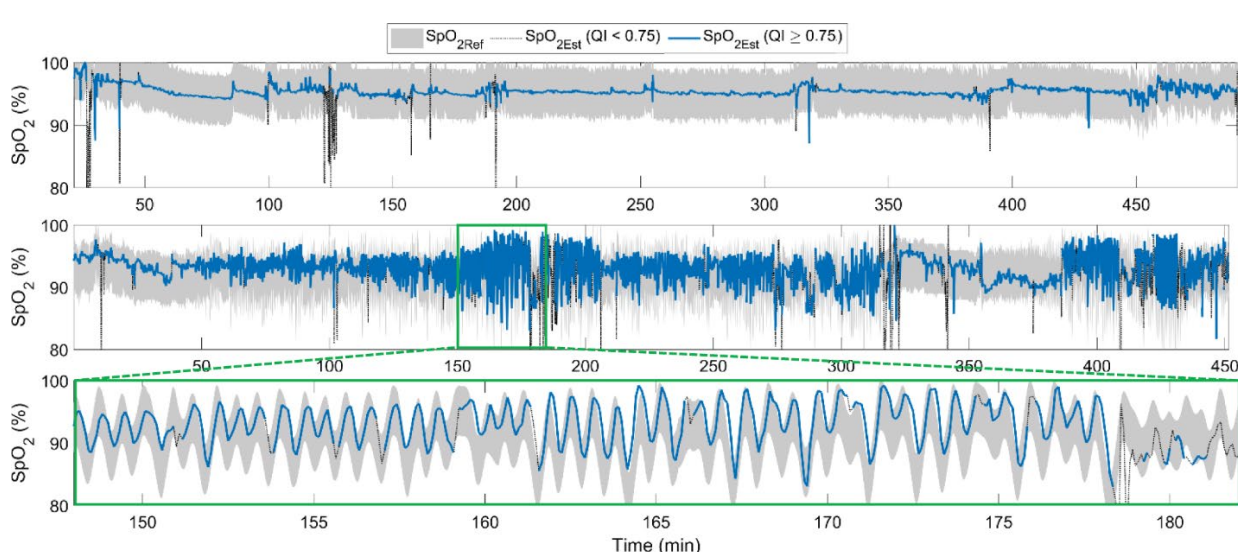


Figure 1: Examples of  $\text{SpO}_2$  estimates. The light grey shaded areas illustrate reference  $\text{SpO}_{2\text{Ref}}$  values  $\pm 4\%$ . The estimated  $\text{SpO}_{2\text{Est}}$  values are shown in black for signals of insufficient quality ( $\text{QI} < 0.75$ ) or in blue for signals of good quality ( $\text{QI} \geq 0.75$ ). The subplots correspond to: (top) subject with BMI of 45  $\text{kg}/\text{m}^2$  and no sleep apnea; (middle) OSA patient with BMI of 34  $\text{kg}/\text{m}^2$  and severe sleep apnea; (bottom) a zoom view of the same patient.

\* Inselspital, Bern, Switzerland

\*\* St. Claraspital, Basel, Switzerland

<sup>[1]</sup> F. Braun, et al., EMBC 2020, IEEE (2020), in press.

<sup>[2]</sup> P. Renevey, et al., EMBC 2018, IEEE (2018), pp. 2861–2864.

<sup>[3]</sup> G. B. Papini, et al., Physiol. Meas. 41 (2020) 065010.

<sup>[4]</sup> M. Proen  a, et al., EMBC 2018, IEEE (2018), pp. 1502-1505.

# ELAINE—Electronic Fetal Monitoring System

M. Rapin, J. Wacker, G. Yilmaz, J.-A. Porchet, R. Rusconi, C. Meier, R. Delgado-Gonzalo, B. Bonnal, A. Radan<sup>\*</sup>, O. Chételat

The objective of the ELAINE project is to evaluate a new technology of active electrodes in the context of fetal ECG (fECG) monitoring. From measuring a full ECG instead of heartrate-based cardiotocography (CTG), a higher reliability in the monitoring of the health status of the unborn is expected. The system is based on a technology developed to reduce cabling complexity, thus increasing maternal comfort. The technology was initiated under contract by the European Space Agency (ESA) in the context of multi-signal wearable monitoring system. The developed system is currently under test at the Maternity Ward of the University Hospital of Bern (Inselspital), Switzerland.

An unobtrusive electronic fetal monitoring (EFM) system based on wearable sensors can benefit from two main market pushes. The first one is derived from the current interest of obstetricians in replacing the cardiotocography (CTG) systems with an alternative which offers a greater comfort to the prospective mother. The second push is the consumer market with the newly booming industry of femtech (i.e., female technology). This sector includes fertility solutions, period-tracking apps, pregnancy and nursing care, and reproductive system healthcare.

CTG is the most common procedure used for fetal heartrate assessment before and during labor. Ever since its introduction in the late 60s, the benefit of the method has been controversial. Not only the great inter- and intra-observer variability due to visual interpretation of CTG traces seems to be an issue, but also the technical difficulties inherent to the method, namely: data analysis in adipose patients, active fetuses or multiple gestation, confusions between fetal and maternal pulse, assessment during water delivery, strong contractions or changing labor positions of the parturient. Inaccurate CTG interpretation might also lead to unnecessary medical interventions such as caesarean section and vaginal-operative deliveries [1].

Over the last 15 years, CSEM has developed technologies for the measurement of multimodal physiological parameters and which led to a novel architecture of the so-called cooperative sensors based on active electrodes connected via a bus of only two unshielded wires. Thus, this technology significantly reduces the cabling complexity of the sensor system [2]. The wires provide the common reference potential necessary for biopotential measurements and are simultaneously used for synchronization, data transfer, and powering of the sensors.

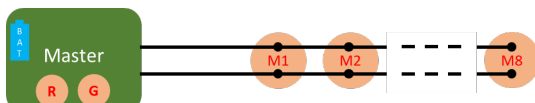


Figure 1: Connection diagram of the ELAINE system comprising a master unit, 8 cooperative sensors (M1 to M8), and a bus made of 2 unshielded wires connecting the master to the cooperative sensors.

As shown in Figure 1, the ELAINE system is made of one master and eight cooperative sensors. Thanks to a subtle architecture of the master sensor providing a low-impedance path for the current induced by electromagnetic disturbances, the wires do not need to be shielded to obtain high-quality ECG measurements [3]. This

low-impedance path is implemented with two skin contacts (namely, the guard and reference electrodes). The system is powered by a single battery integrated in the master. The power is transmitted to the measuring sensors via the same two wires.

Figure 2 shows the ELAINE system during a trial: the cooperative sensors are attached to classical gel electrodes via a snap button and measure the biopotential. The signal is amplified, filtered, and digitized onsite in each cooperative sensor. The digital data is then transmitted to the master via the bus before being wirelessly sent to an external unit. Finally, the measurements are processed to separate the signal into two components: the maternal ECG (mECG) and the fetal ECG (fECG).

Having the analog frontend and digitalization directly placed onto the electrode location increases the input impedance at the electrode and reduces the susceptibility to electromagnetic disturbances. Both are critical to enhance the fECG signal quality. Measurements performed according to IEC 60601-2-25 standard showed that the ELAINE system can measure fECG signals with a rms noise of 2  $\mu$ V (measured over a 10 s period with a measurement bandwidth going from 0.05 to 150 Hz).



Figure 2: The ELAINE system measuring 8 fetal ECG leads on a pregnant patient at the Maternity Ward of the University Hospital of Bern (Bern Ethical Committee, Project ID: 2019-01899).

In conclusion, the proposed system allows the measurement of an 8-lead fECG on pregnant woman with a flexible positioning of the cooperative sensors and reduced cabling complexity. From measuring a full fECG instead of heartrate based cardiotocography (CTG), a higher reliability in the monitoring of the health status of the unborn is expected.

\* Inselspital, Bern, Switzerland

[1] Z. Zhao, et al., "A Comprehensive Feature Analysis of the Fetal Heart Rate Signal for the Intelligent Assessment of Fetal State," *J. Clin. Med.* 2018 Aug 20; 7(8). pii: E223.

[2] M. Rapin, et al., "Wearable Sensors for Frequency-Multiplexed EIT and Multilead ECG Data Acquisition," *IEEE Trans. Biomed. Eng.*, vol. 66, no. 3, pp. 810–820, Mar. 2019.

[3] M. Rapin, et al., "Two-wire bus combining full duplex body-sensor network and multilead biopotential measurements," *IEEE Trans. Biomed. Eng.*, vol. 65, no. 1, pp. 113–122, Jan. 2018.

# Interoperable Pig Health Tracking

S. Dasen, P. Liechti, V. Schaffter, P. Theurillat, P. Renevey, C. Moufawad El Achkar, A. Moreira De Sousa, M. Frosio, R. Delgado-Gonzalo, C. Verjus

Livestock farming is a competitive world. While the herd sizes are increasing, it is ever challenging to keep the farm profitable. The FITPIG project aims at improving pig production by reducing piglet mortality, decreasing the use of preventive medicine, and enhancing animal welfare. In the context of the Internet of Food & Farm 2020 (IoF2020), a heartrate monitoring sensor has been developed to help farmers keep up with the health status of their herd.

In most sectors of livestock production, the role of digitalization is growing quickly. Pig production has not always been a frontrunner in this process. Yet, there are plenty of opportunities. The use of a heartrate sensor can help farmers support decisions in the farrowing process, determine when a sow is in heat, and signal health issues.

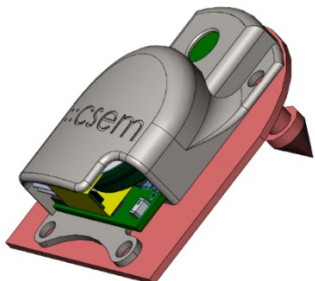


Figure 1: FITPIG embedded heartrate monitoring ear tag sensor.

CSEM, certified ISO 13485 for medical device development, has a long experience in wearable photoplethysmography (PPG) sensors on humans to monitor health parameters such as heartrate (HR), breath rate, blood pressure, etc. This technology has been brought in the field of animal monitoring with an embedded sensor integrated into a commercial off-the-shelf identification ear tag for pigs (Figure 1).

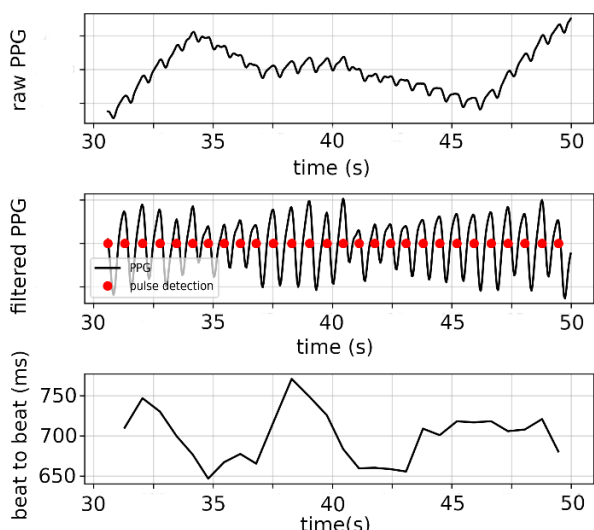


Figure 2: Raw PPG signal (top), filtered signal with pulse detection (middle) and beat-to-beat intervals (bottom).

Two optical bridges (each consisting in a 850 nm near infrared emitter and photodiode receiver) permit to detect beat-to-beat intervals that allow HR calculation (Figure 2). A 3-axis accelerometer is used to control when the PPG acquisition is suitable, to detect motion corrupted segments, and to monitor the daily level of activity of the animal.

PPG also allows the monitoring of breath rate when the animal is still. Figure 3 illustrates a case where a pig has been sedated. It is lying and breathing heavily with small head movements. The respiration component of the signal can be observed.

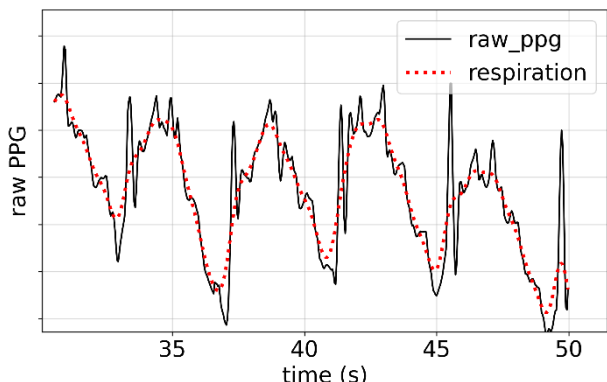


Figure 3: PPG signal from a sedated pig in hyperventilation.

This solution has been deployed first in a farm in Slöv, Sweden (Figure 4). The processed data is collected by a gateway over Bluetooth Low Energy (BLE) and then centralized on the cloud where it is post-processed to identify animals needing a closer attention. As an increase in resting HR is an indicator of fever, an end-user interface allows the farmer and the veterinarian to follow the health of the herd. This technology can also be used for other livestock mammals (e.g., cow, calf, sheep).



Figure 4: Nursing sow equipped with a FITPIG sensor.

FITPIG has demonstrated the feasibility of monitoring HR on a pig using a PPG sensor. Further developments would need an optimization of the power management to remove the heavy and expensive lithium-ion battery.

This project is a use case financed by IoF2020<sup>[1]</sup> in the context of the meat trial work package. IoF2020 has received funding from the European Union's Horizon 2020 research and innovation program under grant agreement no. 731884. CSEM also would like to thank Catherine Ollagnier and Guy Maikoff, from Agroscope - the Swiss centre of excellence for agricultural research, for her help and support.

[1] <https://www.iof2020.eu/>

# Remote Automatic Fall Detection and Activity Monitoring using Smart Wearables

C. Moufawad el Achkar, J. Jorge, E. Muntané-Calvo, M. Gerber, A. Lemkaddem, M. Lemay, C. Verjus

A timely alarm after a fall can save the faller's life and reduce the risk of debilitating injuries. In a connected world, wearable sensors offer a massive opportunity to accurately detect falls and send immediate alarms to family and healthcare providers. At CSEM, we have developed real-time embedded algorithms for unobtrusive fall detection focused on context and activity classification. These algorithms can detect falls more accurately while rejecting false positives. Our solutions target sensors embedded in non-stigmatizing widely available wearable devices.

Falls occur in more than 30% of older adults ( $\geq 65$ ) worldwide and have dire consequences ranging from injuries and fractures to death. The inability to recover after a fall can result in long lying times leading to institutionalization. In recent years, wearable sensors have emerged as potential solutions to the problem of remote fall detection and risk assessment. As wearables get smarter, the field is moving towards full ecosystems such as shown in Figure 1, capable of:

- Detecting a fall using sensors onboard wearables
- Checking the health status of the user
- Sending an alarm to family members or healthcare providers.

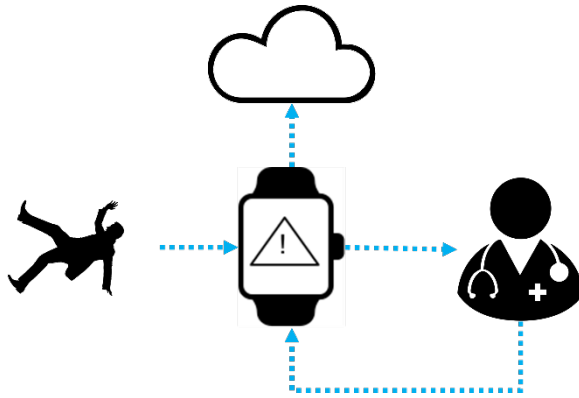


Figure 1: Fall detection ecosystem.

In the EU H2020 project ACTIVAGE, such an ecosystem was deployed with more than 450 users and caregivers as a technical feasibility proof of concept. The users received an alarm in the form of a gentle vibration on their smartwatch with the option to confirm or decline a fall. After one minute, if the alarm was unanswered by the user, communication via message or call was established with a family member or healthcare professional. The users also had the option to send an alarm themselves in case of an undetected fall. Furthermore, remote data collection was implemented through the cloud, enabling the retrieval of detected events for a refined analysis.

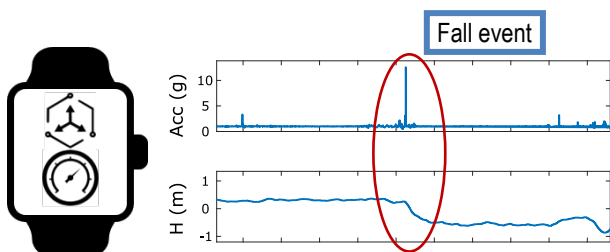


Figure 2: Smartwatch sensor signals during a fall. Acc: accelerometer. H: relative height derived from barometer.

[1] F. Bagalà, C. Becker, A. Cappello, L. Chiari, K. Aminian, J.-M. Hausdorff, J. Klenk (2012), Evaluation of accelerometer-

We built the fall detection algorithm in this ecosystem based on two sensors commonly available in smartwatches, namely accelerometers and barometers. An example of a fall recorded with these sensors is shown in Figure 2.

The proposed algorithm is embedded and works in real time. It receives a continuous stream of data and outputs a fall flag whenever an event is detected. Activity classification runs in parallel to add context to the detection, eliminating a wide range of false positives. This strategy is presented in Figure 3.

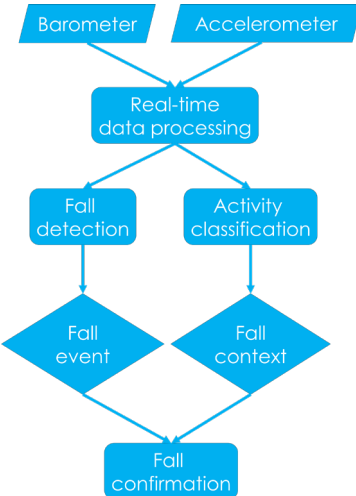


Figure 3: Algorithm structure.

We validated this approach on a dataset of simulated falls in 5 young, healthy participants. The dataset included falls from walking, standing, and during postural transitions. The algorithm achieved a sensitivity of 87% on a total of 90 fall signals, and 95% if very soft falls are excluded. Furthermore, the algorithm was tested with 7 young, healthy participants during daily life activities to check for misclassifications. On a total of 93 hours of measurement, the algorithm produced an average of three false positives per day.

These results are in line with the state of the art [1], and highlight the importance of using real world falls with at-risk persons for fine tuning fall detection algorithms and reducing false positive rate while maintaining a high sensitivity. This is especially true with wrist-worn sensors, since some movements performed during the day generate signal patterns that can resemble falls. The analysis of real-world fall events from at-risk persons is ongoing at CSEM to go beyond the state of the art in fall detection.

The work presented in this report is part of the ACTIVAGE project that has received funding from the EU Horizon 2020 research and innovation program under grant agreement No 73267.

based fall detection algorithms on real-world falls, PloS One, 7(5), e37062.

# SBra—Development of a Sensor-equipped Bra to Evaluate the Feasibility of Detecting Breast Cancer through Temperature and Bioimpedance Measurements

D. Ait Aouit Benouiuoa, J. Wacker, E. Haenni, S. Droz, P. Pilloud, M. Frosio, E. De Cao, F. Braun, J. A. Lahera Perez, I. Kjelberg, P. Heck, O. Chételat

The aim of the project SBra is the demonstration of a sensor-equipped smart bra and algorithms to show the plausibility to detect abnormalities in female mammary tissues, in particular of cancerous origin, with two concurrent measurement techniques, electrical impedance tomography (EIT) and skin contact thermography (SCT). Having produced a first demonstrator, CSEM is currently evaluating its performance on phantom breast models, partially developed in collaboration with the project partner ZTC Technology SA. The long-term objective is to develop a wearable device for use at home or in a doctor's practice, complementing the current costly, error-prone, and potentially harmful diagnosing technologies (mammography, MRI, echography). SBra is a Franco-Swiss collaborative project financed in part by the European Territorial Cooperation Program Interreg France-Switzerland 2014–2020.

According to GLOBOCAN<sup>[1]</sup>, in 2018 breast cancer—with a million diagnosed new cases and about 627 000 deaths—was the main cause for cancer-related deaths in women worldwide. A further reduction of fatalities is possible, since breast cancer can be cured in more than 90% of the cases, when detected in early stages<sup>[2]</sup>.

Currently, mammography is the most effective and popular technique for breast cancer detection, used in individual and/or organized screening. While mammography has undisputed benefits, important disadvantages remain unsolved, namely: risks related to radiation, high number of false positives, pains during the examination due to compression of the breast, and difficulties to access health care in rural areas. In addition, mammography is relatively complex, requires the know-how of specialists, and is therefore costly. Hence, the development of new diagnostic methods that address the aforementioned limitations is key for the public health sector. CSEM developed a demonstrator that examines breast tissue in a non-invasive and unobtrusive manner through a combined measurement of its electrical and thermal properties. The ultimate objective is an effective, comfortable, and portable system in the form of a bra that is capable of detecting abnormalities in the breast.

The design of SBra is guided by mathematical simulations of mammary EIT and SCT as shown in Figure 1. The functionality of the system is first tested on dedicated phantom models which emulate the temperature distribution and the electrical conductivity of breasts with and without cancer (Figure 2).

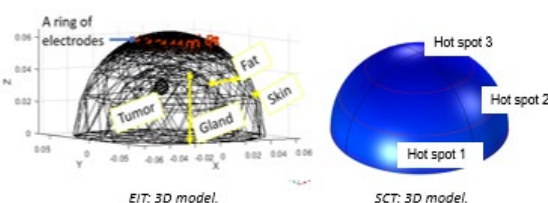


Figure 1: 3D models developed for EIT and SCT design calculations, in Matlab® and COMSOL Multiphysics® environments, respectively.

Noting in the literature that existing breast phantoms are made of perishable materials, we have designed in collaboration with ZTC Technology durable silicone phantoms. One phantom imitates the temperature distribution in the breast; a second phantom imitates the electrical properties of mammary tissues in

frequency range from 50 kHz to 100 kHz. We currently validate the characteristics of the demonstrator on these phantoms.

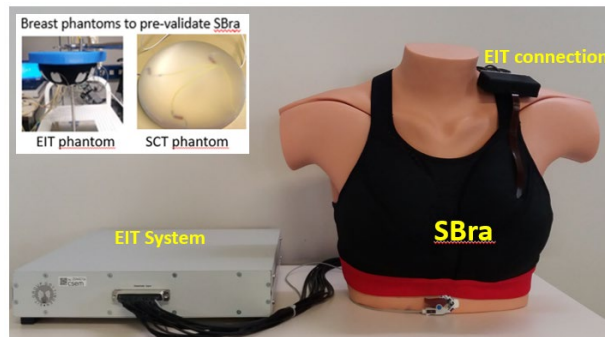


Figure 2: Developed breast phantoms to validate the demonstrator SBra demonstrator for the concurrent measurements of EIT and SCT.

For the EIT design, the optimized parameters are: electrode number and position, drive current levels and frequencies, and current injection and voltage measured patterns. Impedance data is generated by simulation with a given EIT model of a breast for two frequencies (see Figure 1, left). An EIT image is then reconstructed from Weighted Difference Frequency (WDF) measured voltages. To assess the quality of the studied design parameters, the reconstructed WDF EIT image is compared with the model. The figure of merit is the deviation in tumor size  $\Delta TS$  estimation and tumor spot  $\Delta TP$ . Table 1 shows, as an example of EIT simulation results, how the deviation in tumor size  $\Delta TS$  varies with the number of electrodes and their positions.

Table 1: Deviation in tumor size estimation  $\Delta TS$  for different electrode numbers and positions. Tumor size  $TS = 1$  cm, tumor depth (centered)  $TS = 4$  cm.

		Position of electrode ring (1=breast apex; 0=base of breast)								
		0.10	0.20	0.30	0.40	0.50	0.60	0.70	0.80	0.90
Number of electrodes	8	0.82	0.92	1.09	1.22	1.36	1.30	0.73	0.29	0.46
	12	0.83	0.84	0.91	1.00	1.00	2.00	1.04	0.32	0.18
	16	0.66	0.81	0.75	0.85	0.87	1.63	1.26	0.21	-0.09
	20	0.66	0.73	0.76	0.79	0.83	0.92	1.04	0.13	0.34
	24	0.64	0.69	0.77	0.76	0.77	0.76	1.31	0.33	2.15
	28	0.64	0.75	0.72	0.70	0.75	0.73	0.59	0.45	3.25
	32	0.64	0.69	0.71	0.73	0.74	0.63	0.62		

The smallest deviation is obtained with a ring of 16 electrodes as is shown in Table 1, evenly placed on a longitudinal ring at 90% of the height of the breast ( $k= 0.9$ ).

[1] <http://globocan.iarc.fr/Pages/online.aspx>

[2] G. N. Hortobagyi, "The curability of breast cancer: present and future", EJC Supplements, Vol. 1, No. 1 (2003), pp. 24-34.

# Wireless Powering of Ultra-low-power Sensors

A. Fivaz, O. Vorobyov, G. Yilmaz, C. Hennemann, O. Chételat

This study evaluates the remote powering of ultra-low-power sensors with wireless power transfer technology. Magnetic resonance wireless powering was assessed with respect to longitudinal and lateral positions of sensors. The developed solution operates in the ISM band (13.56 MHz). The study showed that wireless powering of ultra-low power sensors at relatively long distances is a realistic approach leading to practical use cases.

Radiofrequency wireless power transfer (WPT) has been well known since the 19<sup>th</sup> century when N. Tesla first studied magnetic resonant coupling (WPT-MRC) to illuminate a tower. This is, however, not a simple topic and Tesla failed in his development. One of the main limitations of WPT-MRC is that the energy transfer efficiency drops as the distance between the source and the sensor increases. The inverse-cube law states that to achieve the same power level at twice the distance one needs to feed eight times as much energy. The other challenge concerns Electromagnetic Safety—exposure shall be limited according to standards and guidelines. WPT could be applied in our daily life in many mobility and household appliances, e.g., for the recharge of mobile phones and headsets.

At CSEM, the feasibility of wirelessly powering ultra-low-power sensors was carried out as a technology study focused on vital signs monitoring in hospitals. A typical setting consists of several sensors placed on a patient admitted in an intensive care unit. Monitoring and recording shall continue when the patient is moved to another service. The current solutions need cumbersome wiring attached from the monitor to the patient. Wireless powering may greatly simplify the whole setup and facilitate the patient mobility between services, as well as the access of the caregivers to the patients. The absence of cables also suppresses the risk of tearing the device away.

A possible use case for ECG monitoring is presented in Figure 1 where CSEM's patented cooperative sensors – attached to a patient by means of a simple uninsulated conductive tape – are wirelessly powered.



Figure 1: ECG monitoring using CSEM's patented cooperative sensors simply connected with conductive tape (no wire).

WPT-MRC has the potential to power up sensors placed on the body, or even implants, but shall fulfill many constraints to reach an acceptable transfer efficiency at a given position of the wireless sensor. The study considered continuous WPT both directly to the sensors and to a battery.

Figure 2 shows a test setup that was used to verify the accuracy of finite elements simulations which were performed.

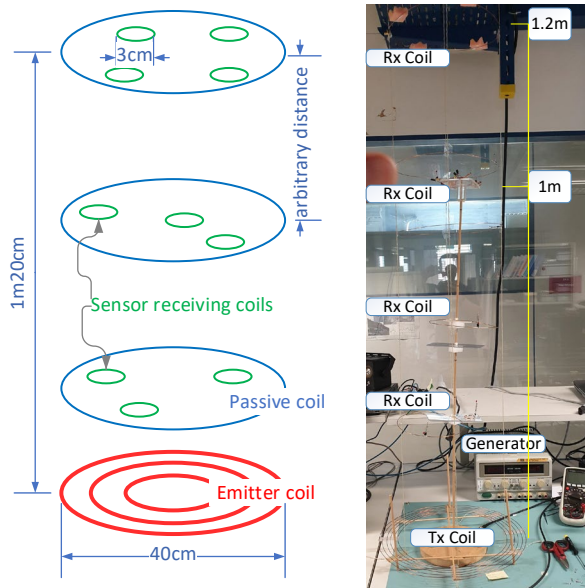


Figure 2: Experimental test setup correlated with simulation.

Several types of WPT solutions have been designed, prototyped, optimized, and tested. Tests and simulations were in good agreement, and simulations (Figure 3) were used to extend the geometry and to evaluate the limits to power directly arbitrarily distributed sensors (coil diameter: 3 cm) with nearly 500  $\mu$ W or a battery (coil diameter: 20 cm) with 10 mW in a volume of roughly  $2 \times 2 \times 2$  m<sup>3</sup> by using at the source only a few watts (typically 2 to 10 W). The free orientation of the sensors has been assessed and, with some other aspects, such as frequency tuning of the coils and limitations of the electromagnetic field strength close to the generator, will require further design steps.

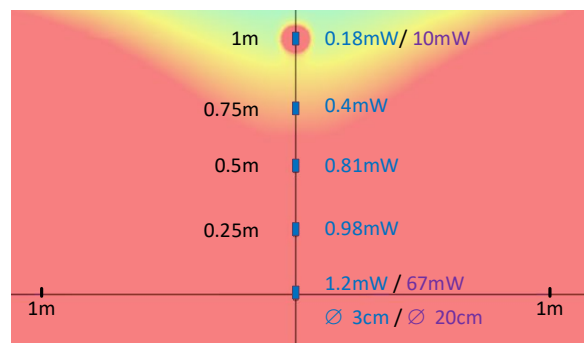


Figure 3: Simulation output example (field intensity (background color) and power versus horizontal and vertical position from a 2 W generator).

The power available in the volume depicted by Figure 3 (cylindrical around the horizontal axis) demonstrates that wireless powering is adapted to such a use case where the needed power is low and the sensor(s) stand(s) in a limited but wide area.

Wirelessly powered cooperative sensors can offer a unique implementation solution for the monitoring of bio-signals by removing the cumbersome arrangement of cabling associated with the usual setup.

# Tissue Discrimination via Electrical Impedance Spectroscopy for Neurosurgical Robots

G. Yilmaz, C. Meier, M. Crettaz, A. de Souza, F. Braun, D. Ferrario, A. Adler, O. Chételat

The BRIDGE project "Towards intelligent sensor-enhanced robotic neurosurgery" proposes a robotic screw placement technology and a surgical approach. It is based on local sensing and mapping techniques of the mechanical and electrical tissue properties, assessed continuously and in real-time while drilling the pedicle screw hole. The technology is developed for spine fusion surgeries, yet the fundamentals of the approach can be applied in other surgical operations involving drilling.

Pedicle screw placement is a central element in most routine spine fusion procedures. During these operations, screws are placed in adjacent vertebrae to join and support two or more of them. Free-hand placement of pedicle screws, a common but complex method for fusion procedures, remains the primary cause of potentially avoidable surgical adverse events due to misplaced screws. The rate of revision surgeries to rectify misplaced screws ranges from 1 to 8%.

Three Swiss partners (ARTORG Center of University of Bern, the Neurosurgery Department of Inselspital, and CSEM) have created a consortium to develop a robotic surgery approach with an ultimate goal of improving the accuracy of the pedicle screw placement to a level of zero misplacement. The proposed solution uses sensor guidance to analyze mechanical and electrical properties of tissues in real-time: (1) drilling force to bone density correlation for tool localization, (2) nerve distance estimation with electrical stimulation, and (3) tissue discrimination via electrical impedance spectroscopy (EIS).

This brief communication focuses on the advances in tissue discrimination via EIS. The fundamental hypothesis of this approach, that EIS allows the detection of transitions from cancellous to cortical bone and from there into the soft tissues (muscle, nerve), stems from the observation that different tissues exhibit different electrical properties such as conductivity and permittivity. However, intra- and inter-subject variabilities of these parameters pose a great challenge - which is further aggravated for the patients who need spine fusion surgeries. We hypothesize that incorporating multiple sensing modalities is key to surmount this challenge.

We have specified an EIS concept (11 frequencies from 10 to 100 kHz, measurement latency < 400 ms) to demonstrate the potential of the approach, as well as to understand its limitations, particularly originating from the measurement itself. Based on this concept, a maximum absolute percentage error <6% for the estimation of the impedance magnitude was recorded using a commercially available EIS device (customized version of ISX-3, Sciospec Inst., Germany) on technical phantoms composed of a wide range of precision loads mimicking tissue impedance. Upon system integration, in-vitro experiments were conducted with a monopolar electrode configuration on a phantom composed of silicone layers with different electrical conductivities. The probe (Figure 1) was inserted and retracted within a pre-drilled hole. Figure 1 shows the transitions between different layers of silicone and the same impedance level could be regained (5, 12, and 7 k $\Omega$ , respectively). Glitches at the transitions occurred due to delayed stabilization at the interface.

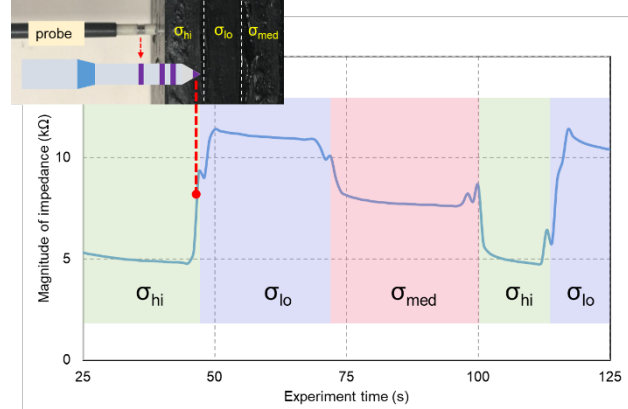


Figure 1: Impedance measurements at 50 kHz performed on a silicone phantom composed of layers with different electrical conductivities show the transition from one layer to another.

During the surgery two types of breaches can occur: frontal (as in Figure 1) and lateral (as in Figure 2). We have shown that lateral breaches are harder to detect [1] and thus concentrated our efforts on optimizing the electrode geometry and position on the probe. Finite element method simulations were performed (EIDORS) to identify the most sensitive configurations to detect lateral breaches (Figure 2). Sensitivity to detect lateral breaches is observed to increase with increasing the surface area of the tip electrode and having a ring electrode on the probe (green curve).

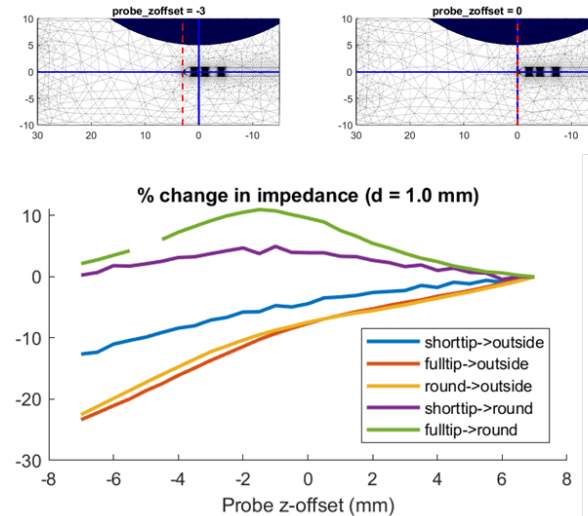


Figure 2: Electrode geometry and position optimization to improve sensitivity to lateral breach detection.

Our current activities focus on (i) designing ex-vivo experiments to validate the acquired knowledge via in-vitro experiments and simulations, and (ii) preparing for potential in-vivo experiments.

[1] Y. Jegge, et al., "Tissue classification during surgical drilling using impedance spectroscopy", EIT 2019, London, UK, 2019, p. 55.

# Soft Structure Designs for 3D-printed Wheelchair Seat Cushions

T. Parkel, I. Stergiou, A. Gautschi\*

CSEM has already demonstrated the great advantage of digital designing custom wheelchair seat cushions for people with paralysis. Within a new project with the Swiss Paraplegic Centre SPZ in Nottwil, a selected range of available materials commonly used to build custom seat cushions has been characterized. By designing turn-key open-cell structures on CAD software, 3D printing them with flexible TPU material, and benchmarking the printed structures against the original materials, CSEM has built a unique database for next-generation multi-soft-zone body interfaces.

Individually shaped wheelchair seat cushions are commonly used to compensate for asymmetries in the body, provide good comfort and prevent decubitus. The current method to build these seat cushions is to stack multiple materials in various layers to achieve the needed pressure release at the neuralgic danger zones on a seating area that tends to cause skin pressure defects. Our goal is to build up a new modular digital material database for the next-generation seat cushions process, including full digital design and 3D printing, in order to transfer the vast existing analog knowledge on material selection and material combination into a digitally customized patient seat cushion/ device.

Nine materials that are most commonly used to build custom made seat cushions for wheelchair drivers were identified. These elastomer foams range from super soft light porous PUR foams to firmer low-density PE material. The materials have been characterized in the form of test cubes. To measure the material characteristics and resulting sitting dynamics (sitting down and changing sitting position) a down-force interval of 5s has been chosen.

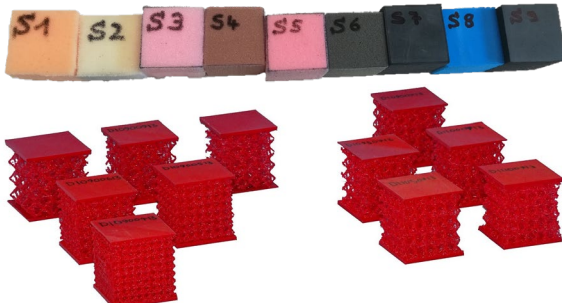


Figure 1: Original material cubes (top), printed lattice test cubes.

Designing and printing cubes with TPU material (shore A80) and different open-celled lattice structures and comparing its characteristic curves with the original material, final changes to the design were made to match the original material characteristics within a range of +/- 5% or (+/- 5N).

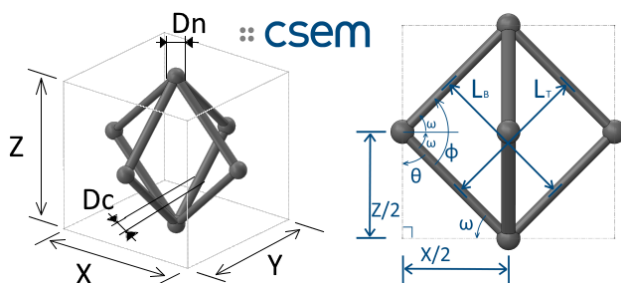


Figure 2: Diamond structure parameters.

\* Swiss Paraplegic Centre SPZ, Nottwil

Changing lattice parameters such as lattice type, lattice core and node diameter, lattice size, the final open-celled cube characteristics could be adjusted.

Most of the examined materials could be reproduced closely with 3D printed lattice structures. Two viscoelastic materials showed very different behavior, which could not be simulated with a lattice structure. Five material structures have been selected as the core set to build the new modular system for printing multiple soft zone devices. These provide enough combination possibilities of stacking different lattice structures to achieve the desired material softness.

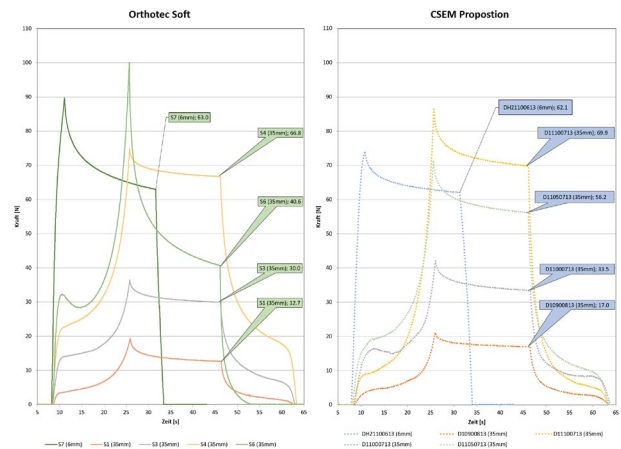


Figure 3: Original material characteristics (left); 3D-printed lattice structure characteristics (right).

Two custom-designed 3D printed seat cushions have been handed over to users and are undergoing a tough user performance test.



Figure 4: 3D printed multi-soft-zone seat cushion in the wheelchair.

# ULTRA-LOW-POWER INTEGRATED SYSTEMS

Alain-Serge Porret

The Ultra-Low-Power (ULP) Integrated Systems program addresses the key challenges and technologies required to build very low power, (often) wirelessly interconnected, embedded smart systems or remote sensing nodes. The availability of such components is central to several global technological trends such as the Internet of Things (IoT) revolution, the advent of wearable technologies for wellness and medical applications (in line with the needs of an aging population), and the generalization of machine-to-machine (M2M) communications required by Industry 4.0.

The IoT is a dramatic extension and generalization of the “wireless sensor networks” approach that CSEM has been promoting since the late 90s. The ultimate goal is to enable the quantification of every piece of useful information captured by a great number of distributed, inexpensive, network-connected, sensor-enabled, computerized devices.

Today's IoT architecture generally mostly relies on fairly “dumb” remote nodes uploading raw data to a centralized processing unit or to the cloud. Distributed sensors (and portable terminals) collect as much data as possible from their environment and dump them in “data lakes” to feed “big data” algorithms. In the process, humongous quantities of raw and mostly useless information is generated, transmitted, stored, and processed, soon to reach yottabyte levels and wasting considerable resources and raising significant privacy-related concerns. This paradigm is also impractical for many industrial and medical applications with high-security or latency constraints.

However, a different model, where information processing occurs upstream, in the sensing node, and only significant events or statistics are communicated, is possible. It emerges more and more as a useful, and in many cases necessary, alternative (“smart edge”). This program focuses on the specialized low-power and/or resource-limited components required to enable

such solutions. It also addresses the needs of many sensors that cannot be physically wired, either because the device is attached to a moving part, is mobile or worn, is implanted, or is not located near a suitable power source, or simply because the wiring required to connect large numbers of remote nodes is costly or impractical. Consequently, such devices:

- Need to be either battery-operated (ideally button batteries lasting years) or rely on harvested energy from their surroundings (toward “zero-battery” devices), leading to a typical power budget in the range of  $10 \mu\text{W}$  (from sub  $\mu\text{W}$  to a few  $100 \mu\text{W}$  range).
- Are required to exchange information wirelessly—since the device is untethered. Wireless transmission of information is energetically very costly, practically  $>10 \text{nJ per bit sent}$  (with overheads), with well above  $1 \text{nJ/bit}$  seemingly being a hard limit for most applications today.
- Should be able to preprocess information locally. Wirelessly transmitting a mean data rate of only  $10 \text{kbit/s}$  (such as for base ECG) costs at a minimum  $100 \mu\text{W}$  of power, and, in practical implementation, likely significantly more. This is larger than the consumption of a commercial medical-grade ECG front end, and much more than the best published research numbers. There are therefore plenty of opportunities to reduce power consumption by using smart local processing to reduce the transmit data rate.

Battery-operated surveillance cameras and keyword spotters illustrate even more clearly these limitations. For such devices, streaming video (respectively sound) continuously is not an option. Only pre-filtered information about detected incidents can be transmitted. This is, of course, only possible if the remote sensing node is equipped with hardware and software components that are sufficiently low-power, yet capable of

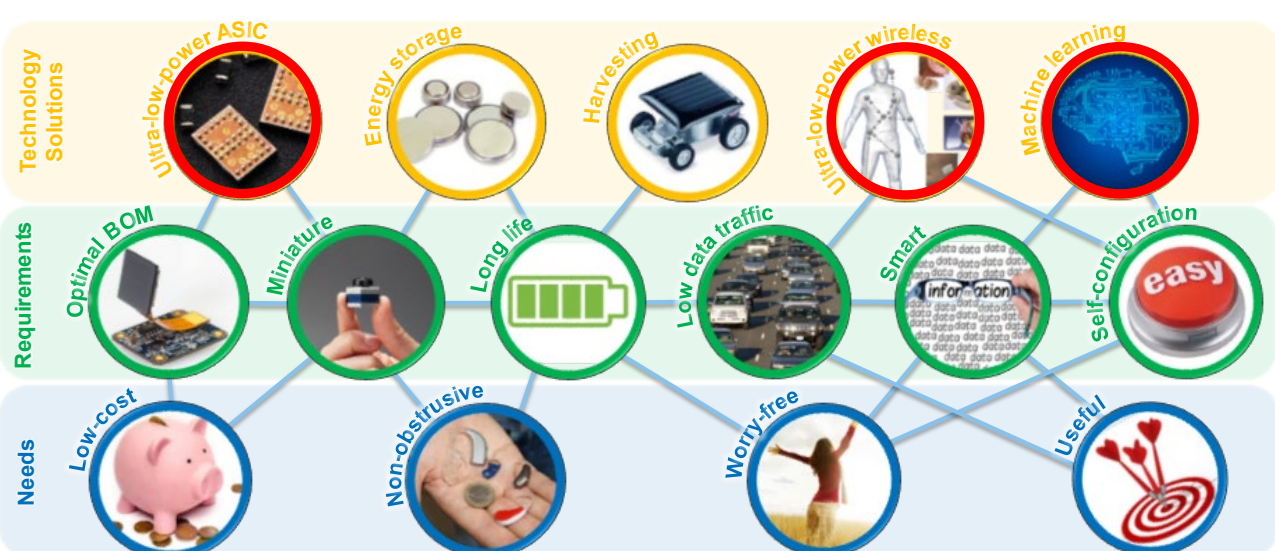


Figure 1: Needs, requirements, and solutions for modern IoT and wearable devices.  
The circles highlighted in red are some of the key challenges covered by the program.

achieving either high levels of data compression or, alternatively, able to understand and classify—at least to a limited extent—the meaning of the collected data. In many practical cases, advanced signal processing techniques are required or even, increasingly, embedded machine learning and artificial intelligence algorithms. Such equipped devices rightly qualify as smart sensors.

### Long-term objectives

This ambitious vision requires significant advances in several fields, ranging from system architectures to hardware devices and algorithms (see Figure 1). It covers energy storage (not studied here, but we rely on the best SoTA devices), energy harvesting sources (investigated in the Photovoltaics and Energy Management program), power management, wireless communications, sensor interfaces, advanced embedded data processing hardware, efficient machine learning algorithms, and resource-limited machine vision.

The markets covered by the program are very diverse, as the generic nature of Figure 1 suggests, and are growing in scope with the continuous development of the Internet of Things. Applications specifically covered by this research program include:

- Consumer electronics (Bluetooth Smart devices, GPS-enabled devices, home automation and security systems, and image processing for occupancy analysis);
- Industrial systems (high-performance sensor interfaces, sensor networks for harsh environments, and optical quality control);
- Metrology (integrated measurement microsystems or optical encoders for various purposes);
- Medical and wellness (implants, vital signs monitoring, and electronic prostheses);
- Automotive (smart sensors in harsh environments, tire monitoring, driver attention monitoring);
- Aeronautics (distributed sensors, touchless man-machine interfaces).

The ULP Integrated Systems program is sub-divided into three research activities. The main areas of attention are indicated below for each.

**Wireless Systems:** (1) Reduction of the effective energy per bit required to send information through a realistic network, with stringent latency, security, robustness, or quality-of-service requirements. (2) Development of high-performance integrated transceivers. (3) Use of electromagnetic waves for ranging, localization and remote sensing (for instance, vital signs monitoring).

**Vision Systems:** (1) Development of very-low-power imagers. (2) Development of machine learning algorithms with a special emphasis on embedded systems. (3) Design of specialized compact smart cameras, inside and outside of the visible spectrum, including multi/hyper-spectral capabilities. (4) 1D to 6D accurate position measurement through optical means.

**System-on-Chip:** (1) Mastering of extremely low power (ELP) subthreshold logic design techniques. (2) Design of ELP mixed-signal sensing interfaces, with an emphasis on vital sign monitoring and timing devices. (3) Dedicated architectures

suitable for ELP logic, including multi-core processors and dedicated accelerators, for example for artificial intelligence inference. (4) Design of the supporting power management circuits.

### Highlights

Improving computing efficiency is crucial for end nodes operating autonomously at the edge. Such improvements can be achieved via many paths, as illustrated by our research. For instance, the paper “Efficient Un-supervised Neural Network Learning for Image Restoration and Generation” (p. 103) focuses on the huge gains that can be achieved by carefully optimizing machine learning algorithms dedicated to image processing. “Efficient neural vision systems based on convolutional image acquisition” (p. 104) demonstrates the benefits that the preprocessing of images in the optical domain can deliver to machine vision systems. Lastly, dedicated hardware approaches are explored in two papers: “A ULP 22 nm system-on-chip with dual-engine hardware acceleration for edge ML inference” (p. 106) and “An ultra-low-power system-on-chip with adaptive body bias” (p. 107).

Traditionally, embedded systems have optimized their power consumption by relying on simple software architectures based on state machines. As the complexity of device functionality increases and additional flexibility is required, a real-time OS (RTOS) becomes mandatory. CSEM continues to develop its own optimized RTOS, as described in “μ111MP—Porting the μ111 RTOS on dual-core Cortex-A7 processor” (p. 109). The efficiency of the approach was also demonstrated by porting very time-critical communication protocols on the OS, without any material penalty, in “Porting low-power wireless protocols on the μ111 real time operating system” (p. 110). Finally, guaranteeing the security of IoT systems is becoming more and more important. An approach to exposing the gaps in a variety of applications is discussed in “IoT SPAT—Security and privacy analysis toolbox for IoT applications” (p. 111).

Wireless communication is another key feature of the IoT that can easily dominate the energy consumption of sensor nodes. CSEM is exploring the benefits of advanced 22 nm CMOS process geometries, not only for digital processing (see above), but also to build better transceivers. This is illustrated in “Bluetooth Dual Mode transceiver in 22 nm CMOS” (p. 112), where a new generation of radio IP allows a reduction in power consumption by a factor of up to 10. The intrinsic speed of CMOS transistors also potentially makes mmWave applications compatible with ultra-low-power, as shown in “A 60 GHz FMCW RADAR-on-chip front-end integrated in 22 nm CMOS” (p. 113). Concomitantly, the algorithms required to process the signal produced by such a radar are discussed in “A novel joint phase processing algorithm for MIMO sensor imaging” (p. 114).

Finally, special antenna applications are described in two papers: “Multipurpose optically transparent planar high-gain passive antenna” (p. 115) and “High-gain sectorial antenna for localization applications” (p. 116).

# Efficient Un-supervised Neural Network Learning for Image Restoration and Generation

D. Honzátko, S. A. Bigdely, E. Türetken, L. A. Dunbar

Digital images are often degraded by undesired artifacts such as noise or blur, which require image restoration tools to remove or reduce them. Many of these tools are nowadays destined for mobile platforms in practical digital imaging applications and there is an ever-growing need for efficient image restoration and generation techniques. We propose new unsupervised algorithms with improved speed and robustness to various types of degradations including *a priori* unknown ones.

With recent advances in deep learning, image restoration has significantly improved in terms of restoration quality. These results, however, rely on an enormous number of ground truth images, both noisy and clean, for training. Adding realistic noise via simulation is complex, so CSEM has been investigating un-supervised techniques to remove the need of a label data set.

## Image Restoration using Plug-and-Play CNN MAP Denoisers

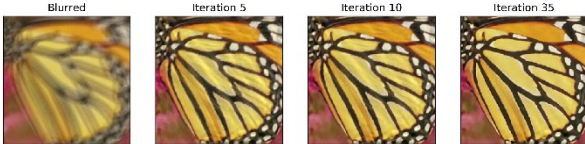


Figure 1: Deblurring iterations of our optimization. Our MAP denoiser network encourages sharp edges and removes undesired artifacts.

Plug-and-play denoisers can be used to perform generic image restoration tasks independent of the degradation type. These methods build on the fact that the Maximum a Posteriori (MAP) optimization can be solved using smaller sub-problems, including a MAP denoising optimization. We present the first end-to-end approach to MAP estimation for image denoising using deep neural networks [1]. We show that our method is guaranteed to minimize the MAP denoising objective, which is then used in an optimization algorithm for generic image restoration. A deblurring example of this optimization process is depicted in Figure 1. As shown on the right, experimental results show that the proposed method can achieve 70x faster performance compared to the state of the art (SOTA) while maintaining the theoretical guarantees of MAP. This brings the method closer to the application in mobile devices.

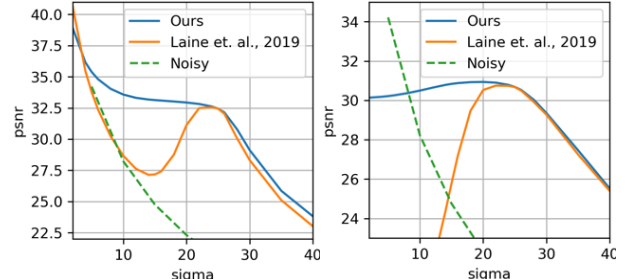
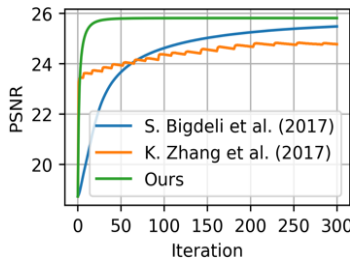


Figure 2: Denoising performance of methods trained with white noise with  $\sigma = 25$  on different test noise variances. Prediction with (left) or and without (right) the knowledge of the noise distribution at inference time.

## Learning Generative Models using Denoising Density Estimators

Learning probabilistic models that can estimate the density of a given set of samples, and generate samples from that density, is one of the fundamental challenges in unsupervised machine learning. We introduce a new generative model based on denoising density estimators (DDEs), which are scalar functions parameterized by neural networks, that are efficiently trained to represent kernel density estimators of the data [3]. Leveraging DDEs, our main contribution is a novel technique to obtain generative models by minimizing the KL-divergence directly. We prove that our algorithm for obtaining generative models is guaranteed to converge to the correct solution. Experimental results demonstrate substantial improvement in density estimation and competitive performance in generative model training. Figure 3 shows that the method is capable of generating realistically looking images.



Figure 3: Results on  $32 \times 32$  images from the CelebA dataset (Liu et al., 2015). (left) generated, (right) real data.

## Summary

In addition to the high accuracy and precision, our techniques have also high computational efficiency. Our method for unsupervised denoising surpasses the SOTA in precision while reducing the computation operations up to a factor of 4. Similarly, our generic image restoration approach improves both speed and precision with respect to other approaches. Finally, we have introduced a new technique in unsupervised density estimation that is significantly more efficient than prior work and can be used as a framework to train generative models.

[1] S. A. Bigdely, et al., "Image Restoration using Plug-and-Play CNN MAP Denoisers", VISAPP (2020).

[2] D. Honzátko, et al., "Efficient Blind-Spot Neural Network Architecture for Image Denoising", 7<sup>th</sup> Swiss Conf. on Data Science (2020).

[3] S. A. Bigdely, G. Lin, T. Portenier, L. A. Dunbar, M. Zwicker, "Learning Generative Models using Denoising Density Estimators", arXiv preprint arXiv:2001.02728 (2020).

# Efficient Neural Vision Systems Based on Convolutional Image Acquisition

P. Pad, S. Narduzzi, C. Kündig, E. Türetken, S. A. Bigdeli, L. A. Dunbar

Despite the recent substantial progress made in deep learning, accuracy, computation time and energy consumption limits the use of this technology in real-time applications on low power and other resource-constrained systems. CSEM has tackled this fundamental challenge by introducing a hybrid optical-digital implementation of a convolutional neural network (CNN) based on engineering the point spread function (PSF) of an optical imaging system.

Practical implementations of convolutional neural networks for vision applications remain in the order of giga multiplication-addition operations (MAdds) despite the significant effort that has been put into lowering this computational cost. This poses a major barrier in many embedded intelligence applications with ultra-low power, small form factor or low-cost requirements which impose strong constraints on the available computational resources to run them in real-time.

Optical systems provide efficient computing capabilities thanks to their inherent parallelism and extremely high speed while effectively consuming no power. Imaging an object through an optical system can be modelled as its convolution with its PSF. Engineering this function has recently become widespread in numerous vision applications such as monocular depth estimation, de-blurring and template matching.

CSEM developed a generic approach for optical convolutions based on amplitude-varying masks to address the challenge of processing incoherent and broadband light that exists in naturally lit scenes. More specifically, we design a compact optical system (Figure 1), made up of an amplitude-only transmittance mask and double lenses, and the ERGO imager [1]. The physical mask is obtained by transcribing the pre-trained weights of a digital convolutional layer onto it such that the PSF function of the optical system closely approximates the convolution kernel. The acquired image is then transmitted to a neural network running on an ultra-low power processor, making the system suitable for real-time embedded inference applications.

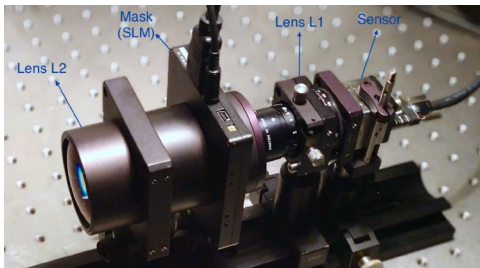


Figure 1: The proposed vision system with a computation-free convolution in optical domain, computation-free activation function in the image sensor, and a processing unit for neural networks.

As a first demonstrator we make an ultra-efficient classification system for the OCR application. We selected the ultra-low power Syntiant NDP101 Neural Decision Processor™ as the processing unit and combined this with the ultra-low power image sensor ERGO. Besides being ultra-low power, the ERGO image sensor enables us to switch between the linear or logarithmic quantization of the pixel values.

In order to obtain the necessary mask pattern, we trained 3 different architectures of the network: a baseline perceptron with

[1] P-F. Ruedi, et al., "An SoC combining a 132 dB QVGA pixel array and a 32b DSP/MCU processor for vision applications", International Solid-State Circuits Conference-Digest of Technical Papers. IEEE (2009).

3 hidden layers, to which we added a large convolutional layer with a kernel size of 240x240, and finally the same network with logarithmic activation after the large convolution to replicate the effect the logarithmic quantization of the ERGO imager. The models were trained on the EMNIST-Digits dataset.

Figure 2 shows the comparison of different techniques on EMNIST-Digits dataset. The accuracy of the baseline model increased from 95.16% to 98.29% by adding the large convolutional layer, which is equivalent to decreasing the error rate by 65% while keeping the computational complexity the same. Afterwards, replacing the linear image sensor quantizer by a logarithmic one, the accuracy further increased to 99.43%. This resulted in 42% decrease of the error rate. It is interesting to note that the computational cost (number of multiplication-addition operations) is reduced by a factor of 250 while the accuracy is decreased only by 0.36% compared to state-of-the-art methods. See the original publication [2] for more experimental results.

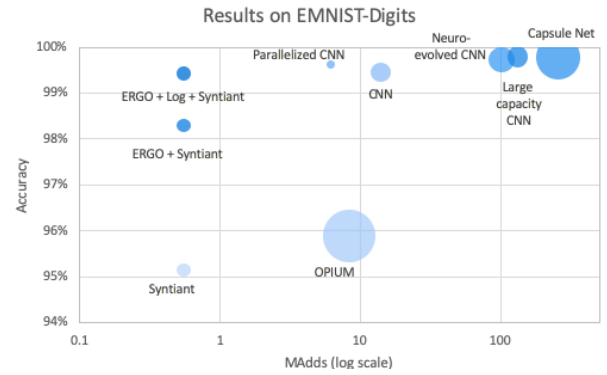


Figure 2: Algorithm performances on the EMNIST-Digits dataset. Our model (ERGO + Log + Syntiant) retains accuracy while significantly reducing the computation power (MAdds).

The similarity of this approach with the extremely efficient mammalian visual system suggests that there is a strong merit in this approach. Both methods record the image in a transformed domain rather than taking raw intensity values. In fact, the idea of recording the scene as a spatial grid of luminosity values, which is how the conventional cameras work, is normally inefficient when the goal is to retrieve high-level information from the scene. That is why in most image processing and computer vision applications the images undergo some transformation (Fourier, wavelets, etc.) to enable efficient processing. The ability to capture the scene in optimal (for each task) transformation domain using optical convolutions, can result in more efficiency of software computation.

In future, this technique can be used to construct efficient vision systems for diverse applications including image compression, depth estimation and presence detection.

[2] P. Pad, et al., "Efficient Neural Vision Systems Based on Convolutional Image Acquisition". IEEE Conference on Computer Vision and Pattern Recognition (CVPR) (2020), 12285-12294.

# AI-based Hand Gesture Recognition System for Improved Human Machine Interaction in Cockpits

H. Sigurthorsdottir, S. A. Bigdeli, S. Saeedi, E. Türetken, L. A. Dunbar

Interest in contact-less Human Computer Interaction (HCI) systems is growing at an accelerated pace due to the recent COVID-19 outbreak. At CSEM, we are developing robust vision-based HCI systems integrated in airplane cockpits and cars. In this study, we present a hand gesture recognition system that achieves 98% accuracy over a diverse set of user participants. The system is comprised of a neural network with convolutional and fully-connected layers that can be run in real-time on low-cost processors with limited computational resources.

With the COVID-19 pandemic, interest in touch-free Human Computer Interaction (HCI), including vision-based hand gesture recognition, has skyrocketed. The worldwide market is expected to grow by a projected US\$ 22.8 billion by 2027 [1] and vision based HCI systems are of particular interest at the moment.

As with many other vision applications, increased accuracy brought by deep learning techniques has recently been a major catalyst for the resurgence of HCI applications. In recent years, interest in HCI has been driven mainly by virtual reality systems, video games, control of robotic systems, and sign language interpretation. These applications are not mission-critical and therefore typically do not require an extremely high-level of accuracy.

At CSEM, we are developing innovative smart vision systems for cockpits in the framework of the CleanSky-sponsored project PEGGASUS \*\*. The goal of which is to create a natural HCI system for pilots to alleviate some of the psychological pressure due to the complexity of modern flight management procedures, tools, and data streams.

When it comes to hand gesture recognition in the cockpit, error tolerance is very low, and security is the priority. Target recognition errors are therefore set below 1%, which is a challenging task for still images that lack temporal information [2].



Figure 1: Depth map (left) and RGB image (right) from the PT1 dataset.

To this end, a hand gesture dataset specifically designed to emulate typical use-cases in the cockpit was collected by the PEGGASUS consortium (hereinafter PT1 dataset). The dataset includes more than 9K sample gestures from 30 subjects, captured by an RGB-D camera (Figure 1). It features five positive static gesture classes, which are selected to be easily

distinguishable as well as a negative class composed of other hand poses usually seen in the cockpit.

We design a convolutional neural network (CNN) that maps its inputs to 6 output classes (5 PT1 gestures and a negative class for irrelevant gestures). The proposed network architecture is illustrated in Figure 2. The network is trained on depth maps only, as RGB images are not reliable in illumination-wise uncontrolled environments such as airplane cockpits.

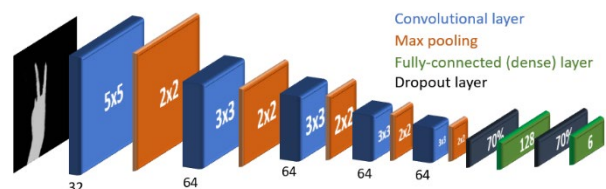


Figure 2: CNN network structure consisting of 5 convolutional blocks with max-pooling layers, and two fully connected layers at the end.

Training the neural network on PT1 led to 65% accuracy due to the relatively small size of this dataset. We therefore looked to transfer-learning to increase this accuracy. To do this first we trained our model on the public EgoGesture dataset [3]. We also resampled the gestures in this dataset to better represent the PT1 distribution. The CNN was benchmarked by hyperparameter-tuning (including the network architecture) on EgoGesture. Data augmentation techniques were used during the training to improve the generalization performance of the model on the PT1 dataset.

The model preformed with 92% accuracy on the EgoGesture validation set and was further fine-tuned on the PT1 dataset to compensate for the differences between the two datasets (camera calibration, capture angle, depth range, etc.). This transfer-learning strategy led to a significant reduction of the errors, bringing the accuracy to 98%.

The trained model will be tested further for robustness on-site in real cockpits. Future directions include incorporating temporal information, embedding the model on edge devices for real-time operation on a low power and computational budget, and using other modalities of sensing such as short-range radars.

[1] R. and M. (n.d.), "Gesture Recognition—Global Market Trajectory & Analytics." Retrieved June 11, 2020, from researchandmarkets.com

[2] B. Liao, et al., "Hand Gesture Recognition with Generalized Hough Transform and DC-CNN Using Realsense", ICIST (2018).

[3] Y. Zhang, et al., "EgoGesture: A New Dataset and Benchmark for Egocentric Hand Gesture Recognition", IEEE TOM (2018).

\*\* This project has received funding from the Clean Sky 2 Joint Undertaking under the European Union's Horizon 2020 research and innovation program under grant agreement No. 821461.



# A ULP 22 nm System-on-Chip with Dual-engine Hardware Acceleration for Edge ML Inference

P. Jokic, E. Azarkhish, R. Catteneo, E. Türetken, V. Moser, P. Nussbaum, S. Emery

Neural network-based object detection algorithms disrupted the field of computer vision, achieving unprecedented detection accuracies in various application domains ranging from large-scale automotive to miniaturized IoT devices. This advance was enabled by the introduction of increasingly deeper and thus more computationally intensive network architectures, challenging the processing hardware. IoT platforms are restricted in size and power, requiring efficient hardware engines to enable on-board processing of such neural network algorithms. We present a system-on-chip, fabricated in an advanced 22 nm CMOS process to provide end-to-end embedded machine learning inference capabilities at the edge.

Smart vision systems provide embedded image analysis capabilities, allowing to implement miniaturized IoT applications for sub-mW face detection as shown in Figure 1. To analyze the acquired images for detecting faces in the field of view, we develop an efficient ultra-low power (ULP) machine learning (ML) inference processor with two ML accelerators.

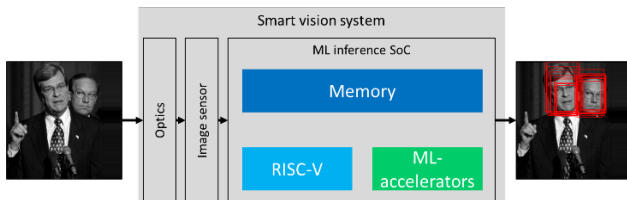


Figure 1: Smart vision system for face detection applications.

The system-on-chip (SoC) is built around CSEM's RISC-V based icyflex-V ecosystem and features 1.2MB of on-chip SRAM memory as well as two ML inference accelerators: one for computing binary decision trees (BDT) and another one for efficiently implementing convolutional neural networks (CNN). A rich set of peripherals allows the SoC to directly connect to an image sensor, allowing to build complete end-to-end solutions without having to add other active components or external memory. The system architecture is illustrated in Figure 2 below.

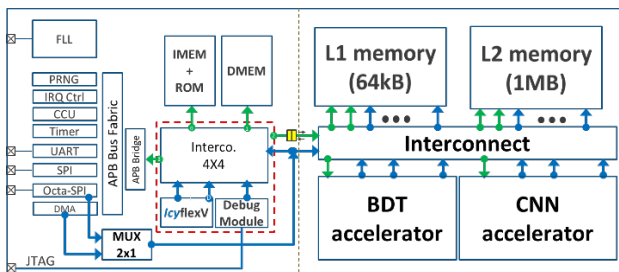


Figure 2: System architecture block diagram.

While CNNs have gained a lot of attention in the last decade, following their success in various object recognition challenges, BDT algorithms have been used for multiple decades. Their simple and scalable computation scheme is based on a cascade of weak classifiers (WC) that allow BDT algorithms to be dynamically adapted (during run-time) to a wide range of algorithmic complexities. Controlling the number of evaluated window positions, the covered range of orientation angles as well as the depth (maximum number of WCs) of the classifier allows to scale both the energy per frame and the analysis accuracy. In the smart vision system use-case this can be exploited by running the BDT algorithm in a low-power setting until a more detailed analysis becomes necessary.

CNNs do not feature such dynamic configurability for trading-off energy per frame versus accuracy but have been shown to tolerate various levels of parameter quantization that enable power reductions by simplifying the processing hardware. Thus,

the CNN accelerator of the presented SoC features multi-precision processing, allowing networks with both 1-bit (binary) or 16-bit precision weights to be computed. Binary weights can reduce the memory footprint by 16x and the dominating multiply-and-accumulate (MAC) operation is simplified to an addition/ subtraction, reducing the energy per operation while allowing larger networks to fit onto the on-chip memory. Each layer can be configured individually, such that networks can consist of layers with different parameter precisions.

The ML inference SoC was fabricated in the GlobalFoundries 22 nm FDX process, enabling a low power consumption at up to 180 MHz clock frequency and a small die area of 3.4mm<sup>2</sup>. Figure 3 below shows the packaged chip with the following main features:

- CSEM icyflex-V core, achieving 3.2 CoreMark/MHz at 2.23 µW/MHz
- Octo-SPI interface with up to 8 parallel data lanes for up to 180 MB/s sensor data transmission
- Dual-accelerator ML cluster (CNN, BDT) reaching a high computational throughput of up to 5.8 GOP/s
- More than 1 MB of shared memory with direct access from the core, the DMA engine and both ML accelerators

The SoC achieves 150 µW average power consumption while running 320x320 pixel face detection at 1 frame per second with more than 98% accuracy. This enables complex ML applications to be implemented in smart IoT devices which are restricted in size and power.

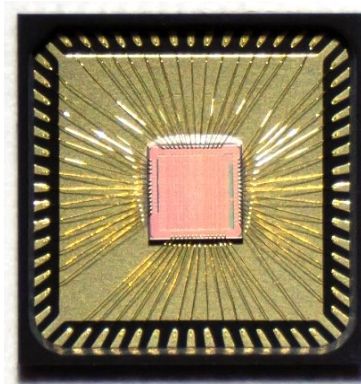


Figure 3: Image of the packaged SoC die.

# An Ultra-low-power System-on-Chip with Adaptive Body Bias

M. Pons Solé, L. Zahnd, Y. Liechti, J.-L. Nagel, V. Moser, E. Azarkhish, R. Cattenoz, T. Mavrogordatos, C. Müller, B. Sporrer, K. Badami, N. Gerber, V. Kopta, E. Pérez Serna, N. Scolari, S. Devise, D. Manic, N. Raemy, S. Emery

The System-on-Chip (SoC) developed is optimized for ultra-low-power applications with increasing battery life constraints. It operates in near-threshold region at 0.6 V and combines user-configurable power management unit (PMU) and bias generator circuits to implement automatic adaptive body bias (ABB) regulation over process, voltage and temperature (PVT) for the icyflex-V core and its memory. It also includes on-chip the icyTRX Bluetooth radio to provide wireless connectivity and ADC/DAC interfaces for sensor applications. Technology used is USJC 55 nm C55DDC which is tailored for low power and body bias control.

ABB mechanism uses transistors body potential as a knob to dynamically control SoC speed and consumption. Reverse bias is used for low-power cases and forward bias is used for high-speed. Figure 1 shows the ultra-low-power SoC implementing ABB. It includes multiple CSEM's designs: 1) icyflex-V [1] (RISC-V based, with 256 kB RAM and 4 kB ROM), 2) icyTRX [2] Bluetooth, 3) low voltage ADC/DAC IPs and 4) PMU and Bias Generator that implement the novel automatic ABB. Thanks to ABB, users can dynamically configure multiple modes of operation of the SoC and control the speed and consumption trade-off. Modes are defined by setting the target clock frequency (e.g. kHz range for Slow mode, MHz range for Fast mode). ABB automatically provides robust operation over PVT for these modes of operation.

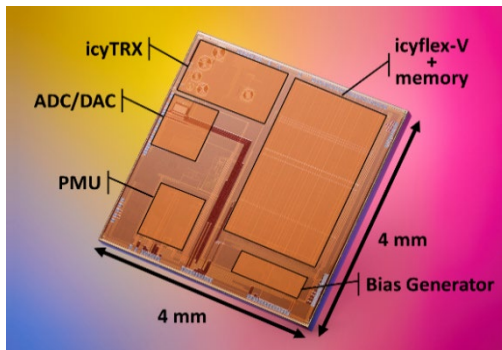


Figure 1: SoC microphotograph.

The different blocks in the SoC can be powered-off using standard power switches and power can also be optimized using ABB. RAM architecture implemented on the SoC is an example of the low-power configurability that can be achieved using ABB. The 256 kB are divided in multiple banks that can be biased independently. When the software requires limited memory, only the minimum size of RAM is active (e.g. configuring Fast or Slow mode) and unused RAM banks are kept in Retention mode. Pushed reverse bias is used for these RAM banks in Retention mode. These banks cannot be accessed but they hold the data and consume as low as 1 pW/bit. Low-power (for Slow and Retention modes) and high-speed (for Fast mode) versions for both PMU and Bias Generator circuits also coexist on-chip. Users can directly select the versions to use or just select the mode of operation (Fast, Slow or Retention mode) and the suitable versions are automatically activated (the others are powered-off for current consumption reduction). Users can also define a frequency target. The Bias Generator circuit will automatically

regulate bias voltages and the clock to ensure functionality over PVT. This Bias Generator circuit is an evolved version from previous works [3] but in this new version a Frequency-Locked Loop circuit (FLL) is used to self-adjust the bias generation and the clock frequency. For that purpose, the FLL includes an oscillator with configurable length that replicates the critical path of the SoC. Mode switching in real-time is supported, allowing the system to adapt to different application phases and obtain optimum consumption results. The SoC can switch for instance from Fast to Slow mode or from Fast to Retention mode and vice versa at any time in the execution of a software. A mode switching specific circuitry takes care of bias voltage continuity over time (avoiding unwanted steps in the bias voltages) and gates the clock while bias voltages are varying (avoiding clock glitches). Figure 2 depicts the SoC's demonstrator. In the application, the SoC is by default in Slow mode (50 kHz setting) and switches to Fast mode (8 MHz setting) using an external trigger (from the Pressure Sensor or the Microphone). Temperature, humidity and current consumption are measured by sensors on-board that are sampled by the on-chip ADC. They are then sent using the icyTRX radio and displayed on a tablet. Power consumption is 10 µA for the Slow mode and 250 µA for the Fast mode. For long periods of inactivity, Retention mode is configured (using pushed reverse bias for the blocks) and consumes 1 µA. In this mode, memories hold the data and SoC clock is gated until the application resumes (for instance, from an external trigger or from an internal timer running on an ultra-low power always-on 32 kHz clock).

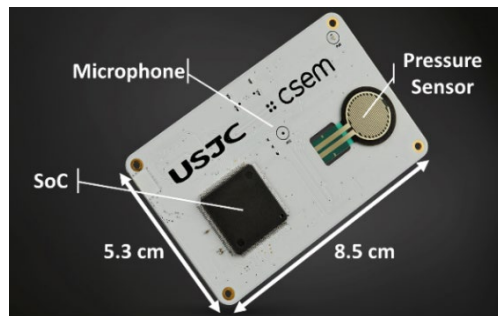


Figure 2: Demonstration board (credit card format).

This ultra-low-power SoC with novel automatic ABB provides robust operation for multiple modes of operation over PVT and can be configured by the user depending on the application needs to obtain best current consumption results. The SoC also provides wireless connectivity and sensor interfaces.

[1] J.-L. Nagel, et al., "icyflex-V-a New Ultra-low-power Processor based on RISC-V Architecture", CSEM Scientific and Technical Report (2019) 116.

[2] V. Peiris, et al., "An Ultra-low-power Bluetooth Smart Integrated Solution", CSEM Scientific and Technical Report (2012) 97.

[3] D. Séverac, et al., "A 0.5 V Near-Threshold Microcontroller Robust over PVT Variations", CSEM Scientific and Technical Report (2017) 142.

# Towards fully Integrated Cooperative Sensors for Vital Signs Monitoring

B. Sporrer, B. Bonnal, K. Badami, J. Wacker, O. Chételat

Cooperative sensors for vital-signs monitoring allow a large number of sensors thanks to their connection to a 2-wire bus used for powering and communication. To keep performance over the shared connection high and keep a sensor node versatile, active circuitry and digital control need to be implemented on each node. In this scenario integrated mixed-signal circuits can provide signal condition, control, and signal transmission, all combined in one package.

The concept of cooperative sensors has been invented and used in various forms and projects within CSEM. The approach aims at avoiding the use of individually connected sensor nodes like commonly found in many biomedical applications such as electrocardiogram (ECG), electroencephalogram (EEG) or bioimpedance measurements. Equipment for these types of measurements usually connect each sensor with at least one individual wire. In many cases this wire must be shielded or even double shielded to bring an unamplified signal to the multi-channel acquisition box. Cooperative sensors on the other hand aim at using a single connection that is shared by all electrodes/ sensor nodes [1].

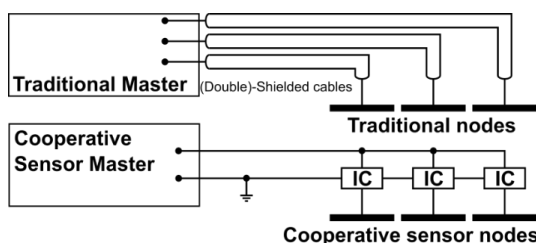


Figure 1: Comparison of vital signs monitoring conventional vs. cooperative approach on example of ECG.

The approach however requires some active circuitry directly placed on each node which, when implemented with discrete components, increases the footprint and the weight of an individual node. The use of an application-specific integrated circuit (ASIC) can counteract this by integrating all required subsystems on the node and therefore minimizing the component count on the sensor. Additionally, the circuits can be optimized for the specific application and reduce the power consumption to the absolute minimum. This can further increase the maximum number of connected channels. For this reason, an ASIC is currently developed for a cooperative sensor system acquiring bioimpedance and sound concurrently. Over the 2-wire bus connection provided to the sensor node the IC has to

- Harvest power to supply the IC operation,
- Synchronize with the system master to allow collision-free communication of data and control, and
- Acquire and pre-amplify the sensed signals with respect to the bus potential.

Figure 2 shows the schematic for the cooperative-sensor node. The supply power is derived from an AC source on the master node with the aid of a rectifier stage. The frequency of the AC supply is chosen not to coincide with any of the signal bands the sensors of the system acquire to avoid crosstalk. The recovered charge is stored on external capacitors that serve as short-term

energy storage. Once the IC is properly synchronized, the harvesting is disabled on predefined time-periods during which one of the nodes can send an acquired analogue value to the master node. The transmission of an analogue sample to the master is a crucial and challenging part of the design. As the system needs to support many nodes multiplexed over a single connection, the time to transmit a single sample needs to be short to keep the sampling rate of individual nodes high and also leave enough time to deliver power to the nodes. Communication of the samples in the analogue domain is done by transferring a controlled charge over the bus. This also releases the IC from the additional task of analogue-to-digital conversion, reducing the power-budget and the complexity of the circuit. The downside of using analogue transmission is the possibility of noise and crosstalk pickup during the process. A clear definition of required dynamic range together with a strategic selection of gain and sampling rate for each application is needed to ensure that transmitter noise stays below the signal's noise floor.

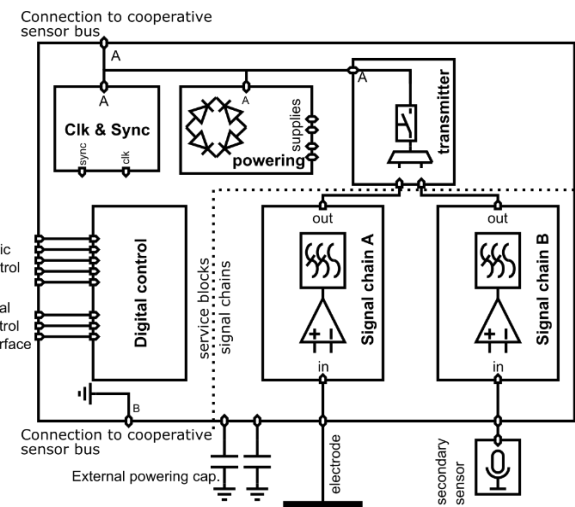


Figure 2: Block diagram of the cooperative-sensing IC.

The IC in Figure 2 contains generic service blocks that are not constrained to a specific application, and signal chains for the electrode and an auxiliary sensor. More than one signal chain can be multiplexed onto the transmit path, which makes the approach very versatile and suitable for a multitude of vital-sign monitoring systems. E.g., the potential from an electrode can be multiplexed with a temperature sensor, a microphone, or other supplementary information.

In summary, the presented IC platform is an important step in the process of developing light weight cooperative-sensor systems that can be adapted to a multitude of different applications for vital-signs monitoring.

[1] M. Rapin, J. Wacker, O. Chételat, "Cooperative sensors: a new wired body-sensor-network approach for wearable biopotential measurement", EAI Endorsed Transactions on Collaborative

# $\mu$ 111MP—Porting the $\mu$ 111 RTOS on Dual-core Cortex-A7 Processor

M. I. Ben Salah, J.-M. Koller, E. Franzi

Multicore processors are common in high-end embedded system/single board computers, often using Linux as their OS. On the other hand, Multicore Real-Time OSes (RTOS) are uncommon. The goal of this exploratory project is to procure an initial insight about the required effort and technical options to adapt our in-house RTOS,  $\mu$ 111, to a multicore processor. The applications of this new kind of RTOS are manifold: Embedded machine learning inference and high reliability processing are typical examples.

The aim of the project is to develop a multicore version of  $\mu$ 111 named  $\mu$ 111MP running on the STM32MP157 processor. The MP157 embeds a dual core Cortex-A7 for high-end processing and a Cortex-M4 for real-time operation. In this project, all the peripherals are controlled by the Cortex-A7 in a symmetric multiprocessor setup (SMP) with instruction cache enabled.

$\mu$ 111 is a CSEM RTOS with dynamic priority processes and a preemptive scheduler. The main operating principles of  $\mu$ 111 are the following (example in Figure 1):

- All the processes move between linked lists depending on their state (not initialized, ready, running, suspended, waiting on a resource).
- When needed the scheduler scans the processes that are suspended and determine if they reached a timeout condition and have a higher priority than the current process. If it is the case, a pre-emption signal is sent to the scheduler.
- Each process has a configurable timeout slot after which the scheduler interrupts the process.
- The scheduler is notified of kernel events (process waiting a specific time, waiting on a specific resource such as. mailboxes, semaphores, etc.) through kernel messages which gives the scheduler information about his call.

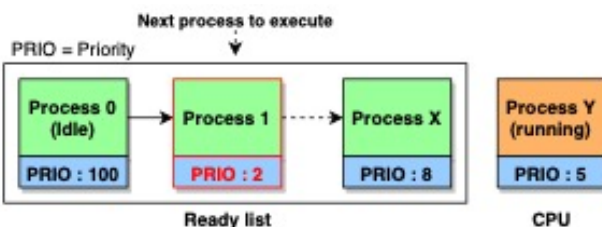


Figure 1:  $\mu$ 111 scheduler selecting next process to run on CPU (lower priority value means higher priority).

The scheduler is split across multiple functions (Figure 2): `sche_chgCxt` handles the scan, moving the processes between the linked-list and the selection of the next process that will be executed. `sche_callbackTrap` analyzes the kernel message to select the linked list on which the scheduler will operate. `temp_testEOTime` checks if any of the suspended processes has reached a timeout. `sche_callbackSlow` wraps arguments to force a preemption when called.

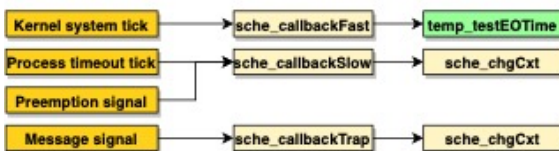


Figure 2: Scheduler call hierarchy.

To provide multiprocessor support the kernel needs to provide inter-CPU locking of shared data structures and consistent shared memory among the CPUs with memory barriers.

**Multicore Scheduling:** To support a multicore execution the kernel has undergone the following changes (example in Figure 3):

- Processes have a parameter defining on which processor they can run (CPU0, CPU1 or both) called affinity.
- Each CPU has a pre-emption signal to reschedule the highest priority process and a specific timeout timer.
- The kernel system tick interrupt can be handled by any CPU.
- The scheduler can run on any CPU and can interrupt both CPU to reschedule new processes.
- When an interrupt that targets both CPUs is raised, only the first CPU to respond will handle it. The second will identify it as a spurious interrupt and resume the interrupted execution.

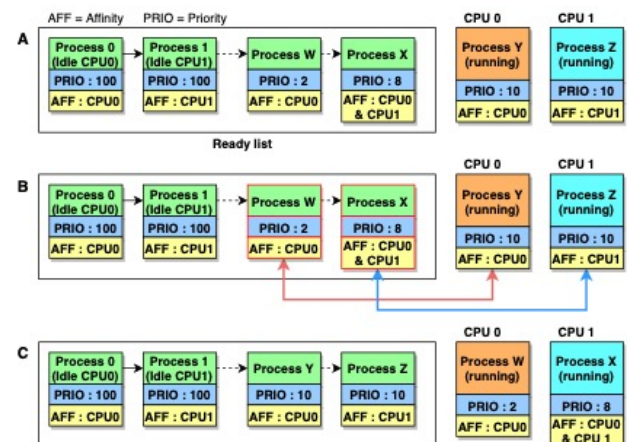


Figure 3: Example of execution of the  $\mu$ 111MP scheduler. A: Scan of the process list that are ready to be run. B: Process W and X are with highest priority and the scheduler will send a pre-emption signal on both CPUs. C: Both CPUs runs the selected processes.

**Supported kernel primitives:** Besides the kernel, a multicore version of  $\mu$ 111 semaphores/mutex has also been implemented and tested. Each kernel primitive will lock the shared global process list when needed, to avoid data races between the CPUs.

**Conclusion & next steps:** The current version of  $\mu$ 111MP is a proof-of-concept which is tightly linked to the SoC architecture, e.g. by using Hardware Semaphore (HSEM) to lock the shared data structures, which introduces high delays due to wait states as it is implemented on another internal bus. The next steps to improve the current implementation are: to enable the data caches and the MMU to handle the cache coherency protocol, to remove HSEM locking and use the ARM specific atomic locking instruction and last but not least to implement a multicore version of the other data structures/services available in  $\mu$ 111 such as mailboxes, signals, memory pool, etc. Another direction of improvement to explore is the development of another kind of schedulers i.e. being cache-aware and using a specific process list per CPU instead of a global process list for both CPUs.

# Porting Low-power Wireless protocols on the μ111 Real-time Operating System

R. Berguerand, L. Bergamini, E. Franzi

With the rapid proliferation of the Internet of Things, the need for low power wireless protocols is expected to grow in the coming years. At the same time, the possibility of running such protocols concurrently with other applications, as made possible by an RTOS (Real-Time Operating System) like μ111, will pave the way to new possibilities in terms of network analysis, machine learning and multitasking, not to mention the ease of porting the protocol from one hardware platform to the other. This work presents a first effort to run two wireless protocols on the μ111 operating system.

Low power wireless protocols have been one of the key enablers for the success of the Internet of Things. Standard solutions, such as Bluetooth Low Energy, are among the market leaders. One of the major reasons for their success is the fact that, apart from being available as standalone solutions running on a custom hardware and firmware, they are well integrated with commercial operating systems (Android OS or OSx, Windows and so on). This is not the case for many existing wireless sensor network protocols, such as the TDMA (Time Division Multiple Access) solutions or CSMA (Carrier Sense Multiple Access)-based WiseMAC [1] protocol, which has been available for many years, but has so far only been available running on dedicated hardware in an OS-less fashion (or with a very trivial OS structure). Recently, CSEM has ported WiseMAC and a novel TDMA protocol also developed by CSEM, to our μ111 RTOS [2]. This solution offers several advantages with respect to the previous OS-less solution, namely:

- Multiple applications can run in parallel on the same processor, enabling both communication and data analysis/decision processes to run at the same time.
- Encapsulation of applications in the OS reduces the risk of fatal errors and improves management.
- Porting from one hardware platform to the other is quicker and safer than in an OS-less environment.

The main challenge with respect to properly porting the WiseMAC and TDMA protocols, was to guarantee that time constraints would be respected, while limiting the usage of radio and CPU for low power operation.

The first step in the porting was to adapt the driver for the radio and the wireless protocols source code to the architecture of the OS, namely the respect of *mutex* (semaphores) to forbid concurrent access to shared resources. The concept of mutex is proper to operating systems: in case a resource is busy, the process is suspended until the resource is released, or if a certain amount of time has passed. The second step was to replace the OS-less scheduler that was formerly used to run the protocols with a scheduler managed by the central OS. To do this, inter-process communication was implemented as depicted in Figure 1. In this case, the process timer updates the software timers periodically (1 ms) using a precise signal (a signal is sent from one process to the other to provide notification of an event, i.e., the passing of 1ms in this case). The process timer informs the protocol of the timeout so that related actions, such as radio

driver commands or protocol functions, can be executed with high time precision.

The first implementation was affected by two issues:

- in the timer process implementation, the CPU could almost never switch to the low power mode, resulting in high power consumption.
- timer resolution was 1ms, so nodes could experience up to a 1ms time shift, which is unacceptable for the TDMA protocol.

Both problems were solved by implementing a new solution using an internal CPU clock that can also run while the processor is asleep and which provides a lower timer resolution of 31 µs, which is acceptable also for the TDMA protocol.

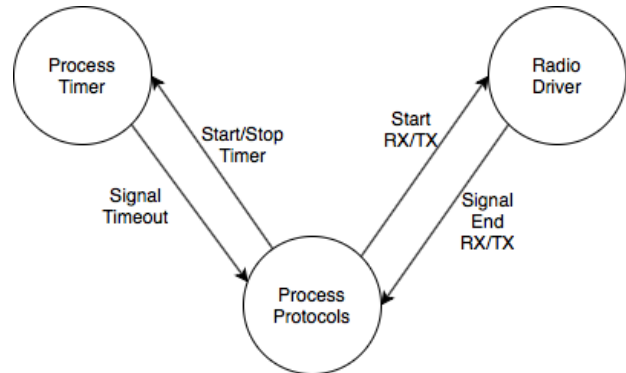


Figure 1: Communication between processes.

To validate the porting of the protocols, preliminary experiments were conducted on a small star-topology network composed of 7 CSEM custom boards featuring an NRF52840 processor. The performance of the protocols, in terms of packet delivery and latency, were found to be comparable to the OS-less version, suggesting that the use of an OS has little to no impact. Ongoing research is focused on measuring the impact on the overall power consumption running the OS vs. the OS-less version of the protocols. The ability to switch from one protocol to the other in real time has also been successfully validated, opening the way to future activities such as the possibility of automatically selecting the more suitable wireless protocol according to traffic conditions among the ones available on the OS. This idea was initially presented in WiseTOP [3], but the use of an OS will allow the implementation of a more advanced traffic analyzer module that will be able to analyze the traffic patterns thanks to machine learning techniques, and automatically switch to the most suitable protocol in real time.

[1] A. El-Hoiydi Amre, J.-D. Decotignie (2004), "WiseMAC: An ultra low power MAC protocol for the downlink of infrastructure", Wireless Sensor networks, International Symposium on Computers and Communications.

[2] E. Franzi (2019), UKOS-III an RTOS for embedded system.

[3] L. Bergamini, J.-D. Decotignie, P. Dallemagne (2018), "WiseTOP: a multimode MAC protocol for wireless implanted devices", 41-50. 10.1145/3273905.3273919.

# IoT SPAT—Security and Privacy Analysis Toolbox for IoT Applications

D. Vizár, A. Olteanu, C. Kassapoglou Faist

Many IoT applications are comprised of low-end interconnected sensors/actuators, accessed remotely through a cloud. This creates a serious problem in terms of security and privacy, with billions of devices being simultaneously highly exposed to attacks, often inadequately secured, with sensitive user data and even personal safety at stake. A key step towards the development of an IoT application with reliable, cost-effective security is a thorough risk analysis. To this end, we design the IoT SPAT, a layman-friendly toolbox for security and privacy analysis of IoT applications.

While enabling new business models and generating value, the typical IoT application paradigm (massive numbers of inexpensive connected Things) also opens a huge opportunity for computer crime with dire consequences (vulnerable self-driving cars, connected toys prone to eavesdropping, health information leakage, traffic light sabotage etc.). At the same time, the applications that apply this IoT paradigm are very diverse in terms of security and privacy requirements, sensitivity of personal information and the quality of the hardware platforms used. Moreover, many IoT products are cost-sensitive, leaving little-to-no margin for security features. While standards, frameworks and recommendations exist concerning how to secure an IoT application (mostly ISO 27k and NIST CSF), applying them is not easy, especially for non-experts; the main obstacles being a high-entry bar in terms of security/privacy expertise, non-specificity to IoT, and/or the amount of effort required. Some frameworks dedicated to IoT applications exist, notably the IoT Security Foundation's (IoT SF) Compliance Framework, which deals with the heterogeneity of security objectives in the IoT through the concept of security classes. While very useful, this framework does not provide any concrete recommendations on how to select the appropriate security class, thus falling short of overcoming all the challenges.

**IoT SPAT.** CSEM has developed the *IoT SPAT*, a toolbox for security and privacy analysis dedicated to the IoT, intended to guide even non-expert analysts through the *complete* process of (1) assessing the risks related to the cyber-security threats to an IoT application and (2) using the results to make an informed selection about the required security and privacy controls for the application. The toolbox consists of (1) a security and privacy analysis method, (2) tools that automatize the most labor-intensive parts of the analysis, (3) a default template with useful assessment data easily adaptable to a variety of IoT applications.

**The method** (see Figure 1) couples a risk assessment following NIST SP 800 30<sup>[1]</sup>, together with the IoT SF Compliance Framework<sup>[2]</sup>, for selection of security and privacy controls. NIST SP 800 30 constitutes a formal backbone of the assessment, providing a well-defined system for risk quantification. For resource effectiveness and layman-friendliness, its use is kept minimalistic with very high-level threat events (such as "damage due to attack on the Thing"). The methodology of "attack trees" is then used to refine the analysis of each threat event, enhancing the resolution and extending the coverage of various attack vectors in an agile, user-friendly way. An attack tree models a high-level threat event as the root of a directed oriented graph, where nodes describe vulnerabilities, attacker actions and other events, such that all nodes on a path from a leaf to the root constitute an attack, and must be executed/materialized in that

order for the attack to succeed. The results of the risk assessment are finally translated into an input to the IoT SF compliance checklist, which generates a list of security and privacy requirements to be implemented.

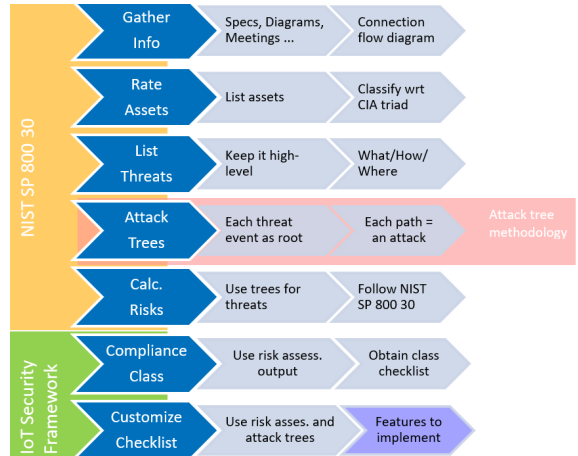


Figure 1: IoT SPAT security and privacy analysis method.

**The tools** accompanying the method are (1) an MS Visio stencil for efficient and visual system modelling, (2) a Python/Graphviz-based tool for creating attack trees, (3) an MS Word template for risk assessment report with embedded instructions, step-by-step and (4) an MS Excel template for risk quantification tables with macros automating most of the work. The attack tree tool turns an attack tree source file into a visual representation of the tree, using a custom syntax, which allows the likelihood of each node to be estimated individually. When the representation is compiled, the tool automatically evaluates the overall success likelihood of the top-level threat event using the individual likelihoods.

**The templates.** To maximize usability by the intended, broad audience, a set of default templates is provided to speed up the analysis process, as well as, to assist potential non-expert users in obtaining meaningful results. The following templates are provided: (1) a sample list of threat sources (aka attackers), (2) a sample list of high-level threat events per (generic) IoT system component, (3) an attack tree per default threat event.

**Conclusion.** The assessment method has been successfully applied to a personal fitness application modelled after Riva Digital, and the in the EU project OffshoreMuster. The experience gained from these two use cases shows that the analysis process with the IoT SPAT is indeed efficient, generates meaningful results and helps gain insight on the overall threat landscape, as well as the weak points, of a given application. The next steps identified are enhancing the template with more real-world data, and integrating the tools under a single UI (e.g. web based).

[1] G. Stoneburner, A. Y. Goguen, A. Feringa, "Sp 800-30. risk management guide for information technology systems" (2002).

[2] A. Abhay Soorya, "IoT Security Compliance Framework" (2019).

# Bluetooth Dual Mode Transceiver in 22 nm CMOS

N. Raemy

The emergence of TWS is driving rapidly increasing demand for low power Bluetooth wireless. CSEM's Bluetooth Dual Mode transceiver provides Bluetooth Classic performance on a Bluetooth Low Energy power budget, offering the possibility of radically increased autonomy, along with enhanced audio streaming quality thanks to its superior link budget and robustness to interferers.

Wireless audio is today the biggest single market for Bluetooth. According to the Bluetooth SIG (Special Interest Group) 1.2 billion Bluetooth audio chips were shipped in 2020. Driven partly by smartphone manufacturers removing the jack plug from latest models, a large part of this growth is coming from True Wireless System (TWS) earbuds, which is estimated today to account for 38% of the headphone market. Furthermore, Apple have announced they would no longer deliver headphones as standard with new I-phones (Android is set to follow), creating a huge opportunity for TWS earbuds: the market is estimated to be 400m units in 2021.

While the demand is clear, TWS is not without its challenges, particularly due to the tiny space available for batteries and electronics. Early models suffered from short playtime, as well as poor audio performance. The race is now on to extend battery lifetime to several hours, as well as improving the user experience with audio enhancements and features such as integrated voice assistants. All these features however consume energy, and wireless is one of the main contributors.

CSEM has developed a Bluetooth Dual-mode (DM) transceiver combining Bluetooth Classic EDR for streaming audio along with Bluetooth Low Energy (BLE) for low power data transfer, as well as for future LE Audio streaming. This transceiver, named IcyTRX-DM, offers game-changing autonomy on a battery cell, an industry-leading budget link for reliable audio streaming and excellent resilience to interferers [1]. IcyTRX-DM uses GlobalFoundries' 22 nm FD-SOI CMOS process which offers extremely low leakage and low supply voltages. Indeed GlobalFoundries (GF) has partnered with CSEM to accelerate the availability of this outstanding silicon IP. CSEM is part of GF's Global Ecosystem of partners, allowing preferred access to engineering support and shuttle runs, as well as marketing promotion via GF's worldwide channels.

While CSEM is already a leading supplier of BLE transceivers, the requirements for ultra-low-power dual-mode operation required significant modifications of the architecture; the use of 22 nm CMOS allows use of a highly digital architecture including an all-digital PLL. Additional innovations include a rapid crystal oscillator to support highly duty-cycled power management schemes, as well as integrated low-drop-out regulators (LDOs) and an enhanced digital interface for support of multiple Bluetooth controller topologies. The radio offers 2Mbps for a flexible audio experience, as well as full BT5.2 compatibility including Long Range (coded S2 & S8) and Direction Finding (DF) BLE options, along with a flexible modem compatible with 802.15.4 2015 and other modulations. BLE only or BT Dual Mode options are available.

A partial test chip was fabricated at the end of 2019 in order to validate critical block functionality, in particular for the new functions, and a full test-chip is now available (see Figure 1).

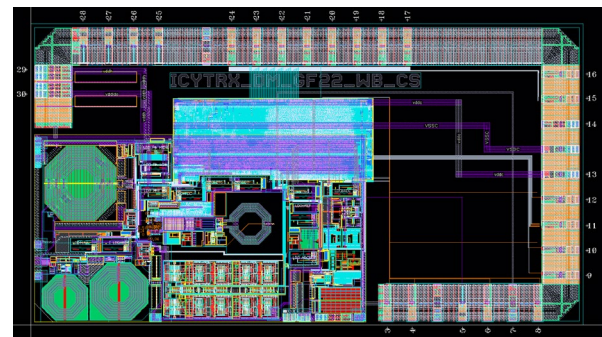


Figure 1: IcyTRX-DM chip.

The radio features a 0.8 V RF core voltage and two power modes: a 0.8 V low-power mode with +3 dBm output power, and a 1.6 V high-power mode up to +10 dBm. A single ended 50Ω RF port with integrated matching means the RF XTAL is the only external component needed. The GFSK transmission modulation spectrum is shown in Figure 2. This plot results from a max hold measurement done on several BLE packets sent at +10 dBm output power with fast ramp-up/down.

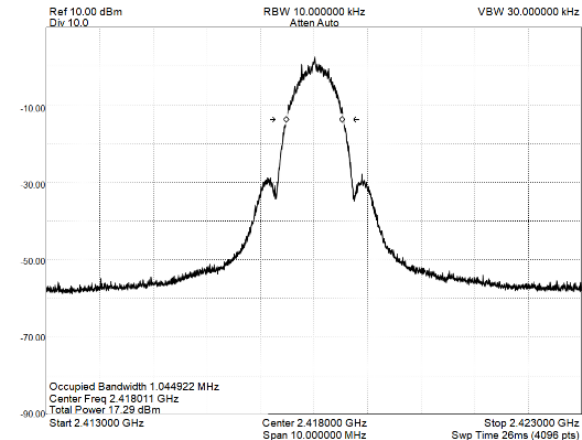


Figure 2: Tx GFSK modulation spectrum.

Lead customer reaction so far has been excellent, confirming the outstanding performance of IcyTRX-DM. Some lead-customers are already looking ahead to next generation products for which additional features are required: certain customers prefer TSMC to GlobalFoundries for their CMOS foundry, and CSEM is planning to introduce a TSMC-22 version later in 2021. In addition, several customers have requested higher output power to allow improved compatibility with streaming audio from mobile phones; while by no means trivial, a modification of the transmitter architecture is being trialed to allow to increase output power by 3-10 dB without degradation of other parameters.

[1] N. Raemy, "Dual-mode Bluetooth Silicon IP in 22 nm CMOS", CSEM Scientific and Technical Report (2019) 108.

# A 60 GHz FMCW RADAR-on-Chip Front-end Integrated in 22 nm CMOS

E. Le Roux, F. Chicco, S. Cerida Rengifo

CSEM is developing a flexible 57-66 GHz FMCW RADAR IP to be integrated into RADAR-on-Chips for low-power miniature MIMO systems targeting portable and/or long-autonomy short-range applications. We describe here a first integration in 22 nm FDSOI CMOS technology of an LO generation associated with 2x Tx & 2x Rx front-ends.

RADARs take advantage of wideband operation for high resolution and good SNR. In the available worldwide license-free bands, two multi-GHz bands can be considered: the 6-8.5 GHz UWB band and the 57-66 GHz band. The UWB band is of interest for low-power operation and easier integration. However, it is more limited with respect to output power, and range resolution. For miniature systems, it is also limited in angular resolution because of the longer wavelength and relative bandwidth that necessitate much larger antennas.

Compared to FMCW, Pulsed-RADARs, are simpler and less sensitive to Tx-to-Rx isolation. They are however limited in average output power because of the high duty-cycle ratio and limited peak voltage associated with integrated technology. Low-power operation also precludes the use of multi GS/s high-dynamic ADCs in Rx: this lowers efficiency because less constrained ADCs are usually associated with distance or dynamic range sweeping, i.e. multiple pulses per range acquisition are needed. FMCW does not suffer from this approach. Additionally, for reduced constraints in terms of energy per acquisition and/or low required acquisition rate, high duty-cycling ratio remains possible [1].

For these reasons, we are integrating a flexible LO generation for operation over the 57-66 GHz band based on an ADPLL. This provides a tunable sweep duration down to 1 ms and a wide closed-loop bandwidth to cope with frequency pulling while maintaining a good sweeping linearity. The LO generation is based on a quadrature DCO swept at carrier frequency in order to minimize Tx silicon surface. Direct quadrature down-conversion is also implemented to minimize Rx silicon surface. A 1-10 MHz chopper is implemented to modulate the transmitted signal in BPSK, in order to eliminate the DC and the DCO-to-Rx leakage, as well as to reduce flicker noise. Different chopper frequencies are used per Tx to separate them on the Rx side by correlation in digital domain.

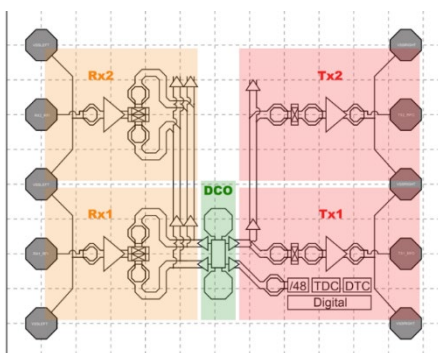


Figure 1: Block diagram of the core.

As illustrated in above Figure 1, 2x Rx & 2x Tx have been integrated to validate a MIMO scheme. The architecture and

layout are scalable: more Tx and Rx slices could be added on the LO distribution paths to address different cost/resolution trade-offs.



Figure 2: 1.25 x 2.5 mm<sup>2</sup> test chip in 22FDX.

Figure 2 above depicts the circuit integrated in a 22 nm FDSOI CMOS from Global Foundry, which offers good performance at 60 GHz and the possibility to also co-integrate powerful and efficient digital processing. LDOs and various RF test structures have also been integrated for characterization. However, the Rx low-IF amplification, filtering and the ADCs are off-chip for the moment. The LO generation has a surface of 0.2 mm<sup>2</sup> and each Rx or Tx has a surface of 0.2 mm<sup>2</sup> including Ø 90 µm 200 µm-pitch pads that are planned for use in characterization via probing, but will also be used in the future for flip-chip assembly.

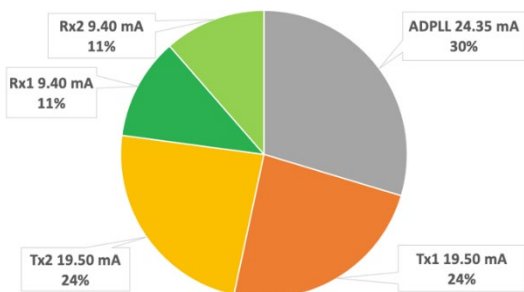


Figure 3: Current consumptions with 0.8 V voltage supply.

For the next integration, we plan to work on reducing the power consumption illustrated in above Figure 3 and completing the system up to ADCs.

[1] Yao-Hong Liu, et al., "A 680 µW Burst-Chirp UWB RADAR transceiver for Vital Sign and Occupancy Sensing up to 15 m distance", ISSCC (2019).

# A Novel Joint Phase Processing Algorithm for MIMO Sensor Imaging

S. Haghishatshoar, J. R. Farserotu, E. Le Roux, P. Dallemande

CSEM is developing a generic MIMO Sensor Imager (MIMOSI) for various sensing applications based on RF mmWave radar technology. Towards this end, we have designed a new joint phase processing algorithm that performs as well as the optimal Doppler FFT for linear phase signals, while overcoming its limitations for nonlinear phase signals arising in a variety of sensing applications.

CSEM develops a generic MIMO Sensor Imager based on RF mmWave radar technology, aiming at covering various sensing applications such as vital signs monitoring, presence detection, see through walls, etc. The approach is to process the phase of the received radar signal across several transmissions to capture the "motion pattern" of subjects and extract relevant information. Phase processing is widely adopted, e.g., in traditional radar Doppler signal processing, to detect moving targets and estimate their velocity (via Doppler FFT). These methods are, however, limited to linear phases (targets moving with a constant radial velocity towards/away from the radar). In the MIMOSI applications, the phase patterns are not linear, which requires new algorithms for joint phase processing under nonlinear priors.

Our numerical simulations show that our new algorithm has almost the same performance as Doppler FFT for linear phases and is able to reliably processes phase at Signal to Noise Ratios (SNRs) that are orders of magnitude lower than the working SNR of per-sample phase processing methods currently in use and described in the literature. As a result, with the new algorithm, we can work with very low signal powers or cover wider ranges.

Joint phase processing extracts the phase signal  $\phi = (\phi[1], \dots, \phi[T])$  from the received signal  $r = (r[1], \dots, r[T])$ , while taking into account the ambiguity of the mapping from  $\phi[n]$  to  $r[n]$ , namely, adding any integer multiple of  $2\pi$  to  $\phi[n]$  yields the same signal  $r[n]$ . This implies that we need additional structure on the phase signal to be able to recover it. [1] shows that the minimal necessary and sufficient condition for the unique recovery of  $\phi$  is given by

$$C: \max_{n \in [T]} |\phi[n] - \phi[n-1]| \leq \pi.$$

Based on this condition, we proposed in [1] a simple per-sample phase recovery algorithm adopted in almost all publicly available real-time demos (especially for vital signs). This algorithm yields a consistent estimation of  $\phi$  at large SNRs when  $\phi$  fulfills condition  $C$ . Although it does not incur any computational delay, it has several crucial drawbacks:

- It is good for high-SNR scenarios (typically larger than 3 dB) such as live demos but not for practical scenarios where SNR can be very low due to low transmit power, low radar cross section of subjects, or their large distance from radar.
- Meeting condition  $C$  typically requires increasing the sampling rate of the signal, thus, using short (low energy) Chirp signals in FMCW radar with lower per-sample SNR.
- This method cannot incorporate the joint structure of the phase signal  $\phi$  such as its periodicity, slow variation, etc.

This motivated us to design a new joint phase processing algorithm, which computes the Likelihood Ratio (LR) function of

the received signal  $r[n]$  in Gaussian noise and constructs the Generalized Likelihood Ratio (GLR) function by computing the maximum of LR with respect to the unknown signal amplitudes. This corresponds to maximizing the following metric

$$\sum_{n \in [T]} g(\phi_r[n] - \phi[n]), \quad \phi \in \Phi, \quad (1)$$

where  $\phi_r[n] = \angle r[n]$ , where  $\Phi$  is the space of all valid phase vectors used as a regularization for joint phase processing, and where  $g$  is a positive function of period  $2\pi$  defined by

$$g(x) = \begin{cases} \sin^2(x), & |x| \leq \frac{\pi}{2}, \\ 1, & \frac{\pi}{2} < |x| \leq \pi, \end{cases} \quad (2)$$

over its single period  $x \in [-\pi, \pi]$ . Depending on our design of the signal transmission in MIMOSI (tuned for specific application), we adopt a suitable convex constraint set  $\Phi$  that allows us to impose on  $\phi$  conditions such as total variation or sparsity in the FFT domain to model its smoothness and periodicity. Unfortunately, even with a convex constraint set  $\Phi$ , the optimization (2) remains nonconvex.

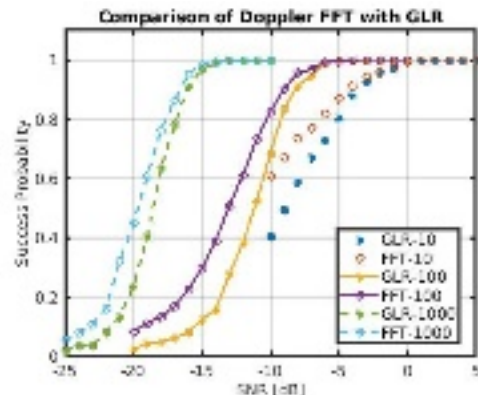


Figure 1: Comparison of Doppler FFT and GLR for different SNR.

Figure 1 illustrates the simulated Doppler FFT with the proposed GLR method for different values of SNR and signal dimensions. In this ideal scenario, phase signal changes linearly and the Doppler FFT is known to be the optimal processing algorithm. Our proposed method has a comparable performance and yields only a minor loss in SNR, especially for large signal dimensions. Also, it processes the phase at very low SNRs (as low as  $-10 \log T$ ), which is almost impossible with the previously adopted per-sample phase processing methods.

Our goal is to extend and use this method for non-linear phase patterns, while keeping efficiency in solving the non-convex optimization problem (2) for the large-dimensional scenarios ( $T \sim 10^3 - 10^5$ ) we may encounter in a variety of sensing applications.

[1] S. Haghishatshoar, J. R. Farserotu, P. Dallemande, "Generic MIMO Sensor Imager: Theoretical Study, Options, and Recommendations", April 2020.

# Multipurpose Optically Transparent Planar High-gain Passive Antenna

A. Vorobyov, P. Dallemande, J. Schleuniger

CSEM designed, prototyped and characterized a high-gain antenna array operating at 2 GHz-5 GHz that is passive and optically semi-transparent. It is used for relaying the RF signal through high attenuation glass structures, while preserving the properties of the glass. The concept uses a semi-transparent conductive material, which is deposited on window glass. It allows for relaying and focusing an RF signal and improving the RF link budget through the window by 7 dB to 10 dB at 2.45 GHz.

The use of a transparent antenna in combination with relatively large unused glass surfaces, such as windows (e.g. on buildings, cars, trains), or even smaller surfaces (e.g. a watch glass or a light bulb) can increase the effective area of the antenna and thus the gain and performance of a wireless device. To this end, CSEM integrates flexible and semi-transparent antennas into devices of all shapes and sizes in order to benefit from unused areas and volumes. This allows for the budget link to be improved, while reducing the impact of the antenna on the device size.

There are several candidate materials suited for making transparent antennas such as spray-on conductive substances or metallic conductive films. Thin film deposition techniques, such as Physical Vapor Deposition (PVD), can be used to produce high conductivity transparent multilayer Transparent Conductive Oxide (TCO), or highly conducting ZnO/silver. This technology, widely used in solar cells, can be employed to develop high performance transparent antennas. Many transparent (physically or electromagnetically) materials, including glass and plastics with curved or flat surfaces, can be processed to integrate an efficient transparent antenna. In addition to improved performance, this technology also offers an increased flexibility in design integration and an efficient use of pre-existing device surfaces.

The transparent antenna solution developed by CSEM is based on the deposition of a conductive layer on a glass window. The antenna can either be completely passive or active when connected to an RF transceiver. It can also comprise several antenna elements assembled into an array. A passive antenna array consists of many small elements distributed so that it forms a beam, increases directivity, etc. For example, the additional directivity and gain provided by forming a beam via a smart window may be used to improve the propagation (link budget of RF signal) inside a building, to relay GPS satellite signals or to drastically improve GSM communications inside the building.

The proposed design serves as a generic basis for developing transparent antennas that may be used for many applications and systems (5G, GPS, GSM, Wi-Fi) operating in various frequency bands:

- Smart buildings (transparent window antenna solutions, PV cell antenna...)
- Automotive (communication, energy harvesting system)
- Security: sensors integrated into the window, e.g. for security and environment monitoring

In the example of Figure 1, the concept is based on the phase gradient of frequency selective surface (right) and an externally placed low gain source antenna ("external antenna"). Circular

shaped elements with a diameter ranging from 1cm to 6cm have been used (Figure 1, left). In real life an external antenna is any antenna built into a portable (e.g. cell phone) or stationary (e.g. WiFi or GSM / LTE routers) devices.

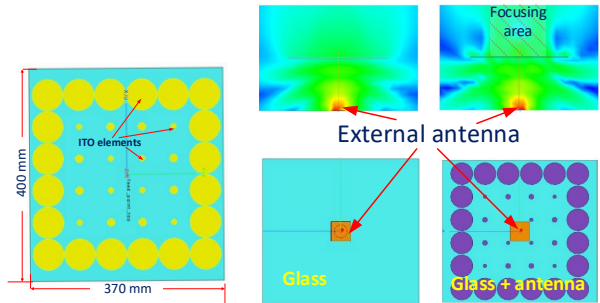


Figure 1: Antenna array theoretical model.

The complexity of the structure (e.g. the number of elements) depends on the application and the required characteristics. All elements are placed on one side of the 3 mm thick glass plate. In this case, the glass plate measures 400 mm by 370 mm. The transparent antennas were designed, manufactured and tested using only CSEM facilities. The measurement results are presented in Figure 2. By comparison with a conventional antenna operating in free space, the passive glass antenna provided an additional 3-4 dB of gain. Considering the losses in the glass and the limitations in the achievable coating thickness, the smart window antenna still increases the gain from 5 dBi to 10 dBi.

A large passive transparent antenna array can potentially improve communication channel budget by up to 15 dB.

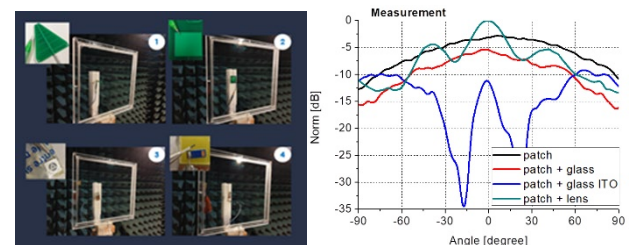


Figure 2: Window antenna characterization with different source antennas (left) and normalized measured antenna gain (right).

The proposed transparent antenna designs leverage and combine the multidisciplinary expertise of CSEM (i.e., antennas, wireless systems, materials) to provide a unique set of mechanical, visual and electro-magnetic properties. The advanced RF antenna can be combined with other aspects (e.g. transparent PV cell antennas) of a smart window, to support multiple functionalities, such as energy-saving, energy harvesting and RF communication.

# High-gain Sectorial Antenna for Localization Applications

A. Vorobyov, C. Hennemann, M. Sénéclauze

This paper presents a new sectorial, high-gain directive antenna operating in the 2.45 GHz band. The purpose of this antenna is to improve the performances of in-door localisation and navigation applications by providing non overlapping reception zones. This antenna was designed to operate indoors and demonstrated very good performances during practical testing. It can be easily optimized for other operational frequencies and applications (e.g. 5G, WiFi, Radio Frequency Identification, radar).

Today, robust indoor positioning is a demanded technology. Monitoring the position of objects is useful to track mobile devices and work equipment, to monitor room occupancy, for logistics, etc. We will focus here only on radio frequency (RF) based methods which, compared to vision-based systems, present the advantage to be independent of lighting conditions.

RF-based indoor localization typically requires two types of RF devices: One affixed to the things to be tracked, and another acting as fixed base stations, the anchors. The system performances of such a system are very dependent of the antenna design, especially on the anchor side.

CSEM has designed and prototyped a high-gain sectorial multi-beam antenna (Figure 1). The antenna is designed to operate at 2.45 GHz with a gain of 10 dBi. This design is based on three optimized high-gain Yagi-Uda antennas, which are geometrically offset by 60 degrees and are excited uniformly through three identical coaxial cables. A standard inexpensive 1.6 mm thick FR-4 substrate has been selected for the antenna prototyping. A metallic reflector placed behind the antennas to improves antenna performance and reduce sidelobe radiation. The final antenna characteristics are summarized in Table 1.

Table 1: High-gain sectorial antenna parameters.

Parameter	Value
Operational frequency [GHz]	2.45
S <sub>11</sub> [dB]	-12 @2.45 GHz
BW [MHz]	250 @-10dB level
Gain (single antenna) [dBi]	~10
Phase center	Common
Dimension (w x l x h) [cm]	34 x 19 x 6

Figure 1 shows one of the basic elements of the antenna (computational model) and the prototyped antenna. The CAD tool used to design and optimize this antenna is HFSS (commercial EM solver from Ansys).

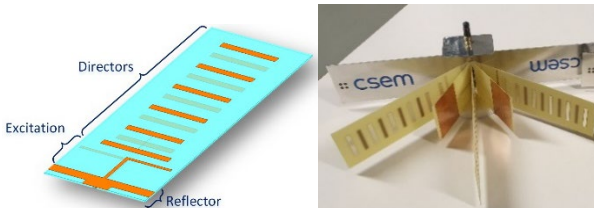


Figure 1: Antenna element model (left) and realized sectorial antenna (right).

The key challenges in such a design are to achieve a common phase reference and a uniform gain of all elements. To meet these challenges, two parasitic elements or back side reflectors were designed and optimized together with the other antenna elements.

Figure 2 shows the simulation and measurement results of the radiation pattern. The gain of the main lobes are about 10 dBi at 2.45 GHz. The left and the right main lobes are tilted at 45 degree

from the central one. Thus, the antenna can monitor three different areas at the same time. The angle between the lobes i can easily be adjusted by shifting the antenna elements position.

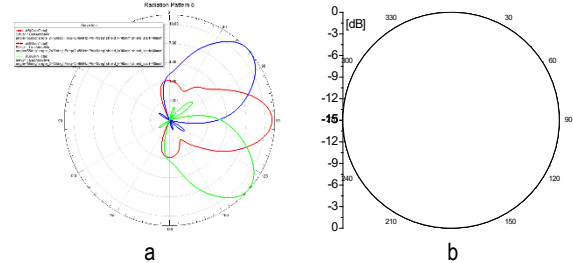


Figure 2: Antenna radiation pattern comparison (@2.45 GHz): HFSS simulation (a) and measured (b).

The sectorial antenna is connected to a Nordic nRF51 DK board Bluetooth evaluation board (EVB) through RF switches. It communicates with an iPad, acting as the monitored thing, and using Bluetooth Low Energy. The EVB measure the received signal strength indication (RSSI) for the three sectorial antenna and transmit them back to the iPad which uses this data to estimate its own position in the room. As shown during a real-time demonstration, a person walking around the room can accurately be monitored between three pre-defined zones (see Figure 3).



Figure 3: Sectorial antenna indoor test @ CSEM showroom.

The proposed antenna solution can be used with different RF-based localisation systems in order to improve their accuracy and robustness. In addition, the antenna can be successfully used in wireless communication systems (e.g. 5G, WiFi.) as a MIMO antenna.

This antenna was developed for Semtech Sàrl as a part of an Innosuisse Project in the field of indoor localisation.

# Dynamic Authorization and Consent in an IoT Ecosystem Dedicated to Healthy Ageing

C. Kassapoglou Faist, D. Vizár

A dynamic authorization framework enabling fine-grained, dynamic access control has been implemented using open-source software and tools. Developed in the context of a large IoT ecosystem for the wellbeing of the elderly, it offers a solution for providing consent, thus enhancing data protection.

The Internet of Things (IoT) has opened tremendous opportunities to enhance the quality of life in a variety of domains. Among others, it offers smart remote monitoring of health indicators, enabling senior citizens to live independently longer at home, with substantial individual and societal benefits. This is the main objective of the H2020 EU Large Scale Pilot project ACTIVAGE, which establishes a European IoT ecosystem extending over nine deployment sites (DS) across the continent, responding to the needs of the elderly, caregivers, service providers and public authorities. In order to realize the ACTIVAGE IoT ecosystem, the project envisions the reuse and scaling up of existing IoT platforms (e.g. frameworks such as Fiware, Sofia, SensiNact, Universaal, openIOT), providing interfaces for interoperability including semantics.

IoT ecosystems present inherent security and privacy risks. In this report, we focus on the implementation of authorization and access control as a security function. The results are twofold: a) a dynamic authorization mechanism has been established, controlling access to the semantic interoperability layer services running above each DS IoT platform in a highly flexible way, and b) the protocols and tools used offer the possibility to a user/data-owner of the platform to manage consents and to control the access rights to his/her private data.

In its essence, the problem is the following. 1) Resources (data, metadata, services, software components etc.) within a distributed environment that are accessible as web applications (an API over HTTPS) must be protected by restricting access. 2) Access rights are determined based on rules (authorization policy, permissions) that may vary in time. Consumers of resources in a distributed environment may be physical persons ("users", using a browser) or other applications ("clients") that act on behalf of a user. Users may be data owners or other requesting parties (e.g. a data analyst).

A typical approach is to place the resources behind Resource Servers (RS - the Policy Enforcement Point-s), and delegate the access decisions to a unique Authorization Server (AS - the Policy Decision Point). Several protocols have been proposed to deal with authorization, often building on the OAuthv2 and OpenID Connect frameworks, which offer identity-based user authentication (log-in), allowing single sign-on through the use of access tokens, signed by the AS and verified by the RS before granting access to a service.

For higher flexibility and scalability, ACTIVAGE targets dynamic authorization, which is characterized by: a) fine-grained rules (best achieved by Attribute-Based Access Control); b) centrally-managed rules (decisions externalized to a single decision point); and c) real-time decisions. The User Managed Access (UMA) protocol by the Kantara Initiative [1] is a good choice to achieve this. UMA distinguishes the roles of the resource owner and the requesting party and it defines an API

dedicated to resource servers (Protection API) for resource registration, permission information retrieval (permission tickets) and token introspection (verification). In addition, it exposes a UMA Grant Token Endpoint to the client, where Requesting Party Tokens (RPT) can be retrieved. Underlying to these interactions is OAuth2, assuring that the RS or the client act on behalf of a person that has been authenticated by the AS.

We used open-source tools to implement this scheme. Specifically, the AS is a Keycloak (KC) server, while the RS is empowered by an Express Gateway (EG) API server [2]. In addition to classic authentication endpoints (e.g. OAuthv2), Keycloak exposes APIs for UMA-compliant authorization services, enabling the protection of resources using ABAC. We used the KC authorization services user interface to specify the ACTIVAGE interoperability layer services as protected resources and define the rules that govern their access (in our example, role attributes were used). On the other hand, benefitting from the ability to customize EG at a very high level, we defined intermediate actions and conditions in the HTTP(S) request/response flows. In this work, we have substantially benefited from open-source software published by the KC and EG communities (Apache2 licenses). Figure 1 depicts the UMA-based authorization workflow being tested in the project.

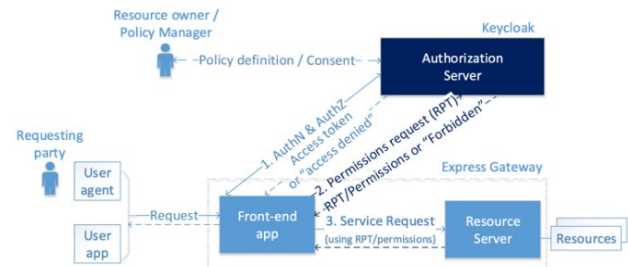


Figure 1: UMA-based dynamic authorization workflow.

Beyond dynamic rules, the UMA workflow and the KC authorization services enable the resource owner to manage fine-grained consent, asynchronously with respect to service runtime. The rules governing the data protection policy of one of the ACTIVAGE deployment sites were defined in KC in order to protect the personal data of the elderly. On top of obvious role-based rules, we added targeted consent in our working example (e.g. a specific user is entitled to see her parent's medical data) and thus test how consent can be enforced, without requiring data owner approval during the service rendering time.

With data protection gaining ever growing importance, this work has enabled us to gain valuable experience using a scalable dynamic authorization framework in an IoT ecosystem. This framework offers a complementary method to cryptographic security that can be applied at most levels of an IoT ecosystem, supporting consent and enhancing data protection.

[1] <https://docs.kantarainitiative.org/uma/wg/rec-oauth-uma-grant-2.0.html>

[2] <https://www.keycloak.org>, <https://www.express-gateway.io/>

# IR-UWB for Precise Ranging and Localization

V. Kopta

The appearance of UWB radios in mobile devices developed by the world's leading manufacturers has opened the door to new applications and business opportunities. CSEM and 3db Access have worked together for more than 7 years on the development of UWB technology for the automotive industry and are now working on a front-end IP that will provide widespread connectivity and compatibility with mobile devices, while assuring state-of-the-art efficiency and low power performance that maximizes the autonomy of battery powered devices.

Ultra-wideband technology (UWB), although present for several decades, came back into focus in the past year. This sudden rise of popularity was fueled by the announcements made by Apple and Samsung that impulse radio (IR) UWB devices will be used in their new smartphones. The key feature of IR-UWB is the capability to provide highly precise distance measurements that could otherwise not be attained with radios commonly found in mobile devices, such as WiFi or Bluetooth. At the moment it is the only technology that can provide secure access (for cars or smart doors and mobile transactions) and enables applications such as personnel tracking in warehouses, augmented reality, or various healthcare and medical applications.

The centimeter-level precision is enabled by extremely short pulses, in the order of 2 ns long, that provide a very fine resolution in time or equivalently, but also result in very large transmitter signal bandwidth ( $> 500$  MHz). The IEEE 802.15.4z standard, released in August 2020, introduced several enhancements to the PHY layer targeting the improvements of integrity, accuracy and security. Two UWB standards are defined today:

- Low-rate pulse UWB PHY (LRP)
- High-rate pulse UWB PHY (HRP)

The HRP is generally more complex and power-hungry but promises higher data-rates and better precision. As such it was adopted for widespread use in smartphones. The high complexity of the HRP is a consequence of the short time between consecutive pulses, which results in inter-pulse interference (IPI) in environments with strong multi-path propagation. Battling the IPI requires heavy digital signal processing and use of specific codes that result in a silicon area that is more than 5 times larger than for similar LRP radios. With the 4 MHz maximum pulse rate of the LRP, typical delay spread of indoor and outdoor channels is shorter than the time between pulses, effectively eliminating the IPI problem and allowing for a significant reduction of power. As a result, the LRP is much more suited for battery powered devices like wearables, key fobs and trackers.

The 7 years long collaboration between CSEM and 3db Access resulted in the first industrial LRP UWB solution that operates in the 6-9 GHz band. The 3DB6830 is currently on the market, integrated in products for secure keyless car access. It achieves 10-15 times lower peak power consumption than similar HRP solutions from competitors. At the same time, it achieves a link budget of more than 90 dB, assuring a minimum range of 120 m in line-of-sight scenarios and guarantees a precision better than 10 cm<sup>[1]</sup>. Other existing solutions either consume an order of

magnitude more power for the similar performance, or they can only achieve a link budget of less than 80 dB.

Recently, the HRP has been selected as the new standard for devices integrated in smartphones. The choice was made based on the expected performance of HRP and knowing that power consumption is not a limiting factor. To address the new market, collaboration between CSEM and 3db continues through an Innosuisse-supported project. The aim of the project is to develop a novel, dual-mode HRP and LRP compatible solution that provides widespread connectivity to commercial devices, together with long autonomy and secure ranging.

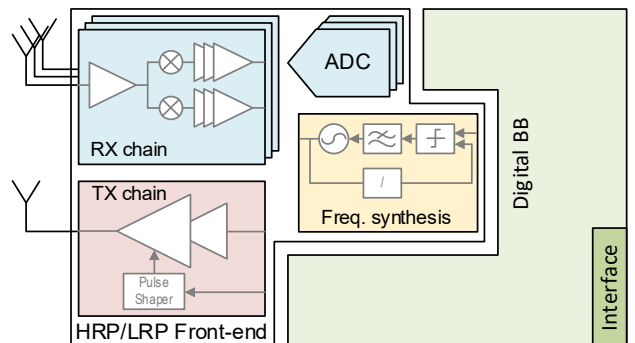


Figure 1: Next generation UWB radio.

The new LRP and HRP compatible RF analog front-end, co-developed by CSEM and 3db, will support different modulations (BPSK, FSK, PPM), channel frequencies, data-rates, and pulse durations. CSEM designed the fast frequency synthesizer, which covers the entire 6-9 GHz band, supports fast frequency switching for the LRP FSK, and provides a coherent, low phase noise carrier signal for the HRP BPSK modulation. The transmitter itself must be able to accommodate a wide range of output power levels, to conform to spectrum limitations and provide a maximum link budget for different pulse rates. A fully integrated solution is targeted, with the quartz crystal and decoupling capacitors being the only needed external components, further reducing the bill of materials, and lowering the price of the product. Integrated, distributed power management will help reduce on-chip coupling and improve performance and consumption of the final product. The TSMC 22 nm technology node has been selected for implementation. The choice is driven by price, reliability as well as performance of the logic circuits needed for the complex combined LRP/HRP digital baseband. To provide support for direction finding and angle of arrival, the future UWB transceiver will contain two or more independent receiver chains. In this way, the targeted transceiver will cover a full range of future applications, while assuring compatibility with a large number of devices.

[1] D. Barras, "Indoor Localization using IR-UWB," CSEM Scientific and Technical Report (2016) 122.

# ANNEXES

## Publications

- [1] R. Abreu, J. Jorge, A. Leal, T. Koenig, P. Figueiredo, "EEG Microstates Predict Concurrent fMRI Dynamic Functional Connectivity States", *Brain Topography*, 34, November 2020, 41-55.
- [2] T. Aderneuer, O. Stefani, O. Fernandez, C. Cajochen, R. Ferrini, "Circadian tuning with metameric white light: Visual and non-visual aspects", *Lighting Research and Technology*, December 2020, 10.1177/1477153520976934.
- [3] G. S. Aglietti, B. Taylor, S. Fellowes, T. Salmon, I. Retat, A. Hall, et al., "The active space debris removal mission RemoveDebris. Part 2: In orbit operations", *Acta Astronautica*, vol. 168, pp. 310-322, Mar 2020.
- [4] D. Ananthanarayanan, J. J. D. Leon, J. Wong, S. Nicolay, A. G. Aberle, J. W. Ho, "Mid-infrared characterization and modelling of transparent conductive oxides", *Solar Energy*, vol. 209, pp. 424-430, Oct 2020.
- [5] M. Auchlin, I. Marozau, D. Z. Bayat, L. Marchand, V. Gass, O. Sereda, "Can automotive MEMS be reliably used in space applications? An assessment method under sequential bi-parameter testing", *Microelectronics Reliability*, vol. 114, p. 7, Nov 2020.
- [6] C. Ballif (2020), "Introduction in Solar Cells and Modules", Ed. A. Shah, *Solar Cells and Modules*, (pp. 1-15), Springer Cham 2020, 10.1007/978-3-030-46487-5.
- [7] M. D. Bassi, L. Benatto, L. Wouk, S. Holakoei, C. K. Oliveira, M. L. M. Rocco, et al., "Correlation between structural and optical characteristics of conjugated copolymers differing by a Si bridge atom", *Physical Chemistry Chemical Physics*, vol. 22 (35), pp. 19923-19931, Sep 2020.
- [8] L. Benatto, M. D. Bassi, L. C. W. de Menezes, L. S. Roman, M. Koehler, "Kinetic model for photoluminescence quenching by selective excitation of D/A blends: implications for charge separation in fullerene and non-fullerene organic solar cells", *Journal of Materials Chemistry C*, vol. 8 (26), pp. 8755-8769, Jul 2020.
- [9] S. Bigdeli, D. Honzatko, S. Susstrunk, L. A. Dunbar, "Image Restoration using Plug-and-Play CNN MAP Denoisers", *Image Restoration using Plug-and-Play CNN MAP Denoisers (Issue)*. Setubal: Scitepress, 2020.
- [10] L. Biggio, I. Kastanis, "Prognostics and Health Management of Industrial Assets: Current Progress and Road Ahead", *Frontiers in Artificial Intelligence*, 3, November 2020, 88.
- [11] E. Borda, L. Ferlauto, J. Schleuniger, A. Mustaccio, F. Lütfi, A. Lücke, S. Fricke, N. Marjanovic, D. Ghezzi, "All-Printed Electrocorticography Array for In Vivo Neural Recordings", *Advanced Engineering Materials*, vol. 22 (3), p. 6, Mar 2020.
- [12] V. Brasch, E. Obrzud, S. Lecomte, T. Herr, "Nonlinear filtering of an optical pulse train using dissipative Kerr solitons," *Optica* 6, 1386-1393 (2019).
- [13] F. Braun, M. Proença, A. Wendler, J. Solà, M. Lemay, J. Thiran, N. Weiler, I. Frerichs, T. Becher, "Noninvasive measurement of stroke volume changes in critically ill patients by means of electrical impedance tomography", *Journal of Clinical Monitoring and Computing*, 34 (5), 903-911.
- [14] F. Braun, C. Verjus, J. Sola, M. Marienfeld, M. Funke-Chambour, J. Krauss, et al., "Evaluation of a Novel Ear Pulse Oximeter: Towards Automated Oxygen Titration in Eyeglass Frames", *Sensors*, vol. 20 (11), p. 11, Jun 2020.
- [15] R. E. Carrillo, M. Leblanc, B. Schubnel, R. Langou, C. Topfel, P. J. Alet, "High-Resolution PV Forecasting from Imperfect Data: A Graph-Based Solution", *Energies*, vol. 13 (21), p. 17, Nov 2020.
- [16] M. Cauz, L. Bloch, C. Rod, L. Perret, C. Ballif, N. Wyrsch, "Benefits of a Diversified Energy Mix for Islanded Systems", *Frontiers in Energy Research*, vol. 8, p. 8, Jul 2020.
- [17] A. Cerreta, R. Gaina, L. Nuccio, I. Marozau, K. Sen, R. D. Prada, et al., "Magneto-transport in La<sub>2</sub>/3Sr<sub>1</sub>/3MnO<sub>3</sub>/YBa<sub>2</sub>Cu<sub>3</sub>O<sub>7</sub>/Alq(3)/Co spin-valves", *Epl*, vol. 129 (3), p. 6, Feb 2020.
- [18] E. Colvill, M. Krieger, P. Bosshard, P. Steinacher, B. A. R. Schnidrig, T. Parkel, et al., "Anthropomorphic phantom for deformable lung and liver CT and MR imaging for radiotherapy", *Physics in Medicine and Biology*, vol. 65 (7), p. 10, Apr 2020.
- [19] M. Dagon, E. Vallat, O. Sereda, J. Gobet, S. Zabihzadeh, F. Marquis Weible, "Nouvelles techniques de contrôle optique de composants en matériaux non-métalliques pour des applications horlogères", *Société Suisse de Chronométrie*, December 2020.

- [20] A. Descoeuilles, J. Horzel, B. Paviet-Salomon, L. L. Senaud, G. Christmann, J. Geissbuhler, et al., "The versatility of passivating carrier-selective silicon thin films for diverse high-efficiency screen-printed heterojunction-based solar cells", *Progress in Photovoltaics*, vol. 28 (6), pp. 569-577, Jun 2020.
- [21] M. Diethelm, L. Penninck, M. Regnat, T. Offermans, B. Zimmermann, C. Kirsch, et al., "Finite element modeling for analysis of electroluminescence and infrared images of thin-film solar cells", *Solar Energy*, vol. 209, pp. 186-193, Oct 2020.
- [22] P. G. Dodds, T. K. Dodds, F. A. Sukachev, D. Zanin, "Arithmetic-Geometric Mean and Related Submajorisation and Norm Inequalities for tau-Measurable Operators: Part II", *Integral Equations and Operator Theory*, vol. 92 (4), p. 60, Jul 2020.
- [23] L. Driencourt, F. Federspiel, D. Kazazis, L. T. Tseng, R. Frantz, Y. Ekinci, et al., "Electrically Tunable Multicolored Filter Using Birefringent Plasmonic Resonators and Liquid Crystals", *ACS Photonics*, vol. 7 (2), pp. 444-453, Feb 2020.
- [24] O. Dupre, A. Tuomiranta, Q. Jeangros, M. Boccard, P.-J. Alet, C. Ballif, "Design Rules to Fully Benefit from Bifaciality in Two-Terminal Perovskite/Silicon Tandem Solar Cells", *IEEE Journal of Photovoltaics*, 10 (3), 9040529, 714-721.
- [25] J. L. Forshaw, G. S. Aglietti, S. Fellowes, T. Salmon, I. Retat, A. Hall, et al., "The active space debris removal mission RemoveDebris. Part 1: From concept to launch", *Acta Astronautica*, vol. 168, pp. 293-309, Mar 2020.
- [26] I. Frerichs, B. Vogt, J. Wacker, R. Paradiso, F. Braun, M. Rapin, et al., "Multimodal remote chest monitoring system with wearable sensors: a validation study in healthy subjects", *Physiological Measurement*, vol. 41 (1), p. 13, Jan 2020.
- [27] B. Gallinet, G. Quaranta, C. Schneider, "Narrowband transmission filters based on resonant waveguide gratings and conformal dielectric-plasmonic coatings", *Advanced Optical Technologies*, November 2020, doi:10.1515/aot-2020-0049.
- [28] Y. Ghamri, M. Proenca, G. Hofmann, P. Renevey, G. Bonnier, F. Braun, et al., "Automated Pulse Oximeter Waveform Analysis to Track Changes in Blood Pressure During Anesthesia Induction: A Proof-of-Concept Study", *Anesthesia and Analgesia*, vol. 130 (5), pp. 1222-1233, May 2020.
- [29] J. S. P. Giraldo, S. Lauwereins, K. Badami, M. Verhelst, "Vocell: A 65-nm Speech-Triggered Wake-Up SoC for 10-mu W Keyword Spotting and Speaker Verification", *IEEE Journal of Solid-State Circuits*, vol. 55 (4), pp. 868-878, Apr 2020.
- [30] F. Grass, B. Pache, F. Butti, J. Sola, D. Hahnloser, N. Demartines, et al., "Fluid management for critical patients undergoing urgent colectomy", *Journal of Evaluation in Clinical Practice*, vol. 26 (1), pp. 109-114, Feb 2020.
- [31] H. Gregory, D. Jean, S. Raoul, B. Guillaume, P. Martin, S. Patrick, "Smartphone-based optical blood pressure monitoring in the acute care setting: Accuracy compared to invasive blood pressure measurement", *Swiss Medical Weekly*, pp. 3S-3S, Oct 2020.
- [32] M. Härmäläinen, L. Mucchi, M. Girod-Genet, T. Paso, J. Farserotu, H. Tanaka, D. Anzai, L. Pierucci, R. Khan, M. Mahtab Alam, P. Dallemande, "ETSI SmartBAN Architecture: The Global Vision for Smart Body Area Networks", *IEEE Access*, 0, 08 2020,
- [33] J. Haschke, G. Christmann, C. Messmer, M. Bivour, M. Boccard, C. Ballif, "Lateral transport in silicon solar cells", *Journal of Applied Physics*, vol. 127 (11), p. 13, Mar 2020.
- [34] S. Holakoei, A. G. Veiga, C. C. Turci, M. F. F. das Neves, L. Wouk, J. P. V. Damasceno, et al., "Conformational and Electron Dynamics Changes Induced by Cooling Treatment on GO:PEDOT:PSS Transparent Electrodes", *Journal of Physical Chemistry C*, vol. 124 (49), pp. 26640-26647, Dec 2020.
- [35] J. Holovsky, S. M. De Nicolas, S. De Wolf, C. Ballif, "Amorphous/Crystalline Silicon Interface Stability: Correlation between Infrared Spectroscopy and Electronic Passivation Properties", *Advanced Materials Interfaces*, vol. 7 (20), p. 7, Oct 2020.
- [36] A. A. Howling, A. Descoeuilles, C. Hollenstein, "Multiple dehydrogenation reactions of negative ions in low pressure silane plasma chemistry", *Plasma Sources Science & Technology*, vol. 29 (10), p. 17, Oct 2020.
- [37] P. Jokic, S. Emery, L. Benini, "Improving Memory Utilization in Convolutional Neural Network Accelerators", *IEEE Embedded Systems Letters (ESL)*, March 2020, 10.1109/LES.2020.3009924.
- [38] S. Karlen, J. Haesler, T. Overstolz, G. Bergonzi, S. Lecomte, "Sealing of MEMS Atomic Vapor Cells Using Cu-Cu Thermocompression Bonding", *Journal of Microelectromechanical Systems*, vol. 29 (1), pp. 95-99, Feb 2020.
- [39] F. Kurth, E. Györvary, S. Heub, D. Ledroit, S. Paoletti, K. Renggli, V. Revol, M. Verhulsel, G. Weder, F. Loizeau (2020), "Organs-on-a-chip engineering", J. Hoeng, D. Bovard, M.C. Peitsch (Eds.), *Organ-on-a-Chip*, (pp. 47-130), Elsevier, 978-0-12-817202-5.

- [40] V. Mitev, N. Torcheboeuf, L. Balet, P. Renevey, M. Krakowski, P. Resneau, *et al.*, "Novel ultra-short light pulse emitters utilizing multiple wide quantum wells", in Novel in-Plane Semiconductor Lasers Xix. vol. 11301 (Issue), A. A. Belyanin and P. M. Smowton, Eds., ed Bellingham: Spie-Int Soc Optical Engineering, 2020.
- [41] V. Mitev, L. Balet, N. Torcheboeuf, P. Renevey, D. L. Boiko, "Discrimination of entangled photon pair from classical photons by de Broglie wavelength", Scientific Reports, vol. 10 (1), p. 9, Apr 2020.
- [42] M. Moncecchi, C. Brivio, S. Mandelli, M. Merlo, "Battery Energy Storage Systems in Microgrids: Modeling and Design Criteria", Energies, vol. 13 (8), p. 18, Apr 2020.
- [43] G. Nardin, C. Dominguez, A. F. Aguilar, L. Anglade, M. Duchemin, D. Schuppisser, *et al.*, "Industrialization of hybrid Si/III-V and translucent planar micro-tracking modules", Progress in Photovoltaics, p. 16.
- [44] J. L. D. Nelis, D. Migliorelli, S. Jafari, S. Generelli, J. Lou-Franco, J. P. Salvador, *et al.*, "The benefits of carbon black, gold and magnetic nanomaterials for point-of-harvest electrochemical quantification of domoic acid", Microchimica Acta, vol. 187 (3), p. 11, Feb 2020.
- [45] E. Obrzud, V. Brasch, T. Voumard, A. Stroganov, M. Geiselmann, F. Wildi, F. Pepe, S. Lecomte, T. Herr, "Visible blue-to-red 10 GHz frequency comb via on-chip triple-sum-frequency generation," Opt. Lett. 44, 5290-5293 (2019).
- [46] D. Ostojic, S. Guglielmini, V. Moser, J. C. Fauchere, H. U. Bucher, D. Bassler, *et al.*, "Reducing False Alarm Rates in Neonatal Intensive Care: A New Machine Learning Approach", in Oxygen Transport to Tissue Xli. vol. 1232 (Issue), P. D. Ryu, J. C. LaManna, D. K. Harrison, and S. S. Lee, Eds., ed Cham: Springer International Publishing Ag, 2020, pp. 285-290.
- [47] T. Portenier, S. Bigdeli, O. Goksel, "GramGAN: Deep 3D Texture Synthesis From 2D Exemplars", June 2020, arXiv:2006.16112v2.
- [48] M. Proenca, F. Braun, M. Lemay, J. Sola, A. Adler, T. Riedel, *et al.*, "Non-invasive pulmonary artery pressure estimation by electrical impedance tomography in a controlled hypoxemia study in healthy subjects", Scientific Reports, vol. 10 (1), p. 8, Dec 2020.
- [49] N. Razek, J. Neves, P. Le Corre, P. F. Ruedi, R. Quaglia, Y. A. R. Dasilva, *et al.*, "Low temperature covalent wafer bonding for X-ray imaging detectors", Japanese Journal of Applied Physics, vol. 59, p. 3, Feb 2020.
- [50] P. Schoettker, J. Degott, G. Hofmann, M. Proenca, G. Bonnier, A. Lemkaddem, *et al.*, "Blood pressure measurements with the OptiBP smartphone app validated against reference auscultatory measurements", Scientific Reports, vol. 10 (1), p. 12, Oct 2020.
- [51] B. Schubnel, R. Carrillo, P.-J. Alet, A. Hutter, "A Hybrid Learning Method for System Identification and Optimal Control", IEEE Transactions on Neural Networks and Learning Systems, 2020, 0.1109/TNNLS.2020.3016906.
- [52] B. Schubnel, R. E. Carrillo, P. Taddeo, L. C. Casals, J. Salom, Y. Stauffer, *et al.*, "State-space models for building control: how deep should you go?", Journal of Building Performance Simulation, vol. 13 (6), pp. 707-719, Nov 2020.
- [53] J. T. Sheridan, R. K. Kostuk, A. F. Gil, Y. Wang, W. Lu, H. Zhong, *et al.*, "Roadmap on holography", Journal of Optics, vol. 22 (12), p. 65, Dec 2020.
- [54] G. A. Soares, T. W. David, H. Anizelli, B. Miranda, J. Rodrigues, P. Lopes, *et al.*, "Outdoor performance of organic photovoltaics at two different locations: A comparison of degradation and the effect of condensation", Journal of Renewable and Sustainable Energy, vol. 12 (6), p. 9, Nov 2020.
- [55] K. R. D. Sousa, L. Benatto, L. Wouk, L. S. Roman, M. Koehler, "Effects of non-halogenated solvent on the main properties of a solution-processed polymeric thin film for photovoltaic applications: a computational study", Physical Chemistry Chemical Physics, vol. 22 (17), pp. 9693-9702, May 2020.
- [56] P. Taddeo, A. Colet, R. E. Carrillo, L. C. Canals, B. Schubnel, Y. Stauffer, *et al.*, "Management and Activation of Energy Flexibility at Building and Market Level: A Residential Case Study", Energies, vol. 13 (5), p. 18, Mar 2020.
- [57] Y. K. Tai, C. Ng, K. Purnamawati, J. L. Y. Yap, J. N. Yin, C. Wong, *et al.*, "Magnetic fields modulate metabolism and gut microbiome in correlation with Pgc-1 alpha expression: Follow-up to an in vitro magnetic mitohormetic study", Faseb Journal, vol. 34 (8), pp. 11143-11167, Aug 2020.
- [58] Y. Tang, K. Petropoulos, F. Kurth, H. Gao, D. Migliorelli, O. Guenat, *et al.*, "Screen-Printed Glucose Sensors Modified with Cellulose Nanocrystals (CNCs) for Cell Culture Monitoring", Biosensors-Basel, vol. 10 (9), p. 17, Sep 2020.
- [59] A.S. Tsagkaris, D. Migliorelli, L. Uttil, D. Filippini, J. Pulkarbova, J. Hajsova, "A microfluidic paper-based analytical device ( $\mu$ PAD) with smartphone readout for chlorpyrifos-oxon screening in human serum", Talanta, 0, 08 2020,

- [60] T. Voumard, T. Wildi, V. Brasch, R. G. Alvarez, G. V. Ogando, T. Herr, "AI-enabled real-time dual-comb molecular fingerprint imaging", *Optics Letters*, vol. 45 (24), pp. 6583-6586, Dec 2020.
- [61] N. Vukovic, J. Radovanovic, V. Milanovic, D. L. Boiko, "Numerical study of Risken-Nummedal-Graham-Haken instability in mid-infrared Fabry-Perot quantum cascade lasers", *Optical and Quantum Electronics*, vol. 52 (2), p. 12, Jan 2020.
- [62] W. L. Weng, R. Bouchand, E. Lucas, E. Obrzud, T. Herr, T. J. Kippenberg, "Heteronuclear soliton molecules in optical microresonators", *Nature Communications*, vol. 11 (1), p. 9, May 2020.
- [63] T. Wildi, T. Voumard, V. Brasch, G. Yilmaz, T. Herr, "Photo-acoustic dual-frequency comb spectroscopy", *Nature Communications*, vol. 11 (1), p. 6, Aug 2020.
- [64] W. Wu, W. Lin, S. H. Zhong, B. Paviet-Salomon, M. Despeisse, Q. Jeangros, *et al.*, "Dopant-Free Back-Contacted Silicon Solar Cells with an Efficiency of 22.1%", *Physica Status Solidi-Rapid Research Letters*, vol. 14 (4), p. 5, Apr 2020.
- [65] P. Wyss, J. Stuckelberger, G. Nogay, J. Horzel, Q. Jeangros, I. Mack, *et al.*, "A Mixed-Phase SiO<sub>x</sub> Hole Selective Junction Compatible with High Temperatures Used in Industrial Solar Cell Manufacturing", *IEEE Journal of Photovoltaics*, vol. 10 (5), pp. 1262-1269, Sept 2020.
- [66] G. Yilmaz, M. Rapin, D. Pessoa, B. M. Rocha, A. M. de Sousa, R. Rusconi, *et al.*, "A Wearable Stethoscope for Long-Term Ambulatory Respiratory Health Monitoring", *Sensors*, vol. 20 (18), p. 14, Sep 2020.
- [67] F. Zanella, G. Basset, C. Schneider, A. Luu-Dinh, S. Fricke, A. M. Madrigal, *et al.*, "Microlens testing on back-illuminated image sensors for space applications", *Applied Optics*, vol. 59 (12), pp. 3636-3644, Apr 2020.
- [68] R.A.Z. Razera, D. A. Jacobs, F. Fu, P. Fiala, M. Dussouillez, F. Sahli, T.C.J. Yang, L. Ding, A. Walter, A. F. Feil, H. I. Boudinov, S. Nicolay, C. Ballif, Q. Jeangros, "Instability of p-i-n perovskite solar cells under reverse bias", *Journal of Materials Chemistry A*, vol. 8 (1), pp. 242-250, Jan 2020.
- [69] A. Ziarati, A. Badiei, R. Luque, M. Dadras, T. Burgi, "Visible Light CO<sub>2</sub> Reduction to CH<sub>4</sub> Using Hierarchical Yolk@shell TiO<sub>2</sub>-xHx Modified with Plasmonic Au-Pd Nanoparticles", *Acs Sustainable Chemistry & Engineering*, vol. 8 (9), pp. 3689-3696, Mar 2020.

## Proceedings

- [1] G. Basset, M. Schnieper, "Transparent DOVIDs Optimized for Readability With any Smartphone", *Optical Document Security 2020*, San Francisco (US), February 2020.
- [2] G. Basset, A. Luu-Dinh, C. Schneider, D. Schlup, S. Perrin, W. Fangting, S. Lecler, "Fabrication of arrays of quasi-micro-beads for massively parallel nanojet super-resolution imaging", *SPIE Photonics Europe 2020*, doi.org/10.1117/12.2555994.
- [3] F. Bennet, L. Burr, D. Schmid, V-D. Hodoroaba, "Towards a method for quantitative evaluation of nanoparticles in suspension via microarray printing and SEM analysis", *NanoSAFE*, Grenoble (FR), 16-20 November 2020, OPUS4-51699.
- [4] S. A. Bigdeli, D. Honzátko, S. Süsstrunk, L. A. Dunbar, "Image Restoration using Plug-and-Play CNN MAP Denoisers", *15th International Conference on Computer Vision Theory and Applications - VISAPP*, Valletta (MT), 27-29 February 2020, arXiv:1912.09299v2.
- [5] D. L. Boiko, "One-Picosecond High-Energy Pulses in Edge-Emitting Laser Devices," in *Conference on Lasers and Electro-Optics*, OSA Technical Digest (Optical Society of America, 2020), paper ATH1K.3.
- [6] V. Brasch, E. Obrzud, S. Lecomte, T. Herr, "Nonlinear filtering with dissipative Kerr solitons", *Photonics West*, San Francisco (US), February 2020, *Proceedings of SPIE* Vol. 11266.
- [7] V. Brasch, E. Obrzud, S. Lecomte, T. Herr, "Nonlinear filtering with dissipative Kerr solitons", *IFCS-ISAF 2020*, Online, July 2020.
- [8] F. Braun, P. Theurillat, M. Proen  a, A. Lemkaddem, D. Ferrario, K. De Jaegere, C. M Horvath, C. Roth, A. K. Brill, Mathieu Lemay, S. R. Ott, "Pulse Oximetry at the Wrist During Sleep: Performance, Challenges and Perspectives", *EMBC 2020 - 42nd Annual International Conferences of the IEEE Engineering in Medicine and Biology Society*, Montr  al, Qu  bec (CA), June 2020.

- [9] L. Burr, D. Schmid, S. Cattaneo, S. Generelli, "Hydrophobicity of nanomaterials measurements for risk assessment", 17th International Conference on Nanosciences & Nanotechnologies – NN20, Thessaloniki (GR), July 2020.
- [10] G. Cattaneo, J. Levrat, H. Li, V. Barth, L. Sicot, A. Richter, C. Colletti, F. Rametta, M. Izzi, M. Despeisse, C. Ballif, "Encapsulant Materials for High Reliable Bifacial Heterojunction Glass/Glass Photovoltaic Modules", Conference Record of the IEEE Photovoltaic Specialists Conference, June 2020, 9300702, 1056-1061.
- [11] G. Cattaneo, R. Tratting, G. Eder, Y. Voronko, D. Moor, F. Jamschek, T. Buchsteine, "BIPV products with innovative glass coatings for low glare photovoltaic façades", Advanced Building Skins 2020, Bern (CH), October 2020.
- [12] S. Chin, V. Mitev, D. L. Boiko, "Frequency blue chirp in Fabry-Perot cavity QCL," in Conference on Lasers and Electro-Optics, OSA Technical Digest (Optical Society of America, 2020), paper AW4M.5.
- [13] C. Colletti, C. Gerardi, B. Strahm, A. Richter, D. Munoz, M. Izzi, J. Levrat, C. Ballif, O. Nielsen, B. Hartlin, B. Melzer, M. Tallian, S. Lombardo, M. Balucani, J. Rentsch, "AMPERE: A successful project to regain European PV manufacture competitiveness", Conference Record of the IEEE Photovoltaic Specialists Conference, June 2020-June, 9300997, 389-393.
- [14] R. Cucu, F. Braun, J. Van Zaen, P. Renevey, A. Lemkadem, K. De Jaegere, C. Horvath, C. Roth, A. Brill, M. Lemay, S. Ott, "Limitations of Unobtrusive Detection of Sleep Disordered Breathing using Heart Rate Variability", DGSM 2020, Essen (DE), October 2020.
- [15] L. Driencourt, F. Federspiel, D. Kazazis, L.-T. Tseng, R. Frantz, Y. Ekinci, R. Ferrini, B. Gallinet, "Electrically tunable filter based on plasmonic phase retarder and liquid crystals", Proc. SPIE. 11290, High Contrast Metastructures IX, February 2020.
- [16] F. Emaury, F. Luetolf, G. Basset, B. Rudin, B. Resan, "Robust ultrafast laser with fiber amplification and pulse recompression", Photonics West, San Francisco (US), February 2020, Proceedings of SPIE vol. 11259.
- [17] A. Faraone, R. Delgado-Gonzalo, "Convolutional-Recurrent Neural Networks on Low-Power Wearable Platforms for Cardiac Arrhythmia Detection", 2nd IEEE International Conference on Artificial Intelligence Circuits and Systems (AICAS2020), Genoa (IT), 23-25 March 2020.
- [18] E. Genzoni, F. Braun, J. Van Zaen, P. Renevey, M. Lemay, E. Pruvot, J. M. Vesin, "Challenging the Limitations of Atrial Fibrillation Detection in the Presence of Other Cardiac Arrhythmias", EMBC 2020 - 42nd Annual International Conferences of the IEEE Engineering in Medicine and Biology Society, Montréal, Québec (CA), June 2020.
- [19] D. Honzátko, S. A. Bigdely, E. Türetken, L. A. Dunbar, "Efficient Blind-Spot Neural Network Architecture for Image Denoising", 7th Swiss Conference on Data Science - SDS, Lucerne (CH), June 2020, 59-60.
- [20] J. Jorge, M. Proença, C. Aguet, J. Van Zaen, G. Bonnier, P. Renevey, A. Lemkadem, P. Schoettker, M. Lemay, "Machine learning approaches for improved continuous, non-occlusive arterial pressure monitoring using photoplethysmography", IEEE EMBC, Montreal (CA), July 2020, 910-913.
- [21] L. Kiener, H. Saudan, F. Cosandier, G. Perruchoud, P. Spanoudakis, J. Rouvinet, "Innovative concept for additive manufacturing of compliant mechanisms", Aerospace European Conference - AEC, Bordeaux (FR), 26 February 2020.
- [22] L. Kiener, H. Saudan, F. Cosandier, G. Perruchoud, V. Pejchal, S. Lani, J. Rouvinet, "Additive manufacturing: innovative concepts of compliant mechanisms", Proc. SPIE. 11451, Advances in Optical and Mechanical Technologies for Telescopes and Instrumentation IV, December 2020.
- [23] F. Kurth, L. Driencourt, F. Lütolf, R. Ferrini, S. Generelli, "Plasmonic Structures for Clinical-Scale Exosome Analysis", Miniaturized Systems for Chemistry and Life Sciences ( $\mu$ TAS 2020), online, 4-9 October 2020.
- [24] A. Lachowicz, G. Christmann, C. Allebé, S. Nicolay, C. Ballif, "Copper Electroplated Metallization for Heterojunction Cells with AZO", Conference Record of the IEEE Photovoltaic Specialists Conference, June 2020, 9300897, 258-260.
- [25] A. Lachowicz, G. Christmann, C. Allebé, S. Nicolay, C. Ballif, "Copper Electroplated Grid on CIGS substrates", Conference Record of the IEEE Photovoltaic Specialists Conference, June 2020, 9300957, 261-262.
- [26] A. Lachowicz, G. Andreatta, N. Blondiaux, A. Faes, J. Diaz Leon, "Project AMELIZ: Patterning techniques for copper electroplated metallization on heterojunction cells", European PV Solar Energy Conference & Exhibition, Paris (FR), September 2020.

- [27] D. Luguern, Y. Benezeth, V. Moser, L. A. Dunbar, F. Braun, A. Lemkadem, K. Nakamura, R. Gomez, J. Dubois, "Remote Photoplethysmography Combining Color Channels with SNR Maximization for Respiratory Rate Assessment", 14th International Symposium on Medical Information Communication Technology - ISMICT, Nara (JP), 20-22 May 2020.
- [28] V. Mitev, N. Torcheboeuf, L. Balet, P. Renevey, M. Krakowski, Ph. Resneau, A. Larue, J.-P. Legoe, Y. Robert, E. Vinet, M. Garcia, O. Parillaud, B. Gerard, D. L. Boiko, "Novel ultra-short light pulse emitters utilizing multiple wide quantum wells", Proc. SPIE 11301, Novel In-Plane Semiconductor Lasers XIX, 113010P, San Francisco (US), February 2020.
- [29] E. Ntavelis, A. Romero, I. Kastanis, L. Van Gool, R. Timofte, "SESAME: Semantic Editing of Scenes by Adding, Manipulating or Erasing Objects", 16th European Conference on Computer Vision - ECCV2020, Glasgow (UK), August 2020.
- [30] E. Ntavelis, I. Kastanis, L. Van Gool, R. Timofte, "Same Same but Different: Augmentation of Tiny Industrial Datasets using Generative Adversarial Networks ", 7th Swiss Conference on Data Science - SDS2020, Luzern (CH), 26 June 2020.
- [31] E. Ntavelis, A. Romero, S. Bigdeli, R. Timofte, "AIM 2020 challenge on image extreme inpainting", European Conference on Computer Vision – ECCV (Online), 23-28 August 2020, 716-741.
- [32] E. Obrzud, V. Brasch, T. Voumard, A. Stroganov, M Geiselmann, F Wildi, F. Pepe, S. Lecomte, T. Herr, "Visible blue-to-red 10 GHz frequency comb via on-chip triple-sum-frequency generation", IFCS-ISAF, Online, July 2020.
- [33] P. Pad, S. Narduzzi, C. Kundig, E. Turetken, S. A. Bigdeli, L. A. Dunbar, "Efficient Neural Vision Systems Based on Convolutional Image Acquisition", The IEEE/CVF Conference on Computer Vision and Pattern Recognition – CVPR, Seattle (US), 14-19 06 2020, 12285-12294.
- [34] V. Pejchal, K. Veideeswaran, V. Hoqui, O. Sereda, M. M. Dadras, "Selective Laser Melting of Aluminium Based Metal Matrix Composites Using Powder Blends", Euro PM2020 Virtu@l Congress, 5-7 October 2020, 6.
- [35] T. Portenier, S. Bigdeli, O. Göksel, "GramGAN: Deep 3D Texture Synthesis From 2D Exemplars", Advances in Neural Information Processing Systems 33 (NeurIPS 2020), arXiv:2006.16112v2.
- [36] R. Prasad, G. Yilmaz, O. Chetelat, M. M. Doss, "Detection of S1 and S2 locations in phonocardiogram signals using zero frequency filter", 45th International Conference on Acoustics, Speech, and Signal Processing - ICASSP, Barcelona (ES), 4-8 May 2020.
- [37] G. Quaranta, C. Schneider, B. Gallinet, "Hybrid plasmonic-dielectric resonant waveguide grating for wavelength-selective diffraction", Proc. SPIE. 11289, Photonic and Phononic Properties of Engineered Nanostructures X, February 2020.
- [38] M. Rapin, J. Wacker, D. Ferrario, E. Haenni, S. Dasen, O. Chételat, "ECG-quality assessment of dry-electrode cooperative sensors", MIE2020, L. Pape-Haugaard, C. Lovis, I. Cort Madsen, P. Weber, P. Hostrup Nielsen and P. Scott, Geneva (CH), April 2020.
- [39] J. Rouvinet, A. Ummel, F. Cosandier, D. Nguyen, V. Schaffter, "PULSAR: development of a mirror tile prototype for future large telescopes robotically assembled in space", Proc. SPIE. 11451, Advances in Optical and Mechanical Technologies for Telescopes and Instrumentation IV, August 2020.
- [40] D. Schmid, G. Oravez, P. Cristofolini, L. Burr, F. Kurth, S. Cattaneo, "Low-cost, versatile colorimetric reader for reactivity assessment of nanomaterials", 17th International Conference on Nanosciences & Nanotechnologies – NN20, Thessaloniki (GR), 7-10 July 2020.
- [41] C. Segarra, R. Delgado-Gonzalo, V. Schiavoni, "MQT-TZ: Secure MQTT Broker for Biomedical Signal Processing on the Edge", 30th Medical Informatics Europe Conference 2020 (MIE2020), Geneva (CH), 28-01 May 2020.
- [42] A. Tuomiranta, J. Cattin, J. Levrat, H. Colin, F. Rametta, O. Dupre, M. Boccard, V. Barth, A. Richter, D. Munoz, C. Colletti, M. Izzi, A. Faes, M. Despeisse, P.-J. Alet, C. Ballif, H. Ghedira, "Comparative Field Performance Assessment of Bifacial Solar Modules", Conference Record of the IEEE Photovoltaic Specialists Conference (2020), 9300612, 1033-1034.
- [43] A. Ummel, G. Perruchoud, P. Schwab, M. Gumy, J. Rouvinet, L. Kiener, "Focus mechanism for EXOMARS mission: lessons learned from preliminary design to space flight model delivery", Proc. SPIE. 11443, Space Telescopes and Instrumentation 2020: Optical, Infrared, and Millimeter Wave, December 2020.

- [44] G. Yilmaz, P. Starkov, M. Crettaz, J. Wacker, O. Chételat, "A Low-Cost USB-Compatible Electronic Stethoscope Unit for Multi-channel Lung Sound Acquisition", XV Mediterranean Conference on Medical and Biological Engineering and Computing – MEDICON 2019, Coimbra (PT), 2020, 1299-1303.
- [45] V. Zubkovs, G. Orawez, E. Rutz, L. Burr, A. A. Boghossian, S. Cattaneo, "Bio-inspired optical sensors for continuous glucose monitoring", 7th Conference Graubünden Forscht, online (CH), 23-24 September 2020.
- [46] V. Zubkovs, G. Orawez, I. Stergiou, A. A. Boghossian, S. Cattaneo, "Optical single-walled carbon nanotube-based bio-sensor for glucose monitoring", Biomedical Photonics Network Meeting, online (CH), 11 December 2020.
- [47] V. Zubkovs, G. Orawez, I. Stergiou, A. A. Boghossian, S. Cattaneo, "Optical sensor for glucose monitoring in cell cultures", Swiss Symposium in Point-of-Care Diagnostics, online (CH), 29 October 2020.

## Conferences and Workshops

G. A. L. Andreatta, A. Lachowicz, N. Blondiaux, A. Faes, C. Allebé, R. Pugin, M. Deispesche, C. Ballif, "Patterns for metallization using self-assembled monolayers", CONFERENCE SAOG 2020, Fribourg (CH), January 2020.

L. Biggio, M. A. Chao, O. Fink, "Uncertainty-aware Remaining Useful Life predictors", Workshop on machine learning for engineering modeling, simulation and design - NeurIPS 2020, December 2020.

L. Biggio, T. Bendinelli, A. Lucchi, G. Parascandolo, "A Seq2Seq approach to Symbolic Regression", 4th Knowledge Representation and Reasoning Meets Machine Learning Workshop (KR2ML 2020), at NeurIPS 2020, December 2020.

C. Brivio, R. E. Carrillo, P.-J. Alet, A. Hutter, "Bestimator™: a novel model-based algorithm for robust estimation of battery SoC", 2020 International Symposium on Power Electronics, Electrical Drives, Automation and Motion (SPEEDAM), Sorrento (IT), June 2020

F. Crivelli, "L'avenir de la fabrication robotisée : Le CSEM, porteur de nouveaux concepts", Le Tout Connecté : la robotique, un levier de compétitivité pour l'économie suisse ?, Delémont (CH), 12 March 2020.

S. Fricke, "Skalierbare Kraft- und Taktilsensoren auf Oberflächen", Neue Anwendungen sensorischer und aktuatorischer Materialien, November 2020.

T. T. Gorecki, W. Martin, "Maestro: A Python library for multi-carrier energy district optimal control design", IFAC World Congress 2020, Berlin (DE), July 2020.

M. Höchemer, T. Schöpe, P. A. E. Schmid, "Qualitätskontrolle mit Deep Learning in der Produktion", Swiss Mechatronics Day 2020, virtual (CH), 1 July 2020.

M. Höchemer, V. Revol, "Industry Grade Lab Automation with AI for Process Control & Predictive Maintenance", Precision Liquid Handling Workshop, Zürich (CH), 15 October 2020.

A. Hutter, "Die Weiterentwicklung der Li-Ionen Batterie", SSM Forum der Technik, 25 May 2020.

A. Hutter, "Les batteries à l'épreuve pratique : résultats actuels de la recherche au CSEM", Journée professionnelle AES - stockage, 3 September 2020.

A. Hutter, "PV self-consumption at its economic optimum - managing heat pumps and electric vehicles", EMPA-PSI-CSEM Technology Briefing -Digital Energy, 11 November 2020.

A. Hutter, "Strategien zur Energieumwandlung auf Quartierebene - Ergebnisse aus dem EU Projekt Pentagon", P2G Expertengespräche, 20 February 2020.

L. Kiener, H. Saudan, F. Cosandier, G. Perruchoud, P. Spanoudakis, J. Rouvinet, "Additive manufacturing: innovative concept of compliant mechanisms", EUSPEN CERN, online, 9 June 2020.

A. Lachowicz, G. Andreatta, N. Blondiaux, A. Faes, C. Allébe, M. Despesse, S. Nicolay, C. Ballif, "Kupfer statt Silber für Solarzellen", 18. Nationale Photovoltaik-Tagung, Lausanne (CH), March 2020.

A. Lachowicz, G. Andreatta, N. Blondiaux, A. Faes, C. Allébe, M. Despesse, S. Nicolay, C. Ballif, "Project AMELIZ: Patterning Techniques for Copper Electroplated Metallization on Heterojunction Cells", 9th Metallization and Interconnection Workshop for Crystalline Solar Cells, Konstanz (DE), October 2020.

D. Luguern, S. Perche, Y. Beneszeth, V. Moser, L. A. Dunbar, F. Braun, A. Lemkaddem, K. Nakamura, R. Gomez, J. Dubois, "An Assessment of Algorithms to Estimate Respiratory Rate from the Remote Photoplethysmogram", The IEEE/CVF Conference on Computer Vision and Pattern Recognition - CVPR, Seattle (US), 14-19 June 2020.

C. Manoli, N. Hendricks, J. Noël, P. Petagna, S. Lani, "Smart Wall Pipes and ducts (SWaP)", Attract Final Conference, online, September 2020.

S. Paoletti, "Innovative diagnostics: sensor solutions for resource-limited settings ", Swiss Symposium in Point of care diagnostics, digital (CH), 29 October 2020.

B. Platerrier, V. Revol, M. Höchemer, "Imagine Talk: How Peter maintains production on track", MSD Symposium, virtual, 14 September 2020.

P. Purwar, M. Höchemer, "Fingerprinting for Industry 4.0", 7th Swiss Conference on Data Science - SDS2020, Luzern (CH), June 2020.

- V. Revol, "CSEM Innovation where technology meets life", Swiss Innovation Forum, Zürich (CH), 18 November 2020
- V. Revol, "Innovative sensor solutions for diagnostics and health monitoring at the point of care", Smart Health, Online (CH), 16 June 2020.
- D. Schmid, "Low-cost, versatile colorimetric reader for reactivity assessment of nanomaterials", Nanotexnology, Thessaloniki (GR), 10 July 2020.
- D. Schmid, "Microfluidic platform for nanomaterials risk assessment", nanoSAFE, Grenoble (FR), 16-20 November 2020.
- D. Schmid, "Smart body sensors", TecDay by SATW Kantonsschule Wohlen, Wohlen (CH), 10 December 2020.
- D. Schmid, "Sustainable technologies for a greener future", OST Coffe Lecture, Buchs SG (CH), 6 October 2020.
- P. A. E. Schmid, A. Steinecker, "Sicherung der Qualität von Produktion und Produkten mit modernen Verfahren der Datenanalyse", microTEC Südwest Clusterkonferenz 2020, Freiburg (DE), 21-22 September 2020.
- P. A. E. Schmid, "Artificial Intelligence - Project LeafEye", Swiss Food Research Innovation Group Meeting - Digitalization Agro-Food, Internet (CH), 18 November 2020.
- P. A. E. Schmid, "Condition Based Maintenance with Deep Learning", 5. F&E-Konferenz zu Industrie 4.0, Zürich (CH), 5 February 2020.
- P. A. E. Schmid, "CSEM – From Space to Industry ", IGLUNA - SWAG SYSTEM, Alpnach (Livestream) (CH), 16 July 2020.
- P. A. E. Schmid, "Datenanalyse für dynamische Wartung und sicheren Anlagenbetrieb", Building Excellence TechOutlook: Energie & Digitalisierung, Internet (CH), 8 April 2020.
- P. A. E. Schmid, "Deep Learning for Industry – from first concept to fully deployed solutions", Roche TIS Forum 2020 - Keynote Lecture, Virtual (CH), 07 September 2020.
- P. A. E. Schmid, "Deep learning keeps Swiss rail network safe", Smart Services Summit (3rd), Internet (CH), 23 October 2020.
- P. A. E. Schmid, E. Schaller, A. Hutter, A. Steinecker, "3 Pitches presenting CSEM Technologies for Building / Energy", Building Excellence - Tech Outlook Event, Rotkreuz (CH), 8 April 2020.

- P. A. E. Schmid, "Künstliche Intelligenz - Revolution im Alltag", SATW TecDay, Wohlen (CH), 10 December 2020.
- P. A. E. Schmid, "Künstliche Intelligenz – Revolution im Alltag", SATW TecJuniors, Landquart (CH), 12 February 2020.
- P. A. E. Schmid, "Künstliche Intelligenz KI – Revolution in der Landwirtschaft?", Jahrestagung der Chartagemeinschaft Digitalisierung: Künstliche Intelligenz – Chance für die Land- und Ernährungswirtschaft, Online (CH), 22 October 2020.
- P. A. E. Schmid, "Neuronales Netzwerk und Deep Learning in der Industrie", Predictive Maintenance, Weinlingen (CH), 3 September 2020.
- P. A. E. Schmid, "Neuronales Netzwerk und Deep Learning in der Industrie", Predictive Maintenance, Weinlingen (CH), 4 September 2020.
- P. A. E. Schmid, "Qualitätskontrolle mit Deep Learning in der Produktion", ETH Fertigungstechnischen Kolloquium: Intelligente Automatisierung in der Produktionstechnik, Zürich (CH), 14 October 2020.
- P. A. E. Schmid, "Referat Industry 4.0 & Machine Learning", HSLU Einführungstage 2020, Rotkreuz (CH), 10 September 2020.
- A. Steinecker, P. A. E. Schmid, M. Höchemer, "Neural Networks - Deep Learning @ CSEM", ANNPR 2020, Winterthur (virtual) (CH), 2-4 September 2020.
- N. Torcheboeuf, V. Mitev, L. Balet, P. Renevey, M. Krakowski, P. Resneau, A. Larrue, J. P. Legoe, Y. Robert, E. Vinet, M. Garcia, O. Parillaud, B. Gerard, D. L. Boiko, "Novel ultra short light pulse emitters utilizing multiple wide quantum wells", European Semiconductor Laser Workshop ESLW 2020, Eindhoven (NL), 4-5 December 2020.
- N. Vukovic, A. Gajic, J. Radovanovic, V. Milanovic, A. Antonov, D. Kuritsyn, V. Vaks, D. Boiko, "Impact of Risken-Nummedal-Graham-Haken Instability on Mid-IR Quantum Cascade Laser Frequency Comb", Photonics Workshop, Kopaonik (RS), 8-12 March 2020.
- V. Zubkovs, G. Oravez, E. Rutz, A. A. Boghossian, S. Cattaneo, "Bio-inspired Optical Sensors for Continuous Glucose Monitoring", Swiss Medtech Day 2020, Bern (CH), 21 September 2020.

## Research Projects

Agroscope	LEAFYE – Development of a hand reader for automatic identification of plant pests
Botnar Research Center for Child Health (BRC)	COVENTE – Improve ventilation safety by means of intra-tracheal pressure monitoring - a short-term and a long-term solution
Botnar Research Center for Child Health (BRC)	DAVINCI – Development and validation of a laminar flow test to detect COVID-19 immunity in saliva
Eurostars	3DBrainScreen – An in vitro 3D brain-on-a-chip model for advanced drug discovery and neurotoxicological assays

Eurostars	AIRSWIM – Airborne instrument for reliable shallow water imaging
Eurostars	COLIDE – Coherent LiDAR demonstration based on a novel swept laser engine in the beyond 2 µm wavelength range
Eurostars	DIAMANT – Direct sensor integration by additive manufacturing technology
Eurostars	EXRIL – Frequency stabilized laser with compact low-cost fiber ferrule based optical reference
Eurostars	FEMTOXIDE – High-power femtosecond laser system based on ytterbium doped sesquioxide crystals
Eurostars	LEVES – Mid-infrared system utilizing LEVEI-crossing chirp-spectroscopy in quantum cascade lasers
Eurostars	MINIHR – A wrist worn wearable device for women for stress detection and management
Eurostars	PREVALE – Preventing anastomotic leakage by developing an anastomotic perfusion measurement device (APM)
Eurostars	SMARTBEAT – ECG system for HRV lifestyle assessment
Interreg	BATHY 3D – Autonomous boat equipped with a LiDAR for precision 3D bathymetry
Interreg	HARISSA – Fabrication de pièces plastiques 3D microstructurées par injection plastiques : applications dentaires, médicales et horlogères
Interreg	INNOSMAD – Maggiore collaborazione trasfrontaliera tra imprese e altri attori dello sviluppo
Interreg	METEOR – Revêtements fonctionnels hautes performances pour composants horlogers, diagnostics et pour l'instrumentation médicale
Interreg	NEODIAM – Développement de nouveaux outils de dépôt de diamant
Interreg	PRODIMED – Développement d'un procédé de revêtement de protection intégrale des dispositifs médicaux
Interreg	SBRA – Smart bra for diagnosing breast cancer
Interreg	V2G STUDY – Vehicle2Grid battery aging study in the frame of RegEnergy project led by Planair
ITER	ITERBOLO – Bolometers prototyping for ITER
SNI – Nanoargovia	DISP-BAT – Development of flow dispersion batteries
SNI – Nanoargovia	PLASPEC – PhD on Plasmonic enhanced photoelectro chemistry
SNI – Nanoargovia	UltraNanoGRACO – Customized, nanostructured grating compressors for high repetition rate ultrafast lasers
SNSF	AMELIZ – Advanced metallization strategies for heterojunction solar cells
SNSF	ASTROTWIN – Dual-comb system for FP calibration used in exoplanet search
SNSF	BIOREACT – Advanced in vitro organ degeneration models for musculo-skeletal research
SNSF	BLUVES – Blue to UV extreme precision astronomical spectroscopy
SNSF	ENHEART – Exploring full content of optical signals to enhance cardiac arrhythmia screening
SNSF	PAPET – Protective, passivating & selective transport layers in perovskite/c-Si tandem solar cells
SNSF	PERSI – Advanced functional perovskites for tandem solar cells
SNSF	PUZZLE – This SNF Ambizione project will develop new brain imaging tools based on ultra-high field (7T) magnetic resonance imaging combined with electroencephalography, to improve the monitoring of human brain structure and function in vivo -- thereby filling critical gaps in the "neuroimaging puzzle"
SNSF	RT-ET – Real-time quality monitoring of engineered tissue for regenerative medicine

SNSF	SALTO – Nitride's semiconductors desposited at low temperatures for photovoltaic
SNSF	SHAMAN – Shadow mask localization of thin films for back-contacted crystalline silicon solar cells & energy harvesters
SNSF / BRIDGE Discovery	FEMTOCHIP – Efficient optical frequency comb generation
SNSF / BRIDGE Discovery	FloCHIP-X – An automated end-to-end microfluidic system for chromatin immunoprecipitation followed by next generation sequencing
SNSF / BRIDGE Discovery	GREENSPACK – Green smart packaging
SNSF / BRIDGE Discovery	POWER – High-performance tandem solar cells with improved stability and cost-competitive manufacturing
SNSF / BRIDGE Discovery	SMARTROBOT – Towards intelligent sensor-enhanced robotic neurosurgery
SNSF / BRIDGE Discovery	VIPS – Ultra-low power visual perception system
Swiss Federal Office of Energy (SFOE)	BAT4SEL – Battery accelerated testing for second life
Swiss Federal Office of Energy (SFOE)	CLEAN-PV – Electrodynamic cleaning for solar pv systems
Swiss Federal Office of Energy (SFOE)	DCSMART – Distribution en courant continu dans les réseaux intelligents
Swiss Federal Office of Energy (SFOE)	HALBION – Half bifacial back-contacted silicon heterojunction solar cells
Swiss Federal Office of Energy (SFOE)	IEA-TASK13 – Performance, operation & reliability of photovoltaic systems
Swiss Federal Office of Energy (SFOE)	OPEN-SESAME – Modelling of energy storages for simulation/optimization of energy systems – open-source energy storage models
Swiss Federal Office of Energy (SFOE)	PAPERWALL – Test and demonstration of new solution for colored PV modules
Swiss Federal Office of Energy (SFOE)	SODA – Solar data analytics for production forecasting and anomaly detection
Swiss Federal Office of Energy (SFOE)	SPET – Flexible Hochleistungskomponenten für die Elektrifizierung von zukünftigen aeronautischen Antriebssystemen basirend auf photoelektrischer Energieerzeugung
Swiss Federal Office of Transport (FOT)	E-HTP – Etude du potentiel de l'hydrogène dans les transports publics
Swiss Food Research	LEAFYE STUDY – Automatic pest detection& classification

## Innosuisse – Swiss Innovation Agency

50041.1 INNO-ENG	4KSIMS	SIM-4KMEMS
47005.1 IP-ICT	ADAPTIVESTORM	An ultra-energy-efficient AI chip for next-gen ICT applications
26245.1 PFLS-LS	AGAT	Automated Goldmann Applanation Tonometer
33572.1 IP-ENG	AMC	Additive Membrane Care
35490.1 IP-ENG	ASYPICK	Fast and robust binpicking for small parts
34738.1 IP-EE	BATMAN	Smart battery management for enhanced balancing and diagnostics of battery cells

29605.1 IP-EE	BESTRADE	Battery energy storage for optimal renewable power trading
37863.1 IP-ENG	BETWEEN	Button with wireless connection for smart crown
18623.1 PFNM-NM	BIOWAVE	Realisation of the BIOWAVE pre-product, a BIOMetric Watch Activated by Veins
27656.1 PFNM-NM	B-SOFT	Beam-shaping optical film technology for LED-based downlights
27049.1 PFES-ES	CBM	Deep learning for condition-based monitoring on railway vehicles
26704.2 PFLS-LS	CERAMIC-TOOTH	Development of a manufacturing solution and surface topography for dental ceramic implant applications, using a novel two-piece implant design
43533.1 IP-ENG	CERANO	Metal oxide thin film deposition is used as a novel sealing process of porous anodized aluminum to increase the durability and corrosion resistance of aluminum components.
35221.1 IP-LS	CEREBRO	ASIC-enabled depth electrodes for neural recording and ablation
38445.1 IP-LS	CHIP-SEQ-CHIP	Automated microfluidic system for standardized and high-throughput chromatin immunoprecipitation (ChIP-sequencing)
50440.1 INNO-ENG	COGI	Compact Gimbal made by additive manufacturing
28345.1 PFNM-NM	CONTACTS	Next generation industrial passivating contacts for high efficiency silicon solar cells manufacturing.
42657.1 IP.ICT	COSIMA	Cooperative sensors for electrographic imaging
38614.1 IP-EE	DAGR	Disruptive innovation in solar energy technologies for building(human) integrated photovoltaic
37705.1 IP-ENG	DALIE	Dry auto-localizing integrated electrodes
33587.1 IP-ICT	DANUBE	High-performance integrated circuits for precise UWB localization
41190.1 IP-ICT	DEEPROFILE	SmartProfile
35855.1 IP-LS	DENOVOCAST	Automated skin tissue formation device
38522.1 IP-LS	DIGITAL-SALIVA	Digital saliva health monitoring device for dental disease prevention with printed biosensors
32348.1 IP-EE	DIPPS	Development of integrated production processes for perovskite/silicon high efficiency photovoltaic
36538.1 IP-LS	DURALOCK	Non-autologous dura substitute with self-sticking properties, a feasibility study
36826.1 INNO-EE	DUSTBUSTER	Dust buster
25365.1 PFNM-NM	EMIRS 2	Development of new infrared light sources for gas detection application.
34950J IP-ENG	ERGO	Ultra-low power image sensor for IoT applications
40657.1 IP-ENG	ESORTER	Vollautomatisches Sortieren von Sendungen bis 30kg stellt nach wie vor eine grosse Herausforderung dar.
43210.1 IP-ICT	FETA	Flexible low-power embedded time series signal accelerator
30156.1 IP-ICT	FINGER-SENSE	Tactile fingertips for service robots
33436.1 IP-ENG	FREE-MLA	Freeform lens and microlens arrays for high-quality lighting systems
31439.1 IP-ENG	FT-MEMS	High accuracy fiber-optic MEMS temperature sensor

41844.1 IP-ICT	GEMTELLIGENCE	Development of software for automated gemstone analysis
41472.1 IP-EE	GIFT	Greenhouse infrared filter technology
25799.2 PFIW-IW	GMD	Predictive maintenance for mill drive power train systems
32074.1 IP-ENG	GOBEYOND	Commercialisation of a breakthrough optical solution in fluorescence imaging for medical diagnostic
25839.2 PFLS-LS	GRAINVIEW	Flow-speed measurement and morphological analysis of food grains
49466.1 INNO-ENG	HEALTH MONITORING TOILET CONCEPT	Health monitoring toilet concept
31841.1 IP-ENG	HEART	High-precision additively manufactured Ti-based active medical device component
29971.1 IP-EE	HELIOS	High efficiency direct and diffused light optimum photovoltaic system
43410.1 IP-ENG	HIHOLO	High quality volume diffraction gratings for digital holography microscopy for enhanced resolution, acceptance angle, and field of view
27655.1 PFNM-NM	HI-NIL	Waveguide-based combiners for augmented reality processed by high refractive index nanoimprint lithography
43539.1 INNO-LS	HomeSTD	Development of urine collection & preparation techniques for use in a rapid, disposable test for chlamydia, gonorrhoea & gonorrhoea resistance
28715.1 IP-LS	HOPE	Hypertension detection through optical blood pressure monitoring in pregnancy by an electronic wearable (HOPE)
49997.1 INNO-ENG	HRFS	High-resolution force sensor
41363.1 IP-LS	IMPLANT	Development of innovative customer-tailored composite multilayers in orthopedic- and trauma surgery
28652.1 IP-ENG	IMPULSE-3DPRINT	Digital printing on 3 dimensional freeform objects
35752.1 IP-ENG	IMPULSE-CLOSEDLOOP	Closed loop manufacturing
35562.1 IP-LS	INFINIPRINT	Multi-material microfluidic printhead for “on-the-fly” formulation for advanced bioprinting
27291.2 PFLS-LS	IN-SITU	Intelligent process control for 3D-bioprinting technology
33074.1 IP-LS	iTooth	An intelligent in-mouth monitoring system for the optimization of dental care
32970.1 IP-ENG	LEADME	Drug screening technology platform based on micro-LED and high resolution MEA
43059.1 IP-ENG	LIFELUB	Development and implementation of a new lubrication technology
35819.1 IP-ENG	LIFI-NED	Light-field near-eye display
35299.1 IP-ENG	LIGHTSAFE	Lightguiding security features
35163.1 IP-ICT	LUBRISAFE	Axino.IoT.LubriSafe – an online quality and safety control system for metal working industry
27435.1 PFNM-NM	MAGNETO	Inspection platform for magnetically oriented optical features
30037.1 IP-EE	MEGAWHITE	New-generation diffuser for industrial production of white PV technology

41268.1 IP-ENG	MEVAM	Mesoscale valve by additive manufacturing for applications in haptic systems
39848.1 IP-LS	MICROHISTO	High throughput histology on microtissues
27901.1 PFLS-LS	MUSCLEANALYSER	Electrical stimulation & optical force measurement apparatus for 3Dprinted muscle tissues in multiwell plate
41091.1 INNO-LS	MYVET	Microfluidic point-of-care cartridge and reader for isothermal amplification
41363.1 IP-LS	Nano-B	Development of innovative customer-tailored composite multilayers in orthopedic- and trauma surgery
41157.1 IP-ICT	OPTIBP ML	Optical blood pressure management smartphone app: OptiBP market launch
37517.1 IP-LS	ORGACHIP	Combined parasite and host models for high-throughput drug pharmacokinetics in animal health
34473.1 IP-ENG	PANORAMA	Powder-based novel raw materials
39699.1 INNO-ENG	PARQUETROBOT STUDY	Preliminary study on Parkett-Schleifroboter
25485.1 PFNM-NM	PERMUT	Investigation of feasibility of MEMS based ultrasonic air transducers for industrial applications
35477.1 IP-LS	PETE	Preeclampsia test at the point of care
34956.1 IP-ENG	PHOMIPRO	Smartphone readable digital scrambled pixelated microstructures for part identification and brand protection
44861.1 INNO-ENG	PIKEPERCH STUDY	Quality control of pikeperch juveniles with digital imaging
28063.1 PFNM-NM	PRECISENSE	Development of a generic, high-performance, low-cost, absolute position sensor prototype
44145.1 IP-ICT	PROXIMITY	Capture system concept validation for in-orbit debris removal demonstration
44098.1 IP-EE	PULSE	Polychromatic universal LED light source and IV extraction for novel solar cell architectures
25422.2 PFIW-IW	PUMPOMAT	Robotergesteuerter Präzisionsmontagearbeitsplatz
45216.1 IP-EE	PVBLIND	Smart modular photovoltaic blind
44587.1 IP-ENG	PYRAMID	High aspect ratio 3D pyramidal probes on CMOS MEA's for in vitro tissue model study
42194.1 INNO-EE	RAPIDE	Reactive power management in district energy systems
40504.1 IP-ENG	REDULAS	Development of advanced femtosecond laser based ultra-precision manufacturing system for smart micro- LED display
36894.1 INNO-ICT	SIDIS	Vision gate for rental cars using machine learning
35418.1 IP-ENG	SLAM4-0	Smart laser manufacturing for precision Industry 4.0
30759.1 IP-EE	SMART-LIGHT	Safe and smart control of blind and lighting
31392.1 IP-EE	SMART-MAT	Advanced materials and design for cost-effective, high-performance and high-reliability SmartWire Connection Technology
35056.1 IP-ENG	SOMBREO	Automatic evaluation of thermoanalytical curves
49680.1 INNO-ENG	SOW	Solar powered watch range extender

39219.1 IP-ENG	SPP-SENS	Sail profile performance sensor
37762.1 INNO-ENG	SPV	Preliminary study on smart pinch valve
16694.2 PFIW-IW	STABILITY	Dynamische Lageregelung für Hydraulikmodule demonstriert an einem Stelzentraktor im Rebberg
34545.1 IP-ENG	STERLING	Improve the production processes of RF components by developing new silver-plating methods
44785.1 INNO-ENG	STONEHENGE STUDY	Automatische Steinprüf anlage
43052.1 IP-ENG	TURBOPREDICTIONS	Steigerung der Effizienz, der Verfügbarkeit und der Lebensdauer von Turbokompressoren aufgrund einer erweiterten Datenerhebung und - Analytik
31512.1 IP-EE	UPPERO	Development of deposition processes for future large-scale production of perovskite based photovoltaic devices
33466.1 IP-ENG	VERSACE	Versatile electrical regulation for spark assisted chemical engraving
46999.1 IP-ICT	VIVALDI	Quality control and high accuracy tracking system for steel mills
48014.1 IP-ENG	WATMON	Drinking water quality monitoring system
18394.1 PFLS-LS	ZEPTOTRACK	Real-time surgical instruments positioning with reference integrated in surgical lamp

## European Commission Projects

H2020 – CS2-CFP10-2019-01 3DGUIDE		Feasibility demonstration of 3D printing for a new efficient production method of mm-wave waveguide antenna
H2020 – NMBP 2016	ACENANO	Analytical and characterisation excellence in nanomaterial risk assessment: A tiered approach
H2020 – IOT 2016	ACTIVAGE	Activating innovative IoT smart living environments for ageing well
H2020 – LCE 2016	AMPERE	Automated photovoltaic cell and module industrial production to regain and secure European renewable energy market
H2020 – Clean Sky	AMPWISE	Autonomous wireless current sensor for aircraft power lines
H2020-ECSEL-2019-2-RIA	ANDANTE	AI for new devices and technologies at the edge
H2020 – ECSEL 2018-1-IA	APPLAUSE	Advanced packaging for photonics, optics and electronics for low-cost manufacturing in Europe
H2020 – Clean Sky 2	AUDACITY	Compact powerful and reliable piezoelectric actuator for landing gear systems
H2020 – LC-SC3-RES-6 2018 BE-SMART		Innovative building envelope for sustainable, modular, aesthetic, reliable and efficient construction
H2020 – ICT 2016	BIOCDX	Miniature bio-photonics companion diagnostics platform for reliable cancer diagnosis and treatment monitoring
H2020 – FETOPEN	CFLOW	Coherent ultrafast long wave infrared communications
H2020 – ECSEL-2019-1-IA	CHARM	Challenging environments tolerant smart systems for IoT and AI
H2020 – IND CE	CITCOM	Complimentary inspection technique based on computer tomography and plenoptic camera for MEMS components
H2020 – ICT 2015	DETOP	Dexterous transradial osseointegrated prosthesis with neural control and sensory feedback

H2020-LC-SC3-EE-2019	DOMOS	Operating system for smart services in buildings
H2020 – ICT 2016	FED4SAE	Federated CPS digital innovation hubs for the smart anything everywhere initiative
H2020 – IOT-2016	FITPIG	HR monitoring of pigs at the ear
H2020 – ICT 2016	FLAIR	Flying ultra-broadband single-shot infrared sensor
H2020 – MSCA-ITN 2016	FOODSMARTPHONE	Smartphone analyzers for on-site testing of food quality and safety
H2020 – SPACE 2018	HEATPACK	New generation of high thermal efficiency components packages for space
H2020-SC1-2019-Single-Stage-RTD	HEDIMED	Human exposomic determinants of immune mediated diseases
H2020-MSCA-ITN-2019	HIDDEN	Hunting invisibles: Dark sectors, dark matter and neutrinos
H2020 – LC-SC3-RES-15 2019	HIGHLITE	High-performance low-cost modules with excellent environmental profiles for a competitive EU PV manufacturing industry
H2020 – LC-SC3-RES-15 2019	HIPERION	Hybrid photovoltaics for efficiency record using integrated optical technology
H2020 – CS2-CFP07-2017-02	HIPNOSIS	Hardware implementation of pilot-non-intrusive cognitive states identification system
H2020 – EEB 2017	HYBUILD	Innovative compact hybrid electrical/thermal storage systems for low-energy buildings
H2020 – EE 2015-2-RIA	INDIGO-2	New generation of intelligent and efficient district cooling systems
H2020 – ICT 2016	INSPEX	Integrated smart spatial exploration system
H2020 – FOF 2016	KRAKEN	Hybrid automated machine integrating concurrent manufacturing processes, increasing the production volume of functional on-demand using high multi-material deposition rates
H2020-FETFLAG-2018-2020	MACQSIMAL	Miniature hot atomic vapor cells-based quantum devices for sensing and metrology applications
H2020-NMBP-FOF-2018	MANUELA	Additive manufacturing using metal pilot line
H2020 – NMBP 2017	MANU-SQUARE	Manufacturing ecosystem of qualified resources exchange
H2020-ICT-2019-2	MEDPHAB	Photonics solutions at pilot scale for accelerated medical device development
H2020 – ICT 2015	MIRPHAB	Mid-infrared photonics devices fabrication for chemical sensing and spectroscopic applications
H2020 – ICT 2017	MOLOKO	Multiplex photonic sensor for plasmonic-based detection of contaminants in milk
H2020 – ECSEL 2019-1-IA	MOORE4MEDICAL	Action for accelerating innovation in electronic medical devices
H2020-BG-2020-1	NAUTILOS	New approach to underwater technologies for innovative, low-cost ocean observation
H2020 – SFS 2018	NUTRISHIELD	Fact-based personalized nutrition for the young
H2020 – EIC-FTI-2018-2020	OFFSHOREMUSTER	An integrated emergency response decision support system for enhancing workers' safety in offshore oil & gas operations

H2020 – NMBP-FOF 2018	OLEDSOLAR	Innovative manufacturing processes and in-line monitoring techniques for the OLED and thin film and organic photovoltaic industries (CIGS and OPV)
H2020-SC1-2019-Single-Stage-RTD	ORGANTRANS	Controlled organoids transplantation as enabler for regenerative medicine translation
H2020 – CS2-CFP07-2017-02	PEGGASUS	Pilot eye gaze and gesture tracking for avionics systems using unobtrusive solutions
H2020-NMBP-TR-IND-2019	PEROCUBE	High-performance large area organic perovskite devices for lighting, energy, and pervasive communications
H2020 – LCE 2017	PERTPV	Perovskite thin-film photovoltaics (PERTPV)
H2020-ICT-2019-2	PHABULOUS	Pilot-line providing highly advanced & robust manufacturing technology for optical free-form micro-structures
H2020 – FETFLAG 2018	PHOG	Sub-poissonian photon gun by coherent diffusive photonics
H2020 – SPACE 2018	PULSAR	Prototype for an ultra large structure assembly robot
H2020 – MSCA-RISE	RDC2MT	Research, demonstration, and commercialization of DC microgrid technologies
H2020 – LC-SC3-RES-4 2018	RE-COGNITION	Renewable cogeneration and storage technologies integration for energy autonomous buildings
H2020 – SEC 2016/7	ROBORDER	Autonomous swarm of heterogeneous robots for border surveillance
H2020 – LCE-2016-SGS	SABINA	Smart bi-directional multi energy gateway
H2020 – ICT 2018-2	SARMENTI	Smart multisensor embedded and secure system for soil nutrient and gaseous emission monitoring
H2020-SC1-2019-Single-Stage-RTD	SBR	Smart bone regeneration
H2020 – SPACE 2018	SELECTOR	Surface mount technology (SMT) compatible electromechanical relay for compact redundancy ring
H2020 – CS2-CFP10-2019-01	SMARTWISE	Smart miniaturized and energy autonomous regional aircraft wireless sensor
H2020 – LC-BAT-2020-3	SPARTACUS	Spatially resolved acoustic, mechanical, and ultrasonic sensing for smart batteries
H2020 – SPACE-2019	SURPRISE	Super-resolved compressive instrument in the visible and medium infrared for Earth observation applications
H2020 – ATTRACT	SWAP	Smart wall pipes and ducts
H2020 – EE 2016/7	TABEDE	Towards building ready for demand response
H2020 – EEB 2016	THERMOSS	Building and district thermal retrofit and management solutions
FP7 – NMP-ENV-EeB	TRIBUTE complement	Take the energy bill back to the promised building performance
H2020 – ICT 2018-2	WELMO	Wearable electronics for effective lung monitoring
H2020 – ICT 2019-2	ZEROAMP	Ultra-low-power computing with survival skills

# European Space Agency, Swiss Space Office, and Swiss Space Center Projects

## ESA Projects

A-CSAC	Advanced concept for chip-scale atomic clocks (NAVISP-EL1-032)
AGAL	Lifetime improvement of the atomic clocks used in Galileo satellites
ATOM	Manufacturing of the complex feature demonstrator for space application made of metal matrix composite (MMC) having the specific modulus >30 GPa·cm <sup>3</sup> /g
CCM-MTG	Development and manufacture of corner cube mechanisms for MTG satellite
CLUPI	CLUPI instrument for Exomars
COMAM	Development of a compliant mechanism based on additive manufacturing
COMO	Coronavirus remote monitoring of outpatients with heart rate, breathing rate and skin temperature
COOLER	Compact opening louver
DANOE	High-dynamic absolute nanometric optical encoder technology assessment for space phase II
ELAINE	Electronic fetal monitoring system
ELISAMET	LISA laser system performance metrology volume 1 – Technical proposal
EUSO-B2	Elegant breadboard LIDAR for extrem universe space observation – Phase B2
EXPOSITION	Integrated flex pivot position sensor
FIFREDO	Fibered frequency doubler at 1560 nm
GERANIUM	Generative artificial intelligence for high performing inversion models
HIGHTS	Highly thermally conductive silver sintered die mounting
HOPP	Photodiode development
IMPROVE	Microvibration simulation and analysis tools
ISABELA	Development of a fine steering mirror breadboard
ISOL	Development of a high performance microvibration isolation system
LAFP	Development of a large angle flex pivot for space applications
LIDISOR2	Development of an experimental optical ranging payload for future Galileo satellites
MACAREW	Magnetic characterization of reaction wheels
MATMAT CCM	Matrix material for programmable flexure mechanism
MBRW	Magnetic bearing-based reaction wheel
MCC-X	Miniaturised motion controller customization for robotic exploration
MDP_CHEF	Cost-effective hermetically sealed chip fuses
MEGA	Micro-fabricated electron gun for atomic clocks
MILA4GROUND	Proof of concept for MILA ground applications
MILEB	Miniaturized imaging LIDAR systems for the landing of spacecraft's
ML-BI-CIS	Microlenses deposition for backside illuminated imagers
NIRS	NIR immersed grating in transmission for high resolution spectroscopy
NPI-BEARING	Miniature magnetic bearings for space actuators
OBSIDIAN	On-board system identification for uncertainty modelling & characterization
OEO	Ultra-low phase noise reference oscillator
OSRC	Digital stabilisation electronics for lasers
PHOTAC	Etude pour une nouvelle génération d'horloge atomique
PRINTHEATERS	Fully printed heaters on CFRP structures for space applications

REAC	Reliability evaluation of MEMS by accumulative tests for space application
R-MTS	Development and fabrication of robust miniature timing source (R-mTS) engineering models (EMs). These R-mTS EMs are double-resonance miniature atomic clocks.
SMARTIES	Design, procurement and qualification testing of a slip ring assembly rotor based on additive manufacturing
SPACEWAVE	Ultra-low phase noise microwave generation with modelocked laser and high-power handling photodiodes
ULTEEM	Ultra-long-term EEG monitoring
WALLIE	Development new TOF detector. Follow-up MILA
WAVEGUIDE	Development of a WGS based on flexible elements

## Industrial Property

### Patent portfolio

In 2020, 10 propositions for new inventions were received internally and 13 new patent applications were filed (12 regular applications and 1 provisional application).

The patent portfolio has been further enhanced by the extension to different countries of 84 patent applications based on prior patent applications (25 cases of "filing under priority" and 59 cases of "entries into national/regional phase").

## Collaboration with Research Institutes and Universities

<i>University</i>	<i>Institute</i>	<i>Professor</i>	<i>Field of collaboration</i>
Agroscope	Animal Production Systems and Animal Health	C. Ollagnier	Vital signs monitoring in livestock (pigs)
AO Research Institute Davos	Regenerative Orthopaedics	S. Grad, M. Stoddart	Bio-sensing
Austrian Institute of Technology (AIT)	Advanced Implant Solutions	L. Sajti	Magnetic inks
Cantonal Hospital St. Gallen	Lung Center	F. Baty, M Bösch	Unobtrusive assessment of sleep apnea using a wrist-worn device
CEA-INES	Heterojunction solar cells Lab	D. Munoz	Silicon heterojunction, metallization
CEA-LETI	DSYS/SSCE	I. Dor	Internet of things
CHUV	Department of Anesthesia	P. Schoettker	Automated pulse oximeter waveform analysis to track changes in blood pressure during anesthesia induction: A proof-of-concept study
CHUV	Head and Neck Surgeons	S. Christian	Multispectral endoscopy for real time delineation in surgery
EMPA	Advanced Materials Processing	P. Hoffmann	Surface texturing / Solid state lighting
EMPA	Functional Inorganic Materials Group	M. Kovalenko	Fluorescence lifetime imaging
EMPA	Laboratory for Thin Films and Photovoltaics	F. Fu	Perovskite based tandem cells
EPFL Lausanne	Advanced Quantum Architecture Laboratory	E. Charbon	Micro-optics
EPFL Lausanne	Automatic Control Laboratory 3 (STI IGM LA3)	C. Jones	Automatic building model identification and optimized control
EPFL Lausanne	Collège de Management de la Techologie	G. de Rassenfosse	Efficient data base collection

<b>University</b>	<b>Institute</b>	<b>Professor</b>	<b>Field of collaboration</b>
EPF Lausanne	Computer Vision Laboratory	P. Fua	Reduced labelling machine learning
EPF Lausanne	ECAL Lab	N. Henchoz	Digital experience - meditation study in collaboration with Ming Shan (Bullet's Taoist center)
EPF Lausanne	ICLAB Integrated Circuits Laboratory	C. C. Enz	60GHz radar, approximate arithmetic, ULP radio and protocol for WiseSkin
EPF Lausanne	Laboratory of advanced semiconductors for photonics and electronics	N. Grandjean	Solid state lighting
EPF Lausanne	Laboratory of Nanobiotechnology	A. Boghossian	Biosensors
EPF Lausanne	Laboratory of Photonics and Quantum Measurements	T. J. Kippenberg	Bridge
EPF Lausanne	LAP Processor Architecture Laboratory	P. lenne	Embedded systems
EPF Lausanne	LESO	J.-L. Scartezzini	Human centric lighting
EPF Lausanne	LIPID	M. Andersen	Human centric lighting
EPF Lausanne	Microengineering	D. Briand, V. Subramanian	Printed electronics
EPF Lausanne	PVLAB	C. Ballif	High performance solar cells and high reliability PV modules
EPF Lausanne	School of Engineering	R. Logé	Materials and alloys
EPF Lausanne	Signal processing laboratory 4	P. Frossard	Privacy preserving machine learning and hierachical computing / Graph machine learning for power forecasting
EPF Lausanne	TCL Telecommunications Circuits Laboratory	A. P. Burg	Good enough circuits, Ultra-low power and sub-threshold design, bias control, library characterization
EPFL Lausanne	Department Engineering Mechanics of Soft Interfaces	J. M. Kolinski	Smart interfaces/coatings
EPFL Lausanne	Laboratory of Physics of Complex Matter	L. Forro	Nanomaterials
ETH Zurich	Computer Vision Laboratory	L. van Gool	Machine learning
ETH Zurich	Data Analytics Lab	T. Hofmann	Machine learning
ETH Zurich	deMello Group	A. De Mello	Microfluidics
ETH Zurich	Department of Chemistry and Applied Biosciences	M. Kovalenko	Fluorescence lifetime imaging
ETH Zurich	Department of Health Sciences and Technology	S. Sturla	Bio-sensing
ETH Zurich	Department of Information Technology and Electrical Engineering	M. F. Yanik	Neuroinformatics

<b>University</b>	<b>Institute</b>	<b>Professor</b>	<b>Field of collaboration</b>
ETH Zurich	Institute for Particle Physics and Astrophysics	A. Rubbia	X-ray read-out circuit characterization
ETH Zurich	Integrated Systems Laboratory	L. Benini	Sub-near-threshold multicore, neural network
ETH Zurich	Mobile Health Systems Lab	W. Karlen	Development and evaluation of a slow wave sleep modulation framework including continuous blood pressure and glucose monitoring
ETH Zurich	Particle Technology Laboratory	S. Abegg	Sensor
Fachhochschule Graubünden (FHGR)	Departement Angewandte Zukunftstechnologien, Institut für Photonics und ICT IPI	U. Hauser-Ehninger	Solid state lighting
Fachhochschule Graubünden (FHGR)	Kompetenzzentrum für Datenanalyse, Visualisierung und Simulation	B. Studer	Bio-sensing
Fachhochschule Nordwestschweiz (FHNW)	Institut für Nanotechnische Kunststoffanwendungen	M. Kristiansen	Micro and nano structuring
Fachhochschule Nordwestschweiz (FHNW)	Institute for Chemistry and Bioanalytics	D. Gygax, L. Suter-Dick	Bio-sensing
Fachhochschule Nordwestschweiz (FHNW)	Institute of Product and Production Engineering	B. Resan	Lasers
FEMTO Besançon	Department Micro Nano Sciences and Systems	F. Chérioux	Nanocoatings
Fondazione Bruno Kessler	Integrated Radiation and Image Sensors	M. Perenzoni	Time-of-flight LiDAR detectors
Geneva University Hospital	Paediatric Emergency Division	M. Rida Benissa	Diagnosis based on AI on chest sounds
HE-ARC La-Chaux-de-Fonds	Engineering – Medical Devices	A. Kaempfer-Homsy	Bio-sensing
Idiap Research Institute	Speech and Audio Processing	P. Motlicek	Modal a people monitoring system using multiple sensing modes (video, audio, ...)
Idiap Research Institute	Speech and Audio Processing	R. Prasad	Detection of QRS landmark in ECG signals
Ifremer	Centre Méditerranée	J. Opderbecke	Bathymetric LiDAR
Imperial College of London, United Kingdom	Faculty of Engineering, Department of Electrical and Electronic Engineering	E. M. Yeatman	Energy harvesting for wireless sensor networks in aerospace applications; smart materials
INAIL (Italian Workers Compensation Authority)	Aids Area and Research and Training Area	R. Sacchetti	Clinical implantation and assessment
IPC-Oyonnax-France	Innovation Plasturgy Composites	L. Tenchine	Injection Molding

<b>University</b>	<b>Institute</b>	<b>Professor</b>	<b>Field of collaboration</b>
Istituto Ortopedico Rizzoli (IOR)	2nd Orthopaedic and Traumatology Clinic	S. Zaffagnini	Clinical implantation and assessment
Katholieke Universiteit, Belgium	Computer Security and Industrial Cryptography group	A. Purnal	Cryptography & security
Leibniz-Institut für Kristallzüchtung (IKZ)	Zentrums für Lasermaterialien	C. Kränkel	New laser crystals for high-power short pulse sources
National Research Council of Italy	Institute of Applied Physics (IFAC)	V. Raimondi	Compressive sensing for space applications
National Technical University of Athens (NTUA)	School of Mechanical Engineering	I. Paraskevas	Systems identification methods
ONERA-France	Meudon Center	M.-C. Mérienne	Pressure sensitive painting
ONERA-France	Modane-Avrieux Center	O. Guillerme, F. Paraz	Pressure sensitive painting
Politecnico Di Torino (POLITO)	Electronics and Telecommunications	E. Magli	Compressive sensing for space applications
Robert-Bosch-Hospital	Clinical of Geriatric Rehabilitation	C. Becker	Fall prediction and detection
Sant'Anna School of Advanced Studies, Pisa	Institute of Communication, Information and Perception Technologies (TeCIP)	A. Bogoni	Photonics radar
Sant'Anna School of Advanced Studies, Pisa	The BioRobotics Institute	C. Cipriani	Artificial wrist, mechatronic couplers, artificial sensors for hand/wrist prosthesis, control algorithms, user assessment tools
Swedish University of Agricultural Sciences	Dept. of Biosystems and Technology	A. Herlin	Vital signs monitoring in livestock (pigs) in the framework of IoF2020
Swiss Institute of Allergy and Asthma Research (SIAF)	Molecular allergology	K. Bärenfaller	Bio-Sensing
Swiss Tropical and Public Health Institute	Department of Medicine	D. Paris	Diagnostics
Università Campus Bio-Medico	Department of Orthopaedics and Trauma Surgery	V. Denaro	Clinical implantation and assessment
Université de Bourgogne	LE2I	J. Dubois	Remote vital signal monitoring
Université de Caen	Department of Neurophysiology	S. Besnard	ADAPTATION - Vital signs monitoring during Christian Clot's expedition in the Valley of Death
University Children's Hospital Basel, UKBB	Department Anesthesiology	T. Erb	Intra-tracheal pressure monitoring
University Hospital Basel	Research Center for Clinical Neuroimmunology and Neuroscience	J. Lorscheider	Improving monitoring solutions for multiple sclerosis patients
University Hospital Inselspital Bern	Department ENT Surgery	M. Caversaccio	Image-guided micro surgery for hearing aid implantation

<b>University</b>	<b>Institute</b>	<b>Professor</b>	<b>Field of collaboration</b>
University Hospital Inselspital Bern	Department of Cardiology and Clinical Research	E. Rexhaj, S. Rimoldi	Clinical validation of a PAP sensor against non-invasive medical gold standard / Clinical study on 24h ambulatory blood pressure monitoring in 70 hypertensive patients using wrist-located optical sensors
University Hospital Inselspital Bern	Department of Cardiovascular Surgery	D. Reineke	Clinical study on non-invasive blood pressure monitoring in 40 patients carrying a left ventricular assist device
University Hospital Inselspital Bern	Department of intensive Care Medicine	J. Schefold, D. Reinecke	Validation of the extended AVA product with the non-invasive measure of the BP in reference to the medical gold standard and with a 40- patient cohort (pregnant women)
University Hospital Inselspital Bern	Lung Cancer Center	G. Kocher	Machine learning for efficient surgery.
University Hospital Inselspital Bern	Sleep-Wake-Epilepsy-Center and NeuroTec	K. A. Schindler	Single-lead electroencephalogram recording using ultra-long-term EEG monitoring (ULTEEM) system – a pilot study / Epilepsy detection and prediction
University Hospital Inselspital Bern	Universitätsklinik für Frauenheilkunde	A. Radan	Introduce artificial intelligence (ai) and machine learning in cardiotocography (CTG) Interpretation to improve clinical use / Wearable system for foetal ECG monitoring
University Hospital Inselspital Bern	Universitätsklinik für Frauenheilkunde	D. Surbek	AI-based decision support system for delivery & Fetal monitoring by transabdominal electrocardiogram recording: the ELAINE pilot project
University Hospital Inselspital Bern	Universitätsklinik für Pneumologie	S. Ott	Unobtrusive assessment of sleep stages using a wrist-worn device
University Hospital of Basel	Cardiology	A. Salome Vischer, T. Burkard	Accuracy of the RIVA digital blood pressure measurement App - a pilot study
University Hospital Zurich	Biomedical optics research laboratory	M. Wolf	Newborn vital signs monitoring based on multiple vision sensors
University of Applied Sciences and Arts of Southern Switzerland (SUPSI)	IDSIA Dalle Molle Institute for Artificial Intelligence	L. M. Gambardella	Machine learning
University of Applied Sciences and Arts of Southern Switzerland (SUPSI)	Institute for Applied Sustainability to the Built Environment	C. Caccivio	Metrology

<b>University</b>	<b>Institute</b>	<b>Professor</b>	<b>Field of collaboration</b>
University of Applied Sciences and Arts, Luzern (HSLU)	CC Electronics	E. Niederberger	Solid state lighting
University of Applied Sciences and Arts, Luzern (HSLU)	Institute of Electrical Engineering	T. Prud'homme	Vision, polarization camera
University of Basel	Chemistry	E. Constable, C. Housecroft	Photochemistry
University of Basel	Psychiatry Hospital / Center for Chronobiology	C. Cajochen	Human centric lighting / Chronobiology
University of Bern	ARTORG Center for Biomedical Engineering	S. Weber	Image-guided microsurgery for hearing aid implantation
University of Bern	Quantum Optics Lab	A. Stefanov	Entangled photons for microscopy
University of Bern – ARTORG	Organs-on-Chip Technologies	O. Guenat	Bio-Sensing
University of Essex, Colchester, United Kingdom	School of Computer Science and Electronic Engineering	L. Citi	Point-process and machine-learning-based neuro-muscular decoding/control algorithms
University of Geneva	Astronomy Department	F. Bouchy	NCCR PlanetS
University of Geneva	Institut de Chimie	T. Burgi	Microstructure of nano particles
University of Geneva	School of Economics and Management	S. Engelke	Non-Contact heart rate monitoring through vision system
University of Geneva	Sensors Group at Institut für Neuroinformatik, U	S.-C. Liu	Neuroinformatics
University of Gothenburg	Department of Orthopaedics	J. Wessberg	Sensory feedback
University of Klagenfurt	Department of Computer Science	A. Roy	Cryptography & security
University of Klagenfurt	Digital Age Research Center	E. Andreeva	Cryptography & security
University of Lorraine	Laboratoire lorrain de Recherche en Informatique et ses Applications	V. Lallemand	Cryptography & security
University of Lund	Department of Biomedical Engineering	C. Antfolk	Prosthetics, decoding of user intent, control, clinical assessment
University of Neuchâtel	Complex Systems Group	V. Schiavoni	Security and data privacy in IoT systems; Usage of trusted execution environments for cloud computation (IntelSGX) and IoT protocols (ARM's TrustZone)
University of Neuchâtel	Institut de Biology	P. Junier, F. Kessler	Ultrastructural investigation
University of Pavia	Department of Chemistry	M. Pesavento	Chemical sensor
University of Sherbrooke	Neonatology	E. Fortin-Pelerin	Evaluation of PAP measurement accuracy in sheep
University of Zurich	Institute of Neuroinformatics	T. Delbrück	On-chip convolutional neural network for visual scene processing

<b>University</b>	<b>Institute</b>	<b>Professor</b>	<b>Field of collaboration</b>
University Politechnica Madrid	Department of Signals, Systems and Radiocommunications	M. Sierra	RF systems & antennas
Vienna University	Department of Physical Chemistry	P. Lieberzeit	Chemical sensor
Wyss Center	Bio and Neuro Engineering	G. Kouvas	Integrated circuits for brain implants

## Teaching

	<b>Title of lecture</b>	<b>Context</b>	<b>Location</b>
L. A. Dunbar	Digital Transformation	EMBA	EPF Lausanne
F. Cosandier	Precision guiding systems for the Swiss Kibble balance	Design of Mechanisms	EPF Lausanne
F. Cosandier	On the revision of the International System of Units	Metrology	EPF Lausanne
M. Dadras	Microscopy	Microscopy and Nanoscopy	University of Neuchâtel
M. Despont	Packaging and hybridization, the valorization of MEMS technologies	Micro- 534 Advanced MEMS 2020 (D. Briand)	EPF Lausanne
N. Marjanovic, F. Zanella	Organic and Printed Electronics	Master course MICRO-505	EPFL Lausanne
R. Pugin	Micro/Nano-structured Functional Surfaces & Components	Highlights in Microtechnology – Summer School	EPF Lausanne

## Theses

### PhD Degrees Awarded in 2020

<b>Name</b>	<b>University</b>	<b>Title</b>
A. Tuomiranta	EPFL	Prediction of Photocurrent in Bifacial Photovoltaic Systems

### CSEM Employees carrying out a PhD & PhD Funded by CSEM

<b>Name</b>	<b>Professor / University</b>	<b>Theme / CSEM Unit</b>	<b>Start year</b>
T. Aderneuer	C. Cajochen / University of Basel	Free form micro-optics for human centric lighting / Center Muttenz	2017
C. Aguet	P. Frossard / EPF lausanne	Generate realistic synthetic PPG data using Generative adversarial networks / Systems	2019
M. Auchlin	V. Gass / EPF Lausanne, Swiss Space Center	New reliability assessment of MEMS components under accumulative testing for space application / Micro&Nano Systems	2017
F. Ayhan	G. Villanueva / EPF Lausanne	LiNbO3 waveguide microfabrication for broadband optical frequency combs for astronomical spectrometers calibration light / Systems	2020
G. Bernard	R. Logé / EPF Lausanne and ESA (partial funding)	Development of a production method of metal matrix composite for space applications using laser powder bed fusion / Micro&Nano Systems	2020
L. Biggio	T. Hofmann / ETH Zurich	Machine learning based domain adaptation and interpretability for time-series / Center Alpnach	2019
B. Bonnal	C. Dehollain / EPF Lausanne	Cooperative sensors / Systems	2019

<b>Name</b>	<b>Professor / University</b>	<b>Theme / CSEM Unit</b>	<b>Start year</b>
G. Borque Gallego	Y. Perriard / EPF Lausanne	Magnetic bearings for space actuators / Systems	2016
S. Cerida Rengifo	C. C. Enz / EPF Lausanne	FMCW radar front-end / Integrated and Wireless Systems	2018
F. Chicco	C. C. Enz / EPF Lausanne	Frequency synthesis for FMCW Radar / Integrated and Wireless Systems	2017
L. Driencourt	E. Constable, C. Housecroft / University of Basel	Plasmon-enhanced water splitting / Center Muttenz	2017
M. Dussouillez	C. Ballif / EPF Lausanne	Perovskite stability / Photovoltaics	2019
Y. El-Zein	K. Huguenin / UNIL	mHealth data privacy / Systems	2019
T. Frei	V. Gass / EPF Lausanne	Thermal management of microsystem in harsh environment / Micro&Nano Systems	2017
Z. Halvorsen	A. De Mello / ETH Zurich	Miniaturized fluid sample preparation for water quality monitoring / Center Alpnach	2017
D. Honzàtko	P. Fua / EPF Lausanne	Defect detection using deep learning / Integrated and Wireless Systems	2018
P. Iurilli	V. Wood / ETH Zurich	State-of-health modeling for batteries / Photovoltaics	2019
S. Jafari	S. Sturla / ETH Zurich	Electrochemical biosensing in food safety / Center Landquart	2017
L. Jeanningsros	J.-P. Thiran / EPF Lausanne	Classification of cardiac arrhythmia based on PPG / Systems	2020
P. Jokic	L. Benini / ETH Zurich	Embedded machine learning / Integrated and Wireless Systems	2017
E. Klauser	E. Karimi / EPF Lausanne	Adaptive control of a micro-vibration isolation system / Systems	2020
T. C. Müller	A. P. Burg / EPF Lausanne	Variation-aware digital design / Integrated and Wireless Systems	2016
S. Narduzzi	S.-C. Liu / ETH Zurich	Ultra-low-power resource algorithms for neuromorphic hardware / Integrated and Wireless Systems	2020
E. Ntavelis	L. van Gool / ETH Zurich	Multimodal learning & generation: Utilizing diverse inputs to generate & manipulate images / Center Alpnach	2019
C. Sainz Martinez	M. Bach Cuadra / CHUV	MRI and EEG processing applied to human brain structure and function / Systems	2020
P. Scharnhorst	C. Jones / EPF Lausanne	Reinforcement learning for building and grid control / Photovoltaics	2019
L. L. Senaud	C. Ballif / EPF Lausanne	Silicon heterojunction solar cells / Photovoltaics	2018
Y. Sepehri	P. Frossard / EPF Lausanne	Smart edge for hierarchical vision systems / Integrated and Wireless Systems	2020
J. Simeunovic	P. Frossard / EPF Lausanne	Graph signal processing for energy grids / Photovoltaics	2019
Y. Tang	O. Guenat / University of Bern, ARTORG	Nanocellulose applications in biosensing / Center Landquart	2017
A. F. Valencia Patino	C. Alippi / Università della Svizzera Italiana	Performance and physical attack security of lattice-based cryptography / Integrated and Wireless Systems	2020

## Commissions and Committees

P.-J. Alet	European Commission, Innovation and Networks Executive Agency: expert European technology and innovation platform – photovoltaics (ETIP-PV): executive committee (member), steering committee (member), “Digital PV and grid” working group (leader) European technology and innovation platform – smart networks for the energy transition (ETIP-SNET): governing board (member) Intersolar Europe: conference committee (chairman), Intersolar Award jury (member)
F. Amez-Droz	CSEM Representative, Swiss Association of Science Journalism
N. Blondiaux	Member of the council of the AET (Academy of Engineering and Technology) Member of the scientific committee of the EUSPEN (European Society of Precision Engineering and Technology)
C. Bosshard	DayOne: Member of Core Team Managing Director of the Swissphotonics NTN Member of M4IVD Board Member of Swissmem Specialty Group Photonics Member of the Board of EPIC (European Photonics Industry Consortium) Member of the Board of Stakeholders of Photonics21 Member of the University Council of the University of Basel
S. Cattaneo	Expert for MSE Master Theses at OST Eastern Switzerland University of Applied Sciences Expert for W.A. De Wigier Foundation Innovation Coach for INOS Innovations Netzwerk Ostschweiz
F. Cosandier	International Scientific Committee, EUSPEN
M. Dadras	Nominated as Professor of University of Neuchâtel
P. Dallemande	Secretary and Swiss representative of Technical Committee 5 "Information Technology Applications", International Federation for Information Processing (IFIP)
R. Delgado-Gonzalo	Expert Group in Digital Health in the Swiss Alliance for Data-Intensive Services
M. Despeisse	n-PV workshop committee, EUPVSEC topic organizer, SolarPower Europe.
M. Despont	Board member of the Swiss-MNT network CSEM and HTA representative at the Micro- and Nano- Technology Workgroup, European Spatial Agency (ESA) Jury Member at the thesis of Etienne Thalmann “Flexure Pivot Oscillators for Mechanical Watches” with Prof. S. Henein Jury Member at the thesis of Matthieu Rüegg ,“Transient Electronics for Smart Biodegradable Medical Implants” with Prof. J. Brugger Member of the editorial board of Microelectronic Engineering Journal (Elsevier) Member of the International Steering Committee of IEEE International Conference on Micro ElectroMechanical Systems (MEMS) Regional Program Chair of the 21st International Conference on Solid-State Sensors, Actuators and Microsystems (Transducers 2021)
L. A. Dunbar	Academic co-Lead of Machine Learning Clinic in the Swiss Alliance for Data-Intensive Services Co-Chair of the Industrial Automation, Communication, Networking and Informatics Track of IEEE ICIT 2021 Members of the subcommittee FA10 on Computer Vision and Human-Machine Interaction in Industrial and Factory Automation,
M. El-Khoury	CNCI Chambre Neuchâteloise du Commerce et de l'Industrie, Neuchâtel Concours International de Chronométrie, Le Locle, Membre du Comité d'honneur Member of the Swiss Academy of Engineering Sciences SATW
S. Emery	Member of the Technical Committee of the IEEE SOI-3D-Subthreshold (S3S) Conference
J. R. Farserotu	Chair and Research Co-ordinator The Hermes Partnership Chair of ETSI Technical Committee Smart Body Area Networks (TC SmartBAN)

O. Fernandez	Member of SciPiL (the Scientific Partnership in Lighting by Luger Research) Member of the Executive Board of the PHABULOU S Pilot Line Association
R. Ferrini	Chair of the Swissphotonics Solid State Lighting - (SSSL) Swiss National Laboratory for Solid State Lighting Managing Director of the PHABULOU S Pilot Line Association Member of SciPiL (the Scientific Partnership in Lighting by Luger Research) Member of the Advisory Board of the Swiss Lighting Forum Member of the Program Committee of the FRED – Forum Romand de l'éclairage et de la domotique
S. Fricke	Chairman of M4IVD Board Member of the Organising Committee, Swiss ePrint 2021
E. Györvary	Board Member of European Organ-on-Chip Society (EUROoC) Core team member of Team Finland in Switzerland Extended Board Member of CSEM Brasil Extended Board Member of the Heterogeneous Technology Alliance (alliance federating the Fraunhofer (microelectronics), VTT, CEA-Tech, and CSEM) & leading the Health & AgriFood Platform Member & CSEM representative of EARTO Working Group on Emerging Technologies for Healthcare Member of the Finnish Chamber of Commerce Member of the Latin American Chamber of Commerce Scientific & Organizing Committee Member of "Next Gen Organ-on-Chip & Organoids" event Scientific Board Member of Swiss Integrative Center for Human health (SICHH), Fribourg Steering Board Member of Innovation Group Digitalization at Swiss Food Research
H. Heinzelmann	Expert, Austrian Research Promotion Agency FFG Expert, German Federal Ministry of Education and Research BMBF Member of the Begleitgruppe Aktionsplan synthetische Nanomaterialien, Federal Office of Public Health FOPH Member of the Executive Board, EARTO Member of the Foundation Board, Switzerland Innovation Member of the Strategic Advisory Board "Produktion der Zukunft", Austrian Federal Ministry of Transport, Innovation and Technology BMVIT Membre du Conseil d'Administration de Centredoc Steering Committee, CCMX Competence Center for Materials Science and Technology
A. Hutter	Commission des énergies et de l'eau de la ville de Neuchâtel Innosuisse expert Vice-President iBAT Association ( <a href="http://www.ibat.swiss">www.ibat.swiss</a> )
C. Joder	Member of the Advisory Board of IAT (Center of Innovation for Assistive Technologies) at Swiss Paraplegic Center, Nottwil
R. Jose James	Chairman Swiss Chapter IEEE Electronic Packaging Society
C. Julia-Schmutz	Communication Coordinator within the Heterogeneous Technology Alliance (HTA) CSEM Representative, BioAlps
H. F. Knapp	Board member for NTN INARTIS Board of Directors member for cluster initiative Toolpoint for Lab Science Jury member for Zinno Ideenscheck Pre-jury member for Swiss Technology Award

G. Kotrotsios	Euripides Scientific Adviser of the Board, Council Member and Adviser of the Council IEEE Subcommittee on Human-Machine in Manufacturing Environment Member of Microcity Consultancy Committee Member of the Advisory Board of the NTN Innovation Booster Photonics Member of the Board of AM-TTC (Advanced Manufacturing Technology Transfer Centers) Initiative Member of the Board of the Heterogeneous Technology Alliance (alliance federating the Fraunhofer (microelectronics), VTT, CEA-Tech and CSEM Member of the Executive Board of EREA (the European Association of Aeronautics Research Centers) Member of the Steering Committee of the SATW Advanced Manufacturing Research Alliance Member of the Swiss Academy of Engineering Sciences SATW Micronarc, member of the Group of Experts Vice Chairman of the Board of Directors of CSEM Brasil
M. Krieger	CSEM Representative Expert Workgroup Data driven Business Models, Swiss Alliance Data intensive services CSEM Representative Greater Zürich Area (GZA) CSEM Representative Innovation Expert Group Food Packaging at Swiss Food Research CSEM Representative SEMI global semiconductor industry association CSEM Representative Smart Card Forum Switzerland (SCF) CSEM Representative Zürcher Handelskammer (ZHK) CSEM Representative, Advanced Factory Automation workgroup of Swissmem (AFA) Member of Scientific Advisory Board of 9th International Precision Assembly Seminar 2020 Kitzbühel, Austria
F. Kurth	Member of the technical program committee, International Conference on Miniaturized Systems for Chemistry and Life Sciences 2020 (mTAS 2020)
M. Lemay	Board Member, Swiss Society for Biomedical Engineering
A. Madrigal	Chair of the Advisory Board of the Space exhibition of the Museum of Transport of Lucerne Chair of the EARTO Working Group Space Research CSEM Representative, General Forum Clean Sky CSEM Representative, Swiss Aeronautics Security and Defense Division of Swissmem (Swiss ASD) CSEM Representative, Swiss Space Industries Group of Swissmem (SSIG) Expert for the evaluation of H2020 proposals in the Space Work Programme of the European Commission Member of the General Assembly of EREA (Association of European Establishments in Aeronautics) and CSEM Delegate in the Aviation Research Groups of the Association Member of the Steering Committee of the Swiss Space Center Member of the Strategic Committee of the Swiss Aeropole
N. Marjanovic	Member of the Organising Committee, Swiss ePrint 2021
S. Mohrdiek	Member of Photonics21 Work Group 6 – Design and Manufacturing of Components and Systems Member of Swissmem Fachgruppe Photonics Swissphotonics, Head of Swiss Photonic Packaging Laboratory (SPPL)
J.-L. Nagel	Member of the Editorial Board of the “Journal of Low Power Electronics” (JOLPE)
S. Paoletti	European Liquid Biopsy Society Member Executive Board member of biotechnet, Switzerland
R. Pugin	Member of the Expert Committee of the Association NTN Innovative Surfaces Member of the Omega Foundation Council Member of the Scientific Committee of the 4M Micro-Nano Manufacturing Association Member of the Scientific Committee of the World Congress on Micro and Nano Manufacturing
V. Revol	Co-Founder and deputy head of the Digital Innovation Hub LifeHub.Swiss ( <a href="http://www.lifehub.swiss">www.lifehub.swiss</a> ) Entrepreneur coach for MicroCity Start-Up Program
D. Ruffieux	Member of the International Technical Program Committee of the European Solid State Circuit Conference (ESSCIRC) in the RF and mmWave Building Blocks

E. Schaller	Member of the Executive Board of sensors.ch, Switzerland
P. A. E. Schmid	Academic co-lead expert group ML-Clinic (ML in Industrial Practice) Swiss Alliance for Data-Intensive Services CSEM Representative Swiss Mechatronics Cluster Founder and regional lead Digital Innovation Hub Robotics & Artificial Intelligence ( <a href="http://www.raisehub.swiss">www.raisehub.swiss</a> ) INOS accredited coach for RIS OST Member expert group Industry 4.0 SATW
P. Steiert	Advisory Board Member for Institute für Chemistry and Biological Chemistry at the ZHAW Advisory Council for cluster initiative Toolpoint for Lab Science Member of the Executive Board for Verein Startup Pilatus
A. Steinecker	CSEM Representative EPoSS and Member of Working Group Robotics CSEM Representative IVAM
D. Ulrich	Co-platform leader IVD & co-chair Swiss Symposium in Point-of-care diagnostics Jury member Best Bündner Tech Start-up award Member Academia Raetica Member Digital meet-up Graubünden

## Prizes and Awards

January 2020	2020 IEEE Lifetime Member to Jean-Do Decotignie.
October 2020	CSEM was awarded 2nd place at the EARTO Innovation Awards 2020, in their Impact Delivered category for its optical blood pressure monitoring technology.
October 2020	Maxime Auchlin and his co-authors' outstanding efforts exploring a novel method for sequential bi-parameter testing to assess the reliability of automotive MEMS for space applications have been honored by ESREF 2020, winning them the 2020 Best Paper Award.
December 2020	Female Digital Innovators 2020 awarded to Samantha Paoletti.



**CSEM SA**

Jaquet-Droz 1  
CH-2002 Neuchâtel

**CENTER ALPNACH**

Untere Gründlístrasse 1  
CH-6055 Alpnach

**CENTER LANDQUART**

Bahnhofstrasse 1  
CH-7302 Landquart

**CENTER MUTTENZ**

Tramstrasse 99  
CH-4132 Muttenz

**ZÜRICH OFFICE**

Technoparkstrasse 1  
CH-8005 Zurich

**CONTACT**

[www.csem.ch](http://www.csem.ch)  
[info@csem.ch](mailto:info@csem.ch)  
[jobs@csem.ch](mailto:jobs@csem.ch)

